The importance of resource allocation for the development and physiology of multicellular organisms

Inaugural-Dissertation

zur Erlangung des Doktorgrades
der Mathematisch-Naturwissenschaftlichen Fakultät
der Heinrich-Heine-Universität Düsseldorf

vorgelegt von

Jürgen Wilhelm Schönborn
aus Leverkusen

Bottrop, Januar 2024

aus dem Institut für Mathematische Modellierung biologischer Systeme
Arbeitsgruppe Systembiologie des Fettstoffwechsels
der Heinrich-Heine-Universität Düsseldorf

Gedruckt mit der Genehmigung der
Mathematisch-Naturwissenschaftlichen Fakultät der
Heinrich-Heine-Universität Düsseldorf

Berichterstatter:

1. Jun.-Prof. Dr. Mathias Beller

2. Prof. Dr. Oliver Ebenhöh

Tag der mündlichen Prüfung: 14.11.2024

Zusammenfassung

Der Stoffwechsel eines Organismus umfasst physikochemische Prozesse, bei denen Substrate in metabolische Zwischenprodukte, sogenannte Metabolite, konvertiert werden, die wiederum in essenzielle zelluläre Bestandteile oder Energie umgewandelt werden. Die Ressourcenallokation bei vielzelligen Organismen bestimmt die Verteilung von Substraten auf kritische Stoffwechselprozesse. Diese Stoffwechselprozesse stehen in ständiger Konkurrenz untereinander, wodurch nicht alle Prozesse gleichzeitig optimiert werden können. Das Verständnis der Ressourcenallokation bei vielzelligen Organismen ermöglicht es uns, Überlebensstrategien und die Auswirkungen von Stoffwechselerkrankungen zu verstehen. Noch sind aber sogar grundlegende Design Prinzipien unklar.

Ziel dieser Arbeit war es, die Einflussfaktoren auf die Ressourcenallokation bei vielzelligen Organismen zu untersuchen. Hierfür wurden biochemische Messungen und metabolische Flussanalysen mittels Flux Balance Analysis durchgeführt. Insbesondere wurde das Wachstum und die Entwicklung von *Drosophila melanogaster* Larven untersucht, um ein besseres Verständnis für die Ressourcenallokation zu erlangen. Diese Untersuchungen zeigten die Auswirkungen unterschiedlicher Wachstumsbedingungen auf die Entwicklung und Ressourcenallokation. Die larvale Entwicklung kann durch die Zugabe verschiedener Metabolite, wie bestimmter Aminosäuren, beschleunigt werden. Diese zusätzlichen Metabolite beeinflussen zugrunde liegende Stoffwechselprozesse und ihre Priorisierung. Die Auswirkung zusätzlicher Ressourcen auf die Entwicklung und den Stoffwechsel wurden durch Wechselwirkungsstudien des Larvenmikrobioms weiter untersucht. Es zeigte sich, dass ausgeschiedene Metabolite Einfluss auf den Metabolismus einzelner Mitglieder des Mikrobioms hatten. Dies kann durch ausgeschiedene Metabolite der Mikrobioms potenziell auch den Stoffwechsel des vielzelligen Wirtsorganismus beeinflussen. Darüber hinaus haben physiologische Studien gezeigt, dass Larvenorgane, wie der Darm, Auswirkungen auf die Ressourcenallokation von sich entwickelnden Larven haben. Diese Studien zeigten, dass der Darm und wahrscheinlich auch andere Organe eine wichtige Rolle bei der Einleitung kritischer Entwicklungsstadien, wie der Verpuppung, spielen und Stoffwechselprozesse bei vielzelligen Organismen regulieren. In dieser Arbeit war es möglich, Ergebnisse vorzustellen, die das Verständnis der Ressourcenallokation und der Auswirkungen physiologischer Eigenschaften auf den Stoffwechsel eines vielzelligen Organismus vertiefen.

Abstract

The metabolism of an organism contains physico-chemical processes in which substrates are converted into metabolic intermediates, known as metabolites, and turned into essential cellular components or energy. Resource allocation in multicellular organisms determines the distribution of substrates to critical metabolic processes. These metabolic processes stand in constant competition with each other, resulting in the inability to optimize all metabolic processes simultaneously. Understanding resource allocation in multicellular organisms enables us to understand survival strategies and the impacts of metabolic diseases. Yet, even fundamental design principles remain unclear.

The aim of this work was to investigate the influencing factors on resource allocation in multicellular organisms. For this purpose, biochemical measurements and metabolic flux analyses using Flux Balance Analysis were performed. Specifically, the growth and development of *Drosophila melanogaster* larvae were investigated to achieve a better understanding of resource allocation. These studies revealed the effects of different growth conditions on development and resource allocation. The larval development can be accelerated by the addition of different metabolites, such as certain amino acids. These additional metabolites directly affect underlying metabolic processes and their prioritization. This effect of additional resources on development and metabolism were further investigated through larval microbiome interaction studies. It was observed that secreted metabolites influenced the metabolism of individual members of the microbiome. This can potentially affect the metabolism of the multicellular host organism through secreted metabolites of the microbiome.

Furthermore, physiological studies of larval organs, such as the gut, have an impact on the resource allocation of developing larvae. These studies revealed that the gut, and more likely other organs, play an important role in determining critical developmental stages, such as the pupation, and regulate metabolic processes in multicellular organisms.

In this thesis, it was possible to present findings that advances the understanding of resource allocation and the impact of physiological properties on the metabolism of a multicellular organism.

Acknowledgments

I want to express my gratitude to Mathias Beller, who gave me the opportunity to work on this project in his working group. I am thankful for the support he offered throughout my project and the time we spend together. Thank you for being an awesome teacher and mentor. I would also like to thank Oliver Ebenhöh as my second referee, for his valuable advice.

I would like to express my sincere thanks to Irfan, Nida, Andrea, Petra, Fiona, and Lisa for their support. Also, thanks to all the other members of the institute of mathematical modelling of biological systems of Heinrich Heine University Düsseldorf.

None of this would have been possible without my family and friends. Thanks to Daniel, Rene, Lucas, Christian, Elisabeth, and Manuel. A special thanks goes to my friend, Zoë, for our valuable discussions and constant motivation. Thank you for everything!

Lastly, I want to express my gratitude to my incredible mother, Halina, my brother, Raimund, and my sister, Angela, and my father, Wilhelm, who have supported me through every aspect of my life.

Table of Contents

1. Introduction

The development and growth of multicellular organisms is orchestrated by complex regulatory processes which are tightly linked to the metabolism. For example, growth is regulated by the quality and quantity of nutrients that an organism absorbs from the environment. These nutrients are resources, which an organism utilizes to fuel its metabolism, enabling it to perform different survival-critical tasks. The process that describes the distribution of nutrients in an organism is called resource allocation. Resource allocation is an adaptive process in response to both external and internal signals. In consideration of the prevailing influences on the organism, resource allocation defines a metabolic strategy aimed at optimizing the fitness of the organism. The optimization of conflicting processes is described in engineering and economy through the concept of Pareto optimality. Here, a set of parameters is optimized toward a specific objective, and improving one parameter leads to a decrease of another, and vice versa. This concept can be applied in the context of resource allocation, a utilization demonstrated in the study of microorganisms (Schuetz et al., 2012). How resource allocation in multicellular organism's work remains unanswered. Disruptions in the organization of the resource allocation network result in possible metabolism-related diseases. Thus, understanding the complex processes that lead to metabolic diseases in multicellular organism is of clinical interest.

1.1. Metabolism

An organism's metabolism is the entirety of physico-chemical processes occurring within cells that convert substrates to metabolites. Substrates are the available resources for metabolic processes that are absorbed from the environment. These metabolites are essential components for cellular structures or serve as an energy source for the organism. Two major groups of reactions dominate the metabolism, anabolic and catabolic reactions (Fig. 1).

Anabolic reactions synthesize complex biomolecules under energy consumption from convertible metabolites (Lehninger et al., 2013). Catabolic reactions on the other hand are reactions that convert available metabolites into energy for the

organism (Lehninger et al., 2013). One prominent metabolic pathway, for example, is Glycolysis, where glucose is converted through other intermediates to pyruvate, which can be used further in other metabolic pathways or channeled to energy production (Lehninger et al., 2013). The coordination of resource allocation among different conflicting metabolic processes of multicellular organisms is complex and determines the survival strategy of the organism (Lambers et al., 1981; van Ankeren and Wheeler, 1985; Roszak and Colwell, 1987).

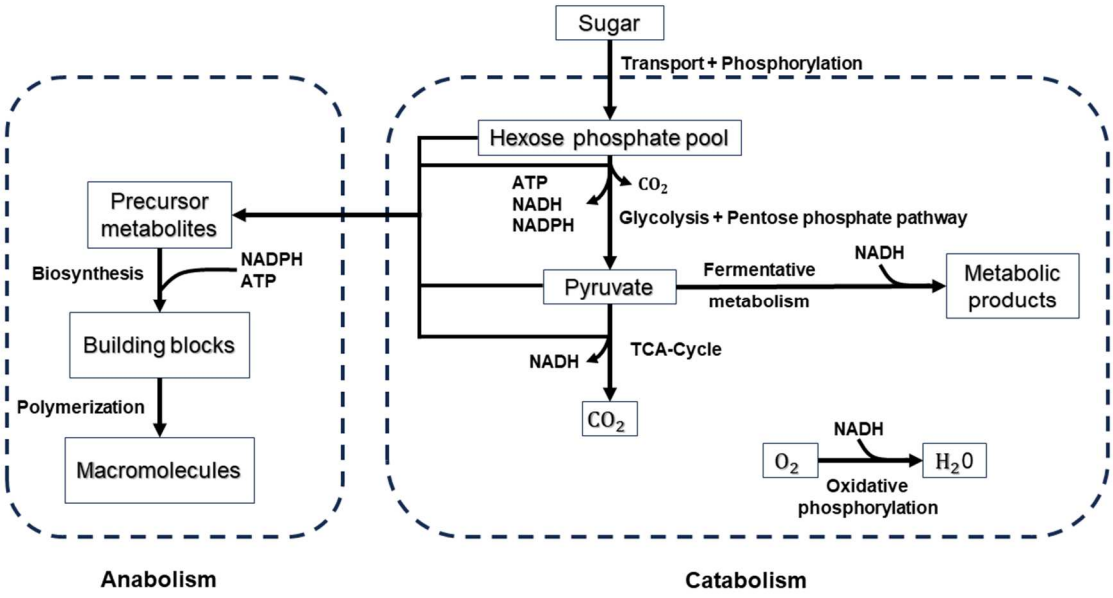

Figure 1: Simplified representation of the core metabolism. Reproduced from Stephanopoulos et al. (1998). Sugars are transported into the cell and enter the hexose phosphate pool. The hexose phosphates are utilized in the glycolysis and/or pentose phosphate pathway to be converted into pyruvate and/or other carbohydrates. Pyruvate can be further utilized to generate energy metabolites through the tricarboxylic acid cycle (TCA-Cycle) or can be used in the production of metabolic products through fermentative metabolism. Intermediates of the glycolysis, TCA-Cycle, and pyruvate can be used to synthesis building blocks. Ultimately, the building blocks can be used to build macromolecules for different cellular structures through polymerization.

The chosen metabolic strategy of an organism plays a determining role for its fitness and appearance (Fux et al., 2005) while the most important aspect of resource allocation form survival-critical processes. As multicellular organisms consist of diverse cell types with distinct functions, they show different patterns of metabolite assimilation (Lehninger et al., 2013). Furthermore, organisms have different behavior patterns depending on their developmental stage and this results in different metabolic patterns. For example, the primary objective of

juvenile organisms is growth, while adult organisms prioritize to maximize their metabolism towards reproduction (Sláma, 1964).

How resource allocation in multicellular organisms' works is to this day an active field of research (Goelzer and Fromion, 2017; Basan, 2018; Russo et al., 2022). The investigation of metabolism and resource allocation becomes crucial, as a compromised metabolism results in different diseases such as obesity, diabetes or organ failures (Baue, 1991; Lumeng and Saltiel, 2011). A better understanding of the metabolism potentially supports the treatment and cure of metabolism related diseases.

1.2. *Drosophila melanogaster*

Drosophila melanogaster, as a holometabolic insect, is a widely utilized model organism in scientific research for investigation of various questions, including those related to metabolism (Baker and Thummel, 2007). The popularity among scientist is explained by several reasons. The fly genome is completely sequenced (Adams et al., 2000), supporting intensive genomic analysis and characterization. Additionally, the fly allows studies of human diseases, as more than 75 % of human disease genes are conserved (Reiter et al., 2001; Chien et al., 2002). Many organs in *Drosophila melanogaster* have analogs in humans. For example, the fly’s oenocytes and fat body have similar functions to the human liver and white adipose tissue (Baker and Thummel, 2007; Li et al., 2019).

The development of *Drosophila* involves different stages. It begins with an embryonic stage, followed by three instar larval stages and ends with pupation, where metamorphosis results in the adult fly (Bate and Martinez Arias, 1993). Completing metamorphosis is the desired objective of the developing larva, which requires reaching the so-called critical weight threshold (Robertson, 1963; Shingleton et al., 2007). If this threshold is not reached, the larvae are not able to survive the metamorphosis. Larvae are able to adjust their developmental program to increase the chance to reach this threshold as larvae can prolong their developmental time under poor nutrient availability (Robertson, 1963). Therefore, the availability of resources has a direct impact on developmental timing, as low amounts of available resources prolong the overall developmental

time (Nunney, 1996). The precise mechanisms how the critical weight threshold function's is not fully understood (Mirth et al., 2005; Mirth and Shingleton, 2012).

The larval stages are especially well suited for the investigation of metabolism and resource allocation as larvae show a constant dietary intake (Aguila et al., 2007), which limits confounding effects of varying meal sizes and nutrient uptake. The larval movement is constant throughout the development (Troncoso et al., 1987) which allows to make assumptions about the energy drain over the course of the larval development. The aim of the larva is to maximize the amount of storage metabolites while growing as fast as possible (Aguila et al., 2007). This is due to the fact that the metamorphosis of larvae to pupae and the following emergence into adulthood is an energetically intensive process (Merkey et al., 2011). In addition to their use in metamorphosis, energy storage metabolites are important for the fertility of adult flies, as low energy storage of metabolites leads to reduced fertility (Robertson, 1963; Nunney, 1996). In contrast, equivalent findings are present in higher organisms such as humans. For example, malnourished men tend to have lower fertility (Sharma et al., 2013; Luque et al., 2017; Leisegang, 2019).

1.3. Microbiome

All higher organisms live in a symbiosis with a high number of different microorganisms, known as the microbiome. In some cases, the number of microorganisms inhabiting the host can be as high as the number of host cells, for example in humans (Sender et al., 2016). The human microbiome shows a high diversity, with studies revealing that it consists of 300 to 1000 different bacteria species (Claesson et al., 2009; Bäckhed, 2012). The microbiome is in many ways useful, as it can increase the nutrient availability (Krajmalnik-Brown, 2012), synthesize important metabolites for the host (Lin et al., 2017; Liu et al., 2020), or interact through secreted metabolites with the host's signaling pathways (Shin et al., 2011; Martin et al., 2019). Dysregulation of the microbiome can lead to various diseases, some of which can be severe. A dysregulated microbiome in humans can cause obesity (Turnbaugh and Gordon, 2009; Tilg and Kaser, 2011), inflammatory bowel disease (Halfvarson et al., 2017) and more. The microbiome

presents a field for research and therapeutic exploration, given its potential benefits, while a dysregulated microbiome can give rise to health issues.

The complexity of the mammalian microbiome, characterized by a broad spectrum of diverse microorganisms, is exceptionally high. Not all microorganisms within the microbiome can be cultured, further complicating the analytical process. Exploring the microbiome of simpler model organisms can help minimize these limitations. In the case of *Drosophila melanogaster*, its microbiome is relatively simple, comprising only 5 to 20 different species (Douglas, 2019; Ludington and Ja, 2020). The microbiome has also a substantial impact on the life quality for *Drosophila*. Laboratory-reared *Drosophila* are not necessarily reliant on the microbiome. Organisms lacking an active microbiome are referred to as axenic (Dougherty, 1959). Research indicates that axenic larvae are still able to fully develop, but the development is prolonged in comparison to non-axenic larva and under malnourishment axenic larvae are unable to survive (Brummel et al., 2004; Shin et al., 2011; Storelli et al., 2011; Ridley et al., 2012). Additionally, the microbiome impacts the expression of host genes, such as metabolism-related genes in *Drosophila* (Erkosar et al., 2014).

These insights reveal that the host-microbiome interactions play an important role in analyzing the metabolism of the host organism, the microorganisms in the microbiome, and their interactions within the microbiome and the host-microbiome system.

1.4. Growth media

The organisms' development is dependent on many different factors, such as the genetic background, its physiology, metabolism, and available resources. Among all factors, available resources are rated one of the most important. Under non laboratory conditions, organisms usually absorb nutrients of varying composition, quantity, and quality. The analysis of an organisms' metabolism and resource allocation depends on the composition of the available resources for digestion (Boggs, 1981).

To investigate the nutritional needs of organisms, three large groups of different growth media are used. First, complex media, where most of the ingredients are undefined (Dougherty, 1959; Jayme and Smith, 2000). Such media consist of complex nutrients, such as yeast (Piper et al., 2014). Studying an organisms metabolism with a complex medium presents challenges, as the majority of components are not fully characterized. This can lead to unknown side effects on the metabolism caused by unidentified ingredients. Second, one can use semi-defined media where nearly all ingredients are defined (Dougherty, 1959). Utilizing a semi-defined medium for metabolic analyses is suitable, as potential side effects caused by the ill-defined dietary components are less complicated to identify. Third, chemically defined media known as *holidic diets* can be used. These media consist of precisely defined elementary ingredients and quantities, making a *holidic diet* ideal for investigating an organisms metabolism and resource allocation. This is particularly valuable for techniques that heavily rely on the accuracy of the parameterized growth medium, such as *in silico* modeling. *Holidic diets* are often classified as a minimal medium, which offers all necessary ingredients for development at a sub-optimal growth rate.

Also for *Drosophila melanogaster* a chemically defined *holidic diet* could be identified (Piper et al., 2014; Piper et al., 2017). For the investigation of resource allocation, defining the amount of individual nutrients is a crucial point as the medium composition is determining the growth of the organism (Waldbauer and Friedman, 1991). Additionally, it offers the systematic alteration of the dietary composition to investigate the developmental impact through different metabolite concentrations. The *holidic diet* offers an excellent base for experimental setups that require the knowledge of the used growth medium for *in vitro* and *in silico* experiments alike.

However, even after changing the amounts of individual or combined *holidic diet* components, the natural growth rate could not be restored. Thus, semi-defined complex media are required to mimic the impact of dietary alterations on the global physiology and developmental timing. For *Drosophila*, a high sugar diet (HSD; Musselman et al., 2011) or low sugar diet (LSD; Millington et al., 2022), are often used. These semi-defined complex media represent extreme diets that are also present in human nutrition. High caloric diets, referred as western diets

(Hariharan et al., 2015), are consisting of food that has a high fat and/or sugar amount, similar to the HSD. Diets with a low amount of sugar are known to support the treatment of different diseases, such as cancer (Agarwal and Maurya, 2018). The understanding of the impact of high or low metabolite concentrations potentially opens ways to establish or support therapies for various diseases.

The microbiome investigation and their host-microbiome are also relying on knowledge of the growth medium (Sommer, 2015). With the use of a defined growth medium, it is possible to draw conclusions about the impact on the growth of the microbiome and the subsequent host-microbiome interactions. To understand the growth of the microbiome within the host, using the hosts growth medium, such as HD medium, is beneficial (Schönborn et al., 2021). Additionally, medium that is designed to optimize the growth of gut bacteria, such as *Acetobacter*-selective medium (ACE medium) for *Acetobacter* strains growth and *Lactobacillus*-promoting medium (MRS medium) for *Lactobacillus* strains (Blum et al., 2013), are beneficial.

It is evident that the choice of growth medium has a significant impact on the outcome of developmental experiments. The selected growth medium can influence the course of development, alter the metabolism of an organism and its microbiome, and determine its fitness.

1.5. Metabolic network

Metabolic networks formalize a set of metabolic processes to model isolated pathways, a single cell, tissue or even an entire organism. Constructing a metabolic network consists of incorporating biochemical reactions, their corresponding educts and products (the metabolites), the required enzymes, and the genes which encode them to model regulatory layers (Lacroix et al., 2008). The entire network is translated into a mathematical model that consists of stoichiometrically balanced biochemical reactions and their associated information (Orth et al., 2010b; Baart and Martens, 2012). This network forms a matrix ($\boldsymbol{S}$) where each row represents a metabolite, and the columns represent reactions (Orth et al., 2010b). The overarching goal is to solve this network by optimization of an objective function, which describes the target of the modeled

network. For many cases, formulating this objective function is a non-trivial task, as for example for a given organ or a complex organism such as an adult mouse due to the sheer number of degrees of freedom available and the varying environmental conditions. In the most intuitive representation, the objective function can be the maximization of biomass production, which is valid for many bacteria reared under constant nutritional conditions. In this case, the objective function equals the biomass function, which summarizes the relative metabolite amounts that are needed to build up mass (Orth et al., 2010b). Other objective functions, for example, used to identify the metabolic conditions needed to maximize the synthesis of a metabolite of interest (García Sánchez and Torres Sáez, 2014). To represent the flow of metabolites that can enter or leave the metabolic network, exchange reactions are used (Orth et al., 2010b).

Thiele and Palsson (2010) created a protocol how metabolic networks can be constructed. To create such a metabolic network a draft model of metabolic reactions is created through genome annotation data of the organism of interest available in biochemical databases. In the following, the draft model is further refined and manually curated. The resulting metabolic model is translated into the mathematical formulation with the addition of constraints, such as flux constrains on the underlying metabolic reactions. This metabolic model is further utilized for network verification, evaluation, and validation.

1.6. Flux Balance Analysis

Flux Balance Analysis (FBA) is an *in silico* method which utilizes metabolic networks in a steady-state (Savinell and Palsson, 1992; Varma and Palsson, 1994; Orth et al., 2010b; Orth et al., 2010a). FBA calculates metabolic fluxes through the metabolic network where all metabolic fluxes are in balance between metabolite formation and degradation.

FBA is formulated as the flux balance equation:

$$\frac{d\boldsymbol{X}}{dt} = \boldsymbol{S} * \boldsymbol{v} = 0 \tag{1}$$

where $\boldsymbol{X}$ is the metabolite concentration vector, t is the time, $\boldsymbol{S}$ is the stoichiometric matrix of the metabolic network and $\boldsymbol{v}$ is the reaction fluxes vector under steady-state conditions. This equation represents an under-determined linear equations system. In a steady-state situation, where metabolite concentrations remain constant, this implies that information of enzyme kinetics is not required for predictions of metabolic processes.

FBA places further restrictions on metabolic flows. Each reactions flux (v_i) is constrained by a flux range to work in a biologically reasonable range. This is defined by:

$$\alpha_i \leq v_i \leq \beta_i \tag{2}$$

where α_i and β_i are the lower and upper bound, respectively, of each flux v_i.

Different classes of reaction flux constraints can be used to narrow the solution space (Covert et al., 2003; Lee et al., 2006). First, the absorption of nutrients is limited by the physiology of the organism which imposes physiochemical constraints and limits the amount of absorption and excretion. Second, enzymes in cells or organisms have different quantities depending on their associated cell compartment that add spatial and topological constraints. Third, the growth medium determines the constitution and quantity of metabolites that are available to enter the organism or metabolic network. Fourth, thermodynamic constraints determine the reversibility of reactions, resulting in reactions having a defined direction within the context of the defined cellular environment.

The flux balance equation with the applied flux constraints forms an enclosed solution space from the nearly infinite available solutions. This solution space is called the null space that contains all possible flux distributions of the available phenotypes (Varma and Palsson, 1994).

Organisms or cells follow a wide range of biological objectives depending on the prevailing conditions and developmental stage. Typical objectives are, for example, growth, energy storage or use, or reproduction. In FBA, these biological objectives can be transformed into a mathematical formulation called the objective function. The objective function is defined as followed:

$$Z = \sum \boldsymbol{c^T} * \boldsymbol{v} \tag{3}$$

where Z represents the objective function, $\boldsymbol{c}$ is a vector of weights on the fluxes of the vector $\boldsymbol{v}$**.** The vector $\boldsymbol{c}$ determines which reactions are involved in the objective functions. This objective function is optimized to find the best solution from the feasible solution space by maximizing or minimizing it. The formulation of this optimization problem is:

$$Maximize\ or\ minimize: Z = \sum \boldsymbol{c^T} * \boldsymbol{v} \tag{4}$$

$$Subject\ to\ \boldsymbol{S} * \boldsymbol{v} = 0 \tag{5}$$

$$and\ \alpha_i \leq v_i \leq \beta_i \tag{6}$$

The solution is a flux distribution optimized for an objective function. This optimal solution can be achieved by different distributions of the metabolic fluxes.

FBA was used in many different investigations regarding an organisms metabolism. Organisms such as *Escherichia coli* (Ow et al., 2009) or *Saccharomyces cerevisiae* (Hjersted and Henson, 2006) were used to investigate growth by maximizing biomass production (Pramanik and Keasling, 1997; Knorr et al., 2007; Schuetz et al., 2007; Thiele and Palsson, 2010). Not only were investigations regarding growth performed, but also the synthesis of cellular structures (Ow et al., 2009), absorption of substrates (Pramanik and Keasling, 1997; Knorr et al., 2007), and the ATP production (Pramanik and Keasling, 1997; Knorr et al., 2007; Schuetz et al., 2007; Ow et al., 2009) in organisms were analyzed.

The formulation of an objective function depends on the knowledge about the targeted organism or cell type, its energy requirements, and the objectives that the organism pursues. By employing FBA, meaningful statements about the metabolism of organisms and cells can be obtained.

1.7. Aim of this thesis

The metabolism of an organism depends severely on the environmental conditions and the available resources. The fitness and phenotype of an organism is determined by the employed metabolic strategy (Fux et al., 2005). How the resource allocation of the available resources in a multicellular organism works is mostly unknown.

The goal of this study was to investigate and expand the knowledge about resource allocation of multicellular organisms. The following questions were raised:

What information is needed to develop a theoretical modeling framework to investigate the resource allocation of a multicellular organism?

Is the accuracy of *in silico* methods high enough to make meaningful statements about the metabolism and resource allocation of multicellular organisms?

What are the principles that the metabolism follows when distributing the resources? What impact does changing environmental conditions have on the metabolism?

Does the microbiome community of a host have a considerable influence among themselves and on the host's resource allocation?

Is the metabolism and therefore the resource allocation influenced by the physiology?

Is the resource allocation in multicellular organisms (Pareto-)optimal?

To address these questions, a combination of *in vivo* and *in silico* studies was performed using the larval stage of *Drosophila melanogaster* as a model system. Ultimately, this work aims to deepen the understanding of the metabolism and to reveal underlying principles of resource allocation in multicellular organisms.

2. Manuscripts

2.1. FlySilico: Flux balance modeling of *Drosophila* larval growth and resource allocation

Authors: Jürgen W. Schönborn, Lisa Jehrke, Tabea Mettler-Altmann, Mathias Beller

Contribution of Jürgen Wilhelm Schönborn:

- wrote the original draft; manuscript correction and proofreading
- designed the experiments/study
- designed figures 2, 3, 6, 7, 8, S1, S2 (B, C, D) and S3 - S9
- significant contribution to figures 1, 4 and 5
- reconstructed the metabolic network model
- parametrization of the metabolic network model
- performed the modeling experiments
- evaluated and analyzed the data

Schönborn, J. W., Jehrke, L., Mettler-Altmann, T., & Beller, M. (2019). FlySilico: Flux balance modeling of *Drosophila* larval growth and resource allocation. Scientific Reports, 9(1), 17156. Reproduced with permission from Springer Nature.

FlySilico: Flux balance modeling of *Drosophila* larval growth and resource allocation

Jürgen Wilhelm Schönborn[1,2$], Lisa Jehrke[1,2$], Tabea Mettler-Altmann[3], Mathias Beller*[1,2]

1 Institute for Mathematical Modeling of Biological Systems, Heinrich Heine University, Duesseldorf, Germany

2 Systems Biology of Lipid Metabolism, Heinrich Heine University, Duesseldorf, Germany

3 Institute of Plant Biochemistry & Cluster of Excellence on Plant Sciences, Heinrich Heine University, Duesseldorf, Germany

* Corresponding author: mathias.beller@hhu.de

$ equal contribution

Abstract

Organisms depend on a highly connected and regulated network of biochemical reactions fueling life sustaining and growth promoting functions. While details of this metabolic network are well established, knowledge of the superordinate regulatory design principles is limited. Here, we investigated by iterative wet lab and modeling experiments the resource allocation process during the larval development of *Drosophila melanogaster*. We chose this system, as survival of the animals depends on the successful allocation of their available resources to the conflicting processes of growth and storage metabolite deposition. First, we generated “FlySilico”, a curated metabolic network of *Drosophila*, and performed time-resolved growth and metabolite measurements with larvae raised on a *Holidic diet*. Subsequently, we performed flux balance analysis simulations and tested the predictive power of our model by simulating the impact of diet alterations on growth and metabolism. Our predictions correctly identified the essential amino acids as growth limiting factor, and metabolic flux differences in agreement with our experimental data. Thus, we present a framework to study important questions of resource allocation in a multicellular organism including process priorization and optimality principles.

Introduction

Balancing limited resources to concurrent processes is an essential task in all areas of life. Every organism, for example, needs to allocate its available resources – mostly in the form of diet-derived nutrients – to concurrent processes such as live sustaining functions, reproduction, or storage metabolite synthesis. While the metabolic pathways involved in these processes, as well as some regulatory signaling pathways, are well established, the overarching design principles governing resource allocation and prioritization are elusive (Dmitriew, 2011; Davison et al., 2014). This is especially true for multicellular heterotrophic organisms, which often have an almost unlimited amount of destinations for channeling their available resources. On top of a plethora of energy consuming processes available to the whole organism (physical movement, growth and reproduction, energy storage metabolite deposition), higher order multicellular organisms are composed of a multitude of organs. This results in an even higher complexity, given that many organs have distinct and different metabolic preferences, which is important during health and disease states (Hood and Terjung, 1990; Votruba and Jensen, 2007; Dashty, 2013). The mammalian brain, for example, depends on sugars for energy production, whereas most other body cells can additionally utilize other energy liberating pathways such as fatty acid beta-oxidation. To this end, a bottom-up understanding of the resource allocation regulation therefore appears close-to impossible based on this complexity and lack of detailed information. Thus, an abstraction in the form of a top-down modeling paradigm has the potential to reveal design principles, which serve as a starting point to investigate resource allocation principles. Yet, the various degrees of freedom available to complex organisms complicate the modeling procedures, as model solving usually targets the optimization (maximizing or minimizing) of a distinct objective function such as e.g. biomass production or growth (Feist and Palsson, 2010). Given that multicellular organisms can have multiple and often conflicting objective functions (e.g. reproduction, longevity), or objective functions without the aim of maximization or minimization (e.g. metabolic processes to sustain survival, growth in terms of sustaining healthy cell turnover, deposition of energy depots), the identification of a single and clear-cut objective function is difficult.

Development, however, appears to represent an exception. The development of most organisms follows a stereotyped program, which involves hard constraints e.g. in terms of the timing or metabolic thresholds. Holometabolous insects, for instance, need to deposit sufficient energy storage amounts to allow metamorphosis into an adult organism, which is often associated with a minimal weight, which is also termed critical weight in insects such as *Drosophila melanogaster* (Moed et al., 1999). Given the variations many organisms face during development – based on e.g. fluctuation in temperature or food supply and quality – developmental programs are at the same time also flexible (Fig. 1A,B).

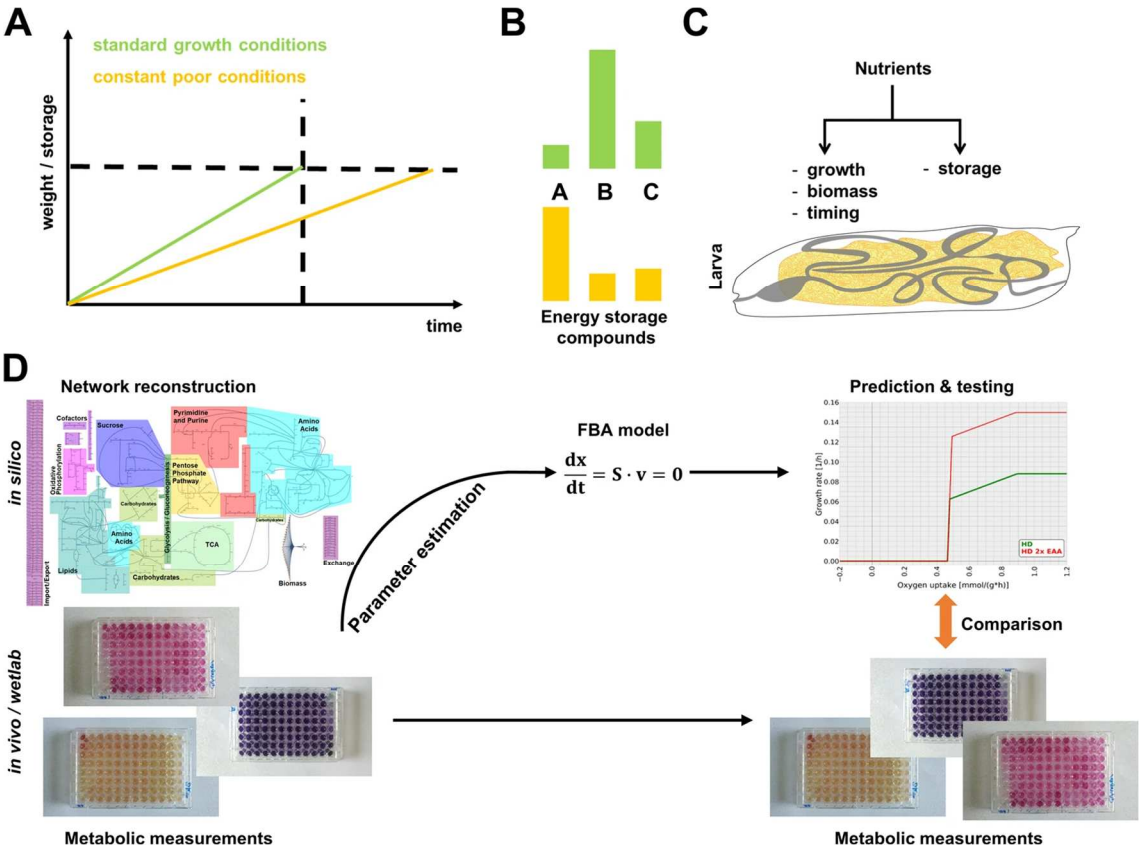

Figure 1: Plasticity of resource allocation and experimental design of the study. (A) Development involves growth and weight gain (in part due to the deposition of storage metabolites) over time. Altered environmental conditions, such as a rich (green) or poor (orange) nutrition results in an altered timing and/or (B) altered energy storage compound levels (compounds A–C show a different relative abundance under rich (green) and poor (orange) nutritional conditions). (C) Nutrients fuel conflicting processes. *Drosophila* larvae need to channel available nutrients to sustain either growth or the formation of storage metabolites. Following nutrient uptake in the gut (shown in grey) copious amounts of triglyceride and glycogen stores are built in the fat body (yellow), which largely fills the body cavity of developing larvae. (D) Our experimental design involved *in silico* and *in vivo* (wet lab) experiments. For the *in silico* studies, we first reconstructed main parts of the *Drosophila* metabolic network. For the parameter estimation, we performed metabolic profiling experiments during the *Drosophila* larval development. Subsequently, the metabolic network served the constraint-based flux balance modeling (FBA). With the FBA models, we predicted the consequences of alterations of the dietary composition and validated the modeling results using targeted experiments. High resolution versions of the metabolic network shown in (D) are provided in Fig. 2 as well as an interactive version of the metabolic network as supplemental data.

The time needed to reach a certain weight or storage threshold necessary to complete development thus can be extended under poor nutritional conditions, for example (Fig. 1A). Besides adjusting the developmental timing, organisms can also alter the relative amounts of their energy storage compounds (Fig. 1B). Thus, development of multicellular organisms should be accessible to modeling campaigns, as there is a clear-cut objective function (growth) and sufficient plasticity (timing and metabolic fine-tuning) to test modeling predictions. A better knowledge of the resource allocation principles potentially answers the question whether the developmental growth and resource allocation are in multicellular organisms also (pareto-)optimal. A pareto-optimality was previously reported for bacterial growth and metabolism (Schuetz et al., 2012). Pareto-optimality was also proposed for certain phenotypic traits of multicellular organisms (Shoval et al., 2012; Szekely et al., 2015), yet this is still under discussion (Edelaar, 2013; Shoval et al., 2013).

Here, we use the larval development of *Drosophila melanogaster* as a model system for the analysis of the resource allocation of a multicellular organism using *in silico* and wet lab experiments (Fig. 1C,D). This system is particularly well suited for this endeavor based on the following key-points: (i) Larval development of *Drosophila* involves a massive increase in size and weight coupled to the deposition of copious energy stores necessary to fuel metamorphosis (Fig. 1C) (Merkey et al., 2011). In order to allow this massive size increase, larvae are constantly eating (Zinke et al., 1999), which facilitates the estimation of energy expenditure and metabolite intake. (ii) *Drosophila* larval development and resource allocation shows an inherent plasticity. Poor nutritional conditions, for example, result in a prolonged developmental timing based on a lowered rate of development (Fig. 1A) (Beadle et al., 1938). This change of developmental timing is often paralleled by an altered metabolite composition of the organism (Levin, 2006; Vijendravarma et al., 2012; Koyama et al., 2014; Martínez et al., 2014). Intriguingly, also e.g. mammals adapt their metabolism to in utero nutritional alterations (Gluckman et al., 2007) and the impact of the nutritional status during development and early life on the later stages is well described in terms of the life history theory (Kuzawa, 2007; Aktipis et al., 2013) and the process of metabolic programming (Bischoff et al., 2018; Limones et al., 2019; Tarry-Adkins et al.,

2019). (iii) For the modeling procedures, we benefitted from a previously published chemically defined, fully synthetic minimal *Drosophila* food (*Holidic diet*; HD) (Piper et al., 2014), which allowed us to clearly define the input of our model. On top of the general advantages of working with small animals, such as the large number of progeny and accessibility of the developmental stages, these characteristics clearly facilitated our investigations.

To target resource allocation in *Drosophila* larval development, we generated the – to the best of our knowledge – to date largest curated metabolic network for fruit flies and subjected it to flux balance analyses. To validate and optimize our metabolic network, we used targeted metabolite quantifications and GC-coupled mass spectrometry metabolomics measurements of larvae grown on the HD. We built the model capturing previously known requirements of *Drosophila* metabolism, such as sterol auxotrophy (Carvalho et al., 2010), and tailored it to incorporate all prominent ingredients of the HD. Our model predictions allowed us to correctly identify the amount of essential amino acids as growth limiting factor. Further, the model predictions resulted in flux differences, which are in line with the measured metabolite alterations associated with growth of the larvae in food with elevated amounts of sucrose or essential amino acids. These proof-of-principle experiments provide a starting point to investigate the optimality principles of multicellular resource allocation.

Results

Drosophila metabolic network reconstruction

In order to model *Drosophila* larval growth and resource allocation, we first constructed a flux balance capable metabolic network covering the biochemical pathways necessary to metabolize the major constituents of the minimal, synthetic medium (*Holidic diet*; HD) (Piper et al., 2014), which we used to grow the fruit flies during the wet lab procedures. On top of the central carbon metabolism, we therefore included e.g. amino acid, lipid, and carbohydrate metabolism (Fig. 2, Table S1, and Interactive Supplementary Fig. 1).

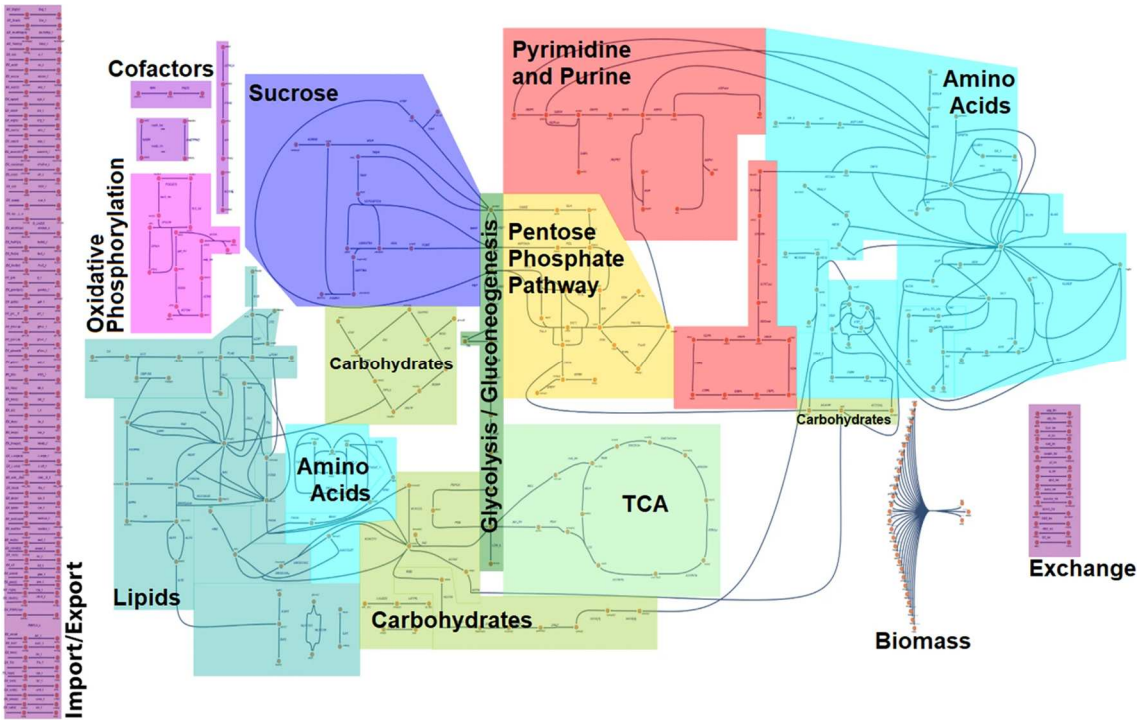

Figure 2: Map of the FlySilico V1.0 metabolic model of *Drosophila melanogaster*. On top of the central carbon metabolism, we included reaction complexes such as the lipid or amino acid metabolic pathways. A main goal was to include the pathways necessary for metabolizing the main constituents of the *Holidic diet* and the pathways covering our experimentally quantified metabolites. For details, please see main text, Table S1 and Interactive Supplementary Fig. 1.

In total, our model – termed FlySilico – covers 363 reactions and 293 metabolites. To date, there are surprisingly only two other *Drosophila* metabolic networks available. The first one focuses on the effects of hypoxia on ATP production (Feala et al., 2007; Coquin et al., 2008; Feala et al., 2009). The other one is a whole-genome computer generated model, which lacks curation (BMID000000141998; https://www.ebi.ac.uk/biomodels-main/BMID000000141998).

For our model reconstruction, we started from scratch and emphasized on avoiding biologically unfeasible reactions (dead-end, blocked, and unbalanced reactions) as well as on minimizing the number of exchange reactions (see methods section). Figure 3 shows a comparison between different aspects of our FlySilico and a selection of previously published other FBA-models of different organisms including the whole genome *Drosophila* model.

Organism	Model ID	# Reactions	# Metabolites	% dead-end reactions	% blocked reactions	% unbalanced reactions	% exchange reactions
E. coli	e_coli_core	95	72	0	0	1.1	21.1
D. melanogaster	FlySilico_v1	363	293	2.5	3.6	0.6	17.6
S. cerevisiae	iMM904	1577	1226	13.5	35.6	3.2	10.4
E. coli	iWFL_1372	2782	1973	9.5	13.8	1.4	14.1
Mouse	iMM1415	3726	2775	13.9	21.3*	0	12.2
Human	RECON1	3741	2766	11.6	34.1*	1.5	11.5
D. melanogaster	BMID000000141998	6198	2873	0.2	0.2*	6.6	46.2

Figure 3: Comparison of FlySilico V1.0 to other publically available metabolic networks. Dead-end reactions result in the production of metabolites, which are not further utilized in the network. Blocked-reactions are not accessible during the solving of the network. Unbalanced reactions are violating the conservation of mass and/or charge. Exchange reactions represent either biologically necessary transporters (such as for the import of nutrients into the system, or naturally occurring transporters for the export of end products), or transport reactions necessary for the modeling, to e.g. eliminate metabolites which are not further processed as the necessary biochemical reactions were omitted from the model. The values marked by an asterisk were calculated using non-loopless conditions. All other values are determined using loopless computations.

While of course still limited in size, our model has a low amount of biologically unfeasible reactions. The importance of this became evident when we performed simulations with the whole genome, *in silico* generated *Drosophila* metabolic network. Here, simulations resulted in a positive Biomass production (Fig. S1) even without any inputs entering the model; i.e. that this model allows perpetual motion. For FlySilico, we did not detect such an artificial and erroneous behavior (data not shown).

Development of a *Drosophila* biomass function based on experimental data

Given our aim to investigate growth and resource allocation, we established the parameters of our model by incorporating experimental data. For this, we grew wildtype Oregon-R *Drosophila* animals on the HD. The complete larval development (until prepupae emerge) appears quasi linear and takes on the HD about 170 hours. In order to follow the development and metabolite profile over time, we collected larvae at three equally spaced time points during development (96, 132 and 168 hours after egg laying; AEL). To determine growth progression over time, we measured the wet and dry weight (Fig. 4A) as well as different size parameters (Fig. S2) of the larvae at the different time points.

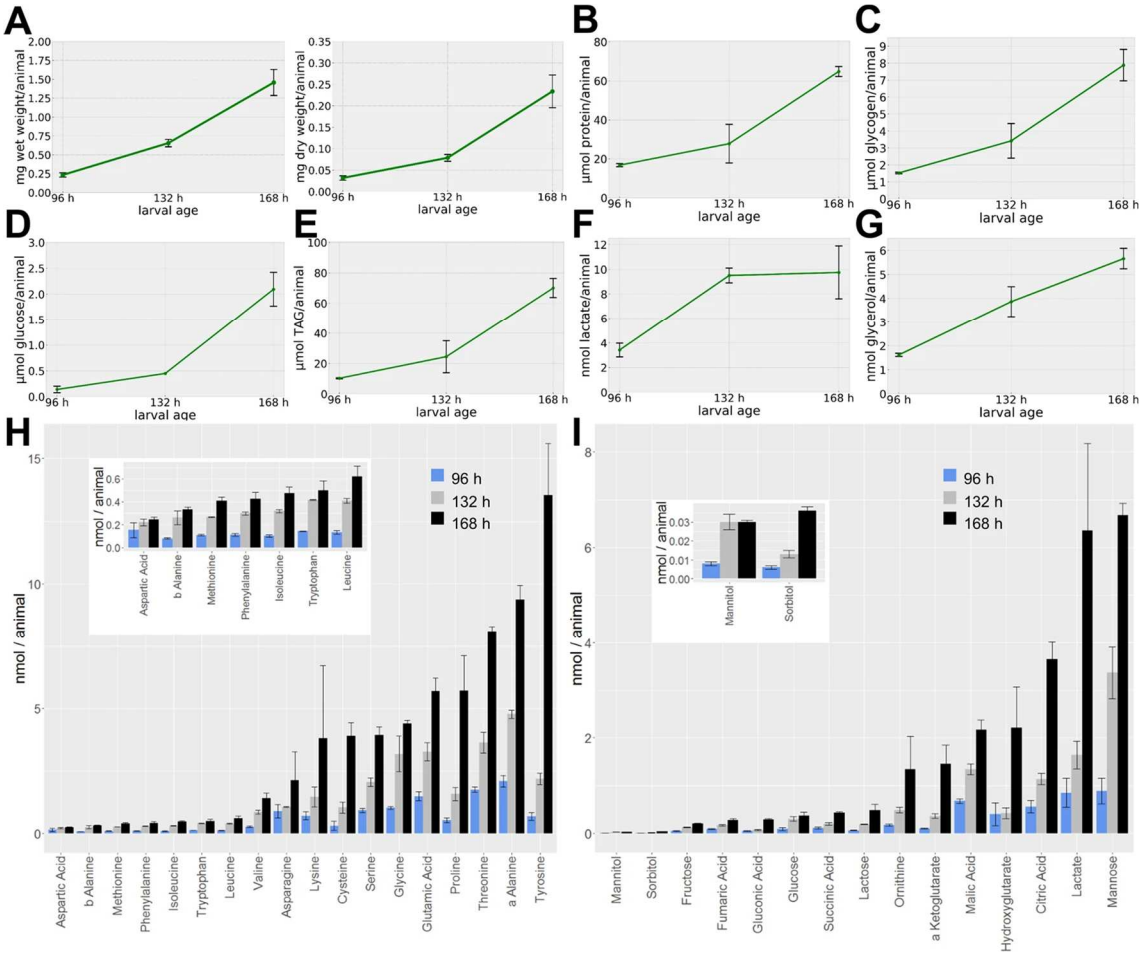

Figure 4: Growth and metabolic profiling of the larval developmental of *Drosophila melanogaster* 96, 132, and 168 hours after egg laying. (A) Wet weight (left plot) and dry weight (right plot) measurements of larvae at the indicated developmental time points. (B–G) Absolute quantification of protein, glycogen, glucose, triglyceride (TAG), lactate, and glycerol levels. The data represent mean values ± standard deviation normalized to the amount of animals per sample of at least triplicate measurements. (H,I) GC-MS metabolomics measurements of proteinogenic amino acids (H) and different metabolites (I) of *Drosophila* larval extracts from the indicated time points. Insets in (H,I) provide a zoom-in view on the low-abundant metabolite data. Metabolites were quantified using five point calibration curves (see methods, Fig. S3, and Table S2) and sorted for increasing abundance during the 168 hours time point.

Larval weight increased almost linear over time (Fig. 4A). The water content was stable with values between 85 and 89 % (Fig. 5A) and unaffected by alterations of the food composition (data not shown).

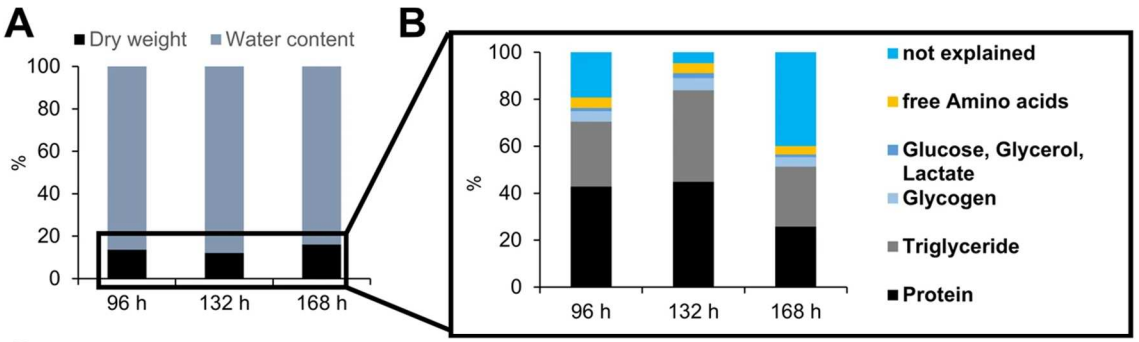

C **BIOMASS:**

0.22812057 ala + 0.07253130 arg + 0.08889074 asn + 0.09052444 asp + 59.276 atp + 0.00326199 clr + 0.05497961 cys + 0.03341084 glc-D + 0.08582346 gln-L + 0.12450671 glu-L + 0.20685442 gly + 0.02221020 glycerol + 0.24597306 glycogen + 59.276 h2o + 0.03930321 his + 0.08637180 ile + 0.06077100 lac-L + 0.15631814 leu + 0.10210655 lys + 0.03615874 met + 0.04767442 phe + 0.14173310 pro + 0.20435090 ser + 0.27972171 TAG + 0.14520307 thr + 0.01216300 trp + 0.09935594 tyr + 0.12118853 val ➔ 59.276 adp + 58.7 h + 59.305 pi

Figure 5: *Drosophila* body composition and biomass function. (A) Water content of *Drosophila* larvae raised on the HD during the three investigated time points. The black part of the stacked bar plots shows the dry mass of the larvae. (B) Our combined targeted and GC-MS metabolite measurements explain on average about 79 % of the dry mass. Triglycerides and protein are the main contributors to dry mass. (C) *Drosophila melanogaster* biomass function based on our experimental data and literature. Green values indicate indices based on the GC-MS measurements and on the absolute biochemical metabolite quantifications, blue indices are based on the absolute biochemical metabolite quantifications. Red indices are based on information from the yeast whole-genome FBA model iMM904 (Mo et al., 2009).

For all time points, we performed absolute quantifications of free protein, glycogen, glucose, triacylglycerol (TAG), lactate, and glycerol (Fig. 4B–G) levels according to established protocols (Jehrke et al., 2018) (see Table S2). Further, we quantified various metabolites of the central carbon metabolism as well as free amino acids by GC-MS metabolomics measurements and external standard curves (Figs 4H,I, S3 and Table S2). Most per animal normalized measurements increased over time, as expected (Fig. 4). Only lactate levels reached a plateau after 132 hours of development. All in all, our measurements explained on average 79 % (for 96 h AEL: ~81 %, for 132 h AEL: ~96 % and for 168 h AEL: ~60 %) of the total dry weight with proteins and TAGs being the major contributors (Fig. 5B). Of course, we can not rule out that the larval midgut contained metabolites from the HD, which we also included in our measurements. Yet, while none of our targeted metabolite measurements covered compounds present in the HD, those represented the most abundant constituents of the larval biomass. The metabolites quantified by the GC-MS metabolomics strategy – which covered also metabolites present in the HD as e.g. the singular amino acids – were only present in minute amounts. Thus, our measurements covered a large

part of the body composition and should provide a sufficient approximation to model larval growth.

In order to perform growth rate simulations, we formulated a biomass function based on the previously reported yeast biomass function of the model iMM904 (Mo et al., 2009). Yet, from the original yeast biomass function, we only utilized the value for the growth associated maintenance (GAM) costs, as this measure is difficult if not impossible to obtain for a multicellular organism. The other coefficients of the biomass function are based on our own measurements (Fig. 5C and methods section). Next, we used the HD food ingredients as constraints for the model solution procedure. Although we already knew the exact composition of the food, we still needed to approximate the amount of food consumed by a single larva over time. Given that the measurement of the amount of internalized solid food is difficult, we decided to follow a theoretical approach (for details see methods section). For this purpose, we used data available for the average number of mouth hook movements ("bites") per minute of larvae. The bites per minute only show low variability across different food compositions (Musselman et al., 2011; Ryuda et al., 2011), suggesting that this assumption is reasonable. Further, we approximated the volume of the mouth of the larva based on previous (Alpatov, 1929) and own measurements (Fig. S2; approximated volume of the mouth = 0.011 mm^3). Calculations based on both parameters resulted in an amount of 0.064 g/h food consumed per hour. We used this approximated food intake amount to calculate for each food ingredient the maximum amount consumed per hour. Of course, the calculated amount of consumed food is likely a prominent overestimation. For example, the larvae will most likely not fill their mouth completely with every bite. Further, not all food ingredients passage the gut barrier with 100 % efficiency and at this point, we do not know the resorption rate for the different nutrients. Thus, we sought to identify a correction factor to limit the nutrient influxes to a reasonable level. For this purpose, we solved the FBA-model with a wide range of diminishing correction factors (Fig. S4) and compared the resulting calculated growth rates with our experimentally determined growth rate of approximately 8.8 % dry weight increase per hour (see methods section). In this way, we identified a correction factor of the calculated food and thus nutritional uptake of about 12.2 %. So far,

little data concerning the food conversion and uptake rates of insects are available. Yet, Waldbauer et al. measured the efficiency of conversion of ingested food to body substance for various Lepidoptera species and found conversion rates ranging from 2 to 38 % (Waldbauer, 1968). Our theory-derived value of 12.2 % thus is in the range of the experimentally determined values of other insects.

Model verification

The first step in our model verification procedure was to test whether it operates in a reasonable manner and whether it recapitulates known behaviors of the fly system, in contrast to e.g. the computer-generated model mentioned above. *Drosophila*, for example, is sterol auxotroph (Carvalho et al., 2010). We built our model to recapitulate this behavior and indeed a steep increase in the growth rate for positive, non-zero sterol uptake rates is visible (Fig. 6A). In contrast, the amount of the non-essential amino acid aspartic acid had no effect on the growth rate, as expected (Fig. 6B).

As a next step, we performed more complex simulations. First, we investigated growth in response to varying oxygen levels. Here, a certain minimal oxygen influx was needed to support suboptimal growth before increasing oxygen levels resulted in a plateau of the growth rate (Fig. 6C). As a test for the predictive power of our system, we decided to test next whether we could predict the impact of diet alterations on the growth and metabolism. While a reduction of certain nutrients would have been possible, we decided to rather test for a possible limitation of certain nutrients given that the growth of the larvae was on the HD much slower as compared to a complex and rich diet. Based on the growth properties of the animals, the HD in fact is classified as a minimal medium, which was designed to mirror dietary restriction characteristics (Piper et al., 2014). Thus, we increased either the amount of dietary sugar or essential amino acids that was possible to enter the model. A doubling of the sucrose input limit had no effect on the calculated growth rate (Fig. 6C). However, when we doubled the amount of essential amino acids (EAA) potentially entering the system, the predicted growth rate prominently increased (Fig. 6D). We subsequently tested our modeling predictions by performing corresponding experiments. Larvae reared on a HD

containing the double amount of sucrose (“2x sucrose food”) indeed did not show an increased growth-associated weight gain as compared to larvae raised on the standard HD (Fig. 6E). Protein levels were even lower than the ones of the control animals at the middle time point (Fig. 6F). Doubling the amount of EAA (“2x EAA food”), however, indeed resulted in a higher growth rate (Fig. 6E) as well as higher amounts of protein (Fig. 6F). Thus, our modeling data are consistent with the experimental results, which suggests a high predictive power of the model.

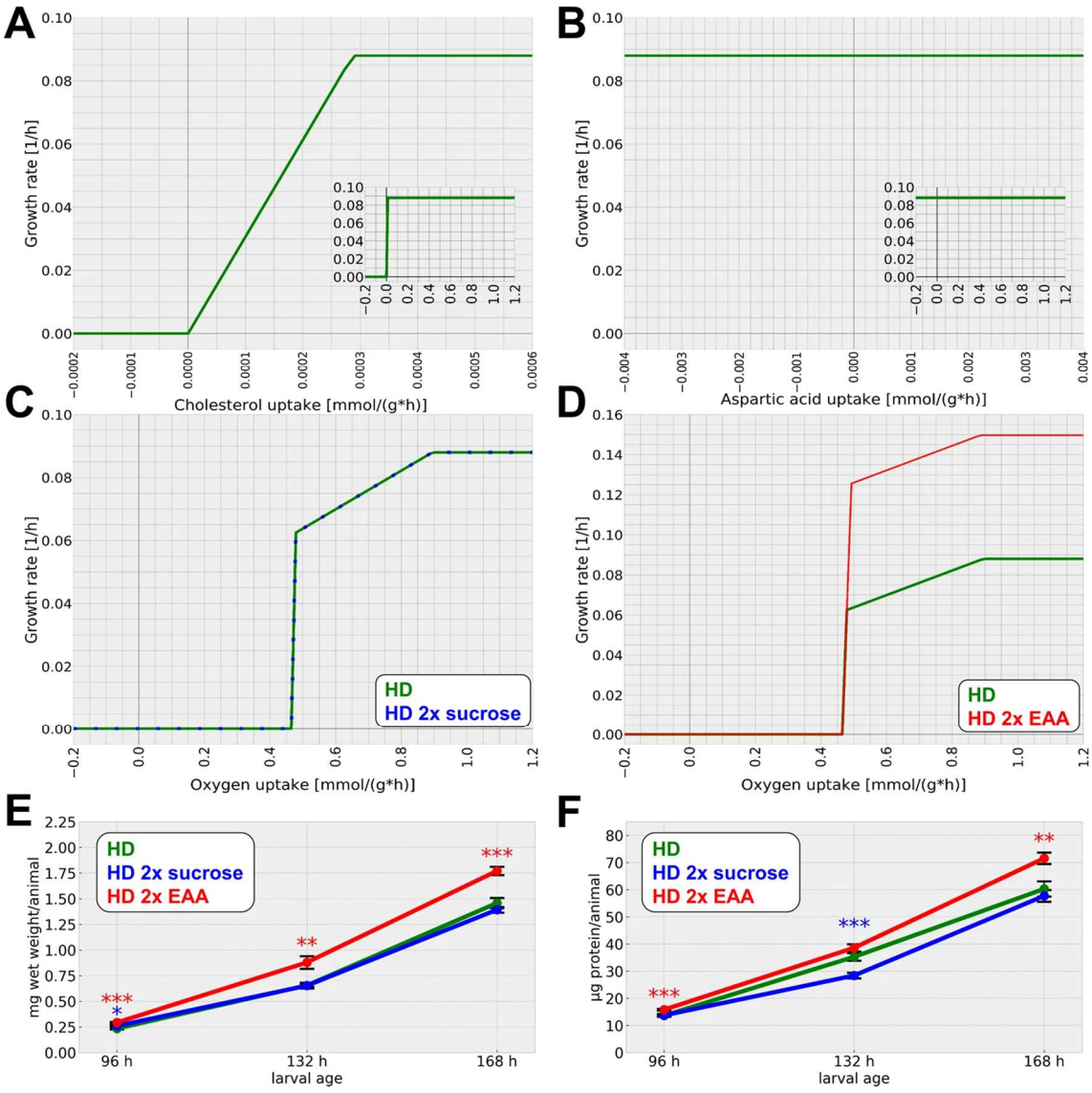

Figure 6: Model verification, predicted growth and comparison to real life. (A–D) Modeled growth rate in response to different input parameter variations. Negative uptake rates correspond to an excretion. (A) A certain level of cholesterol is needed for optimal growth while less result in a suboptimal growth phase. The zoom-in represents a larger cholesterol uptake flux range. (B) Levels of the non-essential aspartic amino acid do not affect biomass production. The zoom-in represents a larger aspartic acid uptake flux range. (C) Oxygen levels need to surpass a threshold to allow biomass production. In the following, the biomass production increases until it reaches a plateau. Increased sucrose levels (blue color) do not alter biomass production as compared to the standard HD (green color). (D) A doubling of the amount of essential amino acids (EAA) increases the biomass production (red color) as compared to the standard HD (green color). (E,F) Experimental testing of our model-based predictions. Animals were either reared on HD (green), HD

containing the double amount of sucrose (blue) or the double amount of EAA (red). The wet weight (E) and protein (F) content of the larvae was measured 96, 132, and 168 hours after egg laying. While the altered sugar content did not affect the growth rate, the addition of more EAA resulted in a higher growth rate (E). The protein measurements show similar results (F). Measurements in (E,F) represent the mean values of three biologically independent experiments. Each experiment consisted of quadruplicate samples. Whiskers represent the standard error of the mean (SEM). Please note that the wet weight data for the HD is identical with the one shown in Fig. 4A. Statistical significance was tested by an unpaired two-sample T-Test for each time point. Significance levels are: *p < 0.05, **p < 0.01, ***p < 0.001.

Modeling resource allocation

As a next step, we investigated whether the model could recapitulate resource allocation differences driven by the increase of sucrose or EAA in the HD. Therefore, we performed a flux variability analysis for our model with the given elevated maximum input limits (Table S3). Subsequently, we percent normalized the maximum and minimum flux values obtained for the 2x sucrose or 2x EAA food, respectively, based on the flux variability values of the standard HD (Table S4). Further, we split the metabolic reactions into functional groups and plotted selected reactions with altered fluxes (Fig. 7).

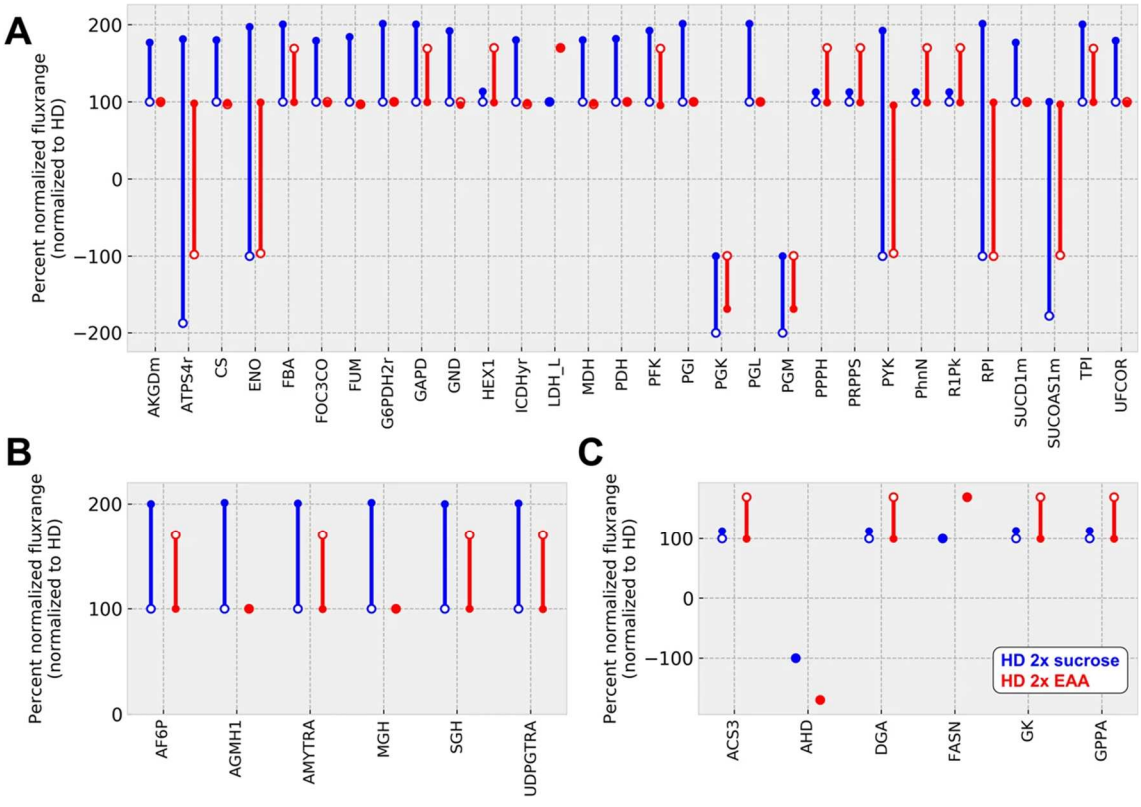

Figure 7: Modeling *Drosophila* larval resource allocation. The figure shows the results of the percent normalized flux variability analysis results for the simulations based on the HD with 2x sucrose (blue) and HD with 2x EAA (red), respectively. In brief, we percent normalized the values of the minimal (open circles) and maximal (filled circles) fluxes on the basis of the results for the standard HD. The sign of the flux percentage indicates the reaction direction, where a positive sign indicates the forward reaction, a negative sign indicates the backwards reaction and values spanning both signs represent reversible reactions. (A) Barplot of the central carbon metabolism flux change of the model solutions for the comparisons HD and HD with 2x sucrose (blue) or HD and HD with 2x EAA (red), respectively. (B) Flux change for the sucrose

metabolism (description as in (A)). (C) Flux change for the lipid metabolism (description as in (A)). Each reaction description can be found in Table S1. Flux variability analysis results are given in Table S3 and the normalized flux data are presented in Table S4.

On the simulated 2x sucrose diet, most reactions of the central carbon metabolism (Fig. 7A) showed a prominently increased maximum flux rate (e.g. FBA = fructose-bisphosphate aldolase, GAPD = glyceraldehye-3-P dehydrogenase, PFK = phosphofructokinase, PGI = glucose-6-P isomerase). On the simulated 2x EAA diet, however, most maximum flux rates did not change, and only the lower flux rate bounds were increased, thus resulting in a more narrow range of possible flux variations (Fig. 7A). For few reactions, the diet alterations resulted in opposite flux changes (HEX1 = hexokinase 1, LDH_L = l-lactate dehydrogenase, PPPH = diphosphate phosphohydrolase, PRPPS = ribose-phosphate diphosphokinase, PhnN = ribose 1,5-bisphosphate phosphokinase, R1Pk = Ribose 1-phosphokinase). The diphosphate phosphohydrolase (PPPH) flux showed a largely increased minimal flux on the simulated 2x EAA diet (Fig. 7A). Diphosphate phosphohydrolase activity takes place very early in the lipid degradation, as it acts as the force to activate fatty acids for the beta-oxidation (Carman and Han, 2006). The higher minimal flux following the elevated EAA input, suggested an enhanced rate of lipid activation, which potentially fuels the elevated growth. Further, the increased flux of the lactate dehydrogenase suggested increased lactate levels of animals reared on the diet with 2x EAA.

As expected, fluxes of reactions involved in sucrose metabolism (AF6P = ATP:D-fructose 6-phosphotransferase, AGMH1 = 1,4-alpha-D-Glucan maltohydrolase AMYTRA = 1,4-alpha-D-Glucan:1,4-alpha-D-glucan 6-alpha-D-(1,4-alpha-D-glucano)-transferase, MGH = maltose glucohydrolase SGH = sucrose glucohydrolase, UDPGTRA = UDP-glucose:glycogen 4-alpha-D-glucosyltransferase) increased prominently if the sucrose input was increased (Fig. 7B). The simulation of elevated EAA levels resulted in increased minimal fluxes of enzymes involved in lipid metabolism (ACS3 = acyl coenzyme A synthetase, DGA = 1,2-diacylglycerol acyltransferase, GK = glycerol kinase, GPPA = alpha-glycerophosphate acyltransferase), as well as situations where both the lower and upper flux limits were elevated (FASN = fatty-acid synthase), which suggest elevated lipid storage levels as a result (Fig. 7C).

When we performed corresponding metabolite measurements with animals raised under the different growth conditions, TAG levels indeed showed a modest, but significant, increase following growth on the 2x EAA diet (Fig. 8A).

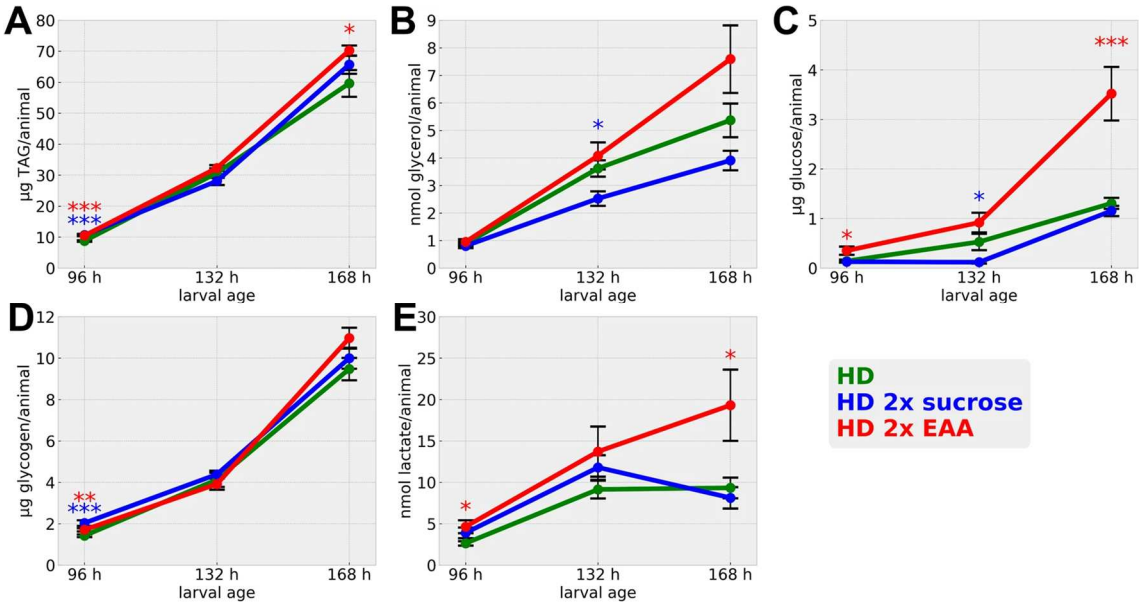

Figure 8: Metabolic profiling of the larval developmental of *Drosophila melanogaster* 96, 132, and 168 hours after egg laying. (A–E) Absolute quantification of triglyceride (TAG), glycerol, glucose, glycogen, and lactate levels. Measurements in (A–E) represent the mean values of three biologically independent experiments. Each experiment consisted of quadruplicate samples. Whiskers represent the standard error of the mean (SEM). Statistical significance was tested by an unpaired two-sample T-Test for each time point. Significance levels are: *p < 0.05, **p < 0.01, ***p < 0.001.

Free glycerol levels showed a larger amount of variation (Fig. 8B). Yet, the trends clearly differed in response to the varying diet compositions. Increased dietary sugar levels resulted in lower levels of free glycerol, whereas increased amounts of EAA resulted in an on average increased free glycerol levels indicative of elevated lipolytic and/or lipogenic activity. Intuitively, we expected an altered sugar content of the animals raised on the 2x sucrose diet. Yet, we did not detect any prominent differences (Fig. 8C), which seems to be in line with the modeling results, which indicate a larger flux of the glycolysis reactions with a simultaneous activation of the complete TCA cycle or the reactions involved in oxidative phosphorylation (Fig. 7A). This increase of flux values suggest that the metabolism of *Drosophila* activates a metabolic program for an overflow metabolism perhaps associated with a larger burning or excretion of sugars. The 2x EAA diet, however, resulted in a significantly higher glucose content of the animals (Fig. 8C), which appears to be in line as the higher flux rate of diphosphate phosphohydrolase or fatty-acid synthase suggest a higher beta-

oxidation besides an increased lipid storage predicted by the model. Glycogen levels were mostly unaffected by the altered nutritional conditions (Fig. 8D). Lactate showed under basal HD growth conditions a plateau 132 hours after egg laying (Figs 4F, 8E). If additional sucrose was present, lactate levels even decreased 132 hours after egg laying (Fig. 8E). The 2x EAA diet yet resulted in statistically increased lactate levels (Fig. 8E), which again is in line with our modeling results, which suggested an increased lactate dehydrogenase flux (Fig. 7A). Thus, we also could largely align our modeled flux values with the corresponding experimental data.

Discussion

Flux balance analyses (FBA) with metabolic networks of heterotrophic multicellular organisms usually appears complicated due to the difficulty of identifying a clear-cut objective function. Further, the various cell types of complex organisms, with their signature gene expression profiles and distinct metabolic and functional tasks, complicate modeling approaches even more. To tackle these difficulties, methods and strategies were designed (Martins Conde, Patricia do Rosario et al., 2016), as for example, to model the metabolic flow in the context of gene regulation or other advanced constraints such as dynamic changes. Here, we decided to use a top-down modeling approach focusing on a generalized and averaged simple model of the growing larva, which we identified as a suitable system for FBA given its clear-cut objective function. We used this simplified model given that many details of the overall organismic physiology are still unclear. Therefore, we rationalized that adding uncertain information might rather act detrimental as compared to a simplified model, which could better catch the more general schemes. A benefit from starting our model mostly from scratch was that we could pay special attention on avoiding dead-end and blocked-reactions (Fig. 3), as well as to assure the biological feasibility of the subsequent FBA modeling results. Our resulting model is to the best of our knowledge the currently most advanced metabolic network of *Drosophila* metabolism and we provide it together with the code to perform FBA analyses in different ready-to-use formats to the community (see methods section). Our initial rationale that a

simple model might be already useful appears valid, given that it is already able to recapitulate basic biology (Fig. 6) and successfully predicted the impact of dietary alterations on the larval growth and metabolism (Figs 6–8). In the future, the refinement of the model by e.g. incorporating gene regulation or a dynamic modeling (Martins Conde, Patricia do Rosario et al., 2016), potentially further enhances the predictive power of the model. While these enhancements will be likely less important for the modeling of a general behavior of the system – and thus general resource allocation questions as there are still many uncertainties resulting in a high number of degrees of freedom –, they will facilitate the studying of new questions. For example, it will be interesting to investigate the interplay between different organs, as well as to study inter-organismal metabolic connections such as between the host and its gut microbiome constituents or host-symbiont/host-parasite mutualism. *Drosophila* is an exquisite model for such kind of studies given its well characterized and relatively simple gut microbiome (Douglas, 2019). Further, the mutualism between insects and the endosymbiont *Wolbachia*, which can also act as pathogen, is well described (Pietri et al., 2016; Landmann, 2019). In *Aedes aegypti*, an impact of an infection with the pathogenic *Wolbachia* strain *wMelPop*, for example, was recently shown to affect the TAG and cholesterol metabolism of the host (Geoghegan et al., 2017). Further, the time-resolved analysis of metabolite amounts as well as the consequences of gene dosage and protein activity alterations, will be interesting avenues to follow.

Our lack of knowledge concerning the energy costs associated with growth and non-growth associated processes (often referred to as GAM – growth associated maintenance, and NGAM – non-growth associated maintenance costs) might appear as a weak spot of our approach. So far, we determined the NGAM values in an iterative process based on the oxygen consumption rate of *Drosophila* S2R+ cells (Da-Ré et al., 2014) (methods section and Fig. S5) and used the GAM values from a yeast model (Mo et al., 2009), as an experimental estimation of the values for *Drosophila* is difficult. Our approach appears legitimate, at least at the current point of time, as simulations testing a wide array of different GAM and NGAM values with our model demonstrated only a limited impact on the biomass production (Fig. S6 and Interactive Supplementary Fig. 2). The impact of GAM and NGAM uncertainties on the resource allocation problem might be bigger. The

size of the linear programming solution space decreases with increasing GAM and/or NGAM values, as fluxes have to compensate for the increased energy requirements as for example the rate of oxygen consumption. Thus, the future estimation of the real GAM and NGAM values for larvae under different physiological conditions is a challenging, yet valuable goal.

We parameterized our model using absolute enzyme-based biochemical quantifications as well as via GC-MS based metabolomics measurements (Figs 4–6 and Table S2). Overall, our measurements explained a large portion of the dry weight of the animals (Fig. 5B). The prominent drop of explained dry weight at 168 hours after egg laying (60 % explained dry mass versus 81 or 95 % (96 or 132 hours after egg laying, respectively)) is intriguing. Given that despite of lactate all metabolites measured by us increased over time (Figs 4 and 8), this result suggests that the production of another metabolite not measured by us is increasing dramatically during this growth phase. Candidates are, for example, nucleic acids or components of the cuticle. In support of this notion, we noted an elevated slope of the larval weight gain from the second to the last time point (Fig. 4A), whereas size increase on the HD rather stalled during this phase (Fig. S2B–D).

The use of the chemically defined HD significantly facilitated the connection of the biological data to the modeling both under basal (Figs 4–8) as well as dietary altered (Figs 4, 6 and 8) conditions. The presence of the chemically defined food is a big advantage as compared to complex and ill-defined food compositions, as uncertainties in terms of the diet obfuscates defining the real inputs entering the system in the experiment as well as the model. An obvious point for optimization is our lack of knowledge concerning the exact amounts of food consumed and metabolite resorption rates. The mouth hook contraction values used by us, for example, could in theory vary in response to different diets. Several reports, however, suggested only a limited impact of the diet on the mouth hook contraction frequencies (Musselman et al., 2011; Ryuda et al., 2011). Nevertheless, in the future, methods that are more sophisticated should be used to eliminate this shortcoming using e.g. radiolabeled tracer experiments, which will also allow the direct estimation of metabolite flux rates. These in turn will allow a much better comparison to the predicted flux rates as our endpoint

measurements. Another point to consider is that the HD represents a minimal medium, which results in a slowed down growth. Here, we started to investigate which nutrients might act as growth limiting factors and our strategy appears to be successful in predicting nutrients allowing a faster growth. For the investigation of resource allocation and optimality principles, the slowed-down growth appears less problematic, given that optimality of resource allocation is situation dependent, and thus an inadequate diet can also be utilized in an optimal manner.

Investigations concerning the minimal nutritional requirements of an organism, as well as concerning the impact of nutritional alterations on the physiology of an organism, is an active field of research (Garcia Caraballo et al., 2014; Besson et al., 2016; Reis, 2016). Our early results with the predictions of the impact of altering sucrose or EAA levels in the food are particularly promising. They suggest that simulations with FlySilico should facilitate the identification of suitable parameter ranges for experiments targeting e.g. the nutritional requirements of larvae and flies or the impact of diet alterations on the metabolic and/or growth phenotype. The future FlySilico-based investigations concerning the impact of varying amounts of essential and branched chain amino acids on growth processes, life history traits such as fecundity, ageing related diseases and cancer will be exciting as these aspects gained a lot of attention recently (Piper et al., 2017; Chen et al., 2018; Knott et al., 2018; Shao et al., 2018).

Drosophila larval growth is marked by an impressive increase in size and mass. This expansion is necessary for a successful completion of metamorphosis, which involves a drastic remodeling of body structures and a food intake cessation. Therefore, the larval development is subject to hard biological constraints. Still, the organism can react to fluctuations in the quality or quantity of food by adjusting the rate of development and resource allocation, e.g. by channeling less nutrients into storage forms (Beadle et al., 1938). Our experiments, where we raised animals on either standard HD or HD supplemented with additional sucrose or EAA (Figs 4, 6 and 8), demonstrate this plasticity. Further, our model predictions correctly identified the growth limiting nutritional parameters and revealed flux differences, which relate to the observed metabolic changes based on the diet alterations. The precision of the model predictions will increase with further improvements as outlined above.

Intriguingly, the metabolic adaptation to altered nutritional conditions are not limited to insects, but have also been described e.g. for mammals (Gluckman et al., 2007). Thus, future investigations targeting other species are possible to test for a possible generalization of our findings.

An important aspect is that solving the flux balance model is by definition following optimality principles. Given that our relatively simple model already was able to result in correct predictions suggests that *Drosophila* resource allocation is operating in a quasi-optimal state. Future studies with additional parameter variations (e.g. cost functions for protein and DNA synthesis and distinguishing different type of organs or tissues (Martins Conde, Patricia do Rosario et al., 2016)) and incorporation of additional fly genotypes and perhaps single gene mutations will help to further elucidate this intriguing possibility.

Materials and Methods

Drosophila fly stocks and rearing

For all our experiments, we used the wild type Oregon-R fly strain reared under standard culture conditions (25 °C, 12 h light-dark rhythm and 60–70 % humidity).

Chemically defined fly medium

The chemically defined (holidic) medium (*Holidic diet*; HD) was introduced in (Piper et al., 2014). Animals developing on HD are viable, fertile, and have no aberrant phenotypes, although the development is slowed-down and the HD is thus classified a minimal medium. Food was prepared according to the instructions of the Piper et al. publication with use of the Yeast-like amino acid composition (“Yaa”). For our perturbation experiments we either added the double amount of sucrose (2x sucrose) or the double amount of essential amino acids (2x EAA).

Larvae collection procedure

In order to minimize a possible impact of environmental effects, we kept the parental density constant with 15 male flies and 30 female flies per vial. These adult flies were kept on a standard complex cornmeal diet (per 100 mL: 0.5 g agar (Becton Dickinson, 214010), 7.1 g polenta (Verival, Pronurel Bio, 265250), 0.95 g soy flour (Bauck Hof, Amazon.de, B004RG3C0I), 1.68 g yeast (Bruggeman, lieferello.de, 14874413), 4 g treacle (Original Grafschafer Goldsaf, lieferello.de, 10231869), 4.5 g malt extract (Demeter, Amazon.de, B00GU029LW), 0.45 mL propionic acid (Acros Organics, 220130010, CAS 79094) and 1.5 mL nipagin (Sigma-Aldrich, H3647-100G) (1:10 stock solution in 70 % Ethanol; Riedel-de Haën, 16202S-1L, CAS 64-17-5) before we transferred them to the chemically defined medium to allow oviposition. After six hours we discarded the parental flies to have a defined time period for the egg-laying. As the maximum time point for collecting larvae we used 168 h after egg laying as afterwards the larvae start to pupariate on the HD. Based on this terminal point, we added two equally spaced time points earlier in development (132 h and 96 h after egg laying, respectively) as growth is quasi linear.

The possibility that larval growth and metabolism is showing a sexual dimorphism appeared intriguing. Pilot experiments using animals reared on the holidic or a standard diet, however, showed that at the latest timepoint used by us female and male larvae do not significantly differ in terms of the size, the triglyceride, glucose or glycogen levels (data not shown). Thus, we did not consider the sex of the animals during our experimental timeframe a prominent factor and therefore collected unsexed larvae 96 h, 132 h and 168 h after egg laying and washed them in PBS with 0.1 % Tween-20 (PBT) for the weight measurements and metabolic assays or in HPLC-graded water for the GC-MS analytics. We used quadruplicates for every condition and collected 25 larvae (96 h) or eight larvae (132 h, 168 h) for the GC-MS and the metabolic assays. For the dry and wet weight measurements, we collected 100 animals from the 96 h time point and 40 animals from the 132 h and 168 h time points, respectively.

Wet and dry weight measurements

For the determination of the wet weight, we transferred the washed larvae into pre-weighed 1.5 mL tubes and weighed them on an analytical scale. The animals were then snap-frozen in liquid nitrogen and dried in an oven at 60 °C with the tube lids open. After 24 h we measured again the weight (= dry weight) and calculated the water content by subtraction of the dry weight from the wet weight.

Larval size measurements

For the larval size measurements, we collected at the indicated time points the animals in ice cold PBS to minimize their movements and to ensure their elongation. Subsequently, we recorded images with a Zeiss SteREO Discovery.V8 dissection microscope, which were analyzed with the Zeiss Zen Software (Zen 2.3 lite – blue edition). For each larva, we measured the area, the length and its width. In total, we performed three biologically independent experiments and measured 20 to 30 animals per repetition.

Biochemical measurements

All targeted biochemical measurements were essentially carried out as described in (Jehrke et al., 2018). We collected the larvae from three different time points and snap-froze the animals in liquid nitrogen before storage at −80 °C. For the homogenization, we used 1 mL 0.05 % Tween 20 in water in 2 mL screw-cap tubes and a Fast Prep FP120 machine (Bio101 Savant). After homogenization and heat-inactivation for 5 minutes at 70 °C, the supernatant was transferred to 1.5 mL tubes as a reservoir for the metabolic assays, which were performed in 96-well plates. We normalized each measurement to the amount of animals per sample.

Protein

The free protein content was measured using the Pierce BCA assay kit (Life Technologies) according to the manufacturer’s instructions. We used bovine

serum albumin (BSA) as a standard to determine the protein content of the samples. The 0.05 % Tween-20 used by us in the homogenization procedure most likely was not sufficient to solubilize also integral membrane proteins. Thus, the protein amounts per animal might represent an underestimation of the real total protein content.

Triglycerides (TAG)

For the determination of the triglyceride levels in the samples, we used the Triglycerides Reagent (Thermo Scientific). We transferred 50 µL of the samples and a serial dilution (1:2 in 0.05 % Tween 20 in water) of the glycerol standard (Sigma Aldrich) to a 96-well plate and added 200 µL of the Triglycerides reagent. The samples and the standard were incubated 45 minutes at 37 °C and the absorbance was read at 510 nm.

Glycerol

The glycerol content of the samples was determined using the Glycerol Assay Kit (Sigma-Aldrich). We followed the manufacturer's instruction for fluorometric measurements.

Glucose and Glycogen

For the determination of glucose and glycogen, we used the GO Assay Reagent (Sigma-Aldrich) and a modified form of a protocol described in Tennessen et al. (2014). For both measurements, we transferred 30 µL of the undiluted samples and the standards to a 96-well plate. We added 100 µL GO reagent to measure free glucose and 100 µL GO reagent with amyloglucosidase (1 µL per 1 mL GO reagent) to measure the total glucose content (free glucose plus glucose liberated from the glycogen). After 60 minutes incubation by 37 °C we stopped the reactions by adding 100 µL 12 N H_2SO_4 and measured the absorbance at 540 nm. We calculated the glycogen content by subtraction of the free glucose from the total glucose content.

Lactate

For the quantification of lactate, we used the Lactate Assay Kit (Biovision). We transferred 50 µL of the pre-diluted samples (1:50) to a 96 well plate and followed then the manufacturer's instruction for fluorometric measurements.

Cholesterol

Measurements were performed as described in Werthebach et al. (2019).

GC-MS measurements

Metabolites were extracted using 105 µL chloroform and 245 µL methanol. After incubation for 1 h at −20 °C we added 560 µL HPLC grade water twice. The samples were centrifuged for two minutes at high speed in a table top centrifuge at 4 °C and the aqueous phases were collected for the GC-MS measurements (in total about 1.3 mL).

For the metabolite analysis a gas chromatography – mass spectrometry (GC-MS) system (7200 GC-QTOF from Agilent) was used as described in Fiehn et al. (2000). The data were analyzed with the Mass Hunter Software (Agilent). For absolute quantifications, we used five different dilutions of the standard mix (resulting in effective metabolite concentrations: 1 µM, 5 µM, 10 µM, 15 µM and 20 µM; Fig. S3) and calculated for each metabolite a standard curve which we used to determine the amount of the respective metabolite in our samples.

Network reconstruction

For the *in silico* reconstruction of *Drosophila melanogaster* growth and metabolism we focused on core metabolic pathways required to metabolize the HD ingredients, and used the cameo package for the Python programming language (Cardoso et al., 2018). The Yeast iMM904 model from the BiGG data base (Mo et al., 2009) and a previously published *Drosophila* model for hypoxia investigations (Feala et al., 2009) served as starting points for our network reconstruction. First, we incorporated major metabolic pathways of the

carbohydrate metabolism (including glycolysis, gluconeogenesis, tricarboxylic acid (TCA) cycle and pyruvate metabolism), the lipid metabolism (with a focus on the glycerolipid metabolism), the energy liberating metabolic reactions (e.g. oxidative phosphorylation) and anaplerotic reactions. Subsequently, we successively integrated metabolic reactions necessary to metabolize the HD ingredients, such as amino acid metabolic pathways (including e.g. glycine, threonine, cysteine, and phenylalanine metabolism), pathways of vitamin synthesis (e.g. folate and riboflavin) and various pathways needed for the transport and synthesis of cofactors. For the initial version of FlySilico we only focused on three different compartments (extracellular, cellular and mitochondrial) and adapted the transport reactions accordingly. We manually curated all reactions by cross-validation with multiple resources (BioCyc - https://biocyc.org/ (Caspi et al., 2016), BRENDA - https://www.brenda-enzymes.org/ (Chang et al., 2009), ChEBI - http://www.ebi.ac.uk/chebi/init.do (Hastings et al., 2016), KEGG - http://www.genome.jp/kegg/ (Kanehisa et al., 2017), PubChem - https://pubchem.ncbi.nlm.nih.gov/ (Wheeler et al., 2008), BiGG - http://bigg.ucsd.edu/ (King et al., 2016), and FlyBase - http://flybase.org/ (Gramates et al., 2017)) and paid special attention on the biochemical pathways and the genetics of *Drosophila melanogaster*. We attached to each reaction a confidence score based on evidence of sequence, physiological, genetic or biochemical data (as previously suggested by e.g. Thiele and Palsson (2010)). Reactions required for the modeling, but without any evidence of correctness, received the lowest confidence scores. FlySilico version 1.0 covers 293 metabolites and 363 reactions. Supplemental Table S1 summarizes all pathways, reactions and metabolites present in the model.

Constraint-based modeling

After the reconstruction process, the coefficients of the mass-balanced reactions form a mathematical representation as stoichiometric matrix S. The constraint-based modeling approach follows equation:

$$\frac{d\boldsymbol{X}}{dt} = \boldsymbol{S} * \boldsymbol{v} = 0 \quad (1)$$

with

$$\alpha_i \leq v_i \leq \beta_i \quad (2)$$

where x is a vector with all metabolites, S is the stoichiometric matrix and v is a vector with all fluxes under steady state conditions. The lower (α_i) and upper (β_i) bounds to each flux v_i impose additional constraints to the system. The null space of S includes any v that satisfies the solution under this steady state assumption with the given constraints. The model is solved by optimizing the system for a given objective function, i.e. the primary goal of an organism (such as biomass production for fast growing unicellular organisms as for example *E. coli*), using linear programming. A detailed explanation of constraint-based modeling, flux balance analysis and linear programming is provided e.g. in: Orth et al. (2010) or Kauffman et al. (2003). For our model solutions we compared solutions allowing loops as well as loopless (Price et al., 2002; Schellenberger et al., 2011) variants (Fig. S7). The loopless solution reflects the biology better, and thus we used this method throughout the study unless otherwise noted.

Flux variability analysis

Flux variability analysis (FVA (Gudmundsson and Thiele, 2010)) is a computational method to identify the maximum and minimum fluxes of reactions from a given network while it preserves a certain network state (e.g. maximum biomass production rate). FVA solves two optimization problems for each reaction v_i after solving a given objective function.

$$\begin{gathered} max_v/min_v\ v_i \\ subject\ to\ \boldsymbol{S} * \boldsymbol{v} = 0 \\ c^T * \boldsymbol{v} \geq \gamma * Z_0 \\ \alpha_i \leq 0 \leq \beta_i \end{gathered} \quad (3)$$

where $Z_0 = c^T v_o$ is an optimal solution for the objective function, γ is a parameter which controls the optimality of the solution (suboptimal: $0 \leq \gamma < 1$; optimal: γ = 1), **c** is the vector which represents the linear objective function.

Calculation of biomass and uptake rates

In order to identify an appropriate biomass function, we estimated the body composition of differently aged larvae by targeted absolute biochemical quantifications as well as GC-MS based metabolomics measurements. We reasoned that the main larval constituents are water, proteins, carbohydrates and storage lipids given that the latter two are the main storage forms fueling metamorphosis and that the larvae are filled up with the adipose-tissue like storage organ – called the fat body – which is the main storage site for storage lipids and glycogen. The water content could be easily measured by gravimetrics (see above) and on top of free protein, glucose, triglyceride and glycogen amounts, we also determined the levels of lactate and free glycerol by targeted biochemical assays (see above). Our GC-MS measurements further covered metabolites from the central carbon metabolism as well as almost all free amino acids.

Biomass functions usually cover each amino acid separately. Yet, our free protein measurements did not provide such fine-grained information. The GC-MS based metabolomics measurements resulted in the identification of free amino acid amounts; yet three amino acids (arginine, glutamine and histidine) were missing in our measurements. In order to approximate the levels of the different amino acids, we followed a bioinformatics strategy with the reasoning that the amino acid fractions would relate to the respective amino acid frequency across the *Drosophila* proteome. Thus, we first calculated the frequency of each of the twenty classical amino acids in the complete proteome of *Drosophila melanogaster* (http://www.uniprot.org/uniprot/?query=proteome:UP000000803). Figure S8 provides the calculated amino acid frequencies. We based the coefficients on the differences between the first and last time points investigated. Thus, for each measurement we calculated:

$$m_{168h,Metabolite} - m_{96h,Metabolite} = m_{\Delta,Metabolite} \quad (4)$$

Where $m_{\Delta,Metabolite_i}$ represents the weight difference of a metabolite i between 168 h and 96 h in $gram$, $m_{168h,Metabolite_i}$ is the weight of the metabolite i at 168 h in $gram$, and $m_{96h,Metabolite_i}$ is the weight of the metabolite i at 96 h in $gram$. For the amino acids, we could now calculate the individual amino acid weights with the help of the calculated amino acid frequencies:

$$m_{\Delta,Metabolite_i} \widehat{=} m_{AA_i} = m_{\Delta,Protein} * f_{AA_i} \quad (5)$$

where m_{AA_i} shall be equivalent to $m_{\Delta,Metabolite_i}$ and represents the weight of amino acid i in $gram$, $m_{\Delta,Protein}$ is the difference of weight of the protein in $gram$ which was calculated based on equation Eq. 4, and f_{AAi} which represents the frequency of amino acid i from Fig. S8. Metabolite weights from equations Eqs 4 and 5 enable the calculation of an assay-based coefficient for each metabolite for the biomass objective function:

$$x_{Assay,Metabolite_i} = \frac{\frac{m_{\Delta,Metabolite_i}}{M_{Metabolite_i}}}{m_{\Delta,dry}} = \frac{n_{Metabolite_i}}{m_{\Delta,dry}} \quad (6)$$

where $x_{Assay,Metabolite_i}$ represents the coefficient of the metabolite based on assay data in $\frac{mmol}{g}$, $M_{Metabolite_i}$ is the molar mass of metabolite i in $\frac{g}{mmol}$, $m_{\Delta,dry}$ is the larval dry weight difference from 96 h till 168 h in $gram$, and $n_{Metabolite_i}$ is the amount of metabolite i in $mmol$.

The GC-MS analysis quantified free metabolite amounts. In order to calculate a GC-MS coefficient, we calculated the difference of metabolite amounts between 168 h and 96 h by the following equation:

$$n_{\Delta,Metabolite_i} = n_{168h,Metabolite_i} - n_{96h,Metabolite_i} \quad (7)$$

where $n_{\Delta,Metabolite_i}$ represents the difference of amount between 168 h and 96 h from metabolite i in $mmol$, $n_{168h,Metabolite_i}$ is the amount of the metabolite i at 168 h in $mmol$, and $n_{96h,Metabolite_i}$ is the amount of the metabolite i at 96 h in $mmol$. We used the resulting metabolite amounts from equation Eq. 7 to calculate a GC-MS coefficient with the equation:

$$x_{GCMS,Metabolite_i} = \frac{n_{Metabolite_i}}{m_{\Delta,dry}} \quad (8)$$

where $x_{GCMS,Metabolite_i}$ as the GC-MS coefficient of the metabolite i in $\frac{mmol}{g}$, $m_{\Delta,dry}$ is the difference of dry weight between 168 h and 96 h in $gram$, and $n_{Metabolite_i}$ is the amount of metabolite i in $mmol$.

Through equation Eqs 6 and 8 the biomass function coefficient can be calculated for all metabolites with the following equation:

$$x_{Metabolite_i} = x_{Assay,Metabolite_i} + x_{GCMS,Metabolite_i} \quad (9)$$

where $x_{Metabolite_i}$ is the biomass function coefficient of metabolite i, $x_{Assay,Metabolite_i}$ as the assay-based coefficient of metabolite i, $x_{GCMS,Metabolite_i}$ and as the GC-MS-based coefficient of metabolite i. All coefficients of Eq. 9 are in $\frac{mmol}{g}$. *Drosophila melanogaster* is cholesterol auxotroph (Sang and King, 1961; Carvalho et al., 2010). To simulate the cholesterol auxotrophy of *Drosophila*, we included cholesterol in the biomass function based on measurements of cholesterol levels from larvae reared on HD (Fig. S9). The biomass coefficient of cholesterol was calculated according to the equation:

$$x_{Cholesterol} = \frac{\frac{c_{Cholesterol,Protein} * m_{\Delta,Protein}}{M_{Cholesterol}}}{m_{\Delta,dry}} \quad (10)$$

where $x_{Cholesterol}$ is the biomass coefficient for cholesterol in $\frac{mmol}{g}$, $c_{Cholesterol,Protein}$ is the cholesterol mass per protein mass in $\frac{g}{g\ Protein}$, $m_{\Delta,dry}$ is the difference of weight of protein between 168 h and 96 h in $gram$, $M_{Cholesterol}$ is the molar mass of cholesterol in $\frac{g}{mmol}$, $m_{\Delta,dry}$ is the difference of dry weight between 168 h and 96 h in $gram$. The mean value of the cholesterol mass per protein mass of all 3 time points (96 h, 132 h and 168 h) is $c_{Cholesterol,Protein} \approx 5.46\ \frac{ng}{\mu g\ Protein}$.

Approximation of food intake

Given that the absolute quantification of the uptake of solid food by larvae is difficult, and that the measurement of the absorption rate and organismic distribution for each nutrient is close to impossible, we used a theoretical approximation of the food intake as a starting point for our modeling experiments. First, we calculated the maximum volume of the mouth cavity by approximating a cylindrical shape and taking length and diameter measurements of the differently aged larvae into account. We calculated the oral cavity volume according to equation:

$$V_{mouth} = \pi * r^2 * h \quad (11)$$

where V_{mouth} is the volume of the oral cavity in mm^3, π is the mathematical constant, r is the radius of the oral cavity in *mm*, and *h* is the height of the oral cavity in *mm*.

Because the larva grows over time, we estimated the diameter of the larva as the mean of the width of time points 96 h and 168 h and assumed that the diameter of the oral cavity is about half of the larva diameter (the radius of the oral cavity thus is $r = 0.118\,mm$). We took the height of the oral cavity from a publication from Alpatov (1929). Here, the height of the oral cavity is the average of the mean length from larval stages II and III with a value of $h = 0.25\,mm$. Thus, the resulting oral cavity volume according to equation Eq. 11 is $v_{Mouth} = 0.011\ mm^2$.

We approximated the feeding rate using measures of the sclerite reactions per minute from Fellowes et al. (1999) $\left(f_{Feed} = \frac{110}{min}\right)$, with the assumptions that each sclerite reaction completely fills the oral cavity and that all food ingredients are homogeneously distributed. The dietary intake can thus be calculated using the following equation:

$$m_{Dietary} = v_{Mouth} * f_{Feed} * \rho_{holidic} \quad (12)$$

where $m_{Dietary}$ is the dietary intake in $\frac{g}{h}$, v_{Mouth} is the oral cavity volume in mm^3, f_{Feed} is the sclerite reactions per *h*, and $\rho_{holidic}$ is the sum of the mass concentrations of the holdic diet ingredients in $\frac{g}{\mu L}$. Our calculated dietary intake is $m_{Dietary} = 0.064 \frac{g}{h}$.

Our calculation is of course an overestimation given that each sclerite reaction most likely does not fill the mouth volume completely and that the uptake from the gut is not 100 % efficient. To account for this limitation, we introduced a correction factor χ based on our experimental data and simulations by an iterative process. In brief, we calculated all uptake rates with increasing values for the correction factor χ (from 0 to 0.20 in 0.001 steps) and used the different uptake rates to calculate the corresponding growth rate. We selected for χ the value where the calculated growth rate fitted the experimentally determined growth rate best (Fig. S4). We determined the experimental growth rate based on the dry weight measurements during the three time points. We calculated the growth rate between the first and last time point as:

$$\mu_{BIOMASS,Exp} = \frac{\frac{\bar{m}_{t2} - \bar{m}_{t1}}{\Delta t}}{\bar{m}_{t1}} \quad (13)$$

As a result we obtained the experimental growth rate $\mu_{BIOMASS,Exp} = \frac{0.0882}{h}$ and for $\chi = 0.122$ the predicted growth rate $\mu_{BIOMASS,Pred} = \frac{0.088}{h}$. Thus, the corrected dietary intake calculation is:

$$m_{Dietary,Metabolite_i} = m_{Dietary} * \chi * p_{Metabolite_i} \quad (14)$$

where $m_{Dietary,Metabolite_i}$ is the dietary intake of metabolite i in $\frac{g}{h}$, $m_{Dietary}$ is the dietary intake in $\frac{g}{h}$, χ is the correction factor, and $p_{Metabolite_i}$ is the proportion of each metabolite i in the holidic medium.

For the network modelling, all dietary internalizations have to be flux rates or uptake rates, which we calculated as follows:

$$v_{uptake,i} = \frac{m_{Dietary,Metabolite_i}}{M_{Metabolite_i} * m_{\Delta,dry}} \quad (15)$$

where $v_{uptake,i}$ is the uptake rate of metabolite i in $\frac{mmol}{g*h}$, $m_{Dietary,Metabolite_i}$ is the dietary intake of metabolite i in $\frac{g}{h}$, $M_{Metabolite_i}$ is the molar mass of metabolite i in $\frac{g}{mmol}$, and $m_{\Delta,dry}$ is the difference of dry weight between 168 h and 96 h in $gram$.

Summary statement

FlySilico, a flux balance analysis suitable metabolic network of *Drosophila melanogaster* is presented, and its use for the investigation of larval growth and metabolism is demonstrated.

Data availability

The supplementary material consists of the metabolic network reconstruction (Table S1), the raw data of all measurements (Table S2), the result of the flux variability analysis for the different diet simulations (Table S3) and the corresponding flux changes in relation to the standard HD (Table S4). Additionally, we added interactive versions of the metabolic network map (Interactive Supplementary Fig. 1) and the GAM/NGAM plot (Interactive

Supplementary Fig. 2), which corresponds Fig. S6. Further, we provide all raw data, the custom python scripts used for the calculation of the weights of the biomass function and the uptake rates, the model comparison and the main scripts for the model reconstruction and analysis in a zip file for use with the Anaconda Project function (https://anaconda-project.readthedocs.io/en/latest/). Once unzipped, the folder contains all information to create an Anaconda Python environment with the required packages in the appropriate version to run our code and all necessary information to rerun or modify our analyses. A readme file within the folder should guide users through the procedure to get the environment operational. We additionally provide all scripts via GitLab: https://gitlab.com/Beller-Lab/flysilico.

Acknowledgements

We thank Andrea Droste and Katrin Weber for excellent technical support as well as Alberto Marin Sanguino, Claus Jonathan Fritzemeier and Oliver Ebenhöh for fruitful discussions during the initial phase of the project. The project was financed through the German “Bundesministerium für Bildung und Forschung (BMBF)” grant 031A 306 (to M. Beller) and in part by a scholarship of the Jürgen Manchot Foundation (to J.W. Schönborn).

Author information

Author notes

These authors contributed equally: Jürgen Wilhelm Schönborn and Lisa Jehrke.

Authors and Affiliations

Institute for Mathematical Modeling of Biological Systems, Heinrich Heine University, Duesseldorf, Germany

Jürgen Wilhelm Schönborn, Lisa Jehrke & Mathias Beller

Systems Biology of Lipid Metabolism, Heinrich Heine University, Duesseldorf, Germany

Jürgen Wilhelm Schönborn, Lisa Jehrke & Mathias Beller

Institute of Plant Biochemistry & Cluster of Excellence on Plant Sciences, Heinrich Heine University, Duesseldorf, Germany

Tabea Mettler-Altmann

Contributions

J.S., L.J. and M.B. designed the study. J.S. and L.J. established the metabolic network model and performed the modeling experiments. L.J. performed the Drosophila experiments and most of the wet lab procedures. T.M.A. performed the GC-MS experiments. J.S., L.J., T.M.A. and M.B. analyzed the data and prepared graphs. J.S., L.J. and M.B. wrote the manuscript. All authors read and approved the final manuscript.

Corresponding author

Correspondence to Mathias Beller.

Ethics declarations

Competing interests

The authors declare no competing interests.

Additional information

Publisher’s note Springer Nature remains neutral with regard to jurisdictional claims in published maps and institutional affiliations.

Supplementary Information

FlySilico: Flux balance modeling of *Drosophila* larval growth and resource allocation

Jürgen Wilhelm Schönborn, Lisa Jehrke, Tabea Mettler-Altmann, Mathias Beller

We provide all primary data as well as the metabolic network in supplemental tables (please see below). The Python scripts for the flux balance modeling and parameter estimations are provided via GitLab (https://gitlab.com/Beller-Lab/flysilico/) and an Anaconda Project folder to allow reproducible research thanks to a snapshot of a Python working environment with the adequate package versions.

The supplemental information comprises:

- 9 figures (found below)
- Four Supplemental Tables:
    - Table S1: Information for the *Drosophila* metabolic network „FlySilico“
    - Table S2: Wet lab experimental data file
    - Table S3: Flux variability analysis results
    - Table S4: Normalized flux variability results
- Two Supplementary Interactive figures:
    - Supplementary Interactive Figure 1: Interactive Metabolic Network Map
    - Supplementary Interactive Figure 2: Interactive GAM/NGAM/Growth rate plot
- Supplemental Zip File with the code and data necessary to use the FlySilico metabolic network for flux balance analyses and to generate the plots shown in the figures

A

MNXM18_bm + MNXM876_bm + bigg_ala_L_bm + bigg_amp_bm + bigg_arg_L_bm + bigg_asn_L_bm + bigg_asp_L_bm + bigg_atp_bm + bigg_cmp_bm + bigg_cys_L_bm + bigg_damp_bm + bigg_dcmp_bm + bigg_dgmp_bm + bigg_dtmp_bm + bigg_gln_L_bm + bigg_gly_bm + bigg_gmp_bm + bigg_his_L_bm + bigg_ile_L_bm + bigg_leu_L_bm + bigg_lys_L_bm + bigg_met_L_bm + bigg_phe_L_bm + bigg_pro_L_bm + bigg_ser_L_bm + bigg_thr_L_bm + bigg_trp_L_bm + bigg_tyr_L_bm + bigg_ump_bm + bigg_val_L_bm --> bigg_adp_bm + bigg_pi_bm

B

IN FLUXES	OUT FLUXES						OBJECTIVES	
	MNXM10815_i	1e+03	bigg_arachd_i	1e+03	bigg_aicar_i	500	BIOMASS_REAC...	500
	MNXM1158_i	1e+03	bigg_but_i	1e+03	MNXM4091_i	421		
	MNXM12528_i	1e+03	bigg_co2_i	1e+03	MNXM977_i	421		
	MNXM2426_i	1e+03	bigg_co_i	1e+03	bigg_n2_i	411		
	MNXM305_i	1e+03	bigg_cysam_i	1e+03	MNXM59_i	346		
	MNXM369_i	1e+03	bigg_dtdpglu_i	1e+03	bigg_gam1p_i	346		
	MNXM5127_i	1e+03	bigg_gcald_i	1e+03	bigg_maltttr_i	307		
	MNXM53135_i	1e+03	bigg_glyc_i	1e+03	bigg_ins_i	230		
	MNXM7206_i	1e+03	bigg_h2_i	1e+03	MNXM56_i	210		
	MNXM7559_i	1e+03	bigg_no3_i	1e+03	bigg_ascb_L_i	193		
	MNXM7713_i	1e+03	bigg_uamag_i	1e+03	MNXM96041_i	154		
	MNXM92184_i	1e+03	bigg_no2_i	849	bigg_meoh_i	123		
	MNXM9857_i	1e+03	bigg_hpyr_i	689	MNXM18606_i	116		
	bigg_5aop_i	1e+03	MNXM1128_i	579	MNXM1289_i	67.2		
	bigg_ade_i	1e+03	MNXM539_i	500	bigg_alaala_i	39.4		

Figure S1: Modeling growth with the computer generated *Drosophila* metabolic network (BMID000000141998; https://www.ebi.ac.uk/biomodels-main/BMID000000141998). (A) Computational biomass function as provided from the ebi website. (B) FBA solution with no substrate incorporation (missing "in fluxes"). The model predicts a biomass production (column "objectives" shows a value of 500 for the biomass reaction). bm – biomass | i - intra cellular | MNXM18_bm - glutamate(1-) | MNXM876_bm - glycogen | bigg_ala_L_bm - L-alanine zwitterion | bigg_amp_bm - AMP | bigg_arg_L_bm - L-argininium(1+) | bigg_asn_L_bm - L-asparagine zwitterion | bigg_asp_L_bm - L-aspartate(1-) | bigg_atp_bm - ATP | bigg_cmp_bm - CMP | bigg_cys_L_bm - L-cysteine zwitterion | bigg_damp_bm - dAMP | bigg_dcmp_bm - dCMP(2-) | bigg_dgmp_bm - dGMP(2-) | bigg_dtmp_bm - dTMP | bigg_gln_L_bm - L- glutamine zwitterion | bigg_gly_bm - glycine | bigg_gmp_bm - GMP(3-) | bigg_his_L_bm - L-histidine zwitterion | bigg_ile_L_bm - L-isoleucine zwitterion | bigg_leu_L_bm - L-leucine zwitterion | bigg_lys_L_bm - L-lysinium(1+) | bigg_met_L_bm - L-methionine zwitterion | bigg_phe_L_bm - L-phenylalanine | bigg_pro_L_bm - L-proline | bigg_ser_L_bm - L-serine | bigg_thr_L_bm - L-threonine zwitterion | bigg_trp_L_bm - L-tryptophan zwitterion | bigg_tyr_L_bm - L-tyrosine zwitterion | bigg_ump_bm - UMP(2-) | bigg_val_L_bm - L-valine zwitterion | bigg_adp_bm - ADP | bigg_pi_bm - phosphate | MNXM10815_i - beta- methylenecyclopropyl pyruvate | MNXM1158_i - sn-glycerol 1-phosphate(2-) | MNXM12528_i - an \xc5\x93\xc3\xa2-oxo fatty acid | MNXM2426_i - ribonucleoside | MNXM305_i - 2-methyl-3-oxopropanoate | MNXM369_i - 1L-myo-inositol 1,2,3,4,6- pentakisphosphate(10-) | MNXM5127_i - diethylphosphate | MNXM53135_i – fatty aldehyde | MNXM7206_i - a debranched limit dextrin | MNXM7559_i - N-acetyl-D- galactosaminyl-polypeptide | MNXM7713_i - a [protein]-L-tyrosine | MNXM92184_i - CMP-N-glycoloylneuraminate | MNXM9857_i - 2-methylamine-furan phosphate | bigg_5aop_i - 5-aminolevulinate | bigg_ade_i - adenine | bigg_arachd_i – arachidonate | bigg_but_i - butyrate | bigg_co2_i - CO(2) | bigg_co_i - carbon monoxide(1+) | bigg_cysam_i - cysteaminium | bigg_dtdpglu_i - dTDP-alpha-D-glucose | bigg_gcald_i - glycolaldehyde | bigg_glyc_i - alditol | bigg_h2_i - H2 | bigg_no3_i - nitrate | bigg_uamag_i - UDP-N-acetylmuramoyl-L-alanyl-D-glutamate(4-) | bigg_no2_i – nitrite | bigg_hpyr_i - 3-hydroxypyruvate | MNXM1128_i - 1-aminocyclopropanecarboxylic acid zwitterion | MNXM539_i - 1-acyl-sn-glycero-3-phosphoglycerol | bigg_aicar_i - 5- amino-1-(5-phospho-D-ribosyl)imidazole-4-carboxamide(2-) | MNXM4091_i – psoralen | MNXM977_i - ethene | bigg_n2_i - dinitrogen | MNXM59_i - 1,2-diacyl-sn-glycerol | bigg_gam1p_i - alpha-D-glucosamine 1-phosphate(1-) | bigg_maltttr_i - alpha- maltotetraose | bigg_ins_i - inosine | MNXM56_i - formaldehyde | bigg_ascb_L_i - ascorbate | MNXM96041_i - 1-acylglycerophosphocholine | bigg_meoh_i - methanol | MNXM18606_i - hyperforin | MNXM1289_i - oxalatosuccinate(3-) | bigg_alaala_i - D-alanyl-D-alanine

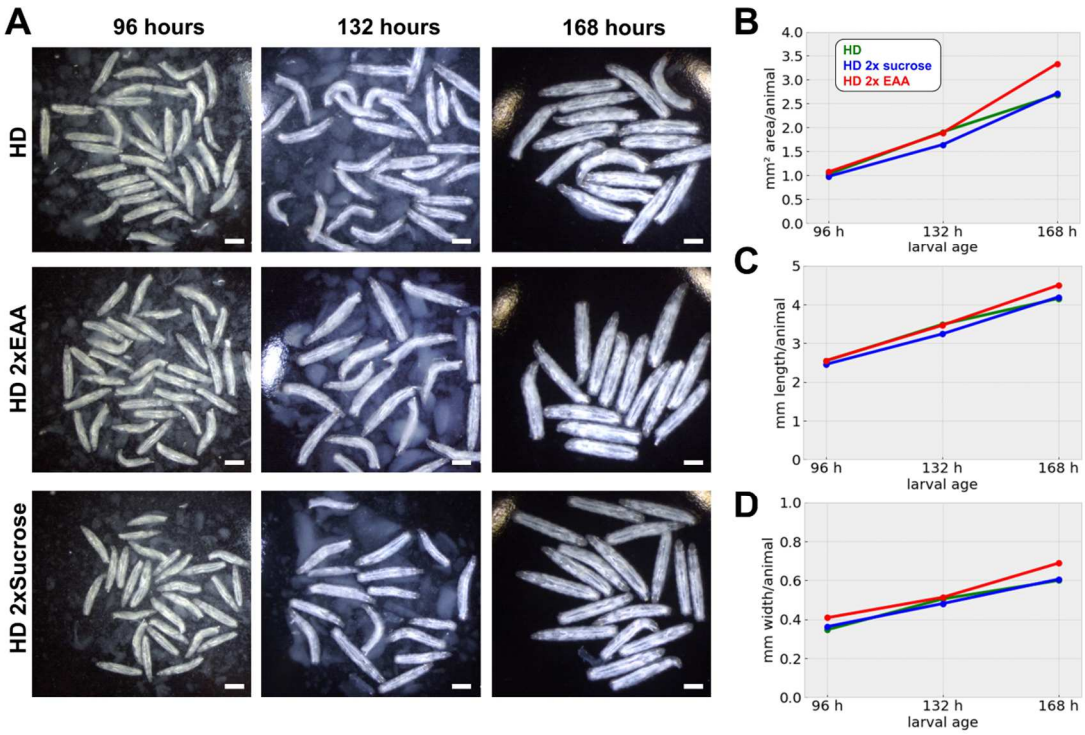

Figure S2: Larval size measurements. (A) Larvae were raised on HD, HD with 2xsucrose or HD with 2x EAA and images were recorded at the indicated time points under a dissecting microscope. The images served the subsequent quantification of the area (B), length (C) and width (D) of the animals across development. Color code in (B-D) is: HD = green, HD with 2x sucrose = blue, and HD with 2x EAA = red. Scalebars in (A) represent 1 *mm*.

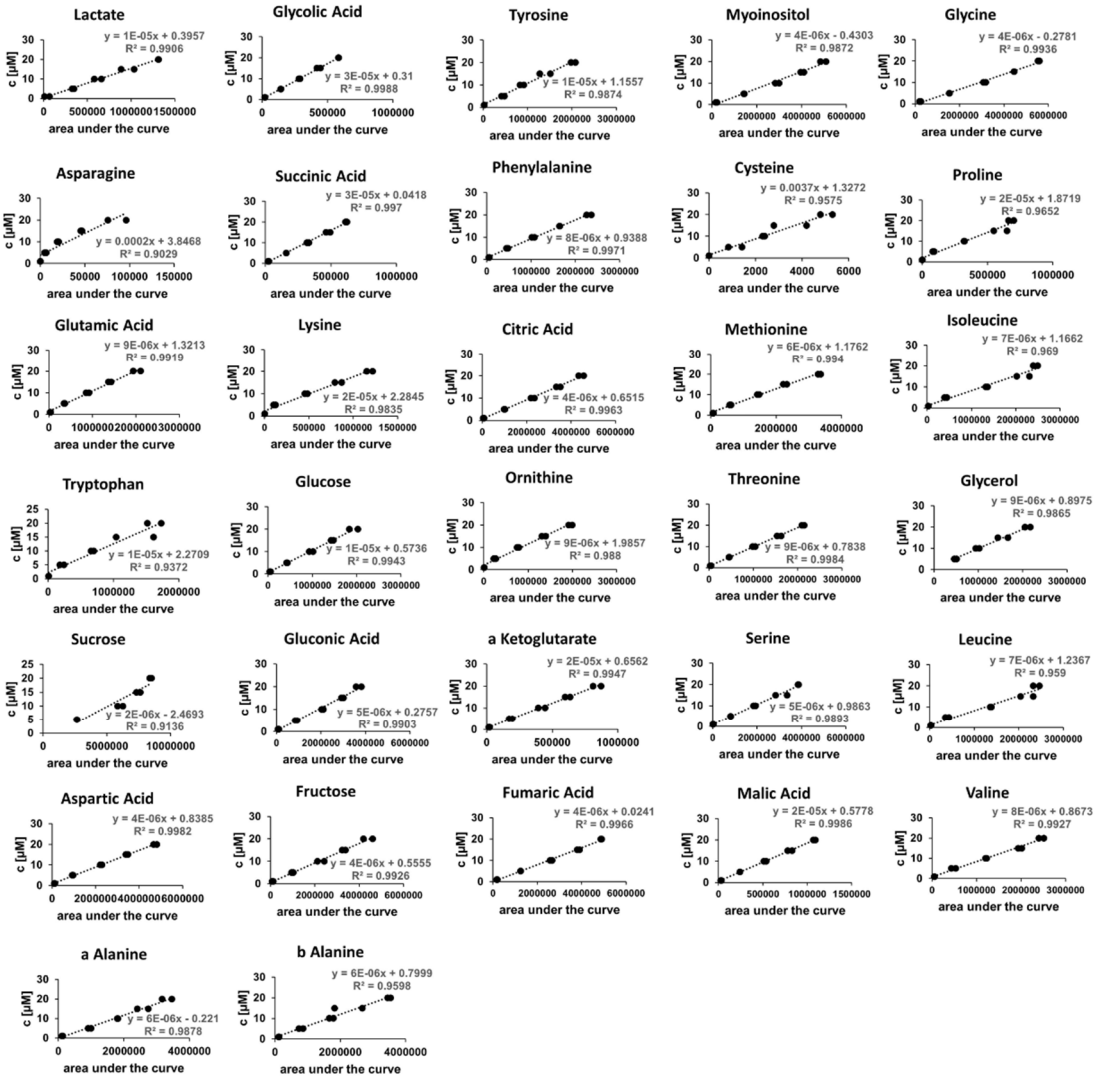

Figure S3: GC-MS calibration curves. Five-point calibration curves for the GC-MS metabolomics measurements (data provided in Table S2).

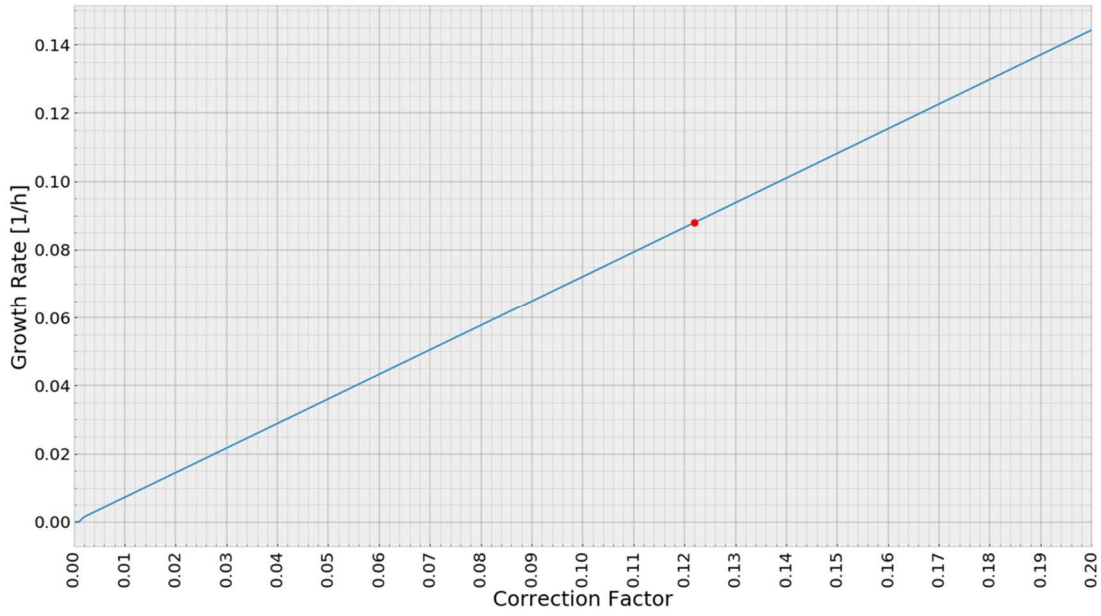

Figure S4: Larval food intake correction factor. Determination of a correction factor for the calculation of the larval food intake rate (for details see main text and methods section).

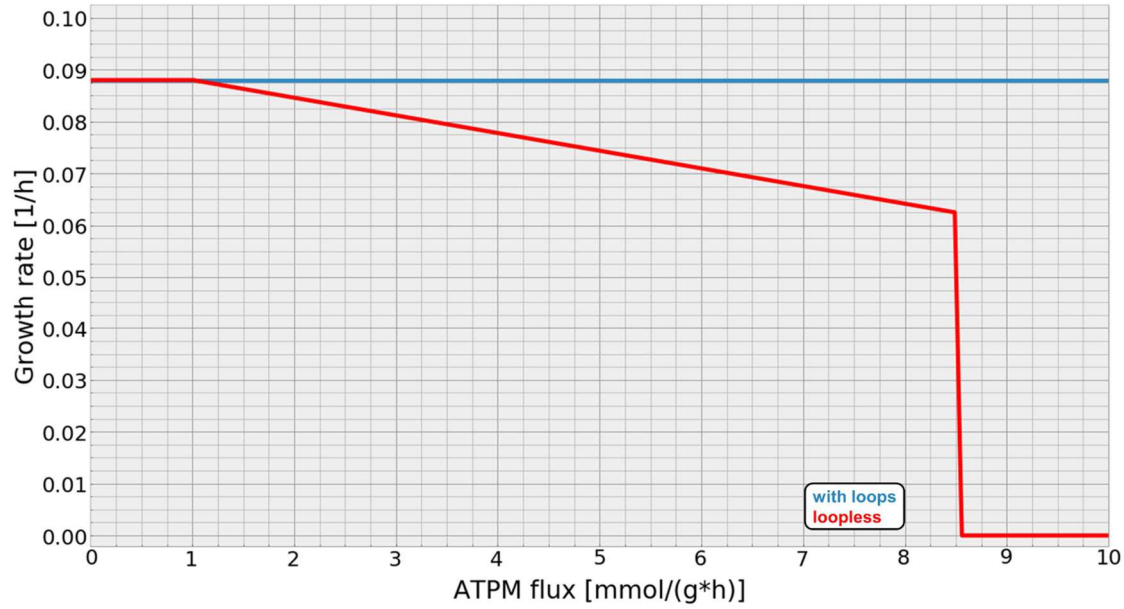

Figure S5: NGAM value determination. Iterative determination of the NGAM value by fixing the oxygen uptake rate to the oxygen consumption rate of S2R+ cells $\left(\mathbf{0.4788}\ \frac{mmol}{g\ dry\ weight*h}\right)$. The last ATPM flux value where growth was still possible was used as the NGAM value $\left(\mathbf{8.55}\ \frac{mmol}{g\ dry\ weight*h}\right)$.

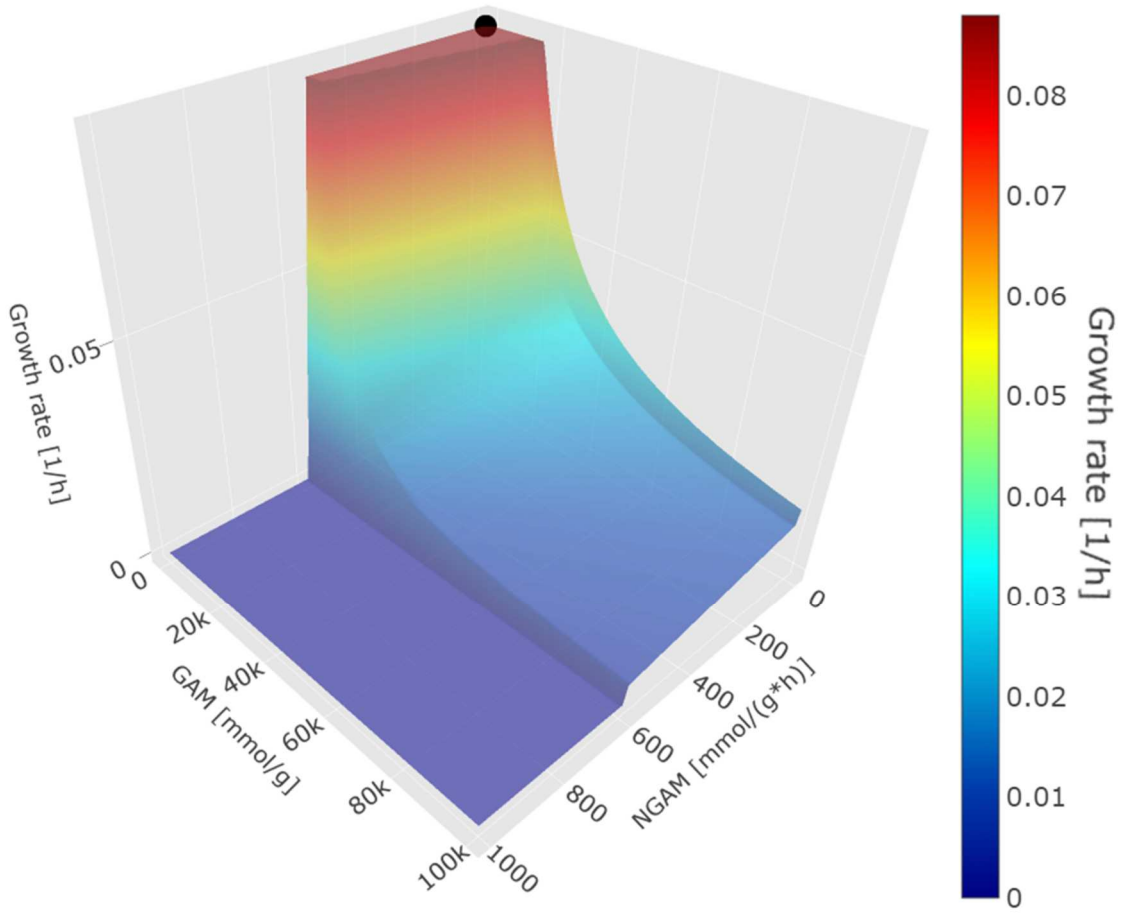

Figure S6: Impact of different GAM and NGAM coefficients on growth rate. Over a large range of values, GAM and NGAM do not prominently affect the maximal growth rate. Only very large values for GAM and NGAM result in a decreased growth rate or the complete cessation of biomass production. The black dot indicates the value set used for NGAM and GAM in our simulations. An interactive version of the figure is provided as Interactive Supplementary Figure 2.

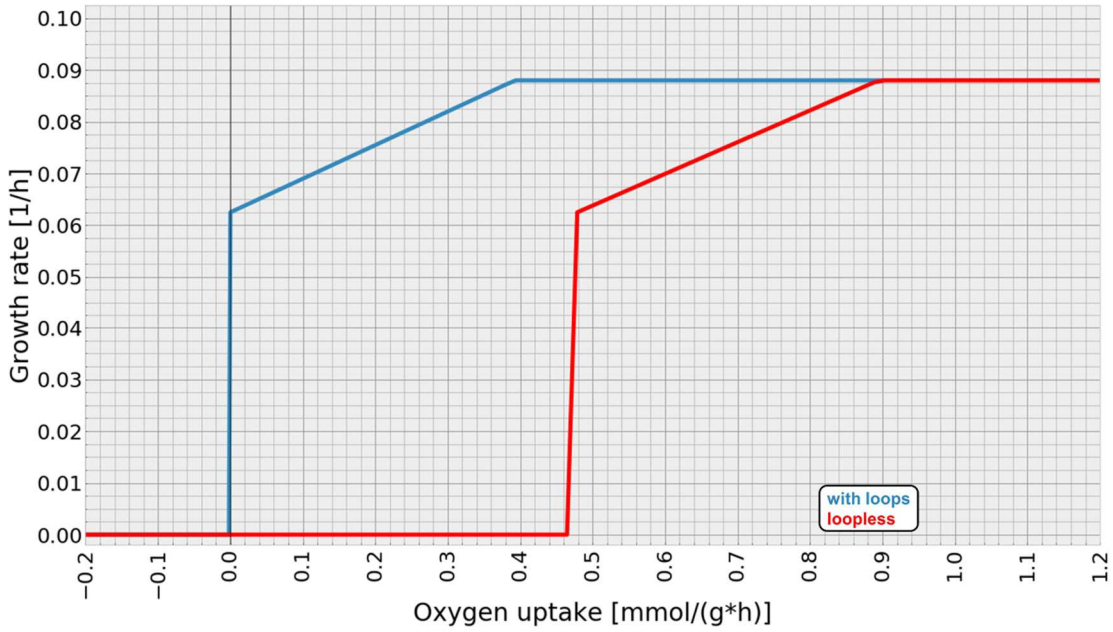

Figure S7: Growth rate solution comparison of loopless and with loop computations. Comparison between solving the FBA with loops (blue color) and loopless (red color). The solution with loops allows growth in the absence of oxygen, which is a biologically infeasible solution. All modeling steps were thus performed using loopless computations.

Amino acid	Frequency f_{AA}
Alanine	0.074
Arginine	0.055
Asparagine	0.047
Aspartic acid	0.052
Cysteine	0.020
Glutamic acid	0.066
Glutamine	0.054
Glycine	0.062
Histidine	0.026
Isoleucine	0.048
Leucine	0.087
Lysine	0.055
Methionine	0.022
Phenylalanine	0.033
Proline	0.058
Serine	0.086
Threonine	0.059
Tryptophan	0.009
Tyrosine	0.028
Valine	0.059

Figure S8: Frequency of amino acids in the *Drosophila* proteome. As we were missing amino acid measurements in the GC-MS/MS experiments, we sought to identify the remaining coefficients by bioinformatics. For details, see methods section.

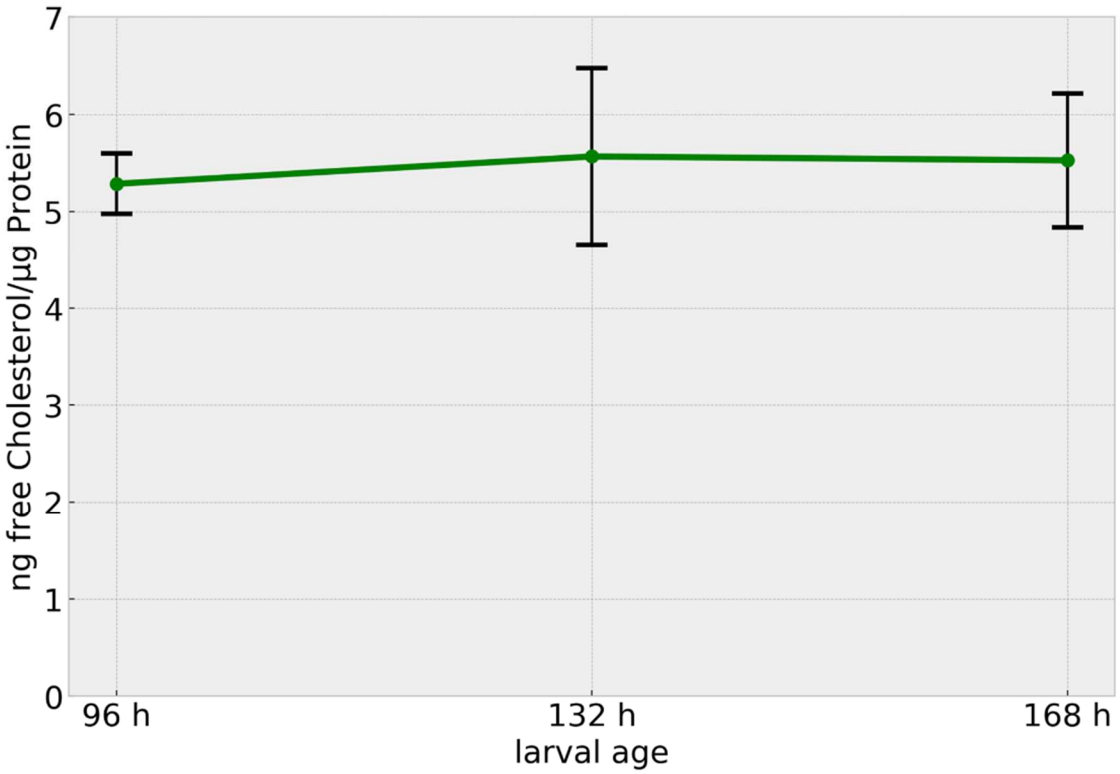

Figure S9: Free cholesterol measurements. We quantified the cholesterol content of larvae reared on the *Holidic diet* (between 96 h and 168 h after egg laying). The determined levels were almost constant.

Interactive Supplementary Figure 1: Interactive version of the FlySilico metabolic network (relates to Fig. 2). For download of the figure, please follow the link to the GitLab repository of the project:

https://gitlab.com/Beller-Lab/flysilico/tree/master/Supplementary_Data

The downloaded html figure file opens in the standard web browser of the system. Please mouse over the different elements of the network to obtain more information, as e.g. the nodes (metabolite details), the edges (reaction details) or the dots in the upper right corners of the colored boxes (reaction block details).

Interactive Supplementary Figure 2 (relates to Fig. S6): Interactive version of the GAM / NGAM simulation plot. For download of the figure, please follow the link to the GitLab repository of the project:

https://gitlab.com/Beller-Lab/flysilico/tree/master/Supplementary_Data

The downloaded html figure file opens in the standard web browser of the system. It can be rotated in all three axis and zoomed / repositioned with the mouse pointer.

References

Aktipis, C.A., Boddy, A.M., Gatenby, R.A., Brown, J.S., and Maley, C.C. (2013). Life history trade-offs in cancer evolution. Nature Reviews Cancer *13*, 883-892. https://doi.org/10.1038/nrc3606.

Alpatov, W.W. (1929). Growth and variation of the larvae of *Drosophila melanogaster*. J. Exp. Zool. *52*, 407-437. https://doi.org/10.1002/jez.1400520303.

Beadle, G.W., Tatum, E.L., and Clancy, C.W. (1938). Food level in relation to rate of development and eye pigmentation in *Drosophila melanogaster*. The Biological Bulletin *75*, 447-462. https://doi.org/10.2307/1537573.

Besson, A.A., Lagisz, M., Senior, A.M., Hector, K.L., and Nakagawa, S. (2016). Effect of maternal diet on offspring coping styles in rodents: a systematic review and meta-analysis. Biological reviews of the Cambridge Philosophical Society *91*, 1065-1080. https://doi.org/10.1111/brv.12210.

Bischoff, A.R., Portella, A.K., Paquet, C., Dalle Molle, R., Faber, A., Arora, N., Levitan, R.D., Silveira, P.P., and Dube, L. (2018). Low birth weight is associated with increased fat intake in school-aged boys. Br J Nutr *119*, 1295-1302. https://doi.org/10.1017/S0007114518000892.

Cardoso, J.G.R., Jensen, K., Lieven, C., Lærke Hansen, A.S., Galkina, S., Beber, M., Özdemir, E., Herrgård, M.J., Redestig, H., and Sonnenschein, N. (2018). Cameo: A Python Library for Computer Aided Metabolic Engineering and Optimization of Cell Factories. ACS Synthetic Biology *7*, 1163-1166. https://doi.org/10.1021/acssynbio.7b00423.

Carman, G.M., and Han, G.-S. (2006). Roles of phosphatidate phosphatase enzymes in lipid metabolism. Trends in Biochemical Sciences *31*, 694-699. https://doi.org/10.1016/j.tibs.2006.10.003.

Carvalho, M., Schwudke, D., Sampaio, J.L., Palm, W., Riezman, I., Dey, G., Gupta, G.D., Mayor, S., Riezman, H., and Shevchenko, A., et al. (2010). Survival strategies of a sterol auxotroph. Development *137*, 3675-3685. https://doi.org/10.1242/dev.044560.

Caspi, R., Billington, R., Ferrer, L., Foerster, H., Fulcher, C.A., Keseler, I.M., Kothari, A., Krummenacker, M., Latendresse, M., and Mueller, L.A., et al. (2016). The MetaCyc database of metabolic pathways and enzymes and the BioCyc collection of pathway/genome databases. Nucleic Acids Research *44*, D471-80. https://doi.org/10.1093/nar/gkv1164.

Chang, A., Scheer, M., Grote, A., Schomburg, I., and Schomburg, D. (2009). BRENDA, AMENDA and FRENDA the enzyme information system: new content and tools in 2009. Nucleic Acids Research *37*, D588-92. https://doi.org/10.1093/nar/gkn820.

Chen, J., Ou, Y., Yang, Y., Li, W., Xu, Y., Xie, Y., and Liu, Y. (2018). KLHL22 activates amino-acid-dependent mTORC1 signalling to promote tumorigenesis and ageing. Nature *557*, 585-589. https://doi.org/10.1038/s41586-018-0128-9.

Coquin, L., Feala, J.D., McCulloch, A.D., and Paternostro, G. (2008). Metabolomic and flux-balance analysis of age-related decline of hypoxia tolerance in *Drosophila* muscle tissue. Molecular Systems Biology *4*, 233. https://doi.org/10.1038/msb.2008.71.

Da-Ré, C., Pittà, C. de, Zordan, M.A., Teza, G., Nestola, F., Zeviani, M., Costa, R., and Bernardi, P. (2014). UCP4C mediates uncoupled respiration in larvae of *Drosophila melanogaster*. EMBO reports *15*, 586-591. https://doi.org/10.1002/embr.201337972.

Dashty, M. (2013). A quick look at biochemistry: carbohydrate metabolism. Clinical Biochemistry *46*, 1339-1352. https://doi.org/10.1016/j.clinbiochem.2013.04.027.

Davison, R., Boggs, C.L., and Baudisch, A. (2014). Resource allocation as a driver of senescence: life history tradeoffs produce age patterns of mortality. Journal of Theoretical Biology *360*, 251-262. https://doi.org/10.1016/j.jtbi.2014.07.015.

Dmitriew, C.M. (2011). The evolution of growth trajectories: what limits growth rate? Biological reviews of the Cambridge Philosophical Society *86*, 97-116. https://doi.org/10.1111/j.1469-185X.2010.00136.x.

Douglas, A.E. (2019). Simple animal models for microbiome research. Nature Reviews Microbiology *17*, 764-775. https://doi.org/10.1038/s41579-019-0242-1.

Edelaar, P. (2013). Comment on "Evolutionary trade-offs, Pareto optimality, and the geometry of phenotype space". Science *339*, 757. https://doi.org/10.1126/science.1228281.

Feala, J.D., Coquin, L., McCulloch, A.D., and Paternostro, G. (2007). Flexibility in energy metabolism supports hypoxia tolerance in *Drosophila* flight muscle: metabolomic and computational systems analysis. Molecular Systems Biology *3*, 99. https://doi.org/10.1038/msb4100139.

Feala, J.D., Coquin, L., Zhou, D., Haddad, G.G., Paternostro, G., and McCulloch, A.D. (2009). Metabolism as means for hypoxia adaptation: metabolic profiling and flux balance analysis. BMC Syst Biol *3*, 91. https://doi.org/10.1186/1752-0509-3-91.

Feist, A.M., and Palsson, B.O. (2010). The biomass objective function. Current opinion in microbiology *13*, 344-349. https://doi.org/10.1016/j.mib.2010.03.003.

Fellowes, M.D.E., Kraaijeveld, A.R., and Godfray, H.C.J. (1999). ASSOCIATION BETWEEN FEEDING RATE AND PARASITOID RESISTANCE IN *DROSOPHILA MELANOGASTER*.

Evolution; international journal of organic evolution *53*, 1302-1305. https://doi.org/10.1111/j.1558-5646.1999.tb04544.x.

Fiehn, O., Kopka, J., Dörmann, P., Altmann, T., Trethewey, R.N., and Willmitzer, L. (2000). Metabolite profiling for plant functional genomics. Nature biotechnology *18*, 1157-1161. https://doi.org/10.1038/81137.

Garcia Caraballo, S.C., Comhair, T.M., Dejong, C.H.C., Lamers, W.H., and Köhler, S.E. (2014). A high-protein diet is anti-steatotic and has no pro-inflammatory side effects in dyslipidaemic APOE2 knock-in mice. Br J Nutr *112*, 1251-1265. https://doi.org/10.1017/S0007114514001986.

Geoghegan, V., Stainton, K., Rainey, S.M., Ant, T.H., Dowle, A.A., Larson, T., Hester, S., Charles, P.D., Thomas, B., and Sinkins, S.P. (2017). Perturbed cholesterol and vesicular trafficking associated with dengue blocking in *Wolbachia*-infected *Aedes aegypti* cells. Nature Communications *8*, 526. https://doi.org/10.1038/s41467-017-00610-8.

Gluckman, P.D., Lillycrop, K.A., Vickers, M.H., Pleasants, A.B., Phillips, E.S., Beedle, A.S., Burdge, G.C., and Hanson, M.A. (2007). Metabolic plasticity during mammalian development is directionally dependent on early nutritional status. Proc. Natl. Acad. Sci. U.S.A. *104*, 12796-12800. https://doi.org/10.1073/pnas.0705667104.

Gramates, L.S., Marygold, S.J., Santos, G.d., Urbano, J.-M., Antonazzo, G., Matthews, B.B., Rey, A.J., Tabone, C.J., Crosby, M.A., and Emmert, D.B., et al. (2017). FlyBase at 25: looking to the future. Nucleic Acids Research *45*, D663-D671. https://doi.org/10.1093/nar/gkw1016.

Gudmundsson, S., and Thiele, I. (2010). Computationally efficient flux variability analysis. BMC bioinformatics *11*, 489. https://doi.org/10.1186/1471-2105-11-489.

Hastings, J., Owen, G., Dekker, A., Ennis, M., Kale, N., Muthukrishnan, V., Turner, S., Swainston, N., Mendes, P., and Steinbeck, C. (2016). ChEBI in 2016: Improved services and an expanding collection of metabolites. Nucleic Acids Research *44*, D1214-9. https://doi.org/10.1093/nar/gkv1031.

Hood, D.A., and Terjung, R.L. (1990). Amino acid metabolism during exercise and following endurance training. Sports Medicine *9*, 23-35. https://doi.org/10.2165/00007256-199009010-00003.

Jehrke, L., Stewart, F.A., Droste, A., and Beller, M. (2018). The impact of genome variation and diet on the metabolic phenotype and microbiome composition of *Drosophila melanogaster*. Sci Rep *8*, 6215. https://doi.org/10.1038/s41598-018-24542-5.

Kanehisa, M., Furumichi, M., Tanabe, M., Sato, Y., and Morishima, K. (2017). KEGG: new perspectives on genomes, pathways, diseases and drugs. Nucleic Acids Research *45*, D353-D361. https://doi.org/10.1093/nar/gkw1092.

Kauffman, K.J., Prakash, P., and Edwards, J.S. (2003). Advances in flux balance analysis. Current Opinion in Biotechnology *14*, 491-496. https://doi.org/10.1016/j.copbio.2003.08.001.

King, Z.A., Lu, J., Dräger, A., Miller, P., Federowicz, S., Lerman, J.A., Ebrahim, A., Palsson, B.O., and Lewis, N.E. (2016). BiGG Models: A platform for integrating, standardizing and sharing genome-scale models. Nucleic Acids Research *44*, D515-22. https://doi.org/10.1093/nar/gkv1049.

Knott, S.R.V., Wagenblast, E., Khan, S., Kim, S.Y., Soto, M., Wagner, M., Turgeon, M.-O., Fish, L., Erard, N., and Gable, A.L., et al. (2018). Asparagine bioavailability governs metastasis in a model of breast cancer. Nature *554*, 378-381. https://doi.org/10.1038/nature25465.

Koyama, T., Rodrigues, M.A., Athanasiadis, A., Shingleton, A.W., and Mirth, C.K. (2014). Nutritional control of body size through FoxO-Ultraspiracle mediated ecdysone biosynthesis. eLife *3*. https://doi.org/10.7554/eLife.03091.

Kuzawa, C.W. (2007). Developmental origins of life history: growth, productivity, and reproduction. American journal of human biology : the official journal of the Human Biology Council *19*, 654-661. https://doi.org/10.1002/ajhb.20659.

Landmann, F. (2019). The *Wolbachia* Endosymbionts. Microbiology Spectrum *7*. https://doi.org/10.1128/microbiolspec.BAI-0018-2019.

Levin, B.E. (2006). Metabolic imprinting: critical impact of the perinatal environment on the regulation of energy homeostasis. Philosophical transactions of the Royal Society of London. Series B, Biological sciences *361*, 1107-1121. https://doi.org/10.1098/rstb.2006.1851.

Limones, M., Sevillano, J., Sánchez-Alonso, M.G., Herrera, E., and Del Ramos-Álvarez, M.P. (2019). Metabolic alterations associated with maternal undernutrition during the first half of gestation lead to a diabetogenic state in the rat. European Journal of Nutrition *58*, 2521-2533. https://doi.org/10.1007/s00394-018-1805-z.

Martínez, D., Pentinat, T., Ribó, S., Daviaud, C., Bloks, V.W., Cebrià, J., Villalmanzo, N., Kalko, S.G., Ramón-Krauel, M., and Díaz, R., et al. (2014). In utero undernutrition in male mice programs liver lipid metabolism in the second-generation offspring involving altered Lxra DNA methylation. Cell metabolism *19*, 941-951. https://doi.org/10.1016/j.cmet.2014.03.026.

Martins Conde, Patricia do Rosario, Sauter, T., and Pfau, T. (2016). Constraint Based Modeling Going Multicellular. Frontiers in Molecular Biosciences *3*, 3. https://doi.org/10.3389/fmolb.2016.00003.

Merkey, A.B., Wong, C.K., Hoshizaki, D.K., and Gibbs, A.G. (2011). Energetics of metamorphosis in *Drosophila melanogaster*. Journal of Insect Physiology *57*, 1437-1445. https://doi.org/10.1016/j.jinsphys.2011.07.013.

Mo, M.L., Palsson, B.O., and Herrgård, M.J. (2009). Connecting extracellular metabolomic measurements to intracellular flux states in yeast. BMC Syst Biol *3*, 37. https://doi.org/10.1186/1752-0509-3-37.

Moed, G.H. de, Kruitwagen, C.L.J.J., Jong, G. de, and Scharloo, W. (1999). Critical weight for the induction of pupariation in *Drosophila melanogaster*: genetic and environmental variation. J Evolution Biol *12*, 852-858. https://doi.org/10.1046/j.1420-9101.1999.00103.x.

Musselman, L.P., Fink, J.L., Narzinski, K., Ramachandran, P.V., Hathiramani, S.S., Cagan, R.L., and Baranski, T.J. (2011). A high-sugar diet produces obesity and insulin resistance in wild-type *Drosophila*. Disease models & mechanisms *4*, 842-849. https://doi.org/10.1242/dmm.007948.

Orth, J.D., Thiele, I., and Palsson, B.Ø. (2010). What is flux balance analysis? Nature biotechnology *28*, 245-248. https://doi.org/10.1038/nbt.1614.

Pietri, J.E., DeBruhl, H., and Sullivan, W. (2016). The rich somatic life of *Wolbachia*. MicrobiologyOpen *5*, 923-936. https://doi.org/10.1002/mbo3.390.

Piper, M.D.W., Blanc, E., Leitão-Gonçalves, R., Yang, M., He, X., Linford, N.J., Hoddinott, M.P., Hopfen, C., Soultoukis, G.A., and Niemeyer, C., et al. (2014). A holidic medium for *Drosophila melanogaster*. Nature methods *11*, 100-105. https://doi.org/10.1038/nmeth.2731.

Piper, M.D.W., Soultoukis, G.A., Blanc, E., Mesaros, A., Herbert, S.L., Juricic, P., He, X., Atanassov, I., Salmonowicz, H., and Yang, M., et al. (2017). Matching Dietary Amino Acid Balance to the *In silico*-Translated Exome Optimizes Growth and Reproduction without Cost to Lifespan. Cell metabolism *25*, 1206. https://doi.org/10.1016/j.cmet.2017.04.020.

Price, N.D., Famili, I., Beard, D.A., and Palsson, B.Ø. (2002). Extreme pathways and Kirchhoff's second law. Biophysical journal *83*, 2879-2882. https://doi.org/10.1016/S0006-3495(02)75297-1.

Reis, T. (2016). Effects of Synthetic Diets Enriched in Specific Nutrients on *Drosophila* Development, Body Fat, and Lifespan. PloS one *11*, e0146758. https://doi.org/10.1371/journal.pone.0146758.

Ryuda, M., Tsuzuki, S., Matsumoto, H., Oda, Y., Tanimura, T., and Hayakawa, Y. (2011). Identification of a novel gene, anorexia, regulating feeding activity via insulin signaling in *Drosophila melanogaster*. The Journal of biological chemistry *286*, 38417-38426. https://doi.org/10.1074/jbc.M111.267344.

Sang, J.H., and King, R.C. (1961). Nutritional Requirements of Axenically Cultured *Drosophila Melanogaster* Adults. Journal of Experimental Biology *38*, 793-809. https://doi.org/10.1242/jeb.38.4.793.

Schellenberger, J., Lewis, N.E., and Palsson, B.Ø. (2011). Elimination of thermodynamically infeasible loops in steady-state metabolic models. Biophysical journal *100*, 544-553. https://doi.org/10.1016/j.bpj.2010.12.3707.

Schuetz, R., Zamboni, N., Zampieri, M., Heinemann, M., and Sauer, U. (2012). Multidimensional optimality of microbial metabolism. Science *336*, 601-604. https://doi.org/10.1126/science.1216882.

Shao, D., Villet, O., Zhang, Z., Choi, S.W., Yan, J., Ritterhoff, J., Gu, H., Djukovic, D., Christodoulou, D., and Kolwicz, S.C., et al. (2018). Glucose promotes cell growth by suppressing branched-chain amino acid degradation. Nature Communications *9*, 2935. https://doi.org/10.1038/s41467-018-05362-7.

Shoval, O., Sheftel, H., Shinar, G., Hart, Y., Ramote, O., Mayo, A., Dekel, E., Kavanagh, K., and Alon, U. (2012). Evolutionary trade-offs, Pareto optimality, and the geometry of phenotype space. Science *336*, 1157-1160. https://doi.org/10.1126/science.1217405.

Shoval, O., Sheftel, H., Shinar, G., Hart, Y., Ramote, O., Mayo, A., Dekel, E., Kavanagh, K., and Alon, U. (2013). Response to comment on "Evolutionary trade-offs, Pareto optimality, and the geometry of phenotype space". Science *339*, 757. https://doi.org/10.1126/science.1228921.

Szekely, P., Korem, Y., Moran, U., Mayo, A., and Alon, U. (2015). The Mass-Longevity Triangle: Pareto Optimality and the Geometry of Life-History Trait Space. PLOS Computational Biology *11*, e1004524. https://doi.org/10.1371/journal.pcbi.1004524.

Tarry-Adkins, J.L., Aiken, C.E., Ashmore, T.J., Fernandez-Twinn, D.S., Chen, J.-H., and Ozanne, S.E. (2019). A suboptimal maternal diet combined with accelerated postnatal growth results in an altered aging profile in the thymus of male rats. The FASEB Journal *33*, 239-253. https://doi.org/10.1096/fj.201701350RR.

Tennessen, J.M., Barry, W.E., Cox, J., and Thummel, C.S. (2014). Methods for studying metabolism in *Drosophila*. Methods *68*, 105-115. https://doi.org/10.1016/j.ymeth.2014.02.034.

Thiele, I., and Palsson, B.Ø. (2010). A protocol for generating a high-quality genome-scale metabolic reconstruction. Nat Protoc *5*, 93-121. https://doi.org/10.1038/nprot.2009.203.

Vijendravarma, R.K., Narasimha, S., and Kawecki, T.J. (2012). Chronic malnutrition favours smaller critical size for metamorphosis initiation in *Drosophila melanogaster*. J Evolution Biol *25*, 288-292. https://doi.org/10.1111/j.1420-9101.2011.02419.x.

Votruba, S.B., and Jensen, M.D. (2007). Regional fat deposition as a factor in FFA metabolism. Annual Review of Nutrition *27*, 149-163. https://doi.org/10.1146/annurev.nutr.27.061406.093754.

Waldbauer, G.P. (1968). The Consumption and Utilization of Food by Insects (Elsevier) *5*, 229-288.

Werthebach, M., Stewart, F.A., Gahlen, A., Mettler-Altmann, T., Akhtar, I., Maas-Enriquez, K., Droste, A., Eichmann, T.O., Poschmann, G., and Stühler, K., et al. (2019). Control of *Drosophila* Growth and Survival by the Lipid Droplet-Associated Protein CG9186/Sturkopf. Cell Reports *26*, 3726-3740.e7. https://doi.org/10.1016/j.celrep.2019.02.110.

Wheeler, D.L., Barrett, T., Benson, D.A., Bryant, S.H., Canese, K., Chetvernin, V., Church, D.M., Dicuccio, M., Edgar, R., and Federhen, S., et al. (2008). Database resources of the National Center for Biotechnology Information. Nucleic Acids Research *36*, D13-21. https://doi.org/10.1093/nar/gkm1000.

Zinke, I., Kirchner, C., Chao, L.C., Tetzlaff, M.T., and Pankratz, M.J. (1999). Suppression of food intake and growth by amino acids in *Drosophila*: the role of pumpless, a fat body expressed gene with homology to vertebrate glycine cleavage system. Development (Cambridge, England) *126*, 5275-5284. https://doi.org/10.1242/dev.126.23.5275.

2.2. Modeling *Drosophila* gut microbe interactions reveals metabolic interconnectivity

Author: Jürgen W. Schönborn, Fiona A. Stewart, Kerstin Maas Enriquez, Irfan Akhtar, Andrea Droste, Silvio Waschina, and Mathias Beller

Contribution of Jürgen Wilhelm Schönborn:

- wrote the original draft; manuscript correction and proofreading
- designed the experiments/study
- designed the graphical abstract, figures and tables
- parametrization of the modeling experiments
- performed the genome reassembly
- performed the modeling experiments
- evaluated and analyzed the modeling data
- devised, contributed and analyzed the growth-promoting experiments

This article was published in iScience; 24(11): Schönborn, J. W., Stewart, F. A., Enriquez, K. M., Akhtar, I., Droste, A., Waschina, S., & Beller, M., Modeling *Drosophila* gut microbe interactions reveals metabolic interconnectivity, 103216, Copyright Elsevier (2021)

Modeling *Drosophila* gut microbe interactions reveals metabolic interconnectivity

Jürgen W. Schönborn[1,2], Fiona A. Stewart[1,2], Kerstin Maas Enriquez[1,2], Irfan Akhtar[1,2], Andrea Droste[1,2], Silvio Waschina[3], and Mathias Beller[1,2,*]

1 Institut für Mathematische Modellierung Biologischer Systeme, Heinrich-Heine-Universität Düsseldorf, 40225 Düsseldorf, Germany

2 Systembiologie des Fettstoffwechsels, Heinrich-Heine-Universität Düsseldorf, 40225 Düsseldorf, Germany

3 Christian-Albrechts-University Kiel, Institute of Human Nutrition and Food Science, Nutriinformatics, Heinrich-Hecht-Platz 10, 24118 Kiel, Germany

* Lead contact: mathias.beller@hhu.de

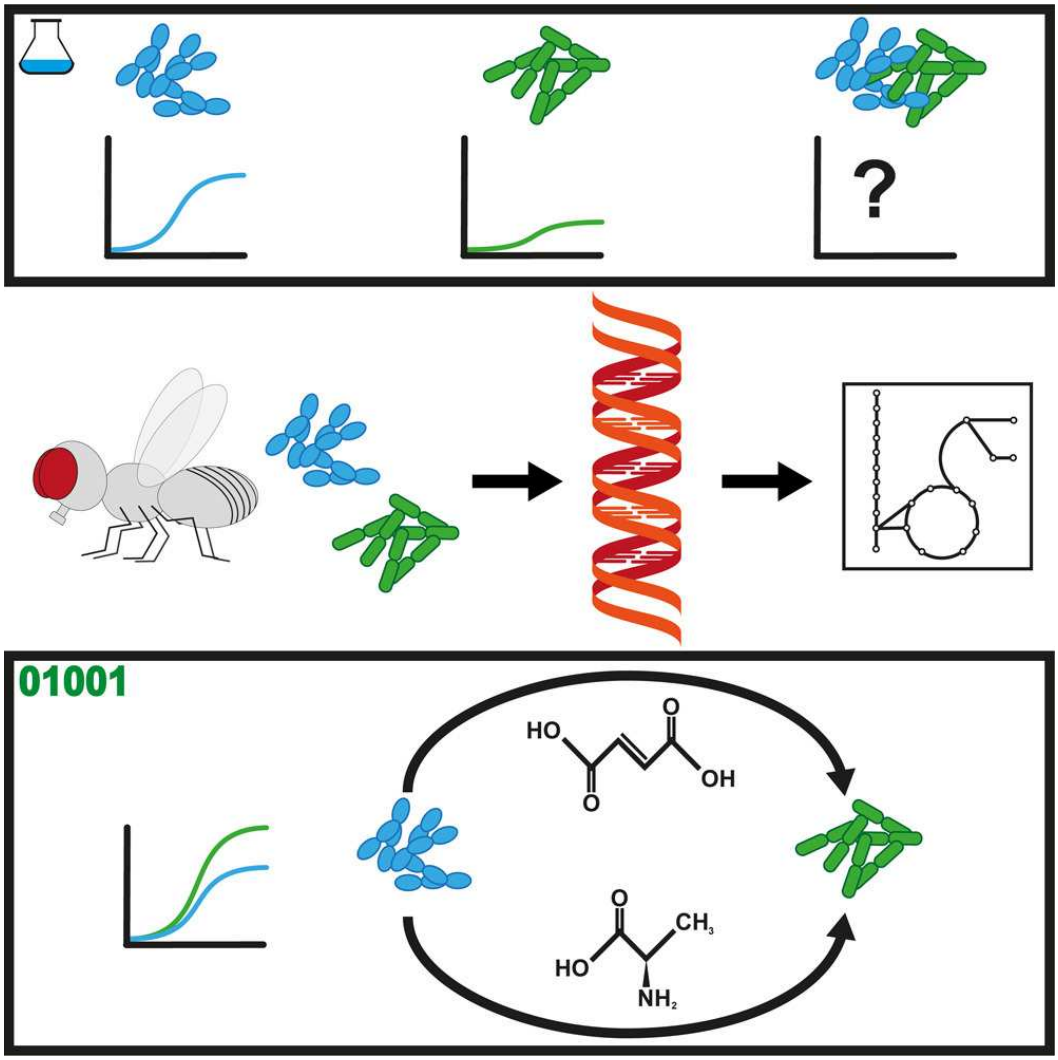

Graphical abstract

Summary

We know a lot about varying gut microbiome compositions. Yet, how the bacteria affect each other remains elusive. In mammals, this is largely based on the sheer complexity of the microbiome with at least hundreds of different species. Thus, model organisms such as *Drosophila melanogaster* are commonly used to investigate mechanistic questions as the microbiome consists of only about 10 leading bacterial species. Here, we isolated gut bacteria from laboratory-reared *Drosophila*, sequenced their respective genomes, and used this information to reconstruct genome-scale metabolic models. With these, we simulated growth in mono- and co-culture conditions and different media including a synthetic diet designed to grow *Drosophila melanogaster*. Our simulations reveal a synergistic growth of some but not all gut microbiome members, which stems on the exchange of distinct metabolites including tricarboxylic acid cycle intermediates. Culturing experiments confirmed our predictions. Our study thus demonstrates the possibility to predict microbiome-derived growth-promoting cross-feeding.

Introduction

Multicellular organisms are inhabited by a vast number of microorganisms, which is generally termed the microbiome. In humans, the number of associated bacteria is in the same range as the cells of the host (Sender et al. 2016) . As an entity, the bacteria encode an overwhelming number of genes and thus expand the metabolic capabilities of the host enormously. We are still at the beginning of understanding this metabolic interplay. Yet, first reports demonstrated an importance of the microbes present in the gut, the so-called gut microbiome, in humans and model organisms for increasing nutrient availability and energy harvest (Krajmalnik-Brown 2012), the production of important bioactive metabolites including branched-chain amino acids (Lin et al. 2017; Liu et al. 2020), the metabolism of pharmaceuticals applied to the host (Clayton et al. 2009; Haiser et al. 2013), or the release of metabolites which affect signaling pathways of the host (Shin et al. 2011; Martin et al. 2019). Thus, the microbiome affects the host far beyond nutrient access. The importance of the gut microbiome can be

seen most prominently in times of a perturbation or altered microbiome composition, which has been linked to many human diseases such as diabetes (Hartstra et al. 2014; Komaroff 2016), obesity (Turnbaugh and Gordon 2009; Tilg and Kaser 2011), autism (Vuong and Hsiao 2017) or inflammatory bowel disease (Halfvarson et al. 2017). Based on the observation that a perturbed microbiome is linked to pathologies, microbiome-focused therapies appear possible. Indeed, microbiome transfer therapies proved effective for the treatment of infections with the pathogen *Clostridium difficile* (Weingarden et al. 2014) and many pro- and prebiotic dietary regimens are already used (Arora et al. 2013).

The microbiome of mammals with hundreds to thousands of different bacterial species is extremely complex. In addition, many of these species cannot be cultured *ex vivo*, which hinders detailed functional analyses. Simpler model organisms can help to overcome these limitations and thus provide access to targeted functional analyses. The microbiome of *Drosophila melanogaster*, for example, only consists of 5–20 different species (Douglas 2019; Ludington and Ja 2020), which makes it much easier to analyze. Still, the gut microbiome of *Drosophila* has a significant impact on many aspects of the hosts' life such as the survival under nutrient limiting conditions, the lifespan of the flies, or the locomotor behavior (Consuegra et al. 2020a; Keebaugh et al. 2018; Ridley et al. 2012; Schretter et al. 2018; Shin et al. 2011; Silva et al. 2020; Storelli et al. 2011; Storelli et al. 2018) The most abundant *Drosophila* gut bacteria belong to the *Lactobacilli*, *Acetobacter*, and *Enterococci* genera. Key species of these bacteria are culturable under standard laboratory conditions (Adair et al. 2018; Broderick and Lemaitre 2012; Erkosar et al. 2013).

The prominent *Drosophila* gut microbiome members *Lactobacillus plantarum* and *Lactobacillus brevis* are Gram-positive rod-shaped lactic acid-producing microaerophilic bacteria from the Firmicutes phylum, which promote the systemic growth of fly larvae under nutrient-limiting conditions (Storelli et al. 2011). In humans, several lactobacilli strains have been shown to confer host health benefits (Marco et al. 2010), and a decline in their abundance is commonly associated with diseases (Aron-Wisnewsky et al. 2020; Heeney et al. 2018; Lee 2020; Schwarzer et al. 2016). *Acetobacter* in contrast are Gram-negative, acetic acid-producing bacteria within the class of alpha-proteobacteria. They can be

isolated from a variety of sources such as fruits and flowers and are often used to generate fermented food, e.g., vinegar (Azuma et al. 2009). *Acetobacter* species are major constituents of the *Drosophila* gut microbiome. Like lactobacilli (Storelli et al. 2011), they contribute to a successful larval development under nutrient-limiting conditions (Shin et al. 2011). This growth-promoting effect was demonstrated to stem on the secretion of acetic acid, which interferes with the insulin signaling pathway of the fly (Shin et al. 2011). This observation underpins the importance of secreted metabolites in terms of an interaction not only with the host but also likely with other members of the gut microbiome. At this point, the beneficial as well as detrimental (e.g., in terms of competition for nutrients) interactions between the microbiome members are not clear. First analyses, however, detected a complex interplay between combinations of the bacterial species and the host, which shapes host fitness through life history trade-offs (Gould et al. 2018). Similarly, also studies with isolated bacteria using growth on agar-based solid media (Sommer and Newell 2018) or chemically defined media (Aumiller 2021) support growth-promoting effects among the bacterial species of the *Drosophila* gut microbiome.

In order to investigate such metabolic interactions, we isolated bacteria from laboratory-reared *Drosophila* and investigated their isolated growth in different media such as *Lactobacillus*-promoting MRS and *Acetobacter*-selective ACE media. Furthermore, we used a synthetic diet suitable to grow *D. melanogaster* (holidic *Drosophila* diet; HD) (Piper et al. 2014). Six bacterial strains were analyzed in total and we resequenced their respective genomes to reconstruct genome-scale metabolic networks. These were used in single and co-culture growth simulations using the BacArena software package (Bauer et al. 2017). Our results reveal co-operative growth of certain bacteria based on the exchange of distinct metabolites including tricarboxylic acid cycle (TCA) intermediates, certain sugars, as well as amino acids in the D- and L-form. In analogous growth experiments, we could confirm the growth-promoting effect of several identified metabolites. Thus, the simulations open the door to systematically investigate the metabolic interplay of gut microbiome constituents and to reveal beneficial metabolites, which can promote the growth of selected gut microbiome constituents.

Results

Bacterial isolation, species identification, and *in vitro* growth characteristics

We started our analysis with the isolation of bacteria from the intestine of *white[-]* and Oregon-R adult flies (see material and methods). First, we isolated in total six morphologically distinct colonies on either *Lactobacillus* growth-promoting MRS- or *Acetobacter*-enriching ACE-agar plates and subsequently extracted the respective genomic DNA of our pure cultures. The 16S rRNA gene region of all clones was amplified by PCR, subcloned, and sequenced to allow species identification by BLAST searches. In total, we isolated two *L. plantarum*, one *L. brevis*, two *Acetobacter indonesiensis*, and one *Acetobacter pasteurianus* strains (see Table 1).

We tested next the growth of the different bacteria in three different growth media (Figures 1 and 2). On top of the commonly used semi-defined MRS (*Lactobacillus* enriching medium; see materials and methods) and ACE (promoting *Acetobacter* growth; see materials and methods) liquid culturing media, we also tested for growth in a chemically defined (holidic diet [HD]) growth medium sufficient to culture *D. melanogaster* (Piper et al. 2014). All isolated lactobacilli were able to grow on the MRS medium (Figure 1A). *L. brevis*, however, showed a lower total growth than the two *L. plantarum* isolates (Figure 1A). On the ACE medium, all lactobacilli only showed low growth (Figure 1B) demonstrating the selectivity of the growth medium. In line with previous results (Consuegra et al. 2020a), *L. plantarum* grew relatively well on the HD, whereas *L. brevis* again only showed a low growth (Figure 1C). To our surprise, growth of the *Acetobacter* isolates did not differ much on the MRS and ACE media (Figures 2A and 2B). *A. indonesiensis* isolates showed prominent growth on the HD (Figure 2C). *A. pasteurianus*, in contrast only showed a relatively poor growth on the HD (Figure 2C). An overview of the experimentally determined growth rates is provided as Figure S1.

Table 1: Sequencing results, genome reassembly, and generated genome-scale model summaries. The upper part of the table summarizes the sequencing results in terms of the number of reads obtained for the six bacterial resequencing reactions. These sequencing results were mapped with the ASA³P software (Schwengers et al. 2020) to the respective reference genomes whose ID as well as NCBI accession is provided. The details of the mapping results in terms of the number and percent of used (as well as unmapped) reads, the number of detected genes, and the genome sequence length are provided. The resequenced genome sequences were subsequently used to build the genome-scale metabolic models (see materials and methods). The lower part of Table 1 provides the details of the six genome-scale models in terms of the number of reactions, metabolites, mapped genes, blocked and unbalanced, as well as exchange reactions. All sequencing, ASA3P, and model data are available at https://doi.org/10.17632/2tgjd6y4zb.1.

	L. plantarum (A2)	L. plantarum (B2)	L. brevis (B6)	A. indonesiensis (A4)	A. indonesiensis (A5)	A. pasteurianus (B5)
Genome assembly						
reads [#]	3587296	3638786	3277616	3319800	3387326	3239340
used reads [#]	2902970	3125105	1917270	2060518	2036898	2077587
used reads [%]	86.2	90.3	59.6	62.2	60.3	66.9
unmapped [#]	495436	353339	1324152	1254692	1345613	1070761
genes [#]	3676	3559	2595	3352	3364	3091
ref. genome sequence length (bp)	3581586	3581586	2340228	3396180	3396180	3007920
reference genome	BDGP2	BDGP2	ATCC 367	NBRC 16471	NBRC 16471	BDGP5
Metabolic models						
reactions [#]	1815	1815	1584	1931	1931	1796
metabolites [#]	1567	1567	1411	1763	1763	1673
genes [#]	657	658	473	631	632	580
blocked reactions [%]	40.1	40.1	41	43.3	43.3	43.7
unbalanced reactions [%]	9.4	9.4	10.2	8.2	8.2	8.5
exchange reactions [%]	9	9	9.9	7.5	7.5	7.7

Bacterium	Isolate	Ref. genome	NCBI ID	Link
Acetobacter pasteurianus	B5	BDGP5	ASM245613v1	https://www.ncbi.nlm.nih.gov/assembly/GCF_002456135.1/
Acetobacter indonesiensis	A4	NBRC 16471	ASM799107v1	https://www.ncbi.nlm.nih.gov/assembly/GCF_007991075.1/
Acetobacter indonesiensis	A5	NBRC 16471	ASM799107v1	https://www.ncbi.nlm.nih.gov/assembly/GCF_007991075.1/
Lactobacillus plantarum	A2	BDGP2	ASM229018v1	https://www.ncbi.nlm.nih.gov/assembly/GCF_002290185.1/
Lactobacillus plantarum	B2	BDGP2	ASM229018v1	https://www.ncbi.nlm.nih.gov/assembly/GCF_002290185.1/
Lactobacillus brevis	B6	ATCC 367	ASM1446v1	https://www.ncbi.nlm.nih.gov/assembly/GCF_000014465.1/

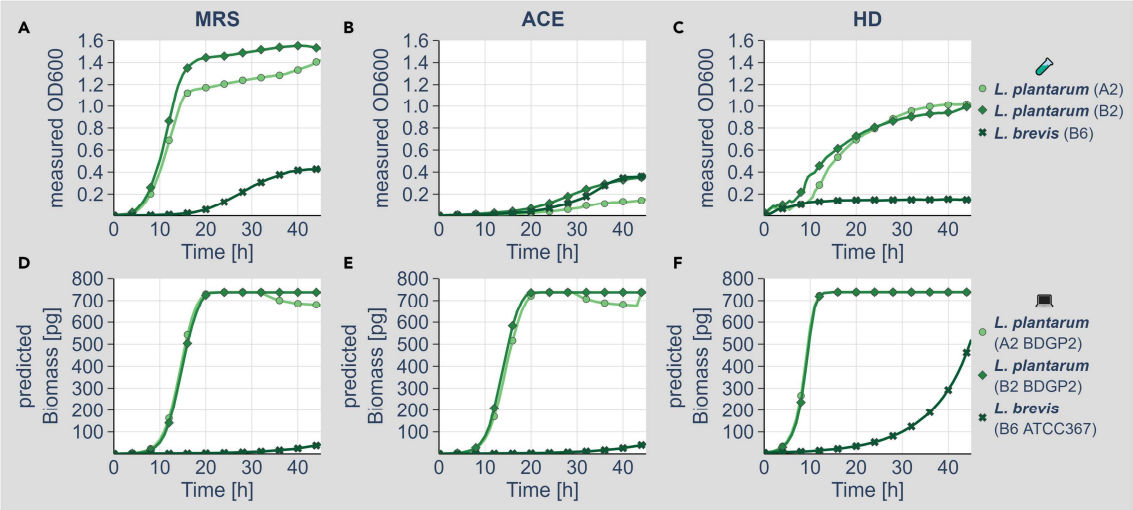

Figure 1: Wet-lab and *in silico* growth of *Lactobacillus* on different media. (A–C) Growth of the *Lactobacillus* isolates *L. plantarum* (A2, light green, dot), *L. plantarum* (B2, medium green, check), and *L. brevis* (B6, dark green, cross) on MRS (A), ACE (B), and HD (C) media. Growth of all bacteria was monitored for at least 45 h in a plate reader without shaking. All cultures were inoculated with a 1:1,000 dilution for MRS and ACE media and with a 1:100 dilution for the HD medium. All cultures had an optically dense pre-culture. Representative growth curves of at least three biologically independent experiments are shown. Growth curves show mean values of triplicate measurements. (D–F) Simulated growth of the same bacteria in the same media as shown in (A–C). For the isolated bacteria, the genomes were resequenced and used

to reconstruct genome-scale metabolic networks. These were used for growth simulations using the BacArena software package (Bauer et al. 2017) in combination with MRS (D), ACE (E), and HD (F) media. *L. plantarum* (A2, light green, dot), *L. plantarum* (B2, medium green, check), and *L. brevis* (B6, dark green, cross) on MRS (D), ACE (E), and HD (F) media. The simulations for each bacterium were run at least 12 times, and the computed growth curves represent the mean values. Detailed model data are available at https://doi.org/10.17632/2tgjd6y4zb.1. Wet-lab (A–C; small reaction tube) and *in silico* data (D–F; computer) are also indicated by the pictograms and labels on the right side of the figure.

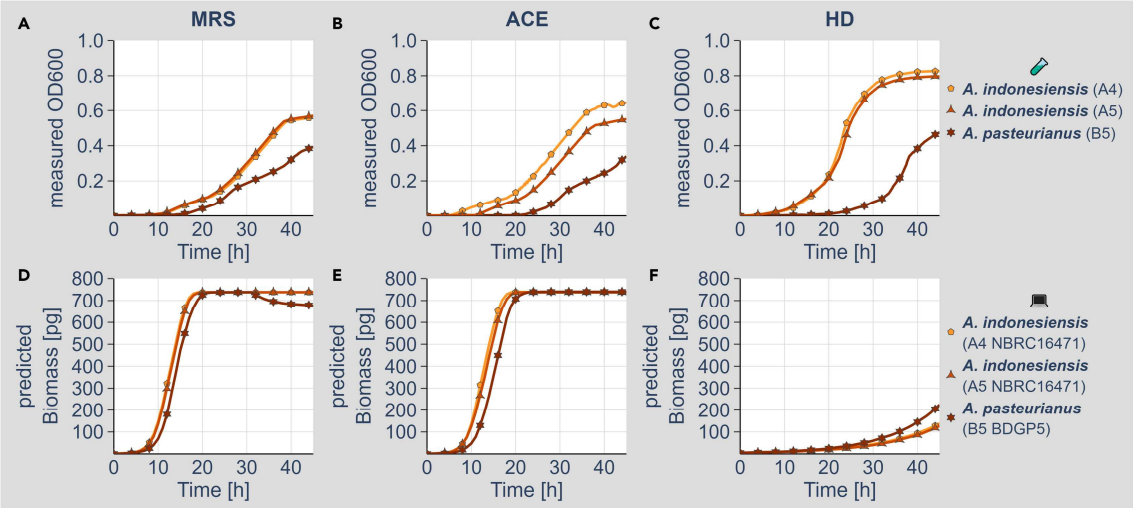

Figure 2: Wet-lab and *in silico* growth of *Acetobacter* on different media. (A–C) Growth of the *Acetobacter* isolates *A. indonesiensis* (A4, light orange, pentagon), *A. indonesiensis* (A5, medium orange, triangle), and *A. pasteurianus* (B5, dark orange, star) on MRS (A), ACE (B), and HD (C) media. Growth of all bacteria was monitored for at least 45 h in a plate reader with shaking. All cultures were inoculated with a 1:1,000 dilution for MRS and ACE media and with a 1:100 dilution for the HD medium. All cultures had an optically dense pre-culture. Representative growth curves of at least three biologically independent experiments are shown. Growth curves show mean values of triplicate measurements. For the isolated bacteria, the genomes were resequenced and used to reconstruct genome-scale metabolic networks. These were used for growth simulations using the BacArena software package (Bauer et al. 2017) in combination with MRS (D), ACE (E), and HD (F) media. (D–F) *A. indonesiensis* (A4, light orange, pentagon), *A. indonesiensis* (A5, medium orange, triangle), and *A. pasteurianus* (B5, dark orange, star) on MRS (D), ACE (E), and HD (F) media. The simulations for each bacterium were run at least 12 times, and the computed growth curves represent the mean values. Detailed model data are available at https://doi.org/10.17632/2tgjd6y4zb.1. Wet-lab (A-C; small reaction tube) and *in silico* data (D-F; computer) are also indicated by the pictograms and labels on the right side of the figure.

The determination of growth of single species cultures is trivial, whereas the determination of the individual contribution of distinct species to the biomass production of a consortium is difficult. Yet, a better understanding of the mutual effect on the growth of bacterial consortia is an intriguing and important question. Modeling experiments are a possibility to overcome this obstacle. For the modeling, an exact knowledge of the nutritional content of the growth medium is very important. Thus, growth of the bacteria on HD was particularly important, as this diet allows the exact description of the input for the modeling experiments. In the past, we already benefitted from this for modeling the growth and metabolism of *Drosophila* larvae (Schönborn et al. 2019). In order to reconstruct the genome-

scale metabolic networks of the isolated bacteria, our next step was to sequence their respective genomes using the Illumina MiSeq platform (see material and methods). In the following, the genomes were assembled using whole-genome information as a scaffold, which we obtained from the NCBI database.

Sequencing of the isolate genomes and model reconstruction

The sequencing runs resulted in 3.2–3.6 Mio reads per genome (see Table 1). The reads were mapped to the whole-genome sequences of *L. plantarum* BDGP2, *L. brevis* ATCC367, *A. indonesiensis* NBRC16471, and *A. pasteurianus* BDGP5, respectively, and further analyzed using the ASA³P software (Schwengers et al. 2020) (the complete dataset is available in the supplement). Between 60% and 90% of the total reads mapped to the respective reference strains (see Table 1).

We reconstructed the genome-scale metabolic models (for a summary cf. Table 1) of our isolated *Drosophila* gut bacteria using the *gapseq* pipeline (Zimmermann et al. 2021). As a last step in the model generation, we used *gapseq*'s in-built gap filling algorithm to enable *in silico* growth of the models on the one hand for the ACE/MRS media and on the other hand for the HD medium (see material and methods and Data S1). This additional step takes composition differences of the varying media into consideration. The ACE and MRS media are semi-defined owing to chemically complex components, which makes the *in silico* representation of the growth environment more difficult. We could explain between 73% and 92% of the unknown complex ingredients (yeast extract, peptone, and meat extract) by the help of information from the literature or the respective manufacturer. For HD such problems do not exist, as this medium is chemically completely defined (Piper et al. 2014). The overview of the diet parametrization is provided in Figure S2 as well as Data S2. In the course of generating the models, we took great care to correct for stochiometric inconsistencies, mass and charge imbalances, as well as metabolite connectivity (see materials and methods section and Table 1). All models were tested for model quality using the MEMOTE tool (Lieven et al. 2020) and resulted in at least 77% model scores (see Data S3 and materials and methods).

In silico biomass and signature metabolite production by the different genome-scale metabolic network models

In order to model growth of the different isolated gut bacteria alone as well as in combination, we performed dynamic and agent-based simulations of bacterial population growth and metabolic fluxes using the BacArena software package (Bauer et al. 2017). In brief, BacArena allows growth simulation of single-species population and multi-species microbial communities in a spatially limited compartment, including the calculations of the changing medium composition due to the metabolite utilization and production by individual bacterial cells. Thus, the metabolism of the organisms is calculated in a time-resolved manner with the biomass production as the objective function (for information concerning the biomass production and objective function, please see material and methods as well as Data S1). BacArena provides the metabolic fluxes, growth pattern, and concentrations of the medium for each time point of each individual species present in the *in silico* experiment. This allows the determination of possible cross-feeding and/or physiological interactions in a multi-species *in silico* culture experiment.

As a starting point, we performed single bacteria growth simulations in the three different media MRS, ACE, and HD. An uncertain parameter was the amount of oxygen entering the system. Acetobacteraceae are aerophilic, whereas lactobacilli are microaerophilic and tolerate only a small amount of oxygen. Furthermore, it is still unknown how much oxygen is present in the larval and adult *Drosophila* gut. Given that our goal was to model the situation within the *Drosophila* gut where the two genera would meet each other, we performed all simulations in the presence of 0.1 mM oxygen, which represents a microaerobic situation (Ito et al. 2002).

Of the lactobacilli, the two *L. plantarum* models showed good growth on all media (Figures 1D–1F). *L. brevis*, in contrast, showed only limited biomass production in the MRS, ACE, and HD simulations (Figures 1D–1F). The *A. indonesiensis* and *A. pasteurianus* models all result in strong biomass production in simulations utilizing the ACE and MRS media (Figures 2D and 2E). On the HD, however, all *Acetobacter* strain model simulations only showed low biomass production

(Figure 2F). When we compared our *in silico* growth simulation results to the actual wet-lab data (Figure S1), our lactobacilli simulations fitted the experimental data overall better. So far, the reasons for the discrepancies of the *Acetobacter* simulations are not clear. Yet, the appropriate simulation of growth magnitudes is inherently difficult using FBA (see discussion) and might depend on many parameters. For our experiments, however, we focused on the identification of growth dependencies and metabolite exchanges, which are only considering relative changes and are thus unaffected by these shortcomings.

Next, we investigated the production of certain signature metabolites by the different models. Several *Lactobacillus* species are able to use the phosphoketolase pathway and are thus heterolactic (Spector 2009). On top of the lactobacilli signature metabolite lactate, heterolactic bacteria also produce acetate. Here, we thus tested for a possible heterolactic behavior of our *L. plantarum* and *L. brevis* models. For the *Acetobacter* models, we did not expect such a behavior and only a prominent production of acetate.

As flux-balance simulations can vary to some extent in terms of individual flux predictions due to stochastic effects, we performed the simulations 100 times to identify the most likely metabolite production behavior (Figure S3). Figures 3 and S4 show representative simulation results (Data S4 is an interactive version of Figure 3, which provides all predicted metabolite productions). Lactate production was mostly limited to *L. plantarum* (B2) on the MRS and ACE diets, *L. plantarum* (A2) on the ACE diet, and *L. brevis* (B6) on the HD (Figures 3 and S3). None of the *Acetobacter* models produced lactate (Figures S3 and S4).

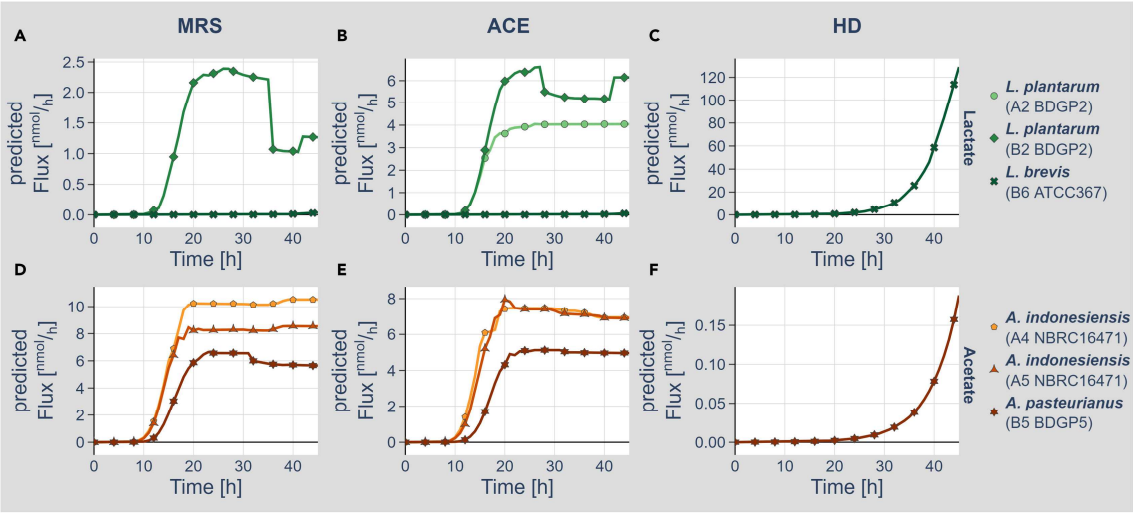

Figure 3: *In silico* production of signature metabolites by the different genome-scale metabolic network models. (A–C) Production of lactate by the *L. plantarum* (A2, light green, dot), *L. plantarum* (B2, medium green, check), and *L. brevis* (B6, dark green, cross) genome-scale models on MRS (A), ACE (B), and HD (C) media, respectively. (D–F) Production of acetate by the *A. indonesiensis* (A4, light orange, pentagon), *A. indonesiensis* (A5, medium orange, triangle), and *A. pasteurianus* (B5, dark orange, star) genome-scale models on MRS (D), ACE (E), and HD (F) media, respectively. Please note that not all models produced the respective signature metabolite on the given medium. Metabolite production curves represent mean values of at least 12 simulation runs. An interactive version of the figure is available as Data S4 and detailed model data are available at https://doi.org/10.17632/2tgjd6y4zb.1.

All *Acetobacter* model simulations resulted in prominent acetate production on the ACE and MRS growth media (Figures 3D, 3E and S3). Yet, on the HD only *A. pasteurianus* (B5) was producing acetate (Figures 3F and S3). For the *Lactobacilli*, only the two *L. plantarum* models showed prominent acetate production on the MRS and ACE media (Figures S3 and S4). On the HD, all *Lactobacilli* showed acetate production (Figures S3 and S4). Altogether, our simulations thus reveal a heterolactic behavior of the isolated lactobacilli as well as demonstrate the expected metabolite production for the *Acetobacter* models. Next, we investigated the co-culturing behavior *in silico*.

Simulating the co-culturing of *Lactobacillus* and *Acetobacter*

Our key question was whether bacteria present in the gut could affect each other's growth. For other gut microbiome members of the fly such beneficial metabolite exchange behavior could be recently demonstrated (Consuegra et al. 2020a; Henriques et al. 2020). For the species isolated in this study, we detected prominent growth differences in the different growth media *in vitro* (Figures 1 and 2) as well as *in silico* (Figures 1 and 2). Our hypothesis was that the growth of

co-cultures could be different from the growth of pure cultures based on the exchange of metabolites. If one is able to predict the impact of an exchange of metabolites between the different species of a gut microbiome as well as the impact of the metabolite exchange, one could design prebiotics, which means metabolites promoting the growth of a certain beneficial gut microbiome constituent. In order to test for such potential growth-promoting effects, we performed simulations comparing the mono-inoculations to all pair-wise combinations of *Acetobacter* and lactobacilli. In order to quantify potential growth effects, we first estimated the predicted biomass production after 45 h for the individual or co-cultured growth. Figures 4A–4C show the color-coded results for all individual and combined growth conditions on the MRS (A), ACE (B), and HD (C) media (all simulation data are available in the supplement). In Figures 4D–4F we highlight three detailed representative modeling outcomes from the overview representation in Figures 4A–4C (orange box in B relates to D, green box in B relates to E, and red box in C relates to F).

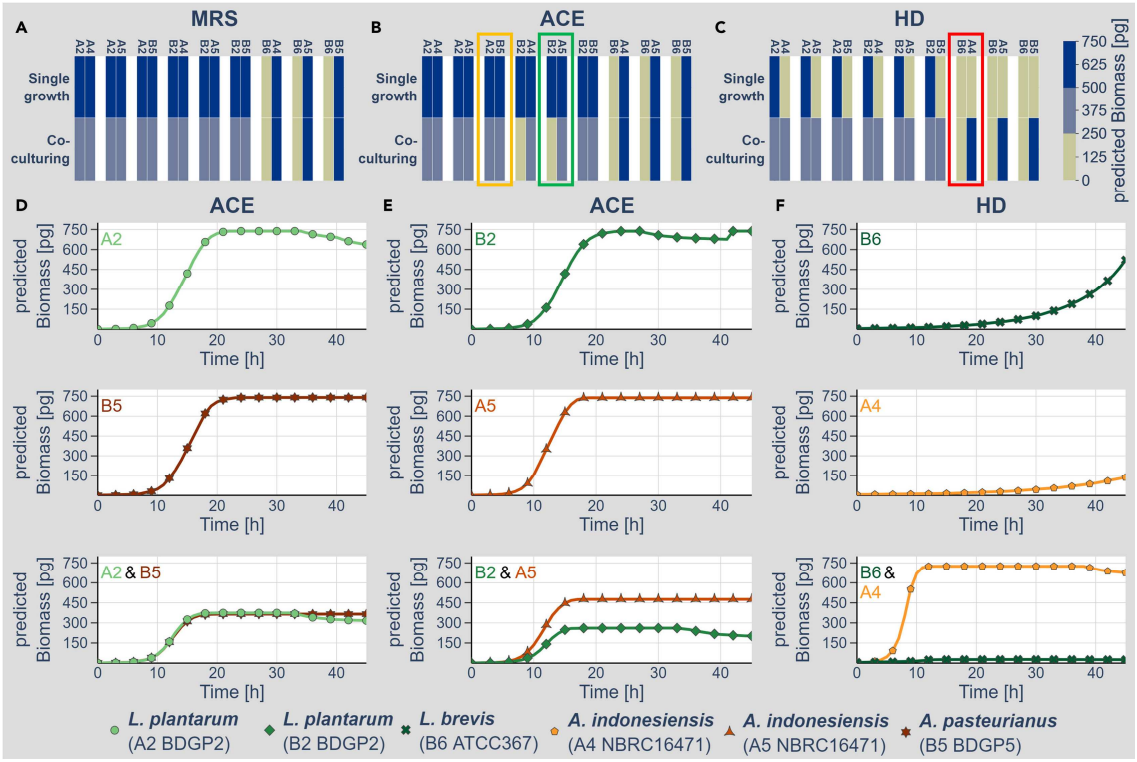

Figure 4: *In silico* co-culturing of *Lactobacillus* and *Acetobacter*. (A–C) We simulated the growth of all individual as well as pair-wise combinations of the *Lactobacilli* and *Acetobacter* models on the MRS (A), ACE (B), and HD (C) media. The plots summarize the color-coded biomass produced after 45 h of simulated growth. Total amount of produced biomass from 0–250 pg: beige, equals no or weak growth; 250–500 pg of predicted biomass: light blue; equals intermediate growth, and 500–750 pg of predicted biomass: dark blue; equals strong growth. (D–F) Detailed time-resolved data for three different examples of single organism growth simulations as well as the simulated growth of the combination of the bacteria. D (refers to orange

box in B) shows an example of the most trivial growth behavior, where the combination of *L. plantarum* (A2, light green, dot) and *A. pasteurianus* (B5, dark orange, star) on the ACE medium limits the growth of each other based on the impact of space and resource competition. E (relates to green box in B) shows an example of a detrimental outcome of the combination of bacteria. *L. plantarum* (B2, medium green, check) and *A. indonesiensis* (A5, medium orange, triangle) grow individually well on the ACE medium. The combination, however, results in a prominent block of the *Lactobacillus* growth, perhaps due to resource competition effects. F (relates to red box in C) shows a probiotic activity of *L. brevis* (B6, dark green, cross) on the growth of *A. indonesiensis* (A4, light orange, pentagon) on the HD. Both bacteria individually only show minute biomass production on the HD, whereas the combination results in a prominent growth of *A. indonesiensis* (A4, light orange, pentagon).

First, we consider the predicted growth curves of singular (upper two panels) or combined (lowest panel) *L. plantarum* (A2) and *A. pasteurianus* (B5) on ACE medium (Figure 4D) as an example of a trivial growth behavior. Both bacteria individually grow very well on the ACE medium. When combined, however, the available space gets limiting and thus both bacteria just reach half of the arbitrarily set maximum possible biomass production of 750 pg. Thus, the two bacteria only affected their mutual growth in terms of a limitation of the available resources. The combination of bacteria, however, can also result in non-trivial growth effects. Simulations with the *L. plantarum* (B2) and *A. indonesiensis* (A5) models on the ACE medium, for example, result individually in very high biomass production (Figure 4E). Yet in combination, the *Acetobacter* model results in higher biomass production, whereas the *Lactobacillus* model results in much lower biomass production (Figure 4E). Thus, the presence of *Acetobacter* apparently limits the biomass production of the *Lactobacillus* model, perhaps by winning the competition about the available resources.

Most striking, however, the combination of *L. brevis* B6 and *A. indonesiensis* A4, which individually produce on the HD only very little biomass in simulations (Figure 4F), results in a surprisingly prominent biomass production of *Acetobacter* (Figure 4F). In fact, the combination of *L. brevis* (B6) and all *Acetobacter* models resulted in such a growth behavior (Figure 4C). Thus, only a small amount of *Lactobacillus* was necessary to allow prominent biomass production of the *Acetobacter* model and *Lactobacillus* serves as a probiotic for *Acetobacter* in our simulations.

Analysis for metabolites exchanged between *Acetobacter* and *Lactobacillus*

The results of our co-occurrence simulations suggest that growth interdependencies between the different gut bacteria exist. Ultimately, the simulations should result in predictions ready to test in *in vivo* experiments. Thus, we concentrated on the following on the growth simulations performed with the HD, as with this defined diet, we can control and fine-tune its constituents. In addition, this diet can also be used in the future to monitor the growth of the bacteria in combination with their natural host *D. melanogaster*. In terms of a probiotic activity of *L. brevis* for *A. indonesiensis* we envisioned that the *Lactobacillus* either removed a growth-inhibiting or secreted a growth-promoting factor thus enabling *Acetobacter* to produce biomass in our simulations. Thus, we monitored the excretion and uptake rates of both bacteria over time within the simulations. For an easier detection of a net efflux or uptake, we formed a quotient between the individual uptake rates and normalized the values (see materials and methods). This allowed us to plot the exchange reactions in a heatmap (Figure 5) where a positive value means that both bacteria take up or excrete the given metabolite and a negative value means that the bacteria show a reciprocal metabolite transport behavior. Thus, a negative value is consistent with the excretion of a given metabolite from one bacterium and the uptake of the same metabolite by the other species. Figure 5 shows the situation after 32 h of growth (see Data S5 for an interactive version of the figure providing the data for all time points). Many transport reactions had a positive sign, and thus the direction of the transport pointed in the same direction in both bacteria. Few reactions, however, consistently showed a negative sign, which is in line with an exchange of the given metabolite. Among those, D-Alanine, L-Arginine, D-Ribose, Acetaldehyde, Fumarate, and Butane-2,3-diol (BDOH) showed the most prominent exchange behavior.

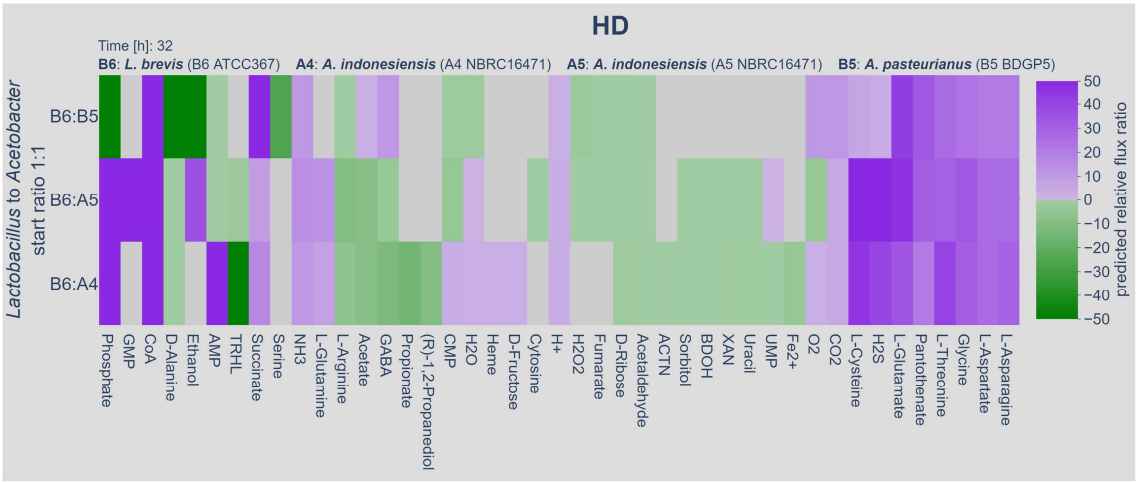

Figure 5: Flux of exchange reactions during the co-culturing of *Acetobacter* and *Lactobacillus* on the HD. We simulated the combined growth of *Acetobacter* and *Lactobacillus* on the HD and monitored the respective fluxes of the exchange reactions (thus, the fluxes representing an uptake or excretion of a given metabolite) over time. Exchange reactions are defined as reactions (or passages) where metabolites can flow in and out of the metabolic network and therefore the organism or cell. They can be subjected to different constraints such as diffusion or Michaelis-Menten kinetics of metabolite transporters, but for most reactions, only boundary thresholds can be set as the real-world flux rates are unknown. Further information on exchange reaction is found in Cotten and Reed 2013; Orth et al. 2010. For the sake of simplicity, we combined the individual fluxes into a normalized quotient, where a positive sign represents the same directionality (e.g., both bacteria secrete a given metabolite) of the individual fluxes and a negative sign represents opposite directionalities (e.g., one bacterium secretes a given metabolite and the other consumes it). The heatmap represents the flux ratios at 32 h of growth (an interactive version of the plot for all time points is provided as Data S5). Gray color represents that the respective metabolite is either not present or only transported by one of the two bacteria (not shown in color scale on the right); green color opposite and lilac color same flux directionalities. Multiple metabolites consistently show opposite flux directionalities across bacterial species combinations and across the time line.

Growth-promoting effect of singular metabolites added to *Acetobacter* cultures

We tested next whether the addition of any of the metabolites shown in Figure 5 to the HD growth medium simulations is sufficient to improve the growth of *A. indonesiensis*, which alone showed only poor biomass production on the HD medium (Figure 6A). Of the 43 metabolites tested (Figure S5), only 10 metabolites showed a growth-promoting effect *in silico*. Those were indeed enriched for the metabolites, which showed a predicted exchange from one bacterial species to the other (negative sign in Figure 5). The *in silico* addition of the TCA intermediate fumarate, for example, resulted in prominently increased predicted biomass production (Figure 6B). The same growth-promoting effect is visible in the *in silico* prediction of D-Ribose added to the HD medium (Figure 6C). No growth-promoting effect was visible when D-Alanine was added to the HD medium in the *in silico* prediction of *A. pasteurianus* B5 (Figure 6D), whereas biomass production of *A. indonesiensis* A4 and A5 was promoted (Figure S5).

Thus, the simulations suggested that already the exchange of a singular metabolite between the bacterial species could result in a growth-promoting effect.

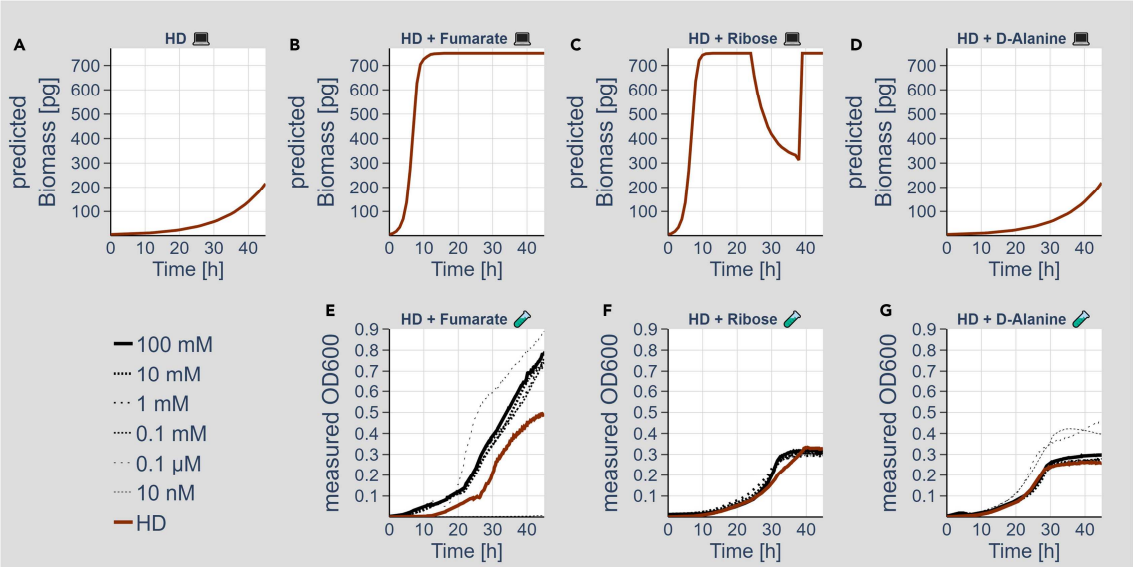

Figure 6: Growth-promoting effect of singular added metabolites. (A–D) *In silico* biomass production of *A. pasteurianus* (B5) on the standard HD. *In silico* biomass production of *A. pasteurianus* (B5) on HD with 10 mM (B) Fumarate, (C) Ribose, and (D) D-Alanine. (E–G) Actual growth measurements of *A. pasteurianus* (B5) on HD (dark orange) with Fumarate (E), Ribose (F), or D-Alanine (G) (10 nM, 0.1 µM, 0.1 mM, 1 mM, and 100 mM; black color and different dashed lines). *In silico* experiments (A, B, C, and D) are represented by the computer, whereas the wet-lab experiments (E, F, and G) are represented by the small reaction tube pictograms.

Finally, we tested for the experimental validation of the predicted growth-promoting effects. For this purpose, we recorded growth curves of *A. pasteurianus* (B5) in HD containing varying concentrations of fumarate (Figure 6E), D-Ribose (Figure 6F), and D-Alanine (Figure 6G). With fumarate and D-Ribose, we selected metabolites that showed *in silico* a prominent growth-promoting effect on all *Acetobacter* species (Figure S5), whereas D-Alanine did not result in a full growth rescue of *A. pasteurianus* (B5), but only the other two *Acetobacter* species (Figure S5). D-Ribose alone was not sufficient to improve the growth of *A. pasteurianus* (B5) prominently (Figure 6F). Yet, the addition of fumarate and D-Alanine in different concentrations showed a prominent positive effect on the growth of the bacteria (Figures 6E and 6G).

Altogether, our results suggest that microbiome members are metabolically connected, thus affecting the growth of individual microbiome members. The strategy presented herein consisting of the isolation of distinct bacteria, their genome sequencing, and subsequent *in silico* modeling of growth and

metabolism thus proved successful to identify metabolite exchange and growth-promoting metabolites. Future experiments targeted to investigate combinatorial effects of metabolite additions as well as the contribution of the hosts' metabolism will further extend our understanding of the complex interplay among the gut microbiome members.

Discussion

In this study, we analyzed multiple members of the *Drosophila* gut microbiome by a combination of *in vitro* and *in silico* experiments. In total, we isolated six bacterial strains from laboratory-reared *Drosophila* flies followed by *in vitro* growth experiments, resequencing, and genome assembly and *in silico* growth and metabolism modeling analyses.

First, we tested for a biomass production of the singular bacteria models on ACE, MRS, and HD. *L. plantarum* was able to generate high amounts of biomass on the ACE medium, whereas *L. brevis* was not (Figures 1D–1F). Similar growth was detected on the MRS medium and on HD. All *Acetobacter* models resulted in high biomass production on the ACE and MRS media and only very low biomass production on the HD (Figures 2D–2F). Our models mostly recapitulated the corresponding actual growth experiments (Figures 1, 2, and S1). Especially the poor growth of the *L. brevis* isolate was detected *in vitro* and *in silico* (Figures 1, 2, and S1). The reason for this growth deficit is to date not clear. For some of the organisms, such as *A. indonesiensis* on the ACE medium, the modeling results deviate from the actual measurements in terms of the magnitude of the effect (Figure S1). This is a problem seen in many modeling approaches, which might be based on a variety and most likely a combination of many parameters, including gaps in the model, confounding factors, and the lack of certain environmental conditions in the modeling procedure. Furthermore, the modeling procedure depends on the requirement to define “exchange reactions,” which are thresholds setting the boundaries for metabolic fluxes going into and out of the model. Although these thresholds can be controlled by different constraints such as diffusion or Michaelis-Menten kinetics of metabolite transporters (Cotten and Reed 2013; Orth et al. 2010), for most of the reactions, these boundaries are not

experimentally validated and thus the model itself is largely underdetermined. Furthermore, also the biology of the given bacterium might be a cause for deviations between the experimental and modeling data. A prerequisite of the FBA procedure is the assumption that an objective function is optimized in terms of a maximization. Often as well as in our study the optimized objective function is biomass production. Previous studies, however, demonstrated that several microorganisms operate at a sub-maximal growth rate (Fischer and Sauer 2005; Schuetz et al. 2007; Schuetz et al. 2012). The reasons for this behavior are not yet always clear.

Altogether, these parameter variations and modeling uncertainties will result not only in deviations of the magnitude of, e.g., biomass production, but also in kinetic differences, e.g., in terms of the growth rate. With variations in the build-up of biomass, also the mass transfer will vary, thus potentially resulting in more prominent differences between the computed and wet-lab results. Important, these confounding characteristics of the modeling procedure apply to the single and the multiple species growth simulations. The latter, however, will of course be even more severely affected by differences in the growth rates of the individual species that make up the consortium as the mass ratios between the species will also affect the mass transfer of metabolites. Furthermore, also the details concerning the juxtaposition (directly neighbored versus located in, e.g., different compartments of the gut) as well as variations in the initial mass ratio, thus the relative abundance of each species, will prominently affect the individual growth rates and mass transfer. Further experimental data including, e.g., localization studies, measurements of the individual abundance of bacterial species, and metabolic labeling experiments to determine flux rates as well as refinements of the models will help to improve the modeling outcome in the future.

Future iterations and refinements of the models will also need to target the optimization of the growth condition parameterization. Our simulations using the HD medium is a first step in the direction of modeling the actual growth conditions within the fly gut, as all bacteria as well as the host can thrive on this medium. The standard diet most often used to rear *Drosophila* is complex and undefined, often containing live or dry yeast, molasses, or treacle, which makes the parameterization and modeling very complex. Also, the exact conditions within

the gut are still not clear as, e.g., metabolite concentrations might vary along the anterior-posterior axis of the gut as well as across the diameter of the gut. Thus, further experimental and modeling work will be needed to decipher these details in the future.

On top of testing the biomass production, model validation also included the analysis of expected signature metabolite production. *Acetobacter*, for example, is known to oxidize sugars or ethanol to acetic acid (Raspor and Goranovic 2008), whereas lactobacilli produce glucose-derived lactic acid as the main product (Hatti-Kaul et al. 2018). Both metabolic models were able to recapitulate this behavior (Figure 3). It is intriguing that the previously described heterolactic metabolism of lactobacilli (Spector 2009) could also be recapitulated for our isolated bacteria (Figure S3) suggesting that our models result in realistic metabolic behavior predictions. Of note, however, some of the predictions need to be considered with care. Our simulations, for example, also revealed the production of H_2O_2 and also H_2S. Both substances can act as inhibitors of bacterial growth, especially in higher concentrations (Alt et al. 1999; Reis et al. 1992). Nevertheless, some *Acetobacter* species were demonstrated to produce H_2S under certain conditions (Ahmad et al. 2004). Thus, so far it is not clear whether the neutral or even positive effect of the presence of these substances on the growth (Figure S5) is real or based on the limitation of FBA to predict correctly growth-inhibiting and detrimental effects of certain metabolites.

The main goal of our study was to test whether we can predict metabolic growth-promoting inter-species interactions. If possible, this could open up the door to design tailored prebiotics to promote or hinder the growth of certain gut microbiome members. For our simulations, we tested all pair-wise combinations of *Acetobacter* and *Lactobacillus* on the three different media ACE, MRS, and HD. Many combinations were neutral in a way that the growth of the singular bacteria was similar or identical in the singular and combination situation (Figures 4A–4C; the complete dataset is provided in the supplement). In case both bacteria showed high growth in single growth simulations, the combination resulted in a competitive situation, which caused both bacteria to grow less (e.g., Figure 4D). On top of these trivial situations, however, we also observed inhibitory and stimulatory interactions. The *L. plantarum* strain B2 and *A. indonesiensis*

strain A5 result in comparable and high biomass production in the ACE medium when grown independently (Figure 4E). The combination, however, does not result in an equal reduction of the biomass to an intermediate level, but in contrast to a much stronger reduction of the *Lactobacillus* biomass production, whereas *Acetobacter* production got increased (Figure 4E). Likely, this effect is based on resource competition, which might also play a role within the gut of the *Drosophila* host. Even more astonishing was the stimulatory effect of combining the individually poor biomass producers *L. brevis* and either of the *Acetobacter* models, which we were able to track down to the exchange of selected metabolites (Figures 4F and S5). For fumarate and D-Alanine, we already were able to confirm the growth-promoting effect by simply adding these metabolites to the HD medium (Figure 6). Ribose, however, did not result in the expected growth rescue. At this point, the reasons for this discrepancy are unclear. Whether additional metabolites could also rescue the growth deficit to a similar extent is at this point unknown. Similarly, it is also not clear how the co-culturing of the organisms in the end affects each other as beneficial and competition effects most likely will play a role and thus a more complex growth effect will arise.

Fumarate and D-Alanine could affect the growth of the bacteria by different means. Thus, we considered different possibilities and cross-validated these using our modeling data. Formally, the metabolites could complement auxotrophies. Based on our modeling and experimental data, however, we exclude this possibility, as the bacteria also grow without the supplementation in the MRS or ACE media (Figures 1 and 2). Furthermore, the compounds could function as additional C- or N-source and enter the metabolism. Fumarate indeed is a central metabolite of the TCA. Thus, its uptake could enhance the overall capacity of the TCA. Various TCA intermediates further serve the biosynthesis of different amino acids, which potentially could also benefit biomass production. For *Acetobacter* pomorum a potential use of fumarate by the enzyme succinate dehydrogenase (EC1.3.5.1, present in TCA) was discussed where fumarate serves as an O-donor for the production of NAD+ and NADP+ from Aspartate (Consuegra et al. 2020b). D-Alanine, in contrast, could be converted first to L-Alanine and subsequently to pyruvate, which serves as a carbon and energy source. When we analyzed the corresponding flux differences of the modeling

performed in the presence or absence of the metabolites in the HD (Figure S6 and Data S6 and S7), we indeed detected a number of corresponding flux changes. First, we consider the situation where D-Alanine was added to the HD. Here, we see an increase in the flux associated with the conversion of D-Alanine to Pyruvate, as expected (Figure S6A). Pyruvate production is further enhanced coming from oxaloglutarate (Figure S6B). Other prominent changes include the change of direction of the fluxes from fumarate to malate and oxaloacetate (Figures S6C and S6D), the production of isocitrate from citrate (Figure S6E), the production of S-Succinyl-dihydrolipoamide from oxaloglutarate (Figure S6F), or the enhanced production of glutamate-derived amino acids such as glutamine (Figure S6G). Many of these enzymatic reactions are also affected by adding fumarate to the HD. Overall, the fumarate-induced flux changes of the TCA reactions are, however, bigger as from D-Alanine. Fumarate also resulted in a third possibility to enhance the pyruvate production coming from oxaloacetate (Figure S6H). The fumarate addition induced higher flux changes, which might provide an explanation for the overall bigger growth rescue phenotype detected in the actual growth experiments (Figure 6E). A recent report also targeted the prediction of *Drosophila* gut microbiome metabolite interactions using *in silico* models (Ankrah et al. 2021). The authors independently also revealed that TCA intermediate metabolites appear to be prominently exchanged between gut microbiome members. In their simulations, the authors used different media than we did, but still found a similar range of exchanged metabolites. Reassuringly, many of the exchanged metabolites are shared by our and the published study. In our extended studies, however, we did not detect a prominent growth-promoting effect for some of these in our simulations (e.g., acetate, succinate, different individual amino acids). Yet, several metabolites detected in both studies (e.g., acetoin, acetaldehyde) clearly resulted in an individual growth-promoting activity (c.f. Figure S5 and Ankrah et al. 2021).

Our results support the possibility to use genome-scale models in combination with agent-based growth simulations to predict meaningful microbiome cooperativity. In the future, extending this approach to additional microbiome constituents and/or the metabolism of the host *D. melanogaster* will be exciting

and perhaps pave the way to analyze also the much more complex microbiomes of higher organisms.

Limitations of the study

There are limitations in the modeling of growth-promoting bacterial metabolic interactions. On the one hand, this is true for the modeling side as outlined above. For example, FBA assumes optimization and maximization of a given parameter such as biomass production, yet organisms sometimes operate at a sub-optimal level. Furthermore, our knowledge of many parameters required for the modeling such as nutrient distribution along the gut, nutrient uptake rates, and transport reaction efficacies are unknown, which results in the necessity to make assumptions that are in the best case imprecise and in the worst case wrong. Further iterations and improvements on the modeling and experimental side might solve some of these shortcomings using, e.g., isotope labeling experiments. On the other hand, uncertainties concerning the biology exist. For example, we used laboratory-reared flies and detected the most prominent microbiome growth interactions on a minimal diet used for the growth of *Drosophila*. In the future, bacteria from wild-reared animals grown under natural conditions should be used, which, however, will be experimentally very challenging. Finally, our analyses were performed with simple consortia. Ultimately, complex mixtures with varying relative microbial species abundancies and consisting of more species will be required to estimate the true importance of metabolic cross-feeding phenomena among gut microbiota.

STAR★Methods

Key resources table

REAGENT or RESOURCE	SOURCE	IDENTIFIER
Bacterial and virus strains		
Acetobacter pasteurianus	This paper	B5
Acetobacter indonesiensis	This paper	A4

Acetobacter indonesiensis	This paper	A5
Lactobacillus plantarum	This paper	A2
Lactobacillus plantarum	This paper	B2
Lactobacillus brevis	This paper	B6
Chemicals, peptides, and recombinant proteins		
L-arginine HCl	Sigma-Aldrich	Cat#A5131
L-alanine	Sigma-Aldrich	Cat#A7627
L-asparagine	Sigma-Aldrich	Cat#A0884
L-aspartic acid	Sigma-Aldrich	Cat#A6683
L-cysteine	Sigma-Aldrich	Cat#C1276
L-glutamic acid monosodium salt monohydrate	Sigma-Aldrich	Cat#G5889
L-glutamine	Sigma-Aldrich	Cat#G3126
Glycine	Sigma-Aldrich	Cat#G7126
L-histidine	Sigma-Aldrich	Cat#H8000
L-isoleucine	Carbolution	Cat#CC10025
L-leucine	Sigma-Aldrich	Cat#L8912
L-lysine HCl	Sigma-Aldrich	Cat#L5626
L-methionine	Sigma-Aldrich	Cat#M9625
L-phenylalanine	Sigma-Aldrich	Cat#P2126
L-proline	Sigma-Aldrich	Cat#P0380
L-serine	Sigma-Aldrich	Cat#S4500
L-threonine	Carl Roth	Cat#T206
L-tryptophan	Sigma-Aldrich	Cat#T0254
L-tyrosine	Sigma-Aldrich	Cat#T3754
L-valine	Sigma-Aldrich	Cat#V0500
Sucrose	Carl Roth	Cat#4661
Cholesterol	Sigma-Aldrich	Cat#C8667
choline chloride	Sigma-Aldrich	Cat#C1879
myo-inositol	Sigma-Aldrich	Cat#I7508
Inosine	Sigma-Aldrich	Cat#I4125
Uridine	Sigma-Aldrich	Cat#U3750
Tween20	Sigma-Aldrich	Cat#P7949
KH2PO4	Grüssing Gmbh	Cat#120171000
NaHCO3	AppliChem	Cat#AP131638
CaCl2.6H2O	Sigma-Aldrich	Cat#442909
CuSO4.5H2O	AcrosOrganics	Cat#A0302205
FeSO4.7H2O	Sigma-Aldrich	Cat#F7002
MgSO4.7H2O	AppliChem	Cat#A6287
MnCl2.4H2O	Sigma-Aldrich	Cat#M3634

ZnSO4.7H2O	Sigma-Aldrich	Cat#Z0251
thiamine (aneurin)	Sigma-Aldrich	Cat#T4625
Riboflavin	Sigma-Aldrich	Cat#R4500
nicotinic acid	Sigma-Aldrich	Cat#N4126
Ca pantothenate	Sigma-Aldrich	Cat#P21210
pyridoxine-HCL	Sigma-Aldrich	Cat#P9755
Biotin	Sigma-Aldrich	Cat#B4501
folic acid	Sigma-Aldrich	Cat#F7876
HPLC	Fisher Scientific	Cat#231-791-2
Fumarate	BLD Pharmatech Gmbh	Cat#BD131629
D(-)-Ribose	AcrosOrganics	Cat#10320164
D-Alanine	Carbolution	Cat#CC10041
Acetic acid glacial	VWR Chemicals	Cat#KRAF20104
Glucose	Fisher Scientific	Cat#10529190
Sodium acetate	Grüssing Gmbh	Cat#121111000
Cycloheximide	AppliChem	Cat#A0879
Peptone	Carl Roth	Cat#8986.2
Yeast Extract	BD Company	Cat#212750
Beef Extract	Carl Roth	Cat#X975
Triammonium citrate	Sigma-Aldrich	Cat#A1332
Tween20	Sigma-Aldrich	Cat#P7949
Ethanol	Honeywell	Cat#32221
MRS agar plates	Thermo Scientific	Cat#CM0361B
Proteinase K	Thermo Scientific	Cat#AM2546
Lysozyme	Sigma-Aldrich	Cat#34046
Phusion HF Polymerase	New England Biolabs	Cat#M0530
Tris-HCL	Roche	Cat#10812846001
EDTA	AppliChem	Cat#1.08452
Triton™ X-100	Sigma-Aldrich	Cat#X100
Bleach	DanKlorix Hygiene Reiniger	N/A
Agar	Becton Dickinson	Cat# 10455513
Polenta	Verival; Pronurel Bio	N/A
Soy flour	Bauck Hof	N/A
Yeast	Bruggeman	N/A
Treacle	Original Grafschafter Goldsaft	N/A
Malt extract	Demeter	N/A
Nipagin	Sigma-Aldrich	Cat# H3647
Propionic acid	Acros Organics	Cat#AC149300010
Tween80	Sigma-Aldrich	Cat#P1754
Critical commercial assays		

TOPO TA Cloning Kit for Sequencing	Invitrogen	Cat#K4575J10
QIAamp DNA Mini Kit	Qiagen	Cat#51304
Deposited data		
Raw and analyzed data	This paper	DOI: 10.17632/2tgjd6y4zb.1
Experimental models: Organisms/strains		
D. melanogaster wildtype strain Oregon-R	Bloomington *Drosophila* Stock Center	BDSC: 5; FlyBase: FBsn0000276
D. melanogaster white[1118]	Vienna *Drosophila* Resource Center	VDRC:60000
Oligonucleotides		
GM3F: AGAGTTTGATCMTGGC	Klindworth et al. 2013	N/A
GM4R: TACCTTGTTACGACTT	Klindworth et al. 2013	N/A
Software and algorithms		
Python 3.8	Python Software Foundation	https://www.python.org
R Studio 1.2.5042	RStudio, Inc.	https://www.rstudio.com
R 3.6.1	R Foundation for Statistical Computing	https://www.R-project.org
BacArena 1.8	Bauer et al. 2017	https://bacarena.github.io
gapseq 1.1	Zimmermann et al. 2021	https://github.com/jotech/gapseq
Plotly 4.14.3	Plotly Technologies Inc.	https://plot.ly

Resource availability

Lead contact

Further requests for resources should be directed to and will be fulfilled by the lead contact, Mathias Beller (mathias.beller@hhu.de).

Materials availability

This study did not generate new materials.

Experimental model and subject details

Fly strains and rearing

The fly lines that were used in this study are *w*^{1118} (*white[-]*) and Oregon-R. Flies were maintained at 25°C with 60–70% humidity and a 12 h light/dark cycle. Standard diet contains 0.5% agar (Becton Dickinson), 7.1% polenta (Verival, Pronurel Bio), 0.95% soy flour (Bauck Hof), 1.68% yeast (Bruggeman), 4% treacle (Original Grafschafter Goldsaft), 4.5% malt extract (Demeter). All diets contained 0.15% nipagin (Sigma-Aldrich) and 0.45% propionic acid (Acros Organics).

Isolation of bacterial species from *Drosophila*

In order to analyze different bacterial species from the gut microbiome of *Drosophila*, both *white[-]* and Oregon-R male flies (9 individuals) were surface sterilized by washing with 10% bleach, 70% ethanol and PBS before homogenization and plating on MRS and ACE agar plates. MRS agar plates (Oxoid, Thermo Scientific) contain (in 1000 mL dH_2O): Agar (15 g), casein peptone, tryptic digest (10 g), meat extract (10 g), yeast extract (5 g), glucose (20 g), Tween 80 (1 g), K_2HPO_4 (2 g), Na-acetate (5 g), $(NH_4)_2$ citrate (2 g), $MgSO_4$ x 7 H_2O (0.2 g), $MnSO_4$ x H_2O (0.05 g), pH 6.2–6.5. ACE agar plates (Blum et al. 2013) contain: (in 1000 mL dH_2O): Agar (15 g), yeast extract (8 g), casein peptone (15 g), glucose (10 g), after autoclaving: acetic acid (3 mL), ethanol (p.a.) (5 mL) and Cycloheximid (100 mg). The plates were incubated at 28°C for three to five days and single colonies were picked and isolated on new agar plates for three rounds to obtain pure cultures. These were then stored in glycerol stocks for later DNA extraction and analysis.

Method details

Single colony PCR and analysis of 16S rRNA genes

Of the different pure cultures single colonies were picked and transferred into PBS buffer containing 200 µg/ml Proteinase K and 10 mg/ml Lysozyme and incubated for 30 min at 37°C and 2 min at 95°C. The samples were centrifuged for 2 min at 13.000 rpm and the supernatant transferred to a new vial. The 16S rRNA Gen was amplified using the GM3F and GM4R primers (Klindworth et al. 2013) using the Phusion Polymerase (New England Biolabs) which produced a product of about 1500 bp. These PCR products were then ligated into the TOP TA Vector (TOPO TA Cloning Kit for Sequencing, Invitrogen) and transformed into chemocompetent *E. coli* DH5alpha according to the manufacturer's instructions. The vector including the insert was extracted from *E. coli* and the insert analyzed by Sanger sequencing (MWG Biotech). The DNA sequence was afterwards subjected to BLAST analysis to identify the isolated bacterial species.

DNA extraction from bacterial species for genome sequencing

The DNA extraction was performed using the Qiagen QiaAmp DNA Mini kit according to the manufacturer's recommendation, with the following modifications. Briefly, an inoculation loop was used to pick bacterial colonies from the pure cultures grown on ACE or MRS agar plates and the bacteria were resuspended in gram-positive lysis buffer (20 mg/ml lysozyme; 20 mM Tris·HCl, pH 8.0; 2 mM EDTA; 1.2% Triton®). The following lysis and purification steps were performed according to the kit's protocol for DNA extraction from gram-positive bacteria.

Liquid media bacteria growth experiments

For the bacterial growth experiment, we prepared pre-cultures in the respective semi-selective medium (MRS for *Lactobacillus* sp. and ACE for *Acetobacter sp.* (Blum et al. 2013)). Subsequently, we either directly used the optical dense overnight culture or adjusted it to an OD600 of 0.8. Next, we performed a 1:1000

(MRS and ACE) or 1:100 (HD) dilution and distributed the bacteria to transparent 96-well flat bottom plates (Sarstedt). The medium was covered with mineral oil and incubated in a BioTek Synergy Mx Plate Reader with (*Acetobacter*) or without (*Lactobacillus*) shaking for at least 48 hours. Optical density was measured every five minutes. Per experiment, all growth curves were measured in at least triplicate and the figures provide mean values.

Whole genome sequencing of isolated bacterial species

The isolated genomic DNA samples from the gut microbiota species were sequenced using the Illumina MiSeq platform following standard procedures. The library preparations and sequencing were performed by the Genomics and Transcriptomics Lab at the HHU.

Genome reassembly

For the genome reassembly the tool ASA³P (Schwengers et al. 2020) was used. ASA³P is an automatic, scalable assembly, annotation, and analysis pipeline for genomes of bacterial origin. The pipeline consists of four steps: Processing, characterization, comparative genomics, and reporting. Each step provides different analysis information about the used sequenced genome through different software tools and databases. While processing and reporting is mandatory, the steps of characterization and comparative genomics is optional and can be skipped by the user. The first step processing includes the task of quality control, genome assembly, scaffolding and annotation. The second step of characterization determines the taxonomy, performs a multi locus sequence typing (MLST) analysis, tries to detect antibiotic resistances (ABRs), a detection of virulence factors (VFs), performs a mapping by using quality clipped reads onto reference genomes provided by the user, and annotates single-nucleotide polymorphisms (SNPs). The third step of comparative genomics consists of the calculation of a phylogenetic tree and of a core, accessory and pan-genome while detecting isolate genes. The last step is a graphical presentation of the pipeline results. All ASA³P results are provided in the supplement.

Reconstruction of bacterial metabolic models

The sequenced genomes were used to reconstruct their genome-scale metabolic models using the *gapseq* analysis pipeline (Zimmermann et al. 2021). We used for the reconstruction and gap-filling step the MRS, ACE and HD as the growth medium. All metabolic models were created combining each genome sequence and every single medium. During the model generation process, we considered in particular stochiometric consistency, mass and charge balance as well as metabolite connectivity and introduced necessary changes following manual curation. In order to test for the quality of our models, we used the MEMOTE analysis pipeline (Lieven et al. 2020). All analysis results are provided as supplemental data. In brief, the models resulted in at least 77% model quality scores. Most importantly, the key requirements for the models all reached at least 99%. The score was only decreased by e.g. missing gene or metabolite annotation cross-references, which we do not focus on in the present manuscript and have no influence on flux predictions in constraint-based modeling. A central part of genome-scale metabolic models is the biomass reaction, which represents the metabolite consumption for the formation of all cell constituents. The biomass reaction is commonly, and also in this study, used as objective function for flux balance analysis (FBA) or FBA-derived simulation techniques. The *gapseq* software automatically adds a biomass reaction to the models based on the organism's Gram-staining phenotype in order to account for biomass composition differences due to differences in the structural characteristics of the cell wall. The exact biomass reaction stoichiometries in *gapseq* are directly derived from ModelSEED (Henry et al. 2010), which in turn derived the biomass reaction definitions from curated genome-scale metabolic models from Escherichia coli (Orth et al. 2010) as a proxy for Gram-negative bacteria and *Bacillus subtilis* (Oh et al. 2007) as a proxy for Gram-positive bacteria. The biomass compositions for all *Lactobacilli* models (Gram-positive) and *Acetobacter* models (Gram-negative) are provided in Data S1.

Constraint-based modeling

Flux balance analysis (FBA; (Orth et al. 2010)) was used to perform the growth and metabolic flux analysis. The mono- and co-culturing *in silico* experiments were performed using the BacArena tool (Bauer et al. 2017), which is also based on FBA.

In silico growth media

In silico experiments used parametrized versions of the experimentally used MRS, ACE and HD media (Supp. Table 1). MRS and ACE medium are semi-defined as the contain complex ingredients such as yeast extract. Therefore, we obtained compositional information from the suppliers of the respective media ingredients (see Data S2). For some media components, which are required to run the simulations, no quantitative information could be obtained. Those compounds were manually curated and added. We limited the number of such manually added compounds to the absolute minimum and provide all media information as supplemental data. The parametrized HD medium is based on the protocol of (Piper et al. 2014), which is completely synthetic and thus did not require any modifications.

Calculation of predicted relative flux ratios

To identify reactions with a higher flux and reactions corresponding to a crosstalk between *Lactobacillus brevis* B6 and the *Acetobacter sp.* we calculated a predicted relative flux ratio for each reaction and time point.

We calculated the predicted relative flux ratio as followed:

$$v_{Ratio,\ \ Reaction\ i,t} = \frac{v_{Lactobacillus\ B6,Reaction\ i,t}}{v_{Acetobacter,Reaction\ i,t}} \quad (1)$$

where $v_{Lactobacillus\ B6,Reaction\ i,t}$ is the flux of the reaction_i of *Lactobacillus* B6 at time point t in $\frac{mmol}{gDW*h}$, $v_{Acetobacter,Reaction\ i,t}$ is the flux of the reaction_i of *Acetobacter sp.* at time point t in $\frac{mmol}{gDW*h}$.

If the predicted relative flux ratio value is between 1 and -1 we calculated the values as followed:

$$v_{Ratio,Reaction\ i,t} = \frac{1}{v_{Ratio,Reaction\ i,t}}\ ; 1 > v_{Ratio,Reaction\ i,t} > -1 \qquad (2)$$

where $v_{Ratio,Reaction\ i,t}$ is the unitless predicted relative flux ratio. We choose this representation of the value range between 1 and -1 to highlight the higher flux value between *Lactobacillus* B6 and the *Acetobacter sp.*.

Calculation of cumulative flux values

In order to analyse the metabolic impact of an additional metabolite in the holidic diet towards the bacteria grown on the media we calculated the cumulative flux for each time point.

First, we calculated the sum of flux values:

$$v_{Sum,M,Reaction\ i} = \sum_{t=0}^{n} v_{M,Reaction\ i} \qquad (3)$$

where $v_{Sum,M,Reaction\ i}$ is the sum of flux values over the time t with medium M in $\frac{mmol}{gDW*h}$, $v_{M,Reaction\ i}$ is the flux value at a time point with medium M in $\frac{mmol}{gDW*h}$.

Next, we calculated the difference of the sum flux values between the standard holidic diet HD and the medium M:

$$v_{\Delta,Reaction\ i} = v_{Sum,HD,Reaction\ i} - v_{Sum,M,Reaction\ i} \qquad (4)$$

where $v_{\Delta,Reaction\,i}$ is the difference between the summed flux values of HD and medium M over the time t.

Finally, we calculated the cumulative flux as followed:

$$v_{cflux,Reacton\,i} = log\left(\left|v_{\Delta,Reaction\,i}\right| + 1\right) \quad (5)$$

where $v_{cflux,Reaction\,i}$ is the cumulative flux value between HD and the medium M for a reaction in $log\left(\frac{mmol}{gDW*h}\right)$. The cumulative flux value can also be calculated for a group of reactions.

Quantification and statistical analysis

Figures represent averaged or representative results of multiple independent experiments or simulations. The figure legends provide details concerning the N of experiments or simulations. Analyses and Plots were performed with custom Python scripts.

Additional resources

All data is available at data.mendeley.com under the URL https://doi.org/10.17632/2tgjd6y4zb.1.

Data and code availability

- Genome resequencing data, the genome-scale metabolic networks and bacterial growth data, as well as all data required to reproduce the figures are deposited at Mendeley Data and is available as of the date of publication at https://doi.org/10.17632/2tgjd6y4zb.1.
- All original code was additionally deposited at our GitLab account and can be accessed via https://gitlab.com/Beller-Lab.
- For any additional questions or information please contact the lead contact.

Acknowledgments

We would like to thank all past and present members of the laboratory for helpful comments and support and the Genomics and Transcriptomics Lab (GTL) of the Heinrich Heine University Düsseldorf for the resequencing of the isolated bacterial species. Funding: The project was financed through the German “Bundesministerium für Bildung und Forschung (BMBF)” grant 031A 306 (to M.B.) and in part by a scholarship of the Jürgen Manchot Foundation (to J.W.S.). S.W. acknowledges support by the Cluster of Excellence 2167 - “Precision medicine in chronic inflammation” - Deutsche Forschungsgemeinschaft. The funders had no role in the study design, analysis, interpretation of the results or the writing of the manuscript.

Author contributions

J.W.S., F.A.S., and M.B. designed experiments. F.A.S., K.M.E., I.A., and A.D. conducted experiments. J.W.S., F.A.S., K.M.E., and M.B. analyzed the data. J.W.S. and K.M.E. performed the resequencing analysis and assembled the bacterial genomes. S.W. reconstructed the bacterial genome-scale metabolic networks, performed the gap filling, and identified the biomass functions. J.W.S. performed the flux-balance simulations and plotted the figures. J.W.S., F.A.S., I.A., S.W. and M.B. wrote the manuscript.

Declaration of interests

The authors declare that they have no competing interests.

Supplemental information

Modeling *Drosophila* gut microbe interactions reveals metabolic interconnectivity

Jürgen W. Schönborn, Fiona A. Stewart, Kerstin Maas Enriquez, Irfan Akhtar, Andrea Droste, Silvio Waschina, and Mathias Beller

A

	Exp. growth rate [1/h]			In silico growth rate [1/h]		
	MRS	ACE	HD	MRS	ACE	HD
L. plantarum A2	0.26	0.11	0.13	0.24	0.26	0.36
L. plantarum B2	0.25	0.09	0.07	0.26	0.24	0.39
L. brevis B6	0.11	0.09	0.14	0.11	0.11	0.12
A. indonesiensis A4	0.10	0.07	0.20	0.29	0.30	0.08
A. indonesiensis A5	0.10	0.10	0.18	0.30	0.30	0.08
A. pasteurianus B5	0.05	0.05	0.20	0.28	0.30	0.09

B

$$\mu_{exp} = \frac{\ln(OD600_t) - \ln(OD600_{t_0})}{t - t_0}$$

$$\mu_{in\ silico} = \frac{\ln\left(\frac{biomass_t}{biomass_{t_0}}\right)}{t - t_0}$$

C

	MRS	ACE	HD
L. plantarum A2	0.02	-0.15	-0.24
L. plantarum B2	-0.01	-0.15	-0.31
L. brevis B6	0.00	-0.01	0.02
A. indonesiensis A4	-0.19	-0.23	0.12
A. indonesiensis A5	-0.20	-0.20	0.10
A. pasteurianus B5	-0.23	-0.25	0.11

In silico higher growth than experiment (delta ≥ - 0.2)

In silico elevated growth than experiment (delta > - 0.15 < - 0.2)

In silico and experimental growth comparable (delta ~ 0)

Experimental growth higher than *in silico* (delta ≥ 0.1)

Figure S1: Growth estimate determination and comparison between wet-lab and *in silico* results, Related to Fig. 1 and Fig. 2. (A) The growth rate of the six isolated bacteria was estimated on the three different media (MRS, ACE and HD) by wet-lab experiments (left part of the table) and using the computed biomass production amounts to calculate *in silico* derived growth rates (right side of the table). The formulas used are provided in (B). (C) We subtracted from the experimentally determined growth rate the *in silico* derived one to get a similarity measure (difference is “delta”). The color-coded delta values obtained are provided in the table.

		MRS	ACE	HD
SUBSTRATE	CPD	Conc. [mM]	Conc. [mM]	Conc. [mM]
GLUCOSE	cpd00027	111.00000	55.50000000	-
SUCROSE	cpd00076	-	-	50
GLUTAMINE	cpd00053	0.06842	0.10947657	12.47000000
GLUTAMATE	cpd00023	19.47937	13.36912934	12.40000000
PHENYLALANINE	cpd00066	4.64919	3.80168291	5.55000000
HISTIDINE	cpd00119	2.27507	1.44367105	4.46000000
LYSINE	cpd00039	7.98960	6.00588276	11.89000000
METHIONINE	cpd00060	1.82976	1.13270777	2.27000000
ARGININE	cpd00051	5.92423	6.18828932	8.17000000
THREONINE	cpd00161	4.58361	2.45970450	10.86000000
VALINE	cpd00156	8.02390	5.97524541	11.41000000
TRYPTOPHAN	cpd00065	0.74426	0.41619742	2.15000000
LEUCINE	cpd00107	9.41526	6.84607761	12.50000000
ISOLEUCINE	cpd00322	5.72539	4.23115042	8.84000000
ALANINE	cpd00035	17.15120	20.51857672	17.82000000
ASPARTIC ACID	cpd00041	10.70624	8.82043576	6.32000000
ASPARAGINE	cpd00132	0.68120	0.94610960	6.35000000
GLYCINE	cpd00033	26.22885	34.96736379	14.43000000
TYROSINE	cpd00069	1.58949	1.02654672	4.64000000
CYSTEINE	cpd00084	0.18727	0.06658344	2.18000000
SERINE	cpd00054	6.34694	3.35902560	7.23000000
PROLINE	cpd00129	14.51403	12.85503344	4.90000000
K+	cpd00205	34.33960	7.49150219	22.00000
CA2	cpd00063	0.05115	0.03717750	1.14000
ZN2	cpd00034	0.01000	0.01000000	0.08700
FE+2	cpd10515	0.004895	0.00501	0.04495
FE+3	cpd10516	0.004895	0.00501	0.04495
RIBOFLAVIN	cpd00220	0.01000	0.01000000	0.00186
FOLATE	cpd00393	0.01000	0.01000000	0.00113
PHOSPHATE	cpd00009	6.34404	3.38629687	22.00000
MAGNESIUM	cpd00254	1.90167	0.25735445	2.08000
MN2+	cpd00030	0.33128	0.01000000	0.00505
BIOTINE	cpd00104	0.01000	0.01000000	0.00060
CU2	cpd00058	0.01000	0.01000000	0.01000
CL-	cpd00099	3.28728	4.50289115	2.64830
PANTOTHENATE	cpd00644	0.01000	0.01000000	0.04949
THIAMIN	cpd00305	0.01000	0.01000000	0.00465
SULFATE	cpd00048	1.77389	0.57464085	2.16687
FOLIC ACID	cpd00393	0.01000	0.01000000	0.00113
URIDINE	cpd00249	0.01000	0.01000000	0.24600
INOSINE	cpd00246	0.01000	0.01000000	0.24200000
NICOTINIC ACID	cpd00218	0.01000	0.01000000	0.06820000
PYRIDOXINE	cpd30645	0.01000	0.01000000	0.01000000
NA+	cpd00971	4.68312	4.49582427	11.90500000
O2	cpd00007	0.10000	0.1	0.10000000
WATER	cpd00001	100.00000	100.00000000	100.00000000
MOLYBDATE	cpd11574	0.01000	0.01000000	-
CO2+	cpd00149	0.01000	0.01000000	0.01
AMMONIUM	cpd00013	8.22335	-	-
CITRATE	cpd00137	8.22335	-	-
ACETATE	cpd00029	59.91674	52.40000000	-
ETHANOL	cpd00363	-	85.60000000	-
CHOLINE	cpd00098	-	-	0.35810
MYO-INOSITOL	cpd00121	-	-	0.02800

Figure S2: Parametrization of the media contents used in this study, Related to Table 1, STAR Methods, and Supplemental File 2. The “CPD” ID refers to the compound descriptor used in the modeling simulations.

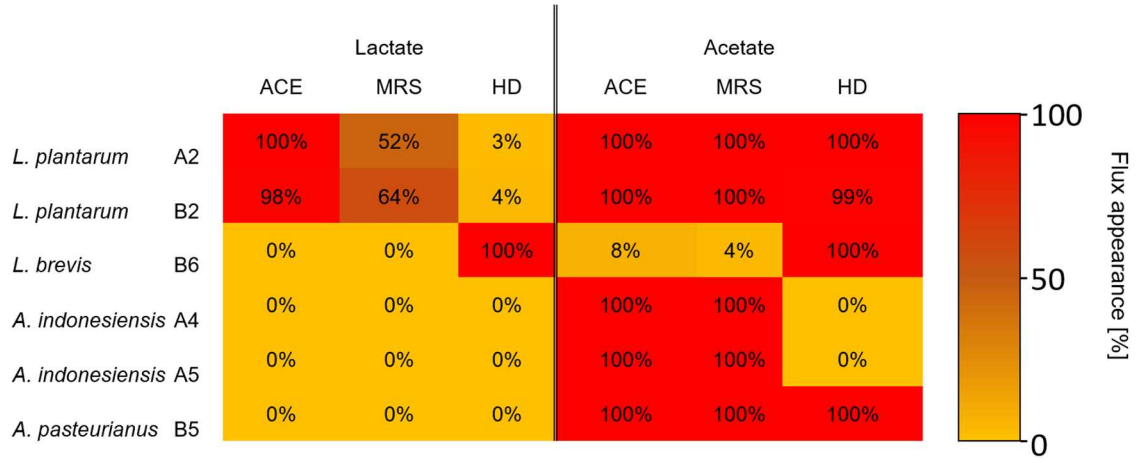

Figure S3: Robustness analysis of the signature metabolite production of *Lactobacilli* and *Acetobacter* bacteria on the three different media, Related to Fig. 3. Simulations were run 100 times and the production of lactate and acetate, respectively, was recorded. As a threshold, metabolite production had to surpass a flux rate of 0.1 nmol / h to count as "flux present". The plots show the color-coded results with red color representing a high fraction of simulation runs with metabolite production and orange shades represent a low fraction of metabolite producing simulation runs.

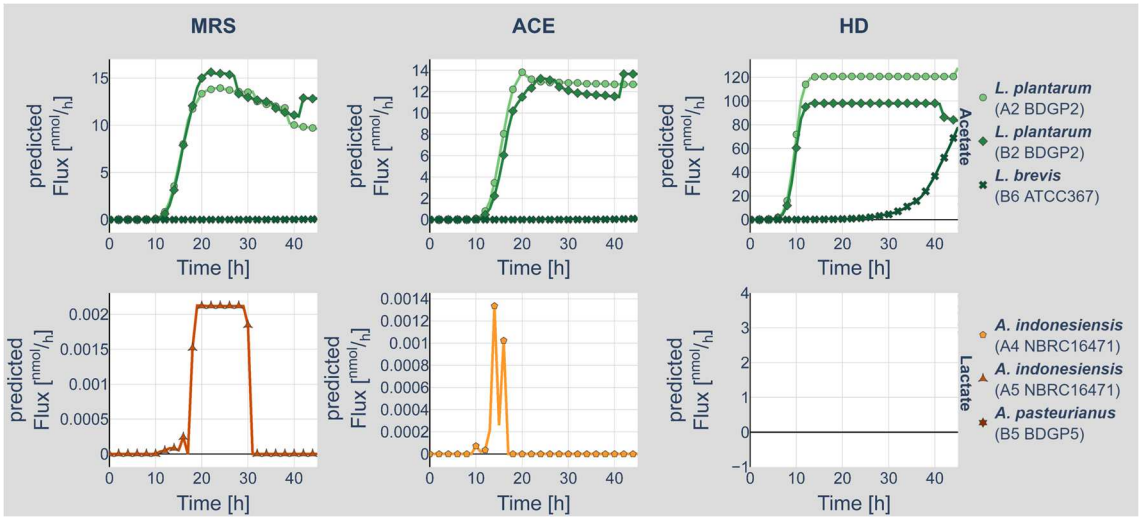

Figure S4: Test for heterolactic behavior of *Acetobacter* and *Lactobacillus* models, Related to Fig. 3. While all *Lactobacilli* were able to produce also acetate (upper row), the *Acetobacter* models failed to produce lactate exceeding our 0.1 nmol / h flux threshold.

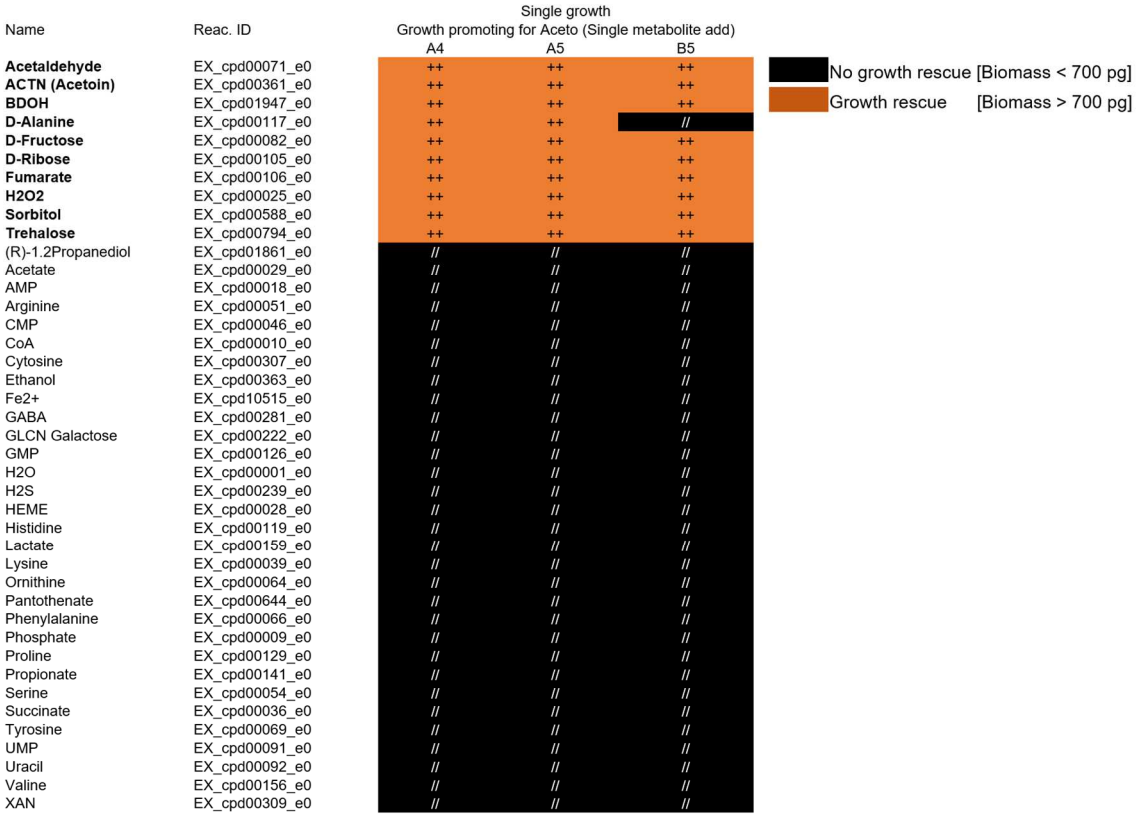

Figure S5: Rescue of the *Acetobacter sp.* growth deficit in the HD by adding singular metabolites, Related to Fig. 5 and Fig. 6. All metabolites which showed an exchange behavior in the combined growth simulations (cf. Figure 5A and supplemental file 2) were added individually to the HD simulations. The simulations were evaluated for a rescue of the growth deficit which is represented by red color in the table. The majority of added metabolites did not alter the biomass production of the model (represented by black color).

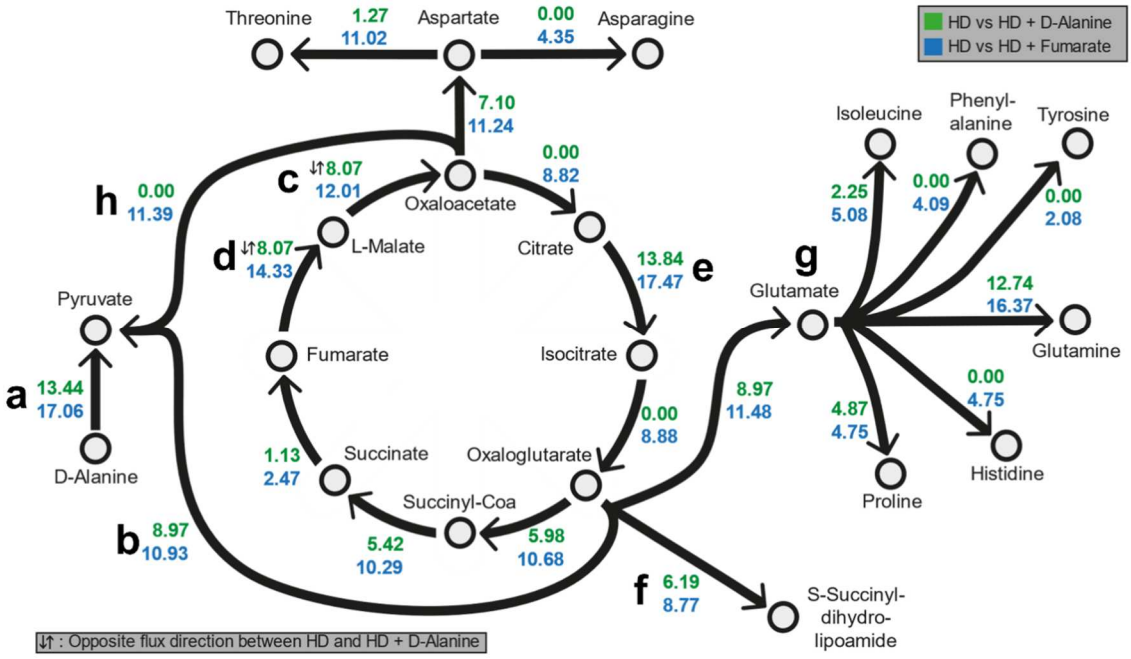

Figure S6: Focused metabolic network with flux differences of *A. pasteurianus* (B5) growth modeled on HD or HD with D-Alanine or HD with fumarate, respectively, Related to Fig. 6. Flux changes were calculated by subtracting the flux present on the HD from the value present in the HD with additive. The result was log normalized. Highlighted reactions are (if multiple reactions are provided, the individual flux values were combined to produce one summarizing value): a) L-Alanine racemase and L-alanine:glyoxylate aminotransferase, b) L-Alanine:2-oxoglutarate aminotransferase, c) Malate-dehydrogenase, d) Fumarase, e) Aconitase, f) 2-oxoglutarate dehydrogenase g) glutamate to isoleucine: L-Isoleucine:2-oxoglutarate aminotransferase; glutamate to phenylalanine: L-Phenylalanine:2-oxoglutarate aminotransferase; glutamate to tyrosine: L-tyrosine:2-oxoglutarate aminotransferase; glutamate to glutamine: L-Glutamate:ammonia ligase (ADP-forming) and L-glutamine:D-fructose-6-phosphate isomerase (deaminating); glutamate to histidine: L-Histidinol-phosphate phosphohydrolase and L-Histidinol:NAD+ oxidoreductase; glutamate to proline: ATP:L-glutamate 5-phosphotransferase and L-glutamate-5-semialdehyde:NADP+ 5-oxidoreductase (phosphorylating) and L-glutamate 5-semialdehyde dehydratase and L-Proline:NADP+ 5-oxidoreductase, h) oxaloacetate carboxy-lyase (pyruvate-forming).

References

Adair, Karen L.; Wilson, Marita; Bost, Alyssa; Douglas, Angela E. (2018): Microbial community assembly in wild populations of the fruit fly *Drosophila melanogaster*. In *The ISME Journal* 12 (4), pp. 959–972. DOI: 10.1038/s41396-017-0020-x.

Ahmad, Iqbal; Sharma, Jyoti; Ahmad, Farah (2004): Isolation and characterization of resistance traits of indigenous strains ofAcetobacter diazotrophicus associated with sugarcane. In *Sugar Tech* 6 (1-2), pp. 41–46. DOI: 10.1007/BF02942616.

Alt, E.; Leipold, F.; Milatovic, D.; Lehmann, G.; Heinz, S.; Schömig, A. (1999): Hydrogen peroxide for prevention of bacterial growth on polymer biomaterials. In *The Annals of Thoracic Surgery* 68 (6), pp. 2123–2128. DOI: 10.1016/S0003-4975(99)00832-2.

Ankrah, Nana Y. D.; Barker, Brandon E.; Song, Joan; Wu, Cindy; McMullen, John G.; Douglas, Angela E. (2021): Predicted Metabolic Function of the Gut Microbiota of *Drosophila melanogaster*. In *mSystems* 6 (3). DOI: 10.1128/mSystems.01369-20.

Aron-Wisnewsky, Judith; Vigliotti, Chloé; Witjes, Julia; Le, Phuong; Holleboom, Adriaan G.; Verheij, Joanne et al. (2020): Gut microbiota and human NAFLD: disentangling microbial signatures from metabolic disorders. In *Nature Reviews Gastroenterology & Hepatology* 17 (5), pp. 279–297. DOI: 10.1038/s41575-020-0269-9.

Arora, Tulika; Singh, Satvinder; Sharma, Raj Kumar (2013): Probiotics: Interaction with gut microbiome and antiobesity potential. In *Nutrition* 29 (4), pp. 591–596. DOI: 10.1016/j.nut.2012.07.017.

Aumiller (2021): A chemically-defined growth medium to support *Lactobacillus* – Acetobacter community analysis. In *bioRxiv* 2021.

Azuma, Yoshinao; Hosoyama, Akira; Matsutani, Minenosuke; Furuya, Naoko; Horikawa, Hiroshi; Harada, Takeshi et al. (2009): Whole-genome analyses reveal genetic instability of *Acetobacter pasteurianus*. In *Nucleic Acids Research* 37 (17), pp. 5768–5783. DOI: 10.1093/nar/gkp612.

Bauer, Eugen; Zimmermann, Johannes; Baldini, Federico; Thiele, Ines; Kaleta, Christoph (2017): BacArena: Individual-based metabolic modeling of heterogeneous microbes in complex communities. In *PLOS Computational Biology* 13 (5), e1005544. DOI: 10.1371/journal.pcbi.1005544.

Blum, Jessamina E.; Fischer, Caleb N.; Miles, Jessica; Handelsman, Jo (2013): Frequent replenishment sustains the beneficial microbiome of *Drosophila melanogaster*. In *mBio* 4 (6), e00860-13. DOI: 10.1128/mBio.00860-13.

Broderick, Nichole A.; Lemaitre, Bruno (2012): Gut-associated microbes of *Drosophila melanogaster*. In *Gut Microbes* 3 (4), pp. 307–321. DOI: 10.4161/gmic.19896.

Clayton, T. Andrew; Baker, David; Lindon, John C.; Everett, Jeremy R.; Nicholson, Jeremy K. (2009): Pharmacometabonomic identification of a significant host-microbiome metabolic

interaction affecting human drug metabolism. In *Proceedings of the National Academy of Sciences of the United States of America* 106 (34), pp. 14728–14733. DOI: 10.1073/pnas.0904489106.

Consuegra, Jessika; Grenier, Théodore; Akherraz, Houssam; Rahioui, Isabelle; Gervais, Hugo; Da Silva, Pedro; Leulier, François (2020a): Metabolic Cooperation among Commensal Bacteria Supports *Drosophila* Juvenile Growth under Nutritional Stress. In *iScience* 23 (6), p. 101232. DOI: 10.1016/j.isci.2020.101232.

Consuegra, Jessika; Grenier, Théodore; Baa-Puyoulet, Patrice; Rahioui, Isabelle; Akherraz, Houssam; Gervais, Hugo et al. (2020b): *Drosophila*-associated bacteria differentially shape the nutritional requirements of their host during juvenile growth. In *PLOS Biology* 18 (3), e3000681. DOI: 10.1371/journal.pbio.3000681.

Cotten, Cameron; Reed, Jennifer L. (2013): Mechanistic analysis of multi-omics datasets to generate kinetic parameters for constraint-based metabolic models. In *BMC bioinformatics* 14 (1), p. 32. DOI: 10.1186/1471-2105-14-32.

Douglas, Angela E. (2019): Simple animal models for microbiome research. In *Nature Reviews Microbiology* 17 (12), pp. 764–775. DOI: 10.1038/s41579-019-0242-1.

Erkosar, Berra; Storelli, Gilles; Defaye, Arnaud; Leulier, François (2013): Host-intestinal microbiota mutualism: "learning on the fly". In *Cell Host & Microbe* 13 (1), pp. 8–14. DOI: 10.1016/j.chom.2012.12.004.

Fischer, Eliane; Sauer, Uwe (2005): Large-scale in vivo flux analysis shows rigidity and suboptimal performance of Bacillus subtilis metabolism. In *Nature Genetics* 37 (6), pp. 636–640. DOI: 10.1038/ng1555.

Gould, Alison L.; Zhang, Vivian; Lamberti, Lisa; Jones, Eric W.; Obadia, Benjamin; Korasidis, Nikolaos et al. (2018): Microbiome interactions shape host fitness. In *Proceedings of the National Academy of Sciences of the United States of America* 115 (51), E11951-E11960. DOI: 10.1073/pnas.1809349115.

Haiser, Henry J.; Gootenberg, David B.; Chatman, Kelly; Sirasani, Gopal; Balskus, Emily P.; Turnbaugh, Peter J. (2013): Predicting and manipulating cardiac drug inactivation by the human gut bacterium Eggerthella lenta. In *Science* 341 (6143), pp. 295–298. DOI: 10.1126/science.1235872.

Halfvarson, Jonas; Brislawn, Colin J.; Lamendella, Regina; Vázquez-Baeza, Yoshiki; Walters, William A.; Bramer, Lisa M. et al. (2017): Dynamics of the human gut microbiome in inflammatory bowel disease. In *Nature Microbiology* 2 (5), p. 17004. DOI: 10.1038/nmicrobiol.2017.4.

Hartstra, Annick V.; Bouter, Kristien E. C.; Bäckhed, Fredrik; Nieuwdorp, Max (2014): Insights into the role of the microbiome in obesity and type 2 diabetes. In *Diabetes Care* 38 (1), pp. 159–165. DOI: 10.2337/dc14-0769.

Hatti-Kaul, Rajni; Chen, Lu; Dishisha, Tarek; Enshasy, Hesham El (2018): Lactic acid bacteria: from starter cultures to producers of chemicals. In *FEMS Microbiology Letters* 365 (20). DOI: 10.1093/femsle/fny213.

Heeney, Dustin D.; Gareau, Mélanie G.; Marco, Maria L. (2018): Intestinal *Lactobacillus* in health and disease, a driver or just along for the ride? In *Current Opinion in Biotechnology* 49, pp. 140–147. DOI: 10.1016/j.copbio.2017.08.004.

Henriques, Sílvia F.; Dhakan, Darshan B.; Serra, Lúcia; Francisco, Ana Patrícia; Carvalho-Santos, Zita; Baltazar, Célia et al. (2020): Metabolic cross-feeding in imbalanced diets allows gut microbes to improve reproduction and alter host behaviour. In *Nature Communications* 11 (1), p. 4236. DOI: 10.1038/s41467-020-18049-9.

Henry, Christopher S.; DeJongh, Matthew; Best, Aaron A.; Frybarger, Paul M.; Linsay, Ben; Stevens, Rick L. (2010): High-throughput generation, optimization and analysis of genome-scale metabolic models. In *Nature biotechnology* 28 (9), pp. 977–982. DOI: 10.1038/nbt.1672.

Ito, Tsukasa; Okabe, Satoshi; Satoh, Hisashi; Watanabe, Yoshimasa (2002): Successional development of sulfate-reducing bacterial populations and their activities in a wastewater biofilm growing under microaerophilic conditions. In *Applied and environmental microbiology* 68 (3), pp. 1392–1402. DOI: 10.1128/AEM.68.3.1392-1402.2002.

Keebaugh, Erin S.; Yamada, Ryuichi; Obadia, Benjamin; Ludington, William B.; Ja, William W. (2018): Microbial Quantity Impacts *Drosophila* Nutrition, Development, and Lifespan. In *iScience* 4, pp. 247–259. DOI: 10.1016/j.isci.2018.06.004.

Klindworth, Anna; Pruesse, Elmar; Schweer, Timmy; Peplies, Jörg; Quast, Christian; Horn, Matthias; Glöckner, Frank Oliver (2013): Evaluation of general 16S ribosomal RNA gene PCR primers for classical and next-generation sequencing-based diversity studies. In *Nucleic Acids Research* 41 (1), e1. DOI: 10.1093/nar/gks808.

Komaroff, Anthony L. (2016): The Microbiome and Risk for Obesity and Diabetes. In *JAMA* 317 (4), pp. 355–356. DOI: 10.1001/jama.2016.20099.

Krajmalnik-Brown (2012): Effects of gut microbes on nutrient absorption and energy regulation. In *Nutr. Clin. Pract. Off. Publ. Am. Soc. Parenter Enter Nutr.* 27, p. 201.

Lee (2020): *Lactobacillus* attenuates progression of non-alcoholic fatty liver disease by lowering cholesterol and steatosis. In *Clin. Mol. Hepatol.*

Lieven, Christian; Beber, Moritz E.; Olivier, Brett G.; Bergmann, Frank T.; Ataman, Meric; Babaei, Parizad et al. (2020): MEMOTE for standardized genome-scale metabolic model testing. In *Nature biotechnology* 38 (3), pp. 272–276. DOI: 10.1038/s41587-020-0446-y.

Lin, Rui; Liu, Wentian; Piao, Meiyu; Zhu, Hong (2017): A review of the relationship between the gut microbiota and amino acid metabolism. In *Amino Acids* 49 (12), pp. 2083–2090. DOI: 10.1007/s00726-017-2493-3.

Liu, Yan; Wang, Yao; Ni, Yueqiong; Cheung, Cynthia K. Y.; Lam, Karen S. L.; Wang, Yu et al. (2020): Gut Microbiome Fermentation Determines the Efficacy of Exercise for Diabetes Prevention. In *Cell metabolism* 31 (1), 77-91.e5. DOI: 10.1016/j.cmet.2019.11.001.

Ludington, William B.; Ja, William W. (2020): *Drosophila* as a model for the gut microbiome. In *PLOS Pathogens* 16 (4), e1008398. DOI: 10.1371/journal.ppat.1008398.

Marco, Maria L.; Vries, Maaike C. de; Wels, Michiel; Molenaar, Douwe; Mangell, Peter; Ahrne, Siv et al. (2010): Convergence in probiotic *Lactobacillus* gut-adaptive responses in humans and mice. In *The ISME Journal* 4 (11), pp. 1481–1484. DOI: 10.1038/ismej.2010.61.

Martin, Alyce M.; Sun, Emily W.; Rogers, Geraint B.; Keating, Damien J. (2019): The Influence of the Gut Microbiome on Host Metabolism Through the Regulation of Gut Hormone Release. In *Frontiers in Physiology* 10, p. 428. DOI: 10.3389/fphys.2019.00428.

Oh, You-Kwan; Palsson, Bernhard O.; Park, Sung M.; Schilling, Christophe H.; Mahadevan, Radhakrishnan (2007): Genome-scale reconstruction of metabolic network in Bacillus subtilis based on high-throughput phenotyping and gene essentiality data. In *Journal of Biological Chemistry* 282 (39), pp. 28791–28799. DOI: 10.1074/jbc.M703759200.

Orth, Jeffrey D.; Conrad, Tom M.; Na, Jessica; Lerman, Joshua A.; Nam, Hojung; Feist, Adam M.; Palsson, Bernhard Ø. (2010): A comprehensive genome-scale reconstruction of Escherichia coli metabolism--2011. In *Molecular Systems Biology* 7 (1), p. 535. DOI: 10.1038/msb.2011.65.

Piper, Matthew D. W.; Blanc, Eric; Leitão-Gonçalves, Ricardo; Yang, Mingyao; He, Xiaoli; Linford, Nancy J. et al. (2014): A holidic medium for *Drosophila melanogaster*. In *Nature methods* 11 (1), pp. 100–105. DOI: 10.1038/nmeth.2731.

Raspor, Peter; Goranovic, Dusan (2008): Biotechnological applications of acetic acid bacteria. In *Critical Reviews in Biotechnology* 28 (2), pp. 101–124. DOI: 10.1080/07388550802046749.

Reis, M. A.; Almeida, J. S.; Lemos, P. C.; Carrondo, M. J. (1992): Effect of hydrogen sulfide on growth of sulfate reducing bacteria. In *Biotechnology and bioengineering* 40 (5), pp. 593–600. DOI: 10.1002/bit.260400506.

Ridley, Emma V.; Wong, Adam C-N; Westmiller, Stephanie; Douglas, Angela E. (2012): Impact of the resident microbiota on the nutritional phenotype of *Drosophila melanogaster*. In *PloS one* 7 (5), e36765. DOI: 10.1371/journal.pone.0036765.

Schönborn, Jürgen Wilhelm; Jehrke, Lisa; Mettler-Altmann, Tabea; Beller, Mathias (2019): FlySilico: Flux balance modeling of *Drosophila* larval growth and resource allocation. In *Sci Rep* 9 (1), p. 17156. DOI: 10.1038/s41598-019-53532-4.

Schretter, Catherine E.; Vielmetter, Jost; Bartos, Imre; Marka, Zsuzsa; Marka, Szabolcs; Argade, Sulabha; Mazmanian, Sarkis K. (2018): A gut microbial factor modulates locomotor behaviour in *Drosophila*. In *Nature* 563 (7731), pp. 402–406. DOI: 10.1038/s41586-018-0634-9.

Schuetz, Robert; Kuepfer, Lars; Sauer, Uwe (2007): Systematic evaluation of objective functions for predicting intracellular fluxes in Escherichia coli. In *Molecular Systems Biology* 3 (1), p. 119. DOI: 10.1038/msb4100162.

Schuetz, Robert; Zamboni, Nicola; Zampieri, Mattia; Heinemann, Matthias; Sauer, Uwe (2012): Multidimensional optimality of microbial metabolism. In *Science* 336 (6081), pp. 601–604. DOI: 10.1126/science.1216882.

Schwarzer, Martin; Makki, Kassem; Storelli, Gilles; Machuca-Gayet, Irma; Srutkova, Dagmar; Hermanova, Petra et al. (2016): *Lactobacillus* plantarum strain maintains growth of infant mice during chronic undernutrition. In *Science* 351 (6275), pp. 854–857. DOI: 10.1126/science.aad8588.

Schwengers, Oliver; Hoek, Andreas; Fritzenwanker, Moritz; Falgenhauer, Linda; Hain, Torsten; Chakraborty, Trinad; Goesmann, Alexander (2020): ASA3P: An automatic and scalable pipeline for the assembly, annotation and higher-level analysis of closely related bacterial isolates. In *PLOS Computational Biology* 16 (3), e1007134. DOI: 10.1371/journal.pcbi.1007134.

Sender, Ron; Fuchs, Shai; Milo, Ron (2016): Revised Estimates for the Number of Human and Bacteria Cells in the Body. In *PLOS Biology* 14 (8), e1002533. DOI: 10.1371/journal.pbio.1002533.

Shin, Seung Chul; Kim, Sung-Hee; You, Hyejin; Kim, Boram; Kim, Aeri C.; Lee, Kyung-Ah et al. (2011): *Drosophila* microbiome modulates host developmental and metabolic homeostasis via insulin signaling. In *Science* 334 (6056), pp. 670–674. DOI: 10.1126/science.1212782.

Silva, Valeria; Palacios-Muñoz, Angelina; Okray, Zeynep; Adair, Karen L.; Waddell, Scott; Douglas, Angela E.; Ewer, John (2020): The impact of the gut microbiome on memory and sleep in *Drosophila*. In *The Journal of experimental biology* 224 (Pt 3). DOI: 10.1242/jeb.233619.

Sommer, Andrew J.; Newell, Peter D. (2018): Metabolic basis for mutualism between gut bacteria and its impact on their host *Drosophila melanogaster*. In *Appl. Environ. Microb.* 85.

Spector, M. P. (2009): Metabolism, Central (Intermediary). In : Encyclopedia of Microbiology: Elsevier, pp. 242–264.

Storelli, Gilles; Defaye, Arnaud; Erkosar, Berra; Hols, Pascal; Royet, Julien; Leulier, François (2011): *Lactobacillus* plantarum promotes *Drosophila* systemic growth by modulating hormonal signals through TOR-dependent nutrient sensing. In *Cell metabolism* 14 (3), pp. 403–414. DOI: 10.1016/j.cmet.2011.07.012.

Storelli, Gilles; Strigini, Maura; Grenier, Théodore; Bozonnet, Loan; Schwarzer, Martin; Daniel, Catherine et al. (2018): *Drosophila* Perpetuates Nutritional Mutualism by Promoting the Fitness of Its Intestinal Symbiont *Lactobacillus* plantarum. In *Cell metabolism* 27 (2), 362-377.e8. DOI: 10.1016/j.cmet.2017.11.011.

Tilg, Herbert; Kaser, Arthur (2011): Gut microbiome, obesity, and metabolic dysfunction. In *The Journal of clinical investigation* 121 (6), pp. 2126–2132. DOI: 10.1172/JCI58109.

Turnbaugh, Peter J.; Gordon, Jeffrey I. (2009): The core gut microbiome, energy balance and obesity. In *The Journal of Physiology* 587 (Pt 17), pp. 4153–4158. DOI: 10.1113/jphysiol.2009.174136.

Vuong, Helen E.; Hsiao, Elaine Y. (2017): Emerging Roles for the Gut Microbiome in Autism Spectrum Disorder. In *Biological Psychiatry* 81 (5), pp. 411–423. DOI: 10.1016/j.biopsych.2016.08.024.

Weingarden, Alexa R.; Chen, Chi; Bobr, Aleh; Yao, Dan; Lu, Yuwei; Nelson, Valerie M. et al. (2014): Microbiota transplantation restores normal fecal bile acid composition in recurrent Clostridium difficile infection. In *American Journal of Physiology-Gastrointestinal and Liver Physiology* 306 (4), G310-9. DOI: 10.1152/ajpgi.00282.2013.

Zimmermann, Johannes; Kaleta, Christoph; Waschina, Silvio (2021): gapseq: informed prediction of bacterial metabolic pathways and reconstruction of accurate metabolic models. In *Genome Biology* 22 (1), p. 81. DOI: 10.1186/s13059-021-02295-1.

2.3. Physiological constraints limiting the growth of *Drosophila* larvae

Author: Jürgen W. Schönborn, Irfan Akhtar, Andrea Droste, Stephanie Wesemann and Mathias Beller

Contribution of Jürgen Wilhelm Schönborn:

- wrote the manuscript
- designed the experiments/study
- designed the graphical abstract, figures and tables
- parametrization of the metabolic network model and modeling experiments
- performed the modeling and wet-lab experiments
- evaluated and analyzed the data

This publication is preprinted at bioRxiv (bioRxiv 2023.12.20.572459; doi: https://doi.org/10.1101/2023.12.20.572459)

Physiological constraints limiting the growth of *Drosophila* larvae

Jürgen Schönborn[1,2], Irfan Akhtar[1,2], Andrea Droste[1,2], Stephanie Wesemann[1,2] and Mathias Beller[1,2]

1 Institut für Mathematische Modellierung Biologischer Systeme, Heinrich-Heine-Universität Düsseldorf, 40225 Düsseldorf, Germany

2 Systembiologie des Fettstoffwechsels, Heinrich-Heine-Universität Düsseldorf, 40225 Düsseldorf, Germany

* Corresponding author: jusch175@hhu.de

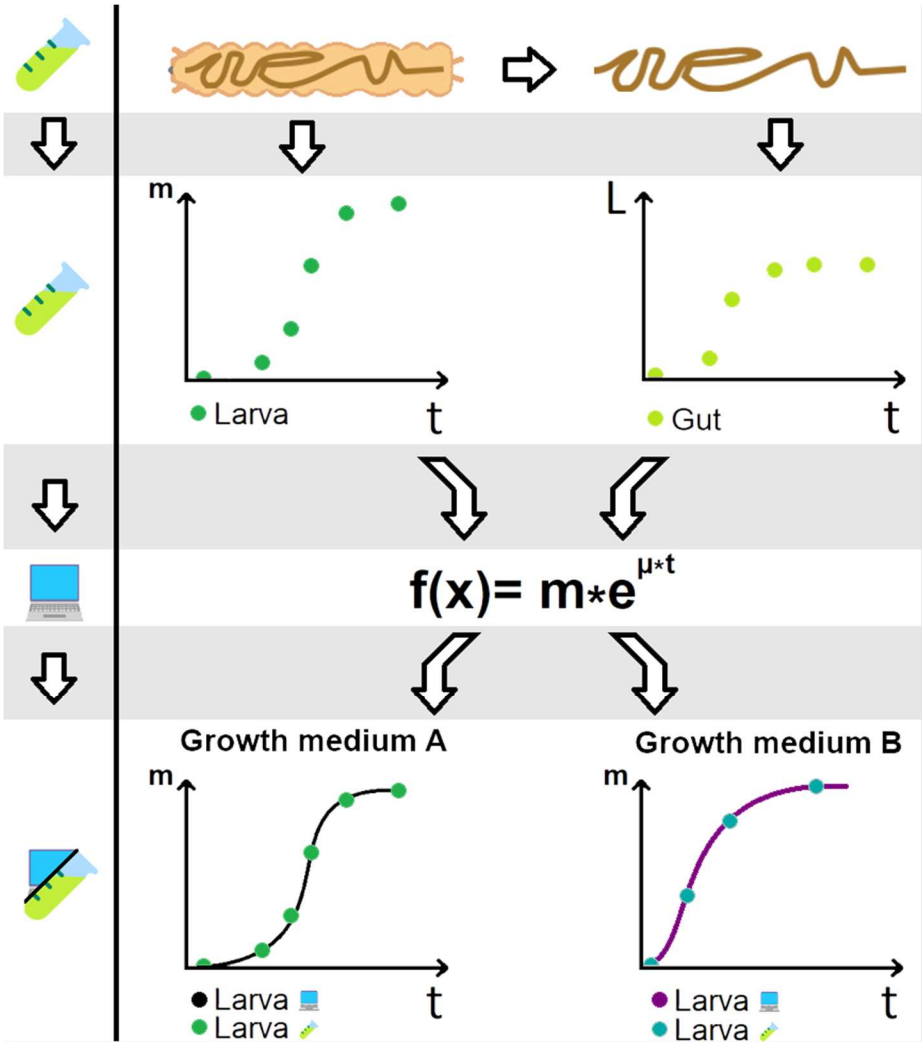

Graphical abstract

Abstract

The phenotype of organisms is the result of complex interactions between physiology, developmental conditions, and intra-organismic processes, such as metabolism and genetic adaptation. Organisms pursue various developmental strategies that depend on factors such as available resources. How organisms regulate and control critical developmental principles is not fully understood. In this study, we investigated the dynamic development of *Drosophila melanogaster* larvae through *in vitro* and *in silico* experiments. First, we enhanced the larval metabolic network FlySilico and its parameters using growth and metabolite measurements. Subsequently, we established a dynamic flux balance analysis approach and incorporated spatial physiological information from the larval gut to improve the prediction results. We successfully predicted larval growth on different media and developmental critical processes, such as the emergence of larval metamorphosis. This expands the ability to investigate and understand the process of the larval critical weight and, furthermore, the influence of critical developmental processes of multicellular organisms on metabolism. Thus, we present an approach to understand the development, metabolism, and the role of physiology in the development of multicellular organisms.

Introduction

Physiology plays a pivotal role in determining the capabilities and developmental outcomes of all organisms. Influences like environmental conditions affect the physiology of organisms. In the progress of organism's growth, malnourished higher organisms often manifest smaller overall sizes, leading to reduced organ or tissue proportions when compared to well-fed counterparts (McCance, 1960). The physiology of all living beings is an expression of their phenotypic traits influenced by diverse genetic responses to the varying environmental conditions experienced by the organism (Mitchell-Olds et al., 2007). Even small organisms like *Drosophila melanogaster* exhibit similar behavioral responses to changes in their environment. Throughout the larval growth stage, *Drosophila* undergoes a quick process of cellular division and specialization, during which numerous

essential genes involved in development are expressed. The progression of this growth phase can be affected by several factors, such as nutrient availability and temperature, which may alter the timing and pace of developmental events. Given its complexity, the growth of *Drosophila* larvae has been a popular model for comprehending the genetic and molecular mechanisms behind growth and development across various higher organisms (Roberts, 2006; Baker and Thummel, 2007; Melcher et al., 2007). Adult flies that developed from larvae raised at 18 °C show decreased mass and size, but exhibit a higher maximum walking speed compared to those developed at 25 °C on the same growth medium (Crill et al., 1996).

Physiology can be altered through genes and signals, although many of the complex interactions between them are still not fully understood as of today. These interactions, often involving a multitude of biological components and pathways, contribute to the distinctive characteristics and behaviors observed in organisms. While understanding these interactions demands a substantial investment of knowledge of the biological components and resources for investigation (Ginzinger, 2002; Tkačik and Walczak, 2011), the outcome is the emergence of a phenotype uniquely specific to the interactions themselves (Wright, 1941; Shingleton, 2010). These phenotypes are possibly easier to quantify as to measure the underlying gene-signal interaction network that led to the phenotype.

Under conditions of unrestricted feeding and stable environmental conditions, the duration of the larval stages, particularly the third instar larval stage, remain constant. This duration is sufficiently long to accumulate a large reservoir of resources, which is essential for beginning and surviving the metamorphosis (Aguila et al., 2007; Merkey et al., 2011). Larvae need to reach the so called “critical weight” (or “critical size”) (Moed et al., 1999). The critical weight is defined as the minimal weight needed to enter and survive the pupation to become an adult fly (Shingleton et al., 2007). Depending on how nutritious the growth medium is, the larvae can grow larger beyond the critical weight. It is known that growth of larvae and their tissue is dependent on the interaction of signal hormones (Riddiford and Ashburner, 1991). In addition, more known and unknown signals, along with genes, interact in various ways towards a complex

gene-signal network that enables the growth in a specific environment. Despite the complexity of the mechanics behind growing in different environments all organisms show distinct phenotypical and morphological features. Those features can be used to derivate the progress of growth to pin down growth phases and their underlying features.

The understanding of the underlying mechanisms of larval growth can be examined in different ways. Wet lab experiments can be conducted to investigate larval growth in terms of size and weight or to explain the genetic factors underlying larval development. The identification of such genetic factors offers valuable insights into the understanding of development but requires extensive labor and complex analysis to obtain meaningful conclusions (Anholt and Mackay, 2004). Furthermore, *in silico* experiments offer a valuable approach to gaining insights into the progression of larval growth during development. For this reason, different approaches can be used. One way to perform meaningful *in silico* experiments is the use of flux balance analysis (hereafter referred to as FBA) in combination with wet-lab experiments. *In silico* experiments with FBA were already successfully used with various organisms: (i) *Escherichia coli* was used to investigate growth, overflow metabolism, and energy consumption (Kauffman et al., 2003; Orth et al., 2010; Zeng and Yang, 2019) (ii) The growth and ethanol production of yeast cultures (Förster et al., 2003; Hjersted and Henson, 2009). (iii) The ATP yield of different carbon sources for human (Swainston et al., 2016). Moreover, FBA was already successfully used to understand the development and environmental impacts on *Drosophila melanogaster* larvae and flies by examining resource allocation, impact of altered growth conditions and the resulting impact on metabolic fluxes (Coquin et al., 2008; Feala et al., 2009; Schönborn et al., 2019; Cesur et al., 2023).

Investigations were made concerning the dynamics of organism's growth, changes in metabolism, nutrient uptake, and metabolite excretion over time using more advanced techniques involving FBA. Dynamic flux balance analysis (hereafter referred to as "dFBA") is one extended version of FBA that allows the investigation of dynamic changes in the simulation conditions, including extracellular concentration changes (Hjersted and Henson, 2006; Meadows et al., 2010; Henson and Hanly, 2014). dFBA enables the prediction of changes in

metabolite concentrations and fluxes both intra- and extracellularly over time. This was enabled through incorporating constraints that change the flux rates over time. This approach has found extensive use in predicting dynamic growth in cell culture dynamics making it suitable for studying cellular metabolism in batch cultures, for example for *E. coli* (Varma and Palsson, 1994) or Yeast (Hjersted and Henson, 2006).

This method illustrates that predicting the growth dynamics of cell batch cultures is feasible, although not all organisms share the same growth conditions as those found in batch cultures. For instance, laboratory-reared *Drosophila melanogaster* grow in an environment that closely resembles a continuous culture growth, where they receive a constant and steady supply of nutrients throughout their entire development with no changing extracellular metabolite concentrations. Therefore, the dFBA approach must be adjusted to effectively predict and describe the growth of organisms like *Drosophila* larvae. This can be achieved by integrating growth-related attributes to the simulations, such as the physiological properties of organisms.

We previously published the curated metabolic network FlySilico (Schönborn et al., 2019) of *D. melanogaster* based on time-resolved growth and metabolite measurements from larvae grown on *holidic diet* (Piper et al., 2014) (hereafter referred to as "HD"). The metabolic network consists of the core metabolism of *Drosophila*. To comprehensively explore larval metabolism across various environmental conditions a biomass function to simulate larval growth was formulated based on experimental metabolite measurements. However, FlySilico, predominantly characterizes the phase of larval growth marked by exponential expansion and potentially overlooking critical insights at the onset and conclusion of larval development.

Considering these limitations, we present an enhanced version of FlySilico. Our goal was to refine predictive accuracy by incorporating the initial and final stage of larval development, with a focus on the larva-to-pupa transition. Additionally, we aimed to identify factors that impose constraints on growth during these crucial developmental phases. First, we improved and expanded the underlying data that are used to determine growth parameters based on experimental

results. Secondly, we constructed a dFBA approach that fits the prediction of larval growth over the time. Thirdly, we show that phenotypes such as morphological attributes can be used to explain the growth through the larval stage of wild-type *Drosophila melanogaster*. We investigated the growth and pupation timing in dependence of their growth environment by using physiological information (such as size and weight) with a dFBA approach. For that we examined the larval gastrointestinal tract (hereafter referred to as "gut") and the larva itself on chemically defined and undefined growth media. Our data provide confirmation that the interplay between physiological characteristics and metabolic processes can effectively be used to estimate both the timing of pupation in larvae and their metabolic patterns during growth.

Results

Detailed analysis of larval growth and development

Our decision to acquire a more extensive dataset was motivated by the observation that the previously published FlySilico dataset lacked coverage of both the initial and final stage of the larval development. It had the potential to overlook significant developmental phases, such as the critical pupation timing. The pupation timing marks the completion of larval development. The inclusion of data about crucial developmental phases assures to improve the precision and quality of insights into larval development.

Under typical conditions, characterized by sufficient nutrient availability, stable temperature, and a wild-type genetic background, the weight increase of developing *Drosophila melanogaster* larvae follows an S-shaped exponential growth pattern, commonly referred to as sigmoidal growth. This growth pattern is evident in our dataset (Fig. 1).

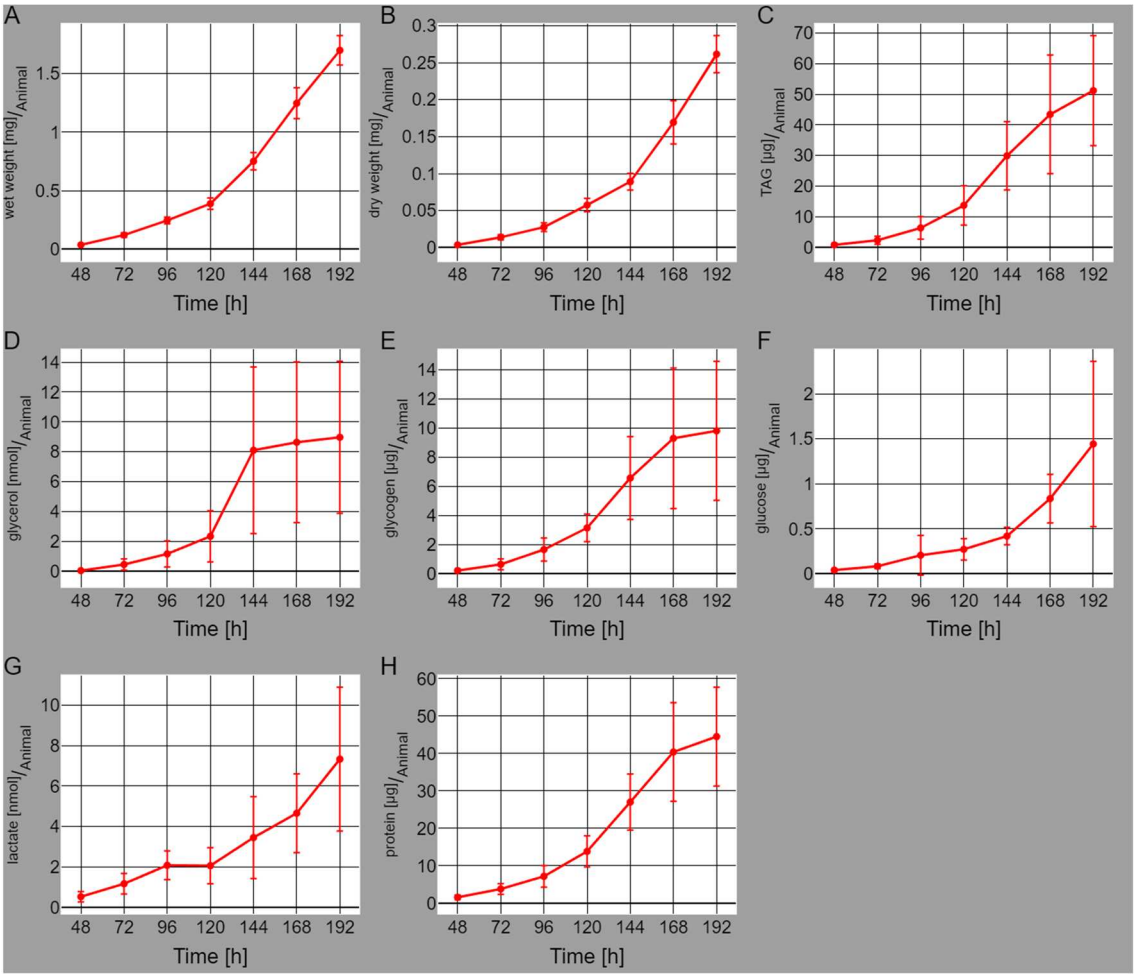

Figure 1: Metabolic profiling of the larval developmental of *Drosophila melanogaster* with growth from 48 to 192 hours after egg laying on holidic diet (HD). Wet weight (A) and dry weight (B) measurements of larvae from 48 hours every 24 hours to 192 hours. (C–H) Absolute quantification of TAG, glycerol, glycogen, glucose, lactate, and triglyceride (TAG) levels. The data is presented as mean values ± standard deviation normalized to the number of animals per sample (triplicate measurements). On average the pupation started around the 192 hours mark.

The data reveal a proportional relationship between the larval growth and the metabolite content, presenting three distinct phases. Initially, the growth progresses moderately, resulting in a lag-like phase. Subsequently, an exponential growth phase occurs, which leads to a third phase where the growth reaches a plateau which ultimately leads to pupation. We measured different larval growth parameters (e. g. larval weight and larval size dimensions) and the metabolic composition in a much more fine-grained and time-resolved manner in comparison to the first data set that we used in the first published FlySilico version (Schönborn et al., 2019).

In-depth enhanced larval *Drosophila* metabolic model

We expanded the previously published metabolic model FlySilico (Schönborn et al., 2019) by incorporating different pathways in greater detail such as the fatty acid biosynthesis and purine and pyrimidine metabolic pathways (Supplementary Table 1). These additional reactions cover the synthesis of macromolecules and polypeptides used to build up important tissues and structures. The current version of FlySilico contains 584 reactions and 326 unique metabolites (Table 1).

Table 1: Comparison of the previously published FlySilico and the FlySilico version from this study. The number of compartments lists the number of cellular compartments present in the respective metabolic network. The count of biomass components denotes the individual metabolite components form the biomass equation of the respective metabolic network.

Model	FlySilico 1.0	FlySilico 2.0	Δ Increase
# Reactions	363	583	+220
# Metabolites	203	326	+123
# Genes	261	443	+182
# Compartments	3	6	+3
# Biomass Components	31	40	+9

The more detailed fatty acid biosynthesis pathway representation was designed to allow us to make more precise statements on how the fatty acids are utilized in the metabolism and in terms of their impact on larval growth, as the fat body of larvae is one of the most important organs for growth and survival for the organism (Zheng et al., 2016). The fat body enables to store as much fatty acids as needed to survive the larval metamorphosis.

Drosophila larvae show a sigmoid weight gain over the course of the development (Fig. 1A, B). This comes with the problem that the growth rate and therefore the biomass function changes over the course of developmental timing. To address this issue while maintaining the use of flux balance analysis to predict the growth we chose to calculate a weighted mean metabolite coefficient for defining the demand of each metabolite essential for growth (view method section). This allows us to use a single coefficient for each metabolite contained in the biomass function over the time of development. Besides the improved single coefficient

for each metabolite in the biomass function we incorporate different important macromolecules into the biomass formulation.

Important structures for larval survival are the mouth-hooks and cuticle which both are made of a protein-chitin-matrix. The mouth-hook functions as the tool to take up nutrients into the organism while the cuticula functions as a stabilizer and protection for the larval body (Chihara et al., 1982; Ashburner, 1989). We include the metabolite chitin into the biomass function based on data from literature. The chitin content of an adult fly is around 7.85 % (Kaya et al., 2016) which we used as an approximation for the content of chitin in a larva.

RNA and DNA play an important role in the growth of every organism by applying significant influence on various aspects of an organism's development (Church and Robertson, 1966; Chícharo and Chícharo, 2008). For instance, anomaly in nucleic acids can contribute to the growth of tumors or other genetic mutations (Loeb et al., 2003). Since the previously published version of FlySilico does not contain any sufficient representation of nucleic acids, this absence limits the ability to make more precise observations. Therefore, meaningful conclusions about the impact and alterations of genetic information during development cannot be made without implementation. Thus, the inclusion of nucleic acids in our modeling is of importance to enhance the precision of the simulation results. We included nucleic acids to the metabolic network in a simplified form. The underlying building blocks of nucleic acids are incorporated into the biomass function. The building blocks are dAMP, dCMP, dGMP and dTMP for DNA and AMP, CMP, GMP and UMP for RNA. All mentioned building blocks received a biomass coefficient based on literature values from the yeast model of Förster et al. (2003). This should sufficiently enhance the predictive power of the larval metabolic network.

Modeling dynamic *Drosophila* larval growth

Flux balance analysis is usually used to predict a flux distribution that minimizes or maximizes a defined objective function (Varma and Palsson, 1994). This objective function can be a biomass function which describes the needed metabolites to synthesis biomass of an organism or a flux that synthesis a metabolite of interest (Kauffman et al., 2003). These predictions are performed

by FBA for a steady-state system. To predict the whole development of an organism like a *Drosophila* larva, the FBA approach needs to be calculated through developmental time which represents a non-typical steady-state system. This can be achieved using dynamic flux balance analysis (dFBA) modeling, where the prediction is performed in a time dependent manner with changing conditions. This technique has been previously demonstrated to successfully predict the growth *of E. coli* within a batch culture (Varma and Palsson, 1994). In a batch culture, *E. coli* relies on initial metabolite concentrations, which gradually evolve over time until all growth-supporting metabolites are consumed.

Drosophila larvae usually do not grow in a batch culture. The larval growth in a laboratory culture occurs usually under constant/overflow metabolite concentrations. The growth of larvae is different to a batch culture growth and has three important key setups: Firstly, the growth medium is usually a homogenous mixed system. Secondly, the metabolites used to grow do not deplete through the development from larva to an adult fly. Thirdly, no significant amounts of metabolic end products accumulate. This growth resembles rather the attributes of a continuous growth culture. The continuous culture growth is described as growth in an environment with steady stream of nutrients which allow growth at a continuous rate over an indefinite time (Novick and Szilard, 1950).

As a result, dFBA that models the growth and changing metabolite concentrations in larval metabolism throughout development, indicates unrestricted growth for a *Drosophila* larva (Supplementary Fig. 1).

Our hypothesis was that a fundamental mechanism limits the unrestricted growth of wild-type *Drosophila* larvae and contributes to the checkpoint regulating the entry into pupation. Therefore, we conducted an analysis of larvae and their various tissues, as the physiological characteristics could manifest the fundamental mechanism in a phenotypic manner (Fig. 2).

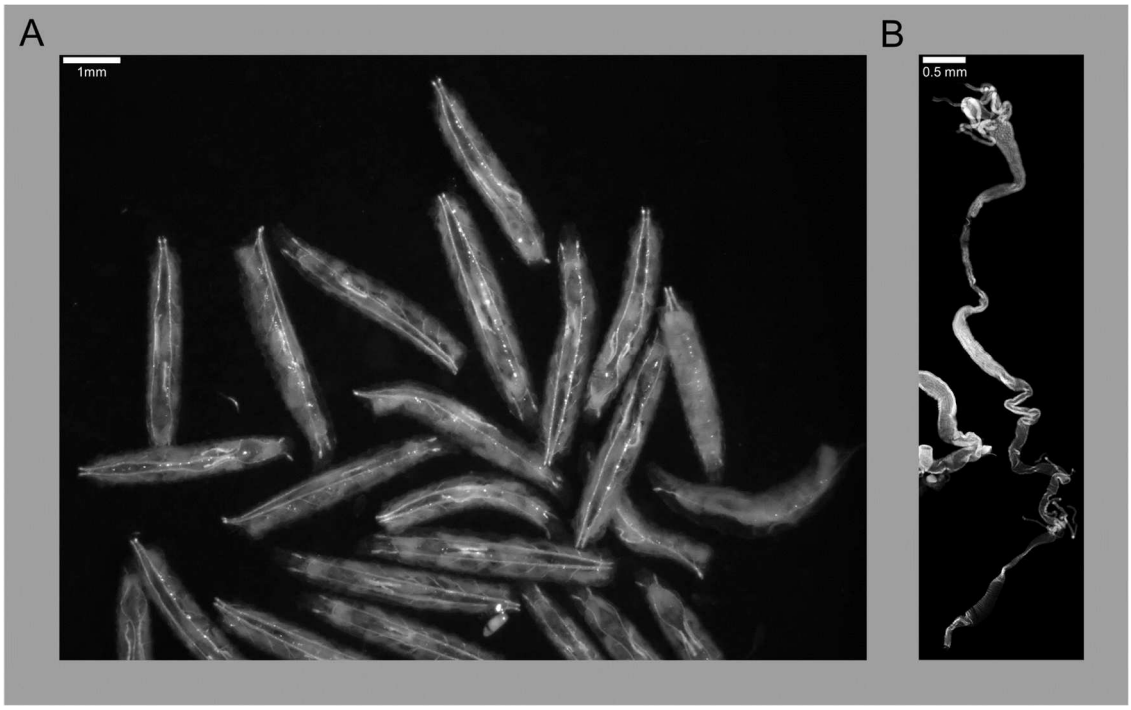

Figure 2: Growth of larvae reared on chemically defined medium. (A) Larvae growing on HD medium at 168 hours AEL. The photo was taken with a Stereomicroscope from Zeiss (SteREO Discovery.V8). The length, width and area were set manually by using the software Zeiss Zen 2.3 lite (blue edition). (B) Example of a dissected larval gut from an individual raised on HD at the 192 hours timepoint AEL. Sample was imaged with an Operetta CLS high content screening microscope (Perkin Elmer) and were recorded with a 20x air objective.

Upon analyzing the larval gut, we observed that the spatial parameters governing gut growth on HD growth medium halt before the larva transition into the wandering L3 stage, marking the onset of pupation (Fig. 3). The termination of gut growth prior to the wandering phase and pupation, presents an opportunity to establish a constraining parameter. This parameter endorses the simulation of larval growth to mimic the natural development observed in the real world.

Modeling the gut as a constraining parameter in growth simulations

To address the previously mentioned issue of unlimited growth in larvae, we implemented a penalty function based on morphological and physiological attributes of the larval gut. The design of this penalty function was inspired by the sigmoidal growth patterns observed in both larval weight (Fig. 1A and B) and gut development (Fig. 2A-C).

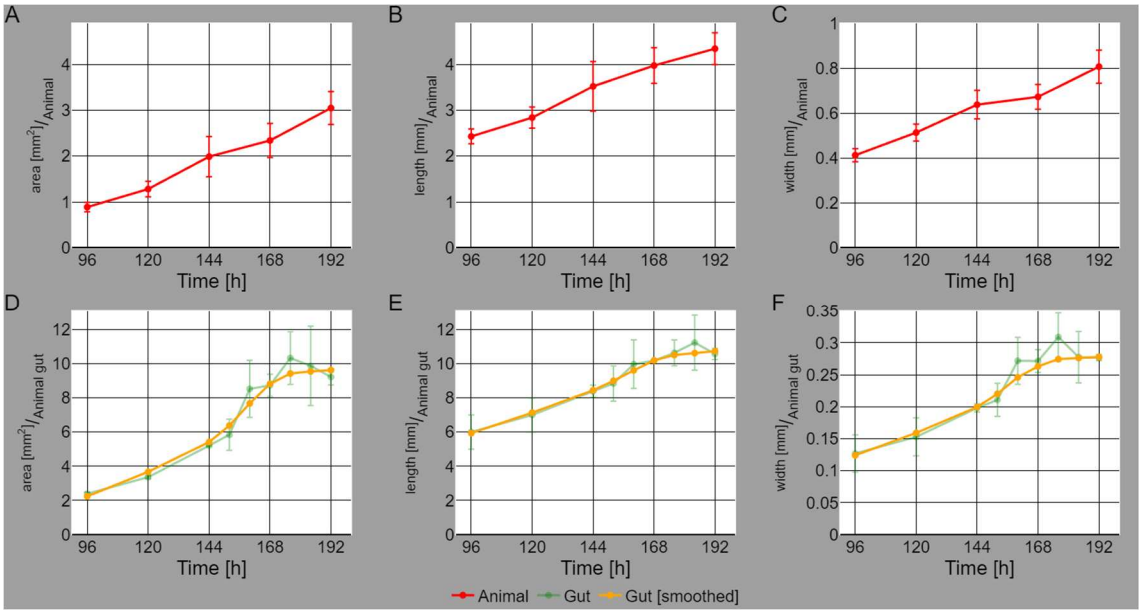

Figure 3: Growth dynamics of *Drosophila melanogaster* larvae and gut. (A-C) Gradual growth in the area, length, and width of developing larvae. The area is calculated based on the length and width of a larvae. Each timepoint consist of at least 20 larvae (triplicate measurements). The data are presented as mean values ± standard deviation normalized to the number of animals per sample. (D-F) Increase of area, length, and width of the gut from developing larvae. The area is calculated based on the length and width for each gut. Each timepoint consist of at least 8 guts (triplicate measurements). The unsmoothed data (shown in green) and smoothed data (shown in yellow) illustrate the sigmoid progression of larval gut growth. Initially, a rapid growth from 96 hours to 168 hours is present which is followed by a nearly plateau from 168 to 192 hours. The data is presented as mean values ± standard deviation normalized to the number of guts per sample (green). On average the pupation started around the 192 hours mark.

The penalty function was implemented to regulate nutrient uptake through the gut and subsequently limit larval growth (see Method section). During the early stages of larval development, the penalty function did not impose any limitations on growth, as the gut efficiently absorb nutrients from the growth medium and allocate the resources fully to larval growth (Fig. 4; Supplementary Fig. 3). As the development further progresses a change in the growth pace is visible which is the result in a decrease of growth rate due to the limitation of the gut function on nutrient uptake (Fig. 4).

This transition is evident during the phase when larvae enter the critical weight range, leading to a stage of minimal to no growth. Simultaneously, growth of the gut declines and its expansion halts (Fig. 3). The penalty function mimics this process as it reduces the nutrient uptake specifically for growth in the simulation. This reduction in nutrient uptake resulted in a decrease in growth rate. As the growth rate continued to decrease, it reaches a point where no further growth was possible. Upon reaching this point, the critical weight is already achieved

and, along with the halting of gut growth, it serves as a signal of the larva's transition towards eventual pupation.

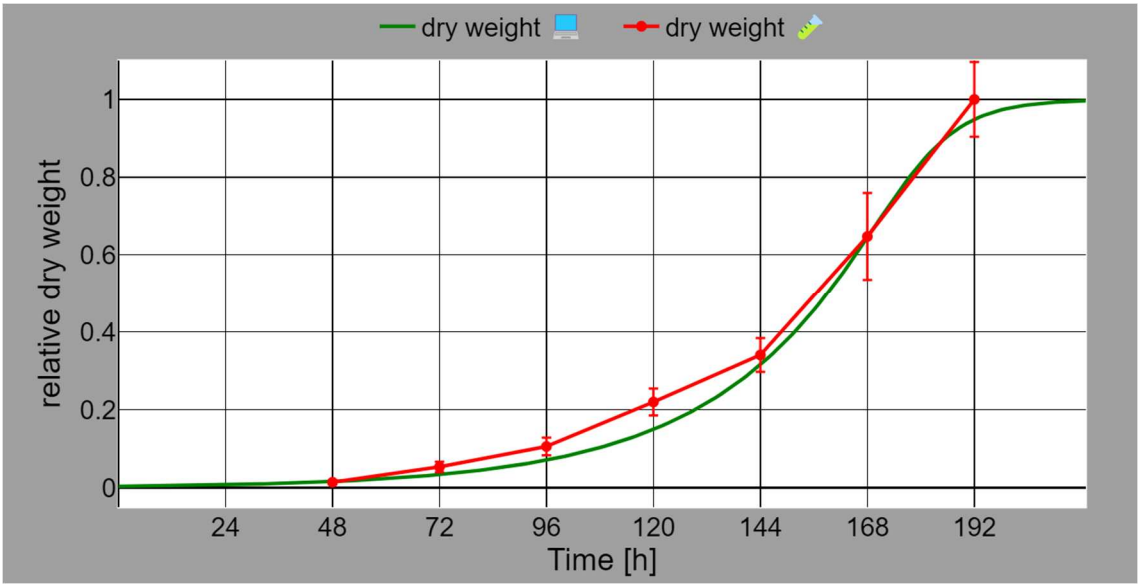

Figure 4: Comparison of *in vitro* and *in-silico* larval growth on chemically defined growth medium. We simulated the *in silico* growth of a larva (green; dry weight) on HD by using the dFBA approach (see method section). The growth of the larva resembles a sigmoidal growth curve till it reaches a plateau starting around 192 hours. The growth of larvae reared *in vitro* (red; dry weight) on HD, starts at 48 hours till 192 hours AEL. The growth *in vitro* shows a small variance in comparison to the *in silico* growth based on the relative dry weight values. On average the pupation started around the 192 hours mark.

The penalty function is mathematically described as a negative sigmoidal function (Supplementary Fig. 3) which runs between 1 and 0. This function is based on different attributes of the larval development which enables the successful integration into the dFBA simulation. The penalty function describes the timing where the larval gut from larvae grown on HD stopped growing. This is roughly around 180 hours after egg laying (AEL) on HD with a function value of 0.5. This is represented by the largest change in the gradient of the function on the timepoint 180 hours AEL which is the turning point of the function (Supplementary Fig. 3). This important time point in the development of larvae under standard conditions grown on HD show a correlation to the critical weight and the end of the development of the gut. Around the turning point of the function a phase is visible which overlaps with the range where the critical weight is reached. This phase of the function starts around 128 hours with a function value of around 1 and ends around 218 hours with a function value of nearly 0. The most crucial impact on the simulation becomes apparent when we observe a particular gradient value, approximately 0.6. This occurs during the time period between

168 hours and nearly 192 hours (Supplementary Fig. 3). Notably, this specific time interval corresponds to the critical weight range, a phase where larvae are capable of initiating pupation. This gradient change results in a sharp decline of the gut function and consequently flattening of the larval growth curve (Fig. 4). This flattening signifies a critical transition point in the larval development process due to the reduced nutrient absorption of the gut.

In summary, the introduction of a negative sigmoidal penalty function based on physiological attributes effectively limits nutrient uptake and controls the growth rate in larvae. This regulation played a crucial role in determining the larva's entry into the wandering L3 phase and subsequent pupation based on the simulation results (Fig. 4). Having successfully run the dFBA simulation of larval growth on HD under standard conditions by incorporating the penalty function (Fig. 4), it is now intriguing to explore whether the current dFBA simulation can accurately predict outcomes in unfamiliar scenarios.

Dynamic growth model verification

The first step in our model verification procedure was to select an unfamiliar scenario for the simulation. We chose to test our simulations on a complex medium called low sugar diet as this diet prominently alters the developmental timing (see method section; hereafter referred to as "LSD"). We defined the underlying growth medium parameters by defining the mediums components and their corresponding amounts (Supplementary Table 2). As LSD is a complex medium, the amount and composition of nutrients available for intake into the metabolic network can vary depending on the complex medium defined for the simulation. This variation in the case of growth, can lead to differences of growth rate in the simulation. Next, we performed growth simulations that were promising as the growth timing was predicted to be much shorter (120 hours for larval grown on LSD in comparison to 192 hours for larval grown on HD).

In the case of the complex LSD medium, the penalty function revealed a shift in the turning point to approximately 100 hours AEL (Supplementary Fig. 4). This is due to the accelerated growth rate in comparison to HD medium. The time point of 100 hours shows a function value of 0.5. The gradient is changing in a range which starts around 76 hours till the end of around 128 hours. This is a smaller

phase where the gradient changes in comparison to the penalty function for the HD and results from the much faster growth of the larva on LSD.

Subsequently, we performed corresponding *in vitro* growth experiments following the initial simulations carried out. We grew larvae on LSD under the same standard conditions as they were grown on HD (see Method section). We measured necessary parameters like weight for larvae reared on LSD (Fig. 5).

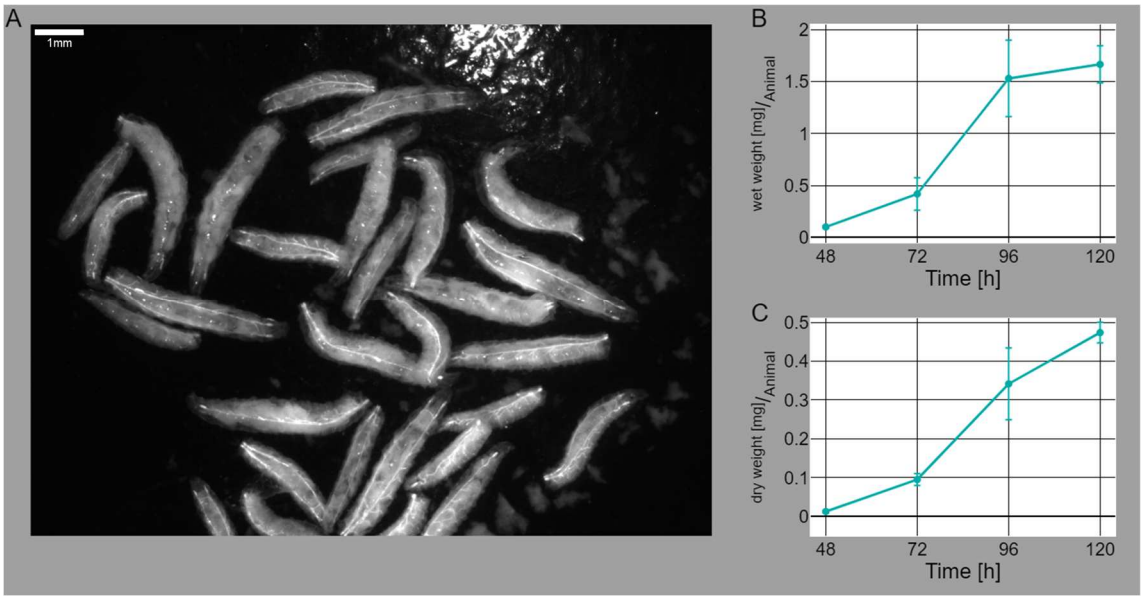

Figure 5: Growth of larvae reared on complex medium. (A) Growing larvae on LSD medium at the timepoint of 72 hours AEL. The photo was taken with a Stereomicroscope from Zeiss (SteREO Discovery.V8). The length, width and area were set manually by using the software Zeiss Zen 2.3 lite (blue edition). Wet weight (B) and dry weight (C) measurements of larvae from 48 hours every 24 hours to 120 hours grown on LSD. Each timepoint consist of at least 50 larvae (duplicate measurements) up to 75 larvae (triplicate measurements). On average the pupation started around the 120 hours mark.

We compared our *in silico* simulations to the experimentally assessed data and found both were in accordance with each other proving the robustness of our *in silico* simulations (Fig. 6). The growth simulation indicated that larvae raised on the LSD medium reveal a developmental period of around 120 hours AEL, mirroring the *in vitro* findings, which also report a 120-hour developmental duration for the larvae.

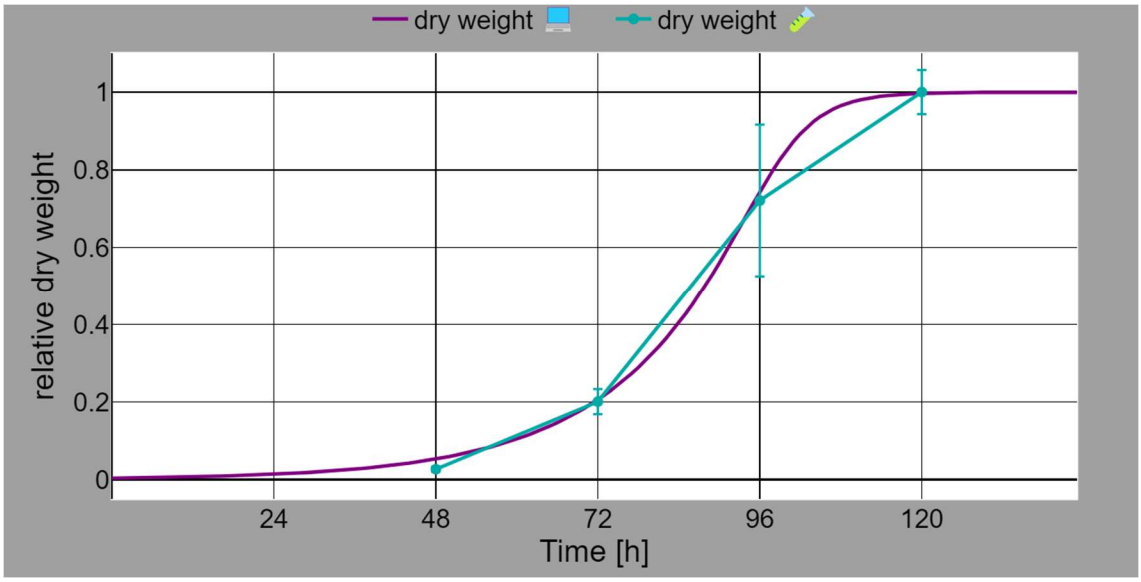

Figure 6: Comparison of *in vitro* and *in-silico* larval growth on complex growth medium. We simulated the *in silico* growth of a larva (purple; dry weight) on HD by using the dFBA approach (see method section). The growth of the larva follows a sigmoidal growth curve till it reaches a plateau starting around 120 hours. Larval growth observed *in vitro* (dark cyan; dry weight) on HD medium, starts from 48 hours till 120 hours AEL. The growth *in vitro* shows a small variance in comparison to the *in silico* growth based on the relative dry weight values.

These results demonstrate the consistency between our modelling data and experimental observations, affirming the validity of employing physiological data in combination with dFBA to predict larval development, even in complex environmental conditions.

Discussion

In this study, we investigated the physiological aspects of *Drosophila melanogaster* larval growth through a combination of *in vitro* experiments and *in silico* simulations. Laboratory-reared wild-type Oregon-R larvae were raised on chemically defined and complex growth medium. Subsequently, we collected physiological and metabolic data, which served as the basis for our *in silico* growth and metabolism modelling analyses.

We translated a fine-grained metabolic profile of growing larvae on HD (Fig. 1) into single coefficients for each metabolite in the biomass function. The growth behavior of *Drosophila* larvae is evidently complex, and a simplistic approach of employing single coefficients for each metabolite in the biomass function falls short of providing a comprehensive explanation for their growth and

metamorphosis dynamics. Nevertheless, streamlined models such as FlySilico, with simplified parameters, offer the advantage to understand fundamental principles and mechanisms of metabolic processes and their consequences. These models are useful for identifying larger metabolic pathways to answer specific biological questions. In the context of larval growth, FlySilico demonstrated which metabolic pathways are essentially required for simulating growth (Schönborn et al., 2019). These models can assist in identifying critical factors and interactions within an organism's metabolism, such as the influence of different nutrients and their quantities on metabolism and growth, as demonstrated in FlySilico (Schönborn et al., 2019). Additionally, in cases where information and data are limited, such models can still provide meaningful insights, whereas large-scale complex models might require additional data. The development of a *Drosophila* larva has different distinct stages (Bate and Martinez Arias, 1993). The developmental process begins with the embryonic stage and progresses through the first, second, and third instar larval stages. Each of these stages show distinct growth patterns and timelines. At the end of the larval development, the larva undergoes a pupation and emerges as an adult fly. The various stages of larval development are expected to have diverse metabolic patterns, much like what is observed during larval embryogenesis (An et al., 2014). The variability in larval growth within a population is noticeable, with some individuals show lower or higher growth rates than others. This variance can be attributed to various factors, such as environmental conditions or genetic backgrounds. To ensure the robustness of conclusions the results are based on the average growth pattern observed in the larval population. Therefore, as distinct metabolic profiles and growth trajectories are expected during different developmental stages, it remains feasible to employ singular coefficients within the biomass function. This approach yields an averaged growth rate over the entire developmental period as these result from the utilization of weighted-average metabolic coefficients. This simplified modelling approach enables the investigation and analysis of larval growth throughout the entire development in simulations with minimal variation to the real world (Fig. 4 and Fig. 1).

Organ growth is influenced by various factors, such as environmental conditions, different signaling pathways, and communication between organs (Andersen et

al., 2013). For that reason, an addition of the FBA simulations is needed to simulate these complex signaling pathways. The incorporation of signaling pathways within FBA models help to understand how signals affect metabolic fluxes, as signaling pathways often regulate metabolic processes (Ward and Thompson, 2012). Incorporating these results could significantly impact the accuracy of FBA simulations, leading to predictions that better mirror real-world scenarios in the best case. Although there are established methods that combining (d)FBA with signaling networks (Papin and Palsson, 2004; Price et al., 2004; Covert et al., 2008), these approaches often face challenges due to the requirement for extensive data. These data are not always readily available or sufficiently detailed for use with FBA (Covert et al., 2001; McKechnie et al., 2010; Hiruma and Kaneko, 2013; Nijhout et al., 2014). The approach we used in this study therefore does not delve into complex signaling pathways. To address these challenges, we have chosen a simpler approach: we assume that the signals and interactions governing organ growth led to specific, defined phenotypes. In other investigations, it has been demonstrated that the physiological functions of various organs contribute to the attainment of developmental stages. For instance, Mirth et al. (2005) observed that the larval organ, the prothoracic gland, plays an important role in determining the critical weight required for the metamorphosis of *D. melanogaster* and secretes growth-related hormones. These characteristics can be effectively translated and integrated into our dFBA approach, making it a more practical and accessible method. It is known that (d)FBA is sensitive to the chosen parameters to a certain degree (Varma and Palsson, 1995). Considering these observations, it becomes evident that the introduction of additional parameters, such as a complex signaling pathway, could significantly alter the predictive outcomes. The prediction of larval growth becomes challenging under such conditions.

The *in silico* approach FBA was improved further into a variation of dFBA. The dFBA approach allows simulations were the larval growth and their metabolic content itself can be analyzed during larval development. The dFBA approach is already established and successfully used for different organisms, such as *E. coli* (Varma and Palsson, 1994). It is an established algorithm that is also implemented in different tools such like the COBRA Toolbox (Heirendt et al.,

2019). The reason why we created an altered version of dFBA is, that the growth of larvae is not possible to be predicted by the unaltered algorithm. The growth of larvae has fundamentally different conditions to a growth scenario for a bacterial culture. The larval growth medium is homogenous mixed and the used metabolites from the medium usually do not deplete through the larval development. Therefore, the metabolite concentration in the medium does not change which is the fundamental condition that the established dFBA algorithms uses as the metabolite concentration changes over the developmental time are calculated (Varma and Palsson, 1994). This results in the case of the larval development into an unlimited growth (Supplementary Fig. 1) which needed to be addressed. To address this issue for dFBA we analyzed different tissues as we hypothesized that physiological properties can be found to solve this unlimited growth issue. We found that the larval gut is a promising candidate to solve the unlimited larval growth.

The larval gut plays a major role in systemic growth. If larvae sense conditions of poor nutrient concentration of the growth medium, the gut crosstalks through signals with the fat body which signals the reduction of larval growth rate (Shin et al., 2011; Storelli et al., 2011; Andersen et al., 2013). Conversely, this signaling activity is not fully understood. In developing larvae, we observed that the larval gut stops to increase in size earlier than the onset of pupation (Fig. 3). As the larval gut plays an important role in larval growth, it provides an entry point for integration into the modelling of the larval growth. The growth of the larval gut and its premature stop were consequently translated into a growth-determining parameter (see Result section) within the *in silico* simulation. This made the prediction of larval growth over the time, including its termination and the correct pupation timing prediction possible (Fig. 4).

Our early results regarding the predictions of *Drosophila* larvae growth on HD through additional physiological and metabolic data are promising. They suggest that simulations with the enhanced model should be able to correctly predict different conditional scenarios.

To ensure the reliability of the growth-determining parameter, additional *in silico* simulations were performed. In these simulations, the growth for larvae raised on

the complex medium LSD were predicted. We reasoned that the successful prediction of the HD growth situation should also elevate the simulations to be able to predict different growth situations of experimentally different conditions. If this is the case, this shows that our approach, to use physiological information for prediction, is valid to be used in changing growth conditions and successful predict those. Based on the previous *in silico* simulations we performed equivalent *in vitro* wet lab experiments on LSD medium (Fig. 5). The simulations revealed that the growth of larvae could be accurately predicted as they align well with the experimental data (Fig. 6). This confirms our assumption that the combination of physiological and metabolic attributes can be used to successfully predict the growth of *Drosophila* larvae on defined and complex growth media.

Shortcomings of predictions based on phenotypical attributes

The presented results show promising findings to understand the larval growth. The performed experiments and simulations show valid results for wild-type OregonR larvae. It is evident that the case of non wild-type larvae is not precisely predictable as the metabolism of the non wild-type can heavily change in comparison to the metabolism of wild-type larvae. Predicting larval growth from mutation-harboring *Drosophila* lines is especially challenging, as these mutations can induce growth-affecting phenotypes (Migeon et al., 1999). Further iterations and improvements on the used dFBA and experimental setup might solve some of these shortcomings by integrating additional genetic information. This could be used to create a simulation that mimics the situation with a mutation background. Ultimately, the introduction of genetic information with rules that constrain the simulation set even more difficulties to interpret the results. The simulation is required to use highly curated genetic information about growth changing mutations if it should be used for dFBA. Addressing the prior mentioned issues will yield valuable insights into growth, physiology, and metabolism.

In conclusion, our findings support the potential of integrating physiological data into metabolic models enabling the generation of valuable growth-related predictions. This study demonstrated that the physiology of complex multicellular organisms stands in relationship with metabolic processes. We could present that gut growth play a role as a regulatory factor for overall organismic growth, a

phenomenon observed in wild-type *D. melanogaster* larvae. The enhanced metabolic model of FlySilico enabled the successful prediction of larval growth over the entire development for various conditions. The incorporation of physiological data from the larval gut enhanced the prediction power of FlySilico, allowing the accurate estimation of developmental critical milestones, including the reach of the critical weight and further the pupation. This enables further in-depth investigations into the mechanisms of critical weight. The extension of this approach to incorporate additional physiological data, potentially involving multiple organs concurrently, holds great promise. These extensions empower the possibility of predicting more favorable growth scenarios.

Ultimately, this approach has the potential to facilitate the translation of these findings to predict even the growth of more complex organisms. Furthermore, this could lead to the possibility to formulate a hypothesis that gut growth and physiology is not only limiting factors for complex organisms like *D. melanogaster* but may also play a crucial role in regulating development and health of extrauterine growing organisms, including humans. We propose that variations in gut physiology, nutrient absorption, and growth in stages, like infants, have a lasting impact on the fitness of individuals and could restrict growth. This hypothesis, along with potentially others, supports future research studies.

Materials and Methods

Fly strains and rearing

The fly lines that were used in this study are Oregon-R. Flies were maintained at 25 °C with 60-70 % humidity and a 12 h light/dark cycle.

Chemically defined fly medium holidic diet (HD)

The chemically defined fly medium HD was used based on the instructions of Piper et al. (2014). The parametrization was performed according to Schönborn et al. (2019).

Complex fly medium low sugar diet (LSD)

The complex fly medium LSD was used based on the complex medium from Backhaus B. et al. (1984) and altered according to Musselman et al. (2011). The parametrization was performed according to Schönborn et al. (2019) and based on the available data of the used ingredients (see Supplementary Table 2). As not all information were unambiguously, we used approximated values.

Metabolic profiling

All data were measured according to the protocols by Schönborn et al. (2019) and under standard conditions on the growth medium *holidic diet* (Piper et al., 2014; Piper et al., 2017) or low sugar diet.

Fixation, histological staining, and mounting

The larval guts were dissected in ice-cold PBS and fixed in RNA-fix (10 % 10x PBS, 10 % 0.5 M EGTA pH 8.0, 10 % Paraformaldehyde, dH20 70 % - 1:1 dilution before use with dH20) for 40 minutes. The RNA-fix solution was removed, and the guts were washed with PBS (1x) for 5 minutes.

Alexa Fluor® 488 Phalloidin (300 U dissolved in 1.5 ml methanol) was used as the staining agent and diluted 1:500 in PBS before direct usage. 1 ml of the diluted Alexa Fluor® 488 Phalloidin solution were used to stain the guts for 30 minutes. After staining the guts were washed with PBS (1x) for 5 minutes.

The guts were mounted on microscope slides in 30 µl Prolong Gold Antifade reagent.

Constraint-based modeling

Flux balance analysis (FBA; Orth et al., 2010) was used to perform the underlying growth simulations and metabolic flux analysis.

Biomass coefficients

We measured the same metabolites in this publication and according to the previously published FlySilico (Schönborn et al., 2019) version. The reason is that the measured metabolites are the most abundant metabolites present in a *Drosophila* larva which should sufficiently represent the growth of the larva. We extended the range where we measured the metabolite contents in comparison to the previously published FlySilico version. Here, we calculated a **w**eighted **m**ean **m**etabolite **c**oefficient (WMMC) for the biomass function. The WMMC should realistically represent a single value of the changing quantity of metabolites to make up the biomass through the larval development. The WMMC is calculated as followed by starting to calculate a polynomial fit $f_x(t)$ of the measured data, where x represents the metabolite and t the timepoint. Next, we used the values of the derivation $f'_x(t)$ at the timepoints where we measured our data of the metabolites and normalized them between 0 and 1 as followed:

$$WMM_x = f'_x(t) * w_{x,t} \tag{1}$$

where WMM_x is the **w**eighted **m**ean of **m**etabolite x in either μg or $nmol$ and $w_{x,t}$ is the measured weight of metabolite x at timepoint t. With the WMM from Equation 1 we can calculate the WMMC:

$$WMMC_x = \frac{\frac{WMM_x}{M_{r,x}}}{w_{\Delta dry}} \tag{2}$$

where $WMMC_x$ represents the weighted mean metabolite coefficient of metabolite x in $\frac{mmol}{g}$, $M_{r,x}$ is the molecular weight of metabolite x and $w_{\Delta dry}$ is the mean weight gain in g. The mean weight gain is calculated as followed:

$$w_{\Delta dry} = \frac{\sum_{t=1}^{n}\left(w_{t,dry} - w_{t-1,dry}\right)}{n} \tag{3}$$

where $w_{t,dry}$ is the dry weight of the larva at timepoint t and $w_{t-1,dry}$ is the dry weight of the larva at the previous timepoint $t-1$.

Additionally, we calculated a chitin biomass coefficient based on data present in the literature. The literature regarding the chitin content of larval *Drosophila* was not clear how large it is. Therefore, we used the chitin content of adult flies to

approximate the content of larval chitin in combination with our data. Kaya et al. (2016) determined the content of chitin in adult fly is 7.85 %.

The chitin biomass coefficient was calculated with the following equation:

$$x_{chitin} = \frac{\frac{w_{dry,192h} * 0.0785}{203.19\ \frac{g}{mol}}}{w_{dry,192h}} \quad (5)$$

where x_{chitin} is the biomass coefficient of chitin represented in the biomass function, $w_{dry,192h}$ is the dry weight in gram dry weight (*gDW*) of a larva at 192 hours AEL on HD, 0.0785 represents the chitin content from literature (Kaya et al., 2016) and $203.19\ \frac{g}{mol}$ is the molar mass of chitin.

The resulting chitin biomass coefficient is $x_{chitin} = 0.3863\ \frac{mmol}{gDW}$.

Growth model equations

The larval growth of *Drosophila* is described by literature as an exponential growth. The growth in our model according to the literature modeled with a basic exponential growth function:

$$m = m_{t-1} * e^{\mu * \Delta t} \quad (4)$$

where m describe the biomass of the larval at the timepoint t in $mgDW$, m_{t-1} describes the biomass of the larval at the previous timepoint $t-1$, μ describes the growth rate derived from the FBA solution and Δt describes the timestep size for which the calculation is.

The uptake rates $v_{x,t0}$ of each most abundant metabolite x in the growth medium HD at the initial timepoint $t0$ where calculated based on the new experimental data according to Schönborn et al. (2019).

The uptake rate at each timepoint in the dynamic FBA (dFBA) approach is calculated as followed:

$$v_{x,t} = v_{x,t0} * f(t)_{gut} \quad (5)$$

where $v_{x,t}$ describes the uptake rate of metabolite x at the timepoint t in $\frac{mmol}{gDW*h}$, $v_{x,t0}$ describes the uptake rate of metabolite x at the initial timepoint $t0$ and $f(t)_{gut}$ describes the dimensionless gut resorption penalty function.

The gut resorption penalty function is defined as following sigmoidal function:

$$f(t)_{gut} = \frac{1}{1 + \frac{t}{t_{\mu,max}}^{24}} \quad (6)$$

where t describes the current timepoint in the dFBA simulation in hours and $t_{\mu,max}$ describes the timepoint where the growth of the larvae should be at maximum in hours. Therefore, $t_{\mu,max}$ is defined as followed:

$$t_{\mu,max} = \frac{\mu_{HD}}{\mu_{max}} * 180 \quad (7)$$

where μ_{HD} describes the growth rate for larvae on HD growth medium in h^{-1}, μ_{max} describes the maximum growth rate of the current simulation time range and 180 hours describes marks the timepoint where the larval gut of larva grown on HD medium enters the plateau-like state (Fig.3 D-F). Furthermore, this timepoint lies within the range when the larvae attain the critical weight threshold while fed on HD medium.

All calculations and predictions are available in the supplementary information presented in a user-friendly way.

Competing interests

The authors declare that they have no competing interests.

Funding

The project was financed through the German “Bundesministerium für Bildung und Forschung (BMBF)” grant 031A 306 (to M. Beller) and in part by a scholarship of the Jürgen Manchot Foundation (to J.W. Schönborn). The funders had no role in the study design, analysis, interpretation of the results or the writing of the manuscript.

Acknowledgements

We would like to thank all members of the laboratory for their helpful comments and support, and Oliver Ebenhöh for his discussions during the initial phase of the project.

Contributions

J.S. and M.B. designed the study. J.S. established the metabolic network and performed the modeling experiments. J.S., A. D., I. A., and S. W. performed the *Drosophila* experiments and wet lab procedures. J.S. and M.B. analyzed the data and prepared graphs. J.S. and M.B. wrote the manuscript.

Supplementary Information

Physiological constraints limiting the growth of *Drosophila* larvae

Jürgen Schönborn, Irfan Akhtar, Andrea Droste, Stephanie Wesemann and Mathias Beller

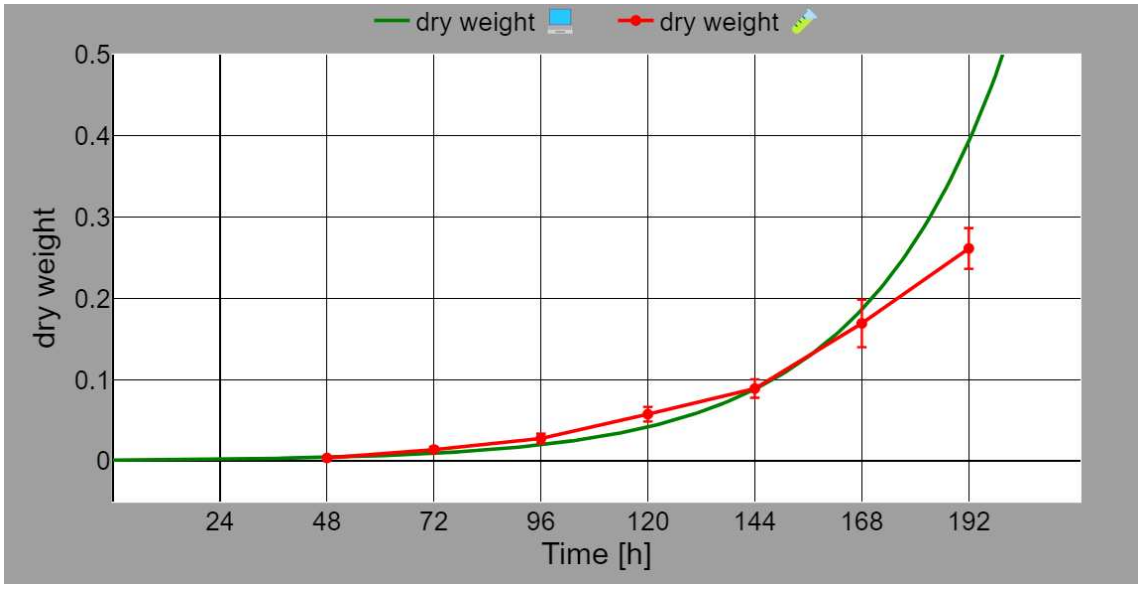

Supplementary Figure 1: Comparison of *in vitro* and *in-silico* larval growth on chemically defined growth medium. Comparison of *in vitro* and *in silico* larval growth on chemically defined growth medium. We simulated the *in silico* growth of a larva (green; dry weight) on HD by using the dFBA approach (see method section) with the addition of the penalty function. The growth of the larva resembles an exponential growth curve with unlimited growth. The growth of larvae reared *in vitro* (red; dry weight) on HD, starts at 48 hours till 192 hours AEL. The growth *in vitro* shows a small variance in comparison to the *in silico* growth till it reaches 168 hours AEL. On average the pupation started around the 192 hours mark.

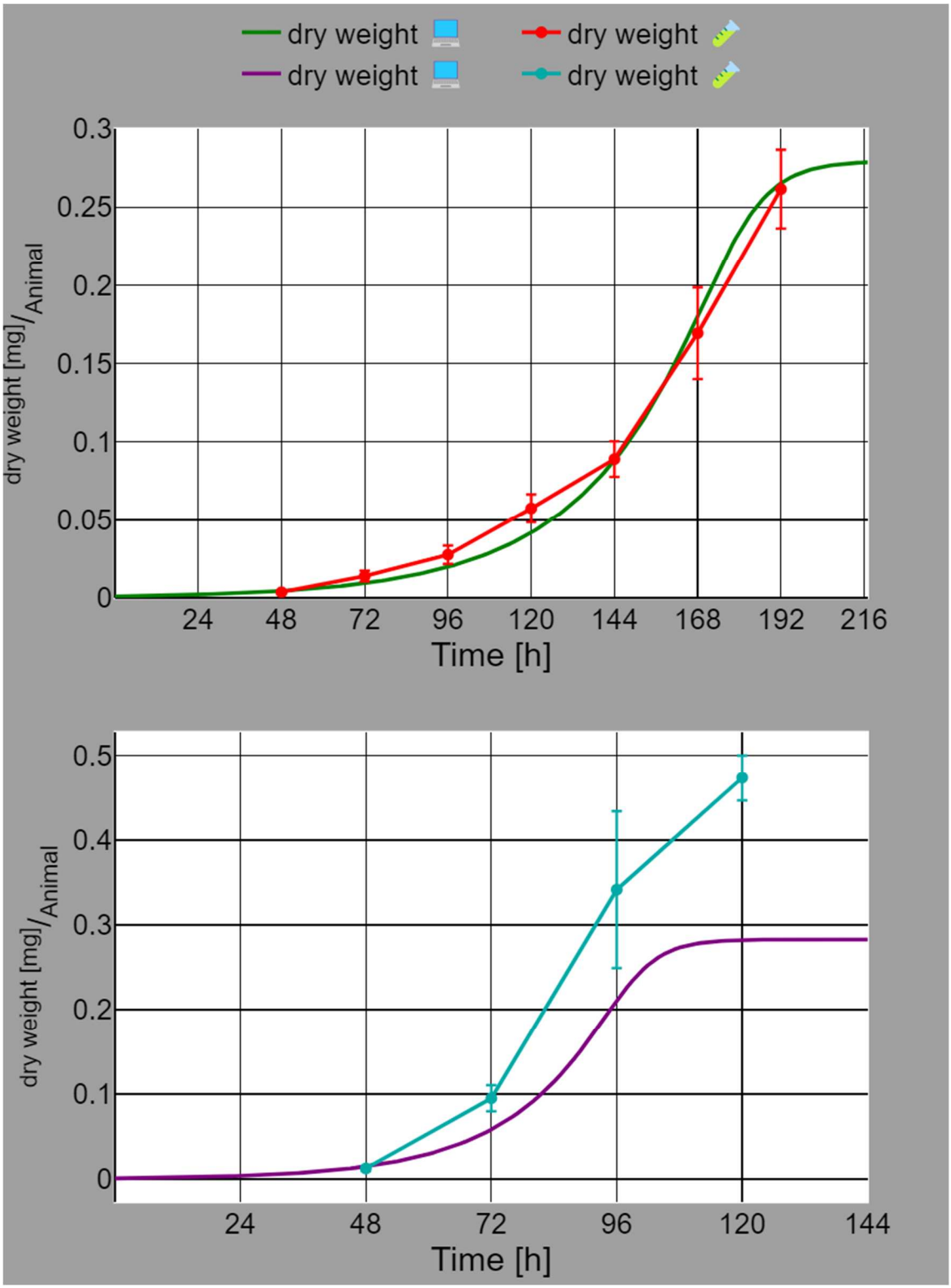

Supplementary Figure 2: Comparison of *in vitro* and *in-silico* larval growth on chemically defined growth medium and complex medium. (A) We simulated the *in silico* growth of a larva (green; dry weight) on HD by using the dFBA approach (see method section). The growth of the larva resembles a sigmoidal growth curve till it reaches a plateau starting around 192 hours. The growth of larvae reared *in vitro* (red; dry weight) on HD, starts at 48 hours till 192 hours AEL. The growth *in vitro* shows a small variance in comparison to the *in silico* growth based on the absolute dry weight values per animal. On average the pupation started around the 192 hours mark. (B) We simulated the *in silico* growth of a larva (purple; dry weight) on HD by using the dFBA approach (see method section). The growth of the larva follows a sigmoidal growth curve till it reaches a plateau starting around 120 hours. Larval growth observed *in vitro* (dark cyan; dry weight) on HD medium, starts from 48 hours till 120 hours AEL. The *in vitro* growth shows a greater

variance when compared to the *in silico* growth data based on the absolute dry weight values per animal. While the *in silico* results do not match the absolute values observed *in vitro*, they do show a similar growth trajectory as they are aligning with the correct timing for the conclusion of growth.

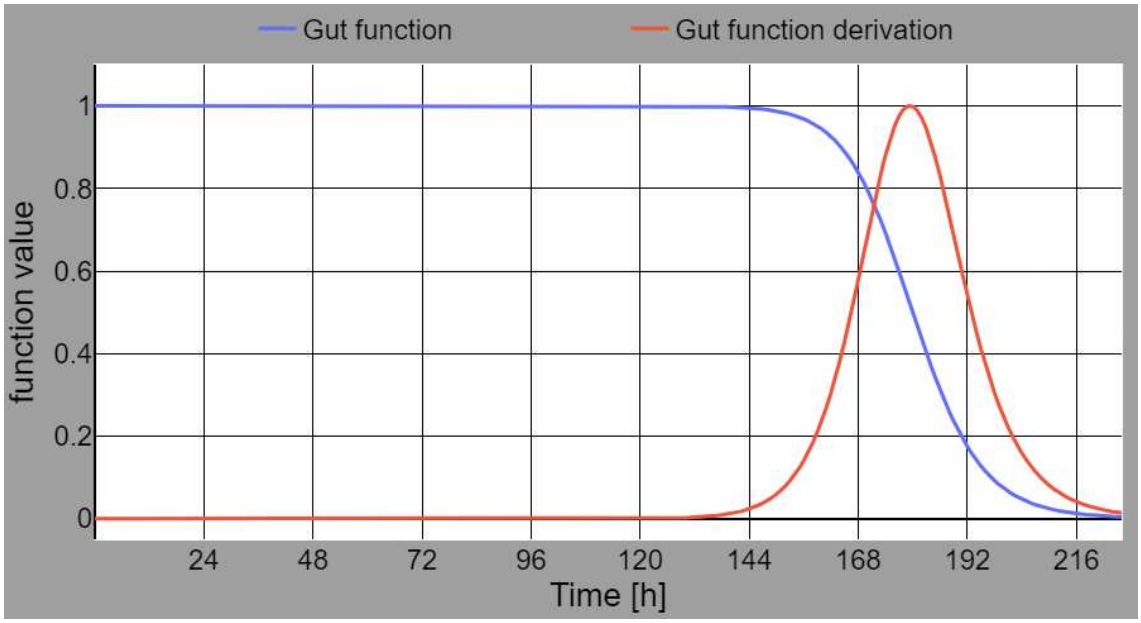

Supplementary Figure 3: Penalty function of the *in silico* simulation based on HD. The penalty function or "gut function" (blue) was formulated as described in the method section. From 0 hours till 128 hours the function value is 1. The gradient starts to change from 128 hours till 218 hours till the function value of nearly 0. The turning point of the function is at 180 hours with a function value of 0.5. The "gut function derivation" (red) is the derivation of the gut function (blue). It shows a function value change in the phase of the gut function where the gradient starts to change. The maximum function value is 1 at 180 hours which is the turning point of the gut function. For better representation the "gut function derivation" values are normalized absolute values.

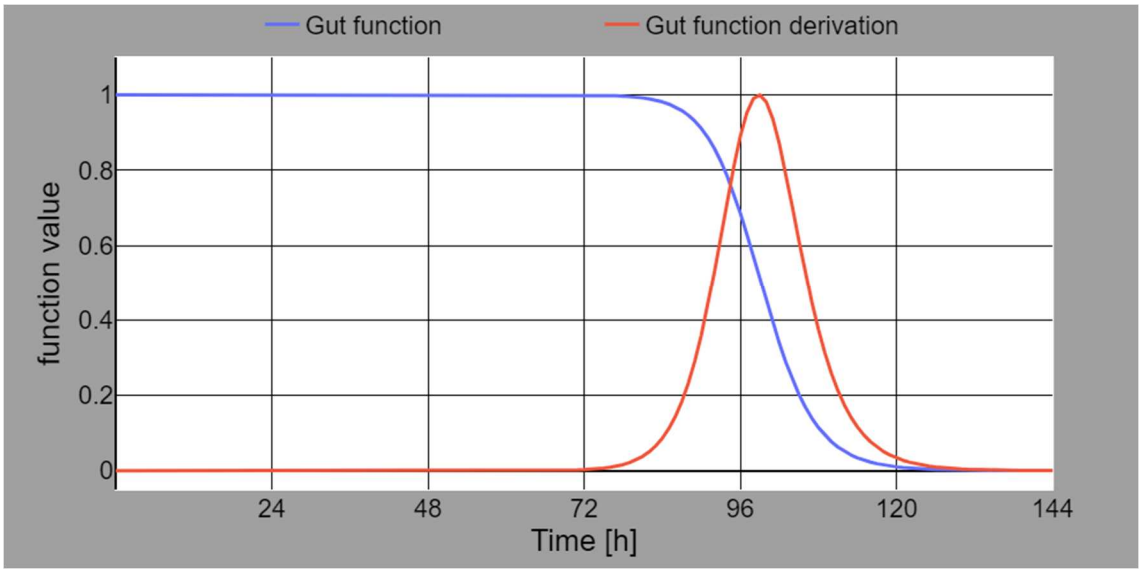

Supplementary Figure 4: Penalty function of the *in silico* simulation based on LSD. The penalty function or "gut function" (blue) was formulated as described in the method section. From 0 hours till 76 hours the function value is 1. The gradient starts to change from 76 hours till 128 hours till the function value of nearly 0. The turning point of the function is at 100 hours with a function value of 0.5. The "gut function derivation" (red) is the derivation of the gut function (blue). It shows a function value change in the phase of the gut function where the gradient starts to change. The maximum function value is 1 at 100 hours which is the turning point of the gut function. For better representation the "gut function derivation" values are normalized absolute values.

Supplementary Table 1: Metabolic reactions added to the present version of FlySilico in comparison to the previously published version.

Supplementary Table 2: Parameterization of the LSD growth medium.

References

Aguila, J.R., Suszko, J., Gibbs, A.G., and Hoshizaki, D.K. (2007). The role of larval fat cells in adult *Drosophila melanogaster*. Journal of Experimental Biology *210*, 956-963. https://doi.org/10.1242/jeb.001586.

An, P.N.T., Yamaguchi, M., Bamba, T., and Fukusaki, E. (2014). Metabolome analysis of *Drosophila melanogaster* during embryogenesis. PloS one *9*, e99519. https://doi.org/10.1371/journal.pone.0099519.

Andersen, D.S., Colombani, J., and Léopold, P. (2013). Coordination of organ growth: principles and outstanding questions from the world of insects. Trends in cell biology *23*, 336-344. https://doi.org/10.1016/j.tcb.2013.03.005.

Anholt, R.R.H., and Mackay, T.F.C. (2004). Quantitative genetic analyses of complex behaviours in *Drosophila*. Nature reviews. Genetics *5*, 838-849. https://doi.org/10.1038/nrg1472.

Ashburner, M. (1989). *Drosophila*. A laboratory handbook. (New York: Cold Spring Harbor Laboratory).

Backhaus B., Sulkowski E., and Schlote F. W. A. (1984). A semi-synthetic, general-purpose medium for *Drosophila melanogaster*. *Drosophila* Information Service, 60:210–212.

Baker, K.D., and Thummel, C.S. (2007). Diabetic larvae and obese flies-emerging studies of metabolism in *Drosophila*. Cell metabolism *6*, 257-266. https://doi.org/10.1016/j.cmet.2007.09.002.

Bate, M., and Martinez Arias, A. (1993). The Development of *Drosophila melanogaster* (Plainview, N.Y.: Cold Spring Harbor Laboratory Press).

Cesur, M.F., Basile, A., Patil, K.R., and Çakır, T. (2023). A new metabolic model of *Drosophila melanogaster* and the integrative analysis of Parkinson's disease. Life science alliance *6*. https://doi.org/10.26508/lsa.202201695.

Chícharo, M.A., and Chícharo, L. (2008). RNA:DNA ratio and other nucleic acid derived indices in marine ecology. International journal of molecular sciences *9*, 1453-1471. https://doi.org/10.3390/ijms9081453.

Chihara, C.J., Silvert, D.J., and Fristrom, J.W. (1982). The cuticle proteins of *Drosophila melanogaster*: stage specificity. Developmental biology *89*, 379-388. https://doi.org/10.1016/0012-1606(82)90326-8.

Church, R.B., and Robertson, F.W. (1966). A biochemical study of the growth of *Drosophila melanogaster*. J. Exp. Zool. *162*, 337-351. https://doi.org/10.1002/jez.1401620309.

Coquin, L., Feala, J.D., McCulloch, A.D., and Paternostro, G. (2008). Metabolomic and flux-balance analysis of age-related decline of hypoxia tolerance in *Drosophila* muscle tissue. Molecular Systems Biology *4*, 233. https://doi.org/10.1038/msb.2008.71.

Covert, M.W., Schilling, C.H., and Palsson, B. (2001). Regulation of gene expression in flux balance models of metabolism. Journal of Theoretical Biology *213*, 73-88. https://doi.org/10.1006/jtbi.2001.2405.

Covert, M.W., Xiao, N., Chen, T.J., and Karr, J.R. (2008). Integrating metabolic, transcriptional regulatory and signal transduction models in Escherichia coli. Bioinformatics (Oxford, England) *24*, 2044-2050. https://doi.org/10.1093/bioinformatics/btn352.

Crill, W.D., Huey, R.B., and Gilchrist, G.W. (1996). Within-and between-generation effects of temperature on the morphology and physiology of *Drosophila melanogaster*. Evolution; international journal of organic evolution *50*, 1205-1218. https://doi.org/10.1111/j.1558-5646.1996.tb02361.x.

Feala, J.D., Coquin, L., Zhou, D., Haddad, G.G., Paternostro, G., and McCulloch, A.D. (2009). Metabolism as means for hypoxia adaptation: metabolic profiling and flux balance analysis. BMC Syst Biol *3*, 91. https://doi.org/10.1186/1752-0509-3-91.

Förster, J., Famili, I., Fu, P., Palsson, B.Ø., and Nielsen, J. (2003). Genome-scale reconstruction of the Saccharomyces cerevisiae metabolic network. Genome Research *13*, 244-253. https://doi.org/10.1101/gr.234503.

Ginzinger, D.G. (2002). Gene quantification using real-time quantitative PCR: an emerging technology hits the mainstream. Experimental hematology *30*, 503-512. https://doi.org/10.1016/S0301-472X(02)00806-8.

Heirendt, L., Arreckx, S., Pfau, T., Mendoza, S.N., Richelle, A., Heinken, A., Haraldsdóttir, H.S., Wachowiak, J., Keating, S.M., and Vlasov, V., et al. (2019). Creation and analysis of biochemical constraint-based models using the COBRA Toolbox v.3.0. Nat Protoc *14*, 639-702. https://doi.org/10.1038/s41596-018-0098-2.

Henson, M.A., and Hanly, T.J. (2014). Dynamic flux balance analysis for synthetic microbial communities. IET Systems Biology *8*, 214-229. https://doi.org/10.1049/iet-syb.2013.0021.

Hiruma, K., and Kaneko, Y. (2013). Hormonal regulation of insect metamorphosis with special reference to juvenile hormone biosynthesis. Current topics in developmental biology *103*, 73-100. https://doi.org/10.1016/B978-0-12-385979-2.00003-4.

Hjersted, J.L., and Henson, M.A. (2006). Optimization of Fed-Batch Saccharomyces cerevisiae Fermentation Using Dynamic Flux Balance Models. Biotechnol Progress *22*, 1239-1248. https://doi.org/10.1002/bp060059v.

Hjersted, J.L., and Henson, M.A. (2009). Steady-state and dynamic flux balance analysis of ethanol production by Saccharomyces cerevisiae. IET Systems Biology *3*, 167-179. https://doi.org/10.1049/iet-syb.2008.0103.

Kauffman, K.J., Prakash, P., and Edwards, J.S. (2003). Advances in flux balance analysis. Current Opinion in Biotechnology *14*, 491-496. https://doi.org/10.1016/j.copbio.2003.08.001.

Kaya, M., Akyuz, B., Bulut, E., Sargin, I., Eroglu, F., and Tan, G. (2016). Chitosan nanofiber production from *Drosophila* by electrospinning. International journal of biological macromolecules *92*, 49-55. https://doi.org/10.1016/j.ijbiomac.2016.07.021.

Loeb, L.A., Loeb, K.R., and Anderson, J.P. (2003). Multiple mutations and cancer. Proceedings of the National Academy of Sciences of the United States of America *100*, 776-781. https://doi.org/10.1073/pnas.0334858100.

McCance, R.A. (1960). Severe undernutrition in growing and adult animals. Br J Nutr *14*, 59-73. https://doi.org/10.1079/BJN19600010.

McKechnie, S.W., Blacket, M.J., Song, S.V., Rako, L., Carroll, X., Johnson, T.K., Jensen, L.T., Lee, S.F., Wee, C.W., and Hoffmann, A.A. (2010). A clinally varying promoter polymorphism associated with adaptive variation in wing size in *Drosophila*. Molecular Ecology *19*, 775-784. https://doi.org/10.1111/j.1365-294X.2009.04509.x.

Meadows, A.L., Karnik, R., Lam, H., Forestell, S., and Snedecor, B. (2010). Application of dynamic flux balance analysis to an industrial Escherichia coli fermentation. Metabolic engineering *12*, 150-160. https://doi.org/10.1016/j.ymben.2009.07.006.

Melcher, C., Bader, R., and Pankratz, M.J. (2007). Amino acids, taste circuits, and feeding behavior in *Drosophila*: towards understanding the psychology of feeding in flies and man. The Journal of endocrinology *192*, 467-472. https://doi.org/10.1677/JOE-06-0066.

Merkey, A.B., Wong, C.K., Hoshizaki, D.K., and Gibbs, A.G. (2011). Energetics of metamorphosis in *Drosophila melanogaster*. Journal of Insect Physiology *57*, 1437-1445. https://doi.org/10.1016/j.jinsphys.2011.07.013.

Migeon, J.C., Garfinkel, M.S., and Edgar, B.A. (1999). Cloning and characterization of peter pan, a novel *Drosophila* gene required for larval growth. Molecular Biology of the Cell *10*, 1733-1744. https://doi.org/10.1091/mbc.10.6.1733.

Mirth, C., Truman, J.W., and Riddiford, L.M. (2005). The role of the prothoracic gland in determining critical weight for metamorphosis in *Drosophila melanogaster*. Current biology : CB *15*, 1796-1807. https://doi.org/10.1016/j.cub.2005.09.017.

Mitchell-Olds, T., Willis, J.H., and Goldstein, D.B. (2007). Which evolutionary processes influence natural genetic variation for phenotypic traits? Nature reviews. Genetics *8*, 845-856. https://doi.org/10.1038/nrg2207.

Moed, G.H. de, Kruitwagen, C.L.J.J., Jong, G. de, and Scharloo, W. (1999). Critical weight for the induction of pupariation in *Drosophila melanogaster*: genetic and environmental variation. J Evolution Biol *12*, 852-858. https://doi.org/10.1046/j.1420-9101.1999.00103.x.

Musselman, L.P., Fink, J.L., Narzinski, K., Ramachandran, P.V., Hathiramani, S.S., Cagan, R.L., and Baranski, T.J. (2011). A high-sugar diet produces obesity and insulin resistance in wild-type *Drosophila*. Disease models & mechanisms *4*, 842-849. https://doi.org/10.1242/dmm.007948.

Nijhout, H.F., Riddiford, L.M., Mirth, C., Shingleton, A.W., Suzuki, Y., and Callier, V. (2014). The developmental control of size in insects. Wiley interdisciplinary reviews. Developmental biology *3*, 113-134. https://doi.org/10.1002/wdev.124.

Novick, A., and Szilard, L. (1950). Description of the chemostat. Science *112*, 715-716. https://doi.org/10.1126/science.112.2920.715.

Orth, J.D., Thiele, I., and Palsson, B.Ø. (2010). What is flux balance analysis? Nature biotechnology *28*, 245-248. https://doi.org/10.1038/nbt.1614.

Papin, J.A., and Palsson, B.O. (2004). The JAK-STAT signaling network in the human B-cell: an extreme signaling pathway analysis. Biophysical journal *87*, 37-46. https://doi.org/10.1529/biophysj.103.029884.

Piper, M.D.W., Blanc, E., Leitão-Gonçalves, R., Yang, M., He, X., Linford, N.J., Hoddinott, M.P., Hopfen, C., Soultoukis, G.A., and Niemeyer, C., et al. (2014). A holidic medium for *Drosophila melanogaster*. Nature methods *11*, 100-105. https://doi.org/10.1038/nmeth.2731.

Price, N.D., Reed, J.L., and Palsson, B.Ø. (2004). Genome-scale models of microbial cells: evaluating the consequences of constraints. Nature reviews. Microbiology *2*, 886-897. https://doi.org/10.1038/nrmicro1023.

Riddiford, L.M., and Ashburner, M. (1991). Effects of juvenile hormone mimics on larval development and metamorphosis of *Drosophila melanogaster*. General and comparative endocrinology *82*, 172-183. https://doi.org/10.1016/0016-6480(91)90181-5.

Roberts, D.B. (2006). *Drosophila melanogaster* : the model organism. Entomologia Exp Applicata *121*, 93-103. https://doi.org/10.1111/j.1570-8703.2006.00474.x.

Schönborn, J.W., Jehrke, L., Mettler-Altmann, T., and Beller, M. (2019). FlySilico: Flux balance modeling of *Drosophila* larval growth and resource allocation. Scientific reports *9*, 17156. https://doi.org/10.1038/s41598-019-53532-4.

Shin, S.C., Kim, S.-H., You, H., Kim, B., Kim, A.C., Lee, K.-A., Yoon, J.-H., Ryu, J.-H., and Lee, W.-J. (2011). *Drosophila* microbiome modulates host developmental and metabolic homeostasis via insulin signaling. Science *334*, 670-674. https://doi.org/10.1126/science.1212782.

Shingleton, A.W. (2010). The regulation of organ size in *Drosophila*: physiology, plasticity, patterning and physical force. Organogenesis *6*, 76-87. https://doi.org/10.4161/org.6.2.10375.

Shingleton, A.W., Frankino, W.A., Flatt, T., Nijhout, H.F., and Emlen, D.J. (2007). Size and shape: the developmental regulation of static allometry in insects. BioEssays : news and reviews in molecular, cellular and developmental biology *29*, 536-548. https://doi.org/10.1002/bies.20584.

Storelli, G., Defaye, A., Erkosar, B., Hols, P., Royet, J., and Leulier, F. (2011). Lactobacillus plantarum promotes *Drosophila* systemic growth by modulating hormonal signals through TOR-dependent nutrient sensing. Cell metabolism *14*, 403-414. https://doi.org/10.1016/j.cmet.2011.07.012.

Swainston, N., Smallbone, K., Hefzi, H., Dobson, P.D., Brewer, J., Hanscho, M., Zielinski, D.C., Ang, K.S., Gardiner, N.J., and Gutierrez, J.M., et al. (2016). Recon 2.2: from reconstruction to model of human metabolism. Metabolomics : Official journal of the Metabolomic Society *12*, 109. https://doi.org/10.1007/s11306-016-1051-4.

Tkačik, G., and Walczak, A.M. (2011). Information transmission in genetic regulatory networks: a review. Journal of physics. Condensed matter : an Institute of Physics journal *23*, 153102. https://doi.org/10.1088/0953-8984/23/15/153102.

Varma, A., and Palsson, B.O. (1994). Stoichiometric flux balance models quantitatively predict growth and metabolic by-product secretion in wild-type Escherichia coli W3110. Applied and environmental microbiology *60*, 3724-3731. https://doi.org/10.1128/aem.60.10.3724-3731.1994.

Varma, A., and Palsson, B.O. (1995). Parametric sensitivity of stoichiometric flux balance models applied to wild-type Escherichia coli metabolism. Biotechnology and bioengineering *45*, 69-79. https://doi.org/10.1002/bit.260450110.

Ward, P.S., and Thompson, C.B. (2012). Signaling in control of cell growth and metabolism. Cold Spring Harbor perspectives in biology *4*, a006783. https://doi.org/10.1101/cshperspect.a006783.

Wright, S. (1941). The physiology of the gene. Physiological Reviews *21*, 487-527. https://doi.org/10.1152/physrev.1941.21.3.487.

Zeng, H., and Yang, A. (2019). Modelling overflow metabolism in Escherichia coli with flux balance analysis incorporating differential proteomic efficiencies of energy pathways. BMC Syst Biol *13*, 3. https://doi.org/10.1186/s12918-018-0677-4.

Zheng, H., Yang, X., and Xi, Y. (2016). Fat body remodeling and homeostasis control in *Drosophila*. Life sciences *167*, 22-31. https://doi.org/10.1016/j.lfs.2016.10.019.

3. Additional Experimental Data

While the previous manuscripts have covered the reconstruction, predictive capabilities, and improvements of the metabolic network of *Drosophila melanogaster* and its associated microbiome, they do not offer a comprehensive in-depth view of other crucial segments of the metabolism. To acquire a deeper understanding of *D. melanogaster's* metabolism, additional experiments were conducted, and theoretical refinements to the metabolic model were investigated.

3.1. Metabolic fluxes

FBA is used to study metabolic fluxes through a steady-state metabolic network. It simulates the metabolic flow through the network and gives resulting metabolic flux patterns that are optimized for a previously defined objective. Metabolic fluxes can be measured and used in combination with metabolic networks to validate results and constrain the metabolic fluxes which enhances the quality and precision of the results from e.g. FBA.

To measure metabolic fluxes in cells or organisms, the use of metabolic tracers is essential. These tracers can be labeled by incorporating radioactive (^{14}C, ^{3}H) or stable isotopes (^{13}C, ^{15}N, ^{2}H) (Crown and Antoniewicz, 2013). The metabolic tracer needs to be introduced to the system of interest which can be single cells (e.g. *E. coli*) or complex organisms (e.g. humans). The metabolic tracer needs considerable time to be incorporated into the metabolism. When enough metabolic tracers are accumulated in the metabolism, the labeled metabolites can be isolated (e.g. through extraction out of microorganisms (Garcia et al., 2008)) and measured. Different techniques can be applied to measure the incorporation of metabolic tracers (Crown and Antoniewicz, 2013), such as nuclear magnetic resonance (NMR; Schleucher et al., 1998), mass spectrometry (MS; Antoniewicz et al., 2007), or tandem mass spectrometry (MS/MS; Antoniewicz, 2013). In the case of radioactive metabolic tracers, the total radioactivity of a metabolite or element is measured (Wolfe and Chinkes, 2005; Crown and Antoniewicz, 2013).

The use of measured metabolic fluxes promises to enhance used parameters for metabolic networks and the prediction quality of *in silico* simulations. The obtained metabolic fluxes can be used with isotopic steady-state metabolic flux analysis (MFA or ^{13}CMFA; Zamboni, 2011). Here, the internal fluxes are fitted to the metabolic labeling measurements and the fitted fluxes describe the flow through metabolism, for example represented in a flux map (Chen et al., 2011).

The idea was to enhance the parametrization of the FlySilico model through the measurement of metabolite fluxes (Chen et al., 2011). On one hand, such measurements offer a means to estimate the rate of nutrient absorption per unit of time. On the other hand, these data can be utilized to determine the minimum and maximum values of fluxes for individual metabolic reactions. Unlike adult flies, the intake of nutrients of larvae is relatively unexplored. Studies on adult fly dietary intake show promising results, particularly through radiolabeling or isotope labeling methods (Deshpande et al., 2014). The prediction accuracy relies, although not exclusively, on the knowledge of the quantity of ingested nutrients. In FlySilico (Schönborn et al., 2019), a theoretical approach was adopted as the information on larval nutrient intake and food utilization is limited. Here, in order to validate these calculated nutrient absorptions or to experimentally determine the larval nutrient absorption, measurements with larvae were conducted using isotope labeling based on established protocols (Li et al., 2018).

Metabolic tracer accumulation

Standard HD medium (Piper et al., 2014) was used for the labeling experiments where sucrose was substituted with glucose. The used glucose was a mixture of 50 % unlabeled and 50 % labeled glucose ($^{13}C_6$-Glucose; Sigma-Aldrich CAS 110187-42-3). Larvae were transferred prior to the sample collection time point to the labeled HD medium. The larvae were reared on the labeled HD medium for 12 hours to ensure enough of the labeled tracer glucose is accumulated for measurements.

Sample collection

The larvae were reared and collected according to established protocols from Schönborn et al. (2019). Larvae developed on HD (Piper et al., 2014), collected from the vials with labeled HD, washed with PBS, dried and frozen in liquid nitrogen. The larvae were four to 8 days old when collected. Each collection time point consists of one sample of larvae from unlabeled HD (40 or 12 larvae) and quadruplicate samples of larvae from labeled HD (40 or 12 larvae).

Tissues (gut and fat body, respectively) were dissected out of the animals in cold PBS and directly transferred to 245 µL methanol before frozen in liquid nitrogen. Each collection time point consists of one sample tissues from unlabeled HD (40 tissues) and quadruplicate sample tissues from labeled HD (40 tissues).

The fresh weight for each sample was measured on an analytical scale before freezing in liquid nitrogen.

Sample preparation

The sample preparation was performed by methanol-chloroform extraction. All samples were kept on ice during extraction. First, 245 µL methanol was added to each larvae sample and followed by homogenization using a mini handheld homogenizer. 105 µL chloroform was added to all samples and carefully vortexed. After the samples were vortexed, the samples were incubated for 1 hour at -20°C.

When the incubation was finished, 560 µL ice cold HPLC water with 15 µL ISTD (internal standard; ribitol) was added to each sample and centrifuged at 14800 rounds per minute (RPM) at 4°C for 2 minutes. 800 µL of each sample were transferred off the top aqueous layer into a new 2 mL centrifuge tube. Additional 560 µL HPLC water were added to the samples and centrifuged again at 14800 RPM for 2 minutes at 4°C. 400 µL were again transferred from each sample off the top aqueous layer into the same 2 mL centrifuge tube. The final extracted samples were stored at -80°C.

Measurements

The samples were measured by Dr. Philipp Westhoff (CEPLAS Metabolomics and Metabolism Laboratory, Heinrich-Heine-Universität Düsseldorf) by Gas chromatography–mass spectrometry (GC-MS; Sparkman et al., 2011). The results were normalized to the ISTD and the fresh weight. Additionally, a correction for the natural abundance of each single isotope was performed. All with the help of IsoCorrectoR (Heinrich et al., 2018).

Results and Discussion

Important metabolites from the core metabolism of *Drosophila melanogaster* were measured (Table 1).

Table 1: Targets of the metabolic labeling measurements. The label "SiX" in "MS ion or MS/MS product ion" describes the derivation of the metabolite through a trimethylsilyl group and the label "LabCX" describes the number of labeled carbons found in the metabolite.

Name	Molecule	MS ion or MS/MS product ion	Pathway
Alanine	Ala1	C5H14N1Si1LabC2	Amino Acid Biosynthesis
Aspertate	Asp1	C9H22N1O2Si2LabC3	Amino Acid Biosynthesis
Citric acid	Cit1	C11H21O4Si2LabC5	TCA-Cycle
Citric acid	Cit2	C14H27O6Si3LabC5	TCA-Cycle
Fumaric acid	Fum1	C9H17O4Si2LabC4	TCA-Cycle
Glycine	Gly1	C9H29N1O2Si3LabC2	Amino Acid Biosynthesis
Malate	Mal1	C9H21O3Si2LabC3	TCA-Cycle
Pyruvic acid	Pyr1	C6H12N1O3LabC3	Glycolysis/Gluconeogenesis
Serine	Ser1	C8H22N1O1Si2LabC2	Amino Acid Biosynthesis
Serine	Ser2	C8H20N1O2Si2LabC2	Amino Acid Biosynthesis
Glutamic acid	Glu1	C10H24N1O2Si2LabC4	Amino Acid Biosynthesis
Lactate	Lac1	C5H13O1Si1LabC2	Glycolysis/Gluconeogenesis
Glucose	Glc1	C8H21O2Si2LabC2	Glycolysis/Gluconeogenesis
Glucose	Glc2	C13H31O3Si3LabC4	Glycolysis/Gluconeogenesis

The results allowed to create a heatmap where the relative abundance of the labeled metabolites is visible (Fig. 2). The heatmap illustrates the flow of the ^{13}C-labeling into metabolites of the core metabolism. Higher relative amounts of labeled metabolites indicate a higher usage of related reactions and therefore a higher activity of the associated metabolic pathways. The label propagated well through the core metabolism as higher amounts of label can be found in nearly all metabolites in the whole larva and in the fat body. A high activity in the TCA-

Cycle is present as core metabolites (Citric acid, Fumaric acid, and Malate) show a higher amount of label, which was expected. It has a high activity throughout the development and additionally higher label amounts of aspartate support this. Oxaloacetate is an important metabolite of the TCA-cycle but its labeling cannot be measured directly. Oxaloacetate's labeling can be inferred through the labeling of aspartate (Antoniewicz, 2018).

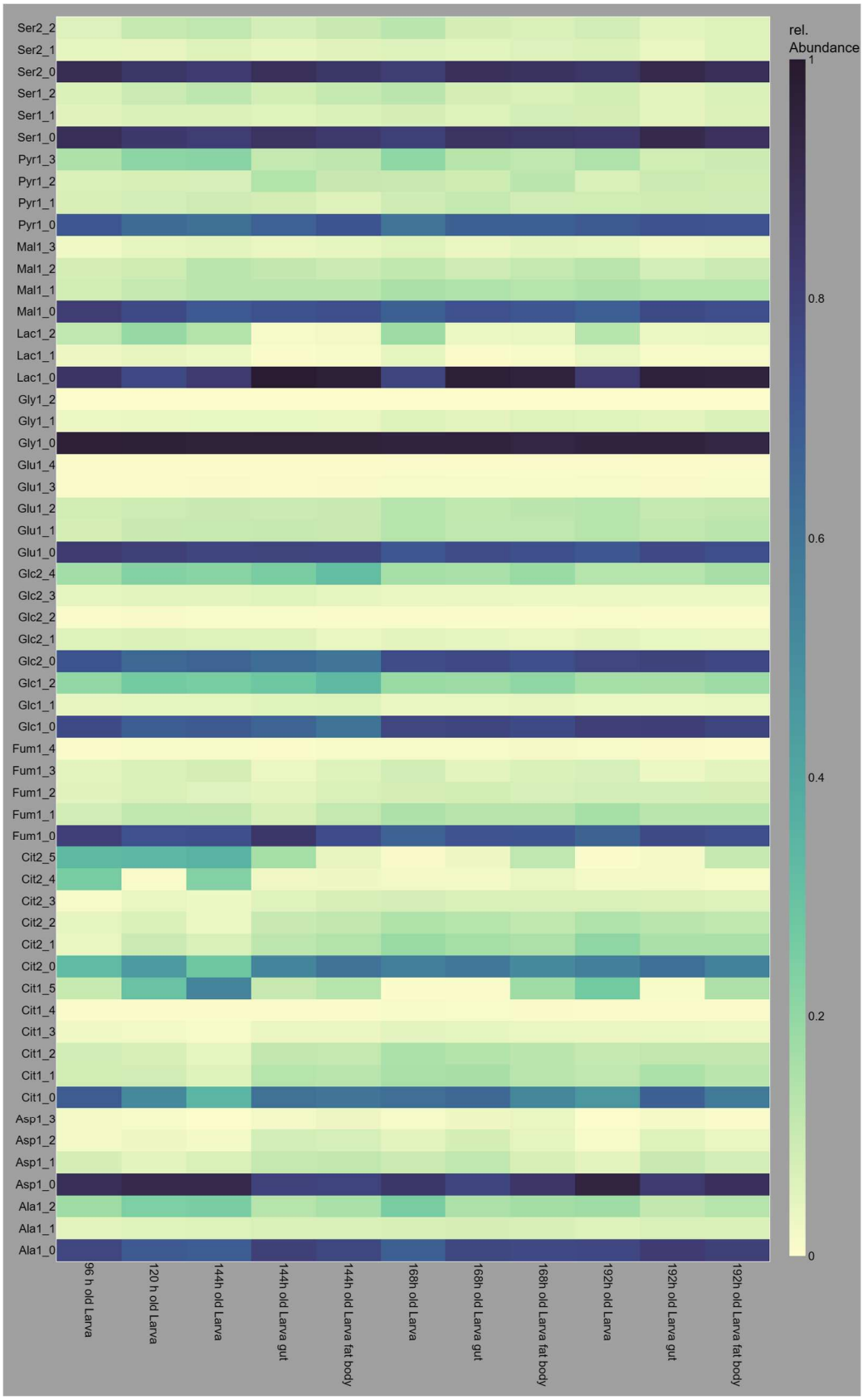

Figure 2: Relative abundance of labeled metabolites during the development of *Drosophila melanogaster* and their organs. The heat map shows the relative abundance of labeled metabolites measured at different developmental time points of the larva or the larval tissues. The index labels are described in Table 1 were the suffix "_X" describes the number of labeled carbons found in the metabolite and not the absolute position of the labeled carbon.

Metabolites, such as pyruvic acid and lactate, have a higher abundance in label throughout the development of the larva which indicates that the glycolysis is active through a large part of the development. On the other hand, the labeled amount of lactate in the larval tissues such as gut and fat body is lower. This suggest that the metabolic utilization of lactate and probably the activity of the glycolysis/gluconeogenesis in those tissues is lower but still present in the organs.

Taken together, the results of the metabolic labeling experiments of developing larvae should permit precise quantifications of fluxes in the core metabolism by using ^{13}CMFA.

The metabolic fluxes can be calculated through different available programs that are based on ^{13}CMFA (Shupletsov et al., 2014; Foguet et al., 2019). ^{13}CMFA utilizes the formulation of so-called propagation rules. These propagation rules describe how the label, that enters the organism, moves through the metabolic network. Based on the propagation rules, ^{13}CMFA can simulate different flux patterns which results in a metabolic label pattern that explain the experimental label pattern. Through further simulation iterations the error between the simulated label pattern and experimental label pattern is minimized.

As a first step, published propagation rules for *E. coli* (Foguet et al., 2019) were used in combination with FlySilico and the measured experimental label pattern. First iterations to calculate a flux pattern that describes the experimental label pattern were not successful (data not shown). Different reasons can be the cause for not being able to successfully calculate a flux pattern. One reason can be that the used propagation rules are not compatible with the larval metabolism. The metabolism of a single cell differs significantly from that of multicellular organisms due to the prominent compartmentalization apparent at multiple levels, including distinct membrane-bound cell organelles and organs. Another reason can be the structure of the metabolic network, which is used as possible dead-ends in the metabolic model, preventing ^{13}CMFA from calculating a flux pattern that can represent the experimental label pattern. The objective that ^{13}CMFA tries to solve and optimize is to predict a metabolic pattern that represent the experimental pattern (Shupletsov et al., 2014) and in FBA, different objectives are optimized,

such as the maximization of growth (Pramanik and Keasling, 1997). This can result in such different flux patterns that prevent the optimization of one method depending on the metabolic network structure.

Solving this problem further analysis of the metabolic network structure need to be done. Nevertheless, it remains to be determined if the applied propagation rules are compatible to be used with FlySilico and therefore the metabolism of a larva. Together, the above data indicate that the determination of metabolic fluxes can be used to optimize the metabolic network of a larva and their parameters should be possible with further optimization of the modeling approach.

3.2. Multi-organ communication network

Multicellular organisms consist of different types of subcellular compartments, cell-types, tissues, and organs. The presence of compartments within organisms establishes a system in which each compartment plays a vital role in generating the energy or metabolites required for the organism to fulfill specific metabolic functions (Li et al., 2022).

Complex organisms, like *D. melanogaster*, show a variety of different organs or tissue-types. The fat body, for example, is the primary energy storage organ and thus accumulates plenty of fat and glycogen during the development of the larva. The stored energy is released during the metamorphosis or during phases within development where the animal lacks sufficient nutrients (transient starvation) to ensure the survival of the larva (Arrese and Soulages, 2010). The metabolism of *D. melanogaster* can experience misregulations reminiscent of human metabolic diseases such as obesity or diabetes e.g. by rearing the animals on a high caloric diet. Many genes that are associated with such diseases are conserved between humans and *Drosophila* (Reiter et al., 2001). This enables the study of metabolic diseases in flies (Musselman and Kühnlein, 2018). Understanding the metabolic impact on the level of organs or tissues-specific level provides a more detailed picture on how metabolic diseases work in organisms. In long term, results regarding the metabolic state of an organ or tissue should lead to more effective and new therapies on how to relieve the symptoms of such metabolic diseases.

Detailed experimental investigations of the metabolism across various organs or tissues has proven to be a challenge, as observed in previous studies (Plauth et al., 1993; van de Kerkhof et al., 2007; Basler et al., 2018). This indicates that detailed experimental investigations need to consider various factors, such as the constant control of the experimental environment, to provide meaningful results. In contrast, metabolic network analysis offers a powerful method to uncover the metabolic profiles of multiple organs, tissues, or cells across different organisms under guaranteed constant conditions (Grafahrend-Belau et al., 2013; Shaw and Cheung, 2018; Thiele et al., 2020; Li et al., 2022).

The modelling of an multi-organ communication network requires the connection of two or more tissues or organs by the exchange of metabolites. Lewis et al. (2010) constructed such a network by connecting an astrocyte metabolic network with the metabolic network of neurons to enable crosstalk. The two networks were able to exchange metabolites with each other and their environment. Following that, multi-tissue networks were reconstructed that allow crosstalk between tissues such as skeletal muscle, liver, and fat tissues of humans (Bordbar et al., 2011; Cordes et al., 2018; Martins Conde et al., 2021). Through these networks, it could be demonstrated that, personalized nutritional compositions could be designed to potentially enhance athletic performance or simulate drug-induced metabolic perturbations safely in patients.

Similar works have also been done for unicellular organisms in the context of the microbiome such as the study performed within this thesis (Schönborn et al., 2021). Diverse bacteria are organized in biofilms or related structures forming communities. This enables the communication and exchange of nutrients between bacteria in proximity. Instead of having metabolic networks of single organs that can communicate in a multi-organ communication network, metabolic models of single unicellular organisms are communicating in an overarching network through metabolic fluxes. This approach of multi-scale modelling was demonstrated by e.g. Bauer et al. (2017). Such an approach was successfully utilized to investigate the host-microbiome interaction between humans and their microbiome (Heinken and Thiele, 2015; Magnúsdóttir and Thiele, 2018).

As far as the available data suggest, metabolic networks of various tissues or organs do not appear to be present for *D. melanogaster*. The reconstruction of a metabolic network for *D. melanogaster* including various organs or tissues would undeniably be beneficial.

Results and Discussion

Reconstruction of a *D. melanogaster* multi-organ communication network

The reconstruction of a multi-organ communication network for *D. melanogaster* was carried out based on the FlySilico metabolic network. Here, the metabolic processes of the entire larva, the larval gut, and the larval fat body were incorporated. The larval gut serves as the primary site for metabolite entry into the metabolism, as its primary function is substrate or metabolite uptake. Metabolites can either be utilized within the gut or transported further into the larva's circulatory system, known as the hemolymph. Within the hemolymph, metabolites can access various parts of the larval body. For an illustrative presentation of the network's structure, please refer to Figure 3.

The reconstruction of the multi-organ communication network used the information about genes present in the different organs. In the metabolic network most reactions are associated with a gene that is present in *D. melanogaster*.

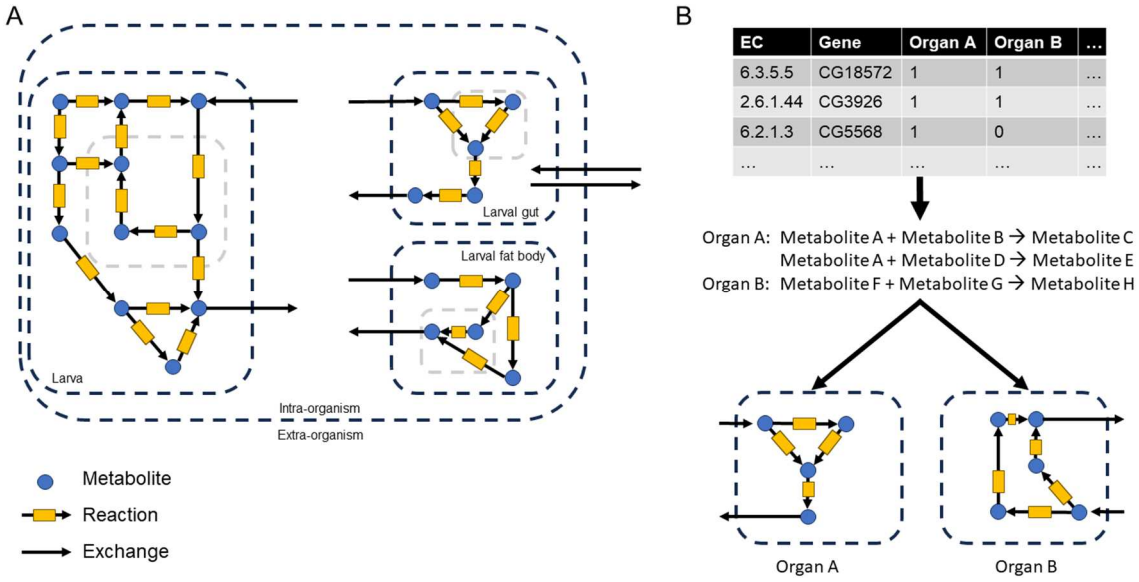

Figure 3: Schematic representation of the multi-organ communication network of *D. melanogaster*. (A) The dotted lines represent the compartment borders where dark blue color represents organ borders or the organism itself. Light grey describes the cell compartment border, such as mitochondria or cytosol. The intra-organism compartment represents the larval hemolymph. The nutrients from the growth medium are found in the extra-organismic environment. The nutrients enter the network through the larval gut, where they are utilized, or they may be further transported into the interior of the organism, known as the hemolymph. Here, the metabolites have access to various parts of the larval body. (B) The metabolic reactions (EC – enzyme commission numbers) associated with genes are matched to gene expression data (FlyAtlas 2; Krause et al., 2022) present in different organs of the larva. The metabolic reactions are then inserted in the associated organ sub-models and necessary reactions (like transport reactions to allow communication between the metabolic networks) were manually added.

The gene expression related to a given metabolic reaction was backed-up by public expression data (FlyAtlas 2; Krause et al., 2022) to identify the most likely gene products carrying out the reactions in the different organs. The matched metabolic reactions are left inside the organ-specific metabolic network and metabolic reactions that could not be matched are deleted. Transport reactions between the different compartments of the multi-organ communication network were added manually to allow the communication through metabolic fluxes.

The resulting multi-organ network consists of 1384 metabolic reactions and 1441 metabolites. The established communication between the single metabolic networks allows metabolic flux through all compartments. The optimization for the original objective function of FlySilico is possible.

With the addition of organs in a whole organism metabolic model, more additions are needed as the initial objective function cannot be used. In FlySilico, the objective function was the biomass function, which describes the building blocks

that make up the overall larval biomass. With the addition of organs, such as the larval fat body, the objective function changes. The fat body's biological purpose is to store as many metabolites as possible for life stages of starvation and to survive the metamorphosis from a larva to an adult fly (Arrese and Soulages, 2010).

As the initial biomass function also describes the storage of lipid metabolites like triacylglycerol (TAG) and glycogen, the biomass function needs to be reformulated. For that purpose, the storage of lipid metabolites needs to be addressed in a new biomass function of the fat body. This biomass function should consist of building blocks that build up the lipid tissue of the fat body and to a large part of TAG and glycogen (DiAngelo and Birnbaum, 2009). The resulting mass from the fat body biomass function then needs to be added to the overall biomass generated from the whole-body biomass function. Additionally, a biomass function for gut growth needs to be formulated to address the growth of the larval gut as it is present as an own organ in the metabolic network. Therefore, each organ that is added to such a network need an own objective function or even multiple objective functions. In the case of larvae, each organ needs a biomass function to describe its growth. The solution of the objective function of each organ needs to be added up to describe the overall larval growth. Each solution of the organ-specific objective function can be analyzed further how the metabolism works in the network and what impact each organ has on the different organs and the overall metabolism. For instance, in the case of a growing gut within an organism, employing a gut biomass growth function as the primary objective may not be justified.

The formulation of such an organic-specific objective function needs extensive metabolic data of each organ. The isolation of the most prominent organs in *Drosophila* larvae are possible which eases the acquiring of such data. Important data that need to be acquired for such a network would be the weight of each organ to determine the contribution to the overall growth. To get further inside to the metabolism and the resource allocation of each organ the metabolic state of each organ should be measured by determining its metabolic content for different developmental timepoints. This should be performed in a similar way as previously done for FlySilico (Schönborn et al., 2019). Furthermore, the data

about the metabolic state can be used to finetune the metabolic fluxes of the organ-specific metabolic networks. This is possible by measuring extensive metabolic flux data for each organ, like the previously measured metabolic fluxes (see 3.1. Metabolic fluxes). The integration of additional multi-omics data into the modelling approach enhances the prediction power and accuracy, which was successfully demonstrated for unicellular organisms (Yoon et al., 2012), plants (Gomes de Oliveira Dal'Molin and Nielsen, 2018) and other higher organisms (Coquin et al., 2008; Magazzù et al., 2021).

For the fat body we treat the storage of metabolites equal to growth. The main purpose of the gut of *Drosophila* is the intake of nutrients but it contributes with his weight-gain also to the overall biomass. Organs, like the brain for example, can be described with a biomass function but also include a sink of energy as the larval brain uses extensive amounts of energy metabolites to function properly. The same is true for the muscles of the larva. This reveals the importance of possible usage of multiple objective functions for each organ.

Altogether, such a multi-organ communication network needs extensive data and investigation of each organ that contribute significantly to growth. This can be carried out by extensive labor but should provide important knowledge of the metabolism of a developing larva. The multi-organ communication network should allow an even more detailed look on how the resource allocation in *Drosophila* larva works, such as the identification of the most active metabolic pathway in each organ and the resulting distribution of the nutrients. This could open the possibility to alter the nutrient composition of the food to enhance specific organ-growth or support the function of a specific organ to a point were eventually a disease state in an organ can be treated or even cured.

4. Discussion and Conclusion

Our understanding of resource allocation in multicellular organisms and the underlying mechanisms driving it is limited. Investigating the metabolic processes that govern resource allocation is an active and evolving field of research (Boggs, 1981; Goelzer and Fromion, 2017; Basan, 2018), but a detailed understanding

remains elusive. However, metabolic networks and approaches such as Flux Balance Analysis have made it practicable to investigate the details of metabolism (Kauffman et al., 2003; Orth et al., 2010b; Basler et al., 2018).

Prior to this work, metabolic networks were used in understanding different questions regarding the metabolism of *D. melanogaster*. Flux balance analysis, combined with extensive metabolomics, enabled the investigation of hypoxia adaptation in hypoxic environments (Coquin et al., 2008; Feala et al., 2009). Further, the energy metabolism and the impact of hypoxic environmental conditions were investigated by analyzing the ATP production (Feala et al., 2007). All these studies were performed in adult flies and provide a more detailed understanding of how the metabolism operates under varying conditions and revealing their consequences. However, these studies were unable to address how resource allocation impacts the development and physiology of *Drosophila*.

The understanding of the metabolism and resource allocation of a developing *D. melanogaster* larva is rather limited. The presented work reveals that the use of data-driven *in vivo* and *in silico* methods provide a viable approach to investigate the metabolism and resource allocation of developing multicellular organisms in detail. The reconstruction of a metabolic model guiding larval metabolism (Manuscript 2.1: Fig. 2) in combination with extensive experimental data to obtain feasible parameters suitable for FBA (Manuscript 2.1: Fig. 4 and 5), allow for successful and detailed predictions of the metabolic state during larval development (Manuscript 2.1: Fig. 6). This allowed to generate a metabolic model of a developing larva and functions as the theoretical modeling framework for future studies of the metabolism and resource allocation. Further *in silico* and *in vivo* investigations, regarding the impact of different growth conditions on the resource allocation (Manuscript 2.1: Fig. 7 and 8), allowed to understand how the metabolic rewiring occurs and why the destination of metabolites changes under different growth conditions. These studies revealed conflicting processes, revealing the optimality of resource distribution and prioritization of certain metabolic processes. The assumption that the predictions are optimal is based on the fact, that flux balance analysis of metabolic networks relies on the principles of optimality. These investigations revealed metabolic principles when distributing resources and how the metabolism changes under changing

environmental conditions. Although the metabolic model primarily covers the core metabolism, it has been demonstrated that accurate predictions can be generated. This capability enables the expression of meaningful insights into the functioning of metabolism and resource allocation in multicellular organisms. In total, *in silico* methods, like FBA, demonstrate the accuracy to correctly predict the metabolic state of a multicellular organism, even under changing growth conditions and how the resource allocation responses to changing environmental conditions. The microbiome of a multicellular organism has a significant impact on both development and fitness. This holds true for *Drosophila* as well. It was possible to demonstrate that isolated most prominent strains of the gut microbiome in *Drosophila* can grow under lab conditions (Manuscript 2.2: Fig. 1 and 2). These bacteria were able to produce strain-typical metabolites *in silico* (Manuscript 2.2: Fig. 3) which suggest a metabolic behavior comparable to the conditions in a *Drosophila* gut. Furthermore, *in silico* co-culturing experiments of different bacterial strains from the microbiome (Manuscript 2.2: Fig. 4 and 5) reveal an expected inter-organism communication through the exchange of metabolites. Depending on the growth medium, different metabolites were produced and secreted from one bacterial strain. These metabolites can be used by other bacterial strains present in the co-culturing. This revealed secreted metabolites promote growth of other bacterial strains (Manuscript 2.2: Fig. 6). Ultimately, these findings emphasize that the co-growth of different bacterial strains could have a positive effect on growth and fitness of bacterial strains, depending on the available resources. Considering that the different bacterial strains of the microbiome secrete various metabolites, it is reasonable to expect that these secretions may have an influence on the host, *Drosophila*. This influence was shown in earlier studies (Storelli et al., 2011) but can be further developed to generate tailored probiotics to enhance the fitness and growth of an organism. The larval and adult microbiome differ slightly in the composition of the bacterial species (Shin et al., 2011). Nevertheless, the data presented support a robust entry point for studies into host-microbiome interactions. Additional supply of metabolites through the microbiome could have a significant impact on the resource allocation under various conditions. This raises new questions on how the metabolism and resource allocation operates and how these processes are

influenced by the resource supply from the microbiome. These questions include for example:

Is there a resource competition between the host and its microbiome, especially the resources acquired by the host? Does the competition result in a long-term impact on the host's metabolism?

Is there an ideal microbiome composition that maximizes a possible growth-promoting effect?

Addressing these and additional questions will be important, as the microbiome in multicellular organisms seem to be factors of significant influence on the host.

Various elements that influence the metabolism of a multicellular organism have been previously discussed, it is reasonable to consider the relationship between physiology, metabolism, and resource allocation. Further investigations were conducted by measuring a detailed time-resolved metabolic profile (Manuscript 2.3: Fig. 1) of developing larvae. Through this metabolic profile the modeling parameters were improved and allowed the investigation of the larval development over the complete larval development. Insights from studies on the physiology of developing larvae revealed differences in growth behavior in organs, like the larval gut, and the whole larval growth (Manuscript 2.3: Fig. 2 and 3). The ability to predict larval growth throughout the entire developmental process was achieved by translating the early halt of larval gut growth into an intake-constraining penalty function. This function was integrated through a dFBA approach (Manuscript 2.3: Fig. 4). For example, the successful prediction of the larval pupation time was possible. Furthermore, we conducted additional *in silico* predictions and *in vivo* growth experiments to confirm that the utilized approach successfully predicted growth patterns and the timing of critical developmental stages under complex environmental conditions (Manuscript 2.3: Fig. 5 and 6). These results highlight the interaction between physiology and resource allocation, where gut growth is dependent on the resources directed towards it. Simultaneously, the larval gut controls the influx of available resources for the entire larva. Various characteristics of an organism's physiology can be used as a useful approximation for supporting investigations of resource allocation and metabolism. Studies by Mirth et al. (2005) and this study show that physiology

has an impact on the resource allocation and development of multicellular organisms. This emerges additional questions such as the following:

How impactful are other organs on the metabolism and resource allocation (e.g. the fat body)?

How is the developmental metabolic strategy of organs under starvation and other not optimal conditions?

What is the impact of genetic alterations on the physiology of multicellular organisms and consequently on the metabolism?

By addressing these questions, the importance of physiology for a developing multicellular organism will be further revealed. Possibly, the first approach to investigate the raised questions is by enhancing the prediction accuracy and precision of the used parameters through metabolic flux measurements (see 3.1. Metabolic fluxes). The interaction between organs in a multicellular organism and their impact on metabolism and resource allocation remains elusive. The investigation of such interactions can be performed by extensive additions to metabolic networks by reconstructing multi-organ communication networks (see 3.2. Multi-organ communication networks). These metabolic networks should provide detailed insights to the mechanics governing the metabolic interactions and their impact on resource allocation.

An important question to address was whether if the resource allocation in multicellular organisms operates according to Pareto optimality. Pareto optimality describes the selection of parameters in a system where the available resources are optimized to a degree that one parameter cannot be improved without worsening another parameter. The Pareto optimality is also used in biology, as studies propose that bacterial growth and metabolism (Schuetz et al., 2012), as well as some phenotypic attributes of multicellular organisms, follow Pareto optimality (Shoval et al., 2012; Szekely et al., 2015). Gaining a deeper understanding of whether resource allocation follows Pareto optimality is the potential usage of 13C metabolic flux analysis (13CMFA). ^{13}CMFA was used to show that bacterial growth and metabolism is working Pareto optimally (Schuetz

et al., 2012), and first steps toward a deeper investigation were performed in this thesis (see 3.1. Metabolic fluxes).

The accurate simulation of growth behavior and metabolic fluxes in various environmental scenarios through FBA suggests that resource allocation in multicellular organisms operates optimally. Whether the simulation strictly obeys to Pareto optimality is difficult to prove, as the principle of Pareto optimality in nature has not been fully demonstrated (Edelaar, 2013; Shoval et al., 2013). Furthermore, it is not completely understood whether a Pareto optimal solution is also a biologically optimal solution. Additional studies need to be performed to determine if the optimal solution from FBA is both a Pareto and biologically optimal solution, through additional experiments such as ^{13}CMFA and the additional statistical testing suggested by Edelaar (2013). The usage of advanced FBA methods, like “Resource Balance Analysis” (RBA; Goelzer et al., 2011), can contribute to answer the question of Pareto optimality and biological optimal solutions. This approach predicts in more detail how available resources are distributed to different defined cellular systems.

Future studies need to tackle these previously raised and more questions to deepen the understanding of the complex interplay of the resource allocation in multicellular organisms. Summarized, the presented studies show that the resource allocation strategy of choice has a remarkable impact on the physiology and development of multicellular organisms.

5. Bibliography

Adams, M.D., Celniker, S.E., Holt, R.A., Evans, C.A., Gocayne, J.D., Amanatides, P.G., Scherer, S.E., Li, P.W., Hoskins, R.A., and Galle, R.F., et al. (2000). The genome sequence of Drosophila melanogaster. Science *287*, 2185-2195. https://doi.org/10.1126/science.287.5461.2185.

Agarwal, N.R., and Maurya, N. (2018). Low Sugar Diet: A New Tool in War Against Tumorigenesis. Proc. Nat. Res. Soc. *2*. https://doi.org/10.11605/j.pnrs.201802009.

Aguila, J.R., Suszko, J., Gibbs, A.G., and Hoshizaki, D.K. (2007). The role of larval fat cells in adult Drosophila melanogaster. Journal of Experimental Biology *210*, 956-963. https://doi.org/10.1242/jeb.001586.

Antoniewicz, M.R. (2013). Tandem mass spectrometry for measuring stable-isotope labeling. Current Opinion in Biotechnology *24*, 48-53. https://doi.org/10.1016/j.copbio.2012.10.011.

Antoniewicz, M.R. (2018). A guide to 13C metabolic flux analysis for the cancer biologist. Experimental & molecular medicine *50*, 1-13. https://doi.org/10.1038/s12276-018-0060-y.

Antoniewicz, M.R., Kelleher, J.K., and Stephanopoulos, G. (2007). Accurate assessment of amino acid mass isotopomer distributions for metabolic flux analysis. Analytical chemistry *79*, 7554-7559. https://doi.org/10.1021/ac0708893.

Arrese, E.L., and Soulages, J.L. (2010). Insect fat body: energy, metabolism, and regulation. Annu. Rev. Entomol. *55*, 207-225. https://doi.org/10.1146/annurev-ento-112408-085356.

Baart, G.J.E., and Martens, D.E. (2012). Genome-Scale Metabolic Models: Reconstruction and Analysis. In Neisseria meningitidis (Humana, Totowa, NJ), pp. 107–126.

Bäckhed, F. (2012). Host responses to the human microbiome. Nutrition reviews *70 Suppl 1*, S14-7. https://doi.org/10.1111/j.1753-4887.2012.00496.x.

Baker, K.D., and Thummel, C.S. (2007). Diabetic larvae and obese flies-emerging studies of metabolism in Drosophila. Cell metabolism *6*, 257-266. https://doi.org/10.1016/j.cmet.2007.09.002.

Basan, M. (2018). Resource allocation and metabolism: the search for governing principles. Current opinion in microbiology *45*, 77-83. https://doi.org/10.1016/j.mib.2018.02.008.

Basler, G., Fernie, A.R., and Nikoloski, Z. (2018). Advances in metabolic flux analysis toward genome-scale profiling of higher organisms. Bioscience reports *38*. https://doi.org/10.1042/BSR20170224.

Bate, M., and Martinez Arias, A. (1993). The Development of Drosophila melanogaster (Plainview, N.Y.: Cold Spring Harbor Laboratory Press).

Baue, A.E. (1991). Nutrition and metabolism in sepsis and multisystem organ failure. The Surgical clinics of North America *71*, 549-565. https://doi.org/10.1016/S0039-6109(16)45433-2.

Bauer, E., Zimmermann, J., Baldini, F., Thiele, I., and Kaleta, C. (2017). BacArena: Individual-based metabolic modeling of heterogeneous microbes in complex communities. PLOS Computational Biology *13*, e1005544. https://doi.org/10.1371/journal.pcbi.1005544.

Blum, J.E., Fischer, C.N., Miles, J., and Handelsman, J. (2013). Frequent replenishment sustains the beneficial microbiome of Drosophila melanogaster. mBio *4*, e00860-13. https://doi.org/10.1128/mBio.00860-13.

Boggs, C.L. (1981). Nutritional and Life-History Determinants of Resource Allocation in Holometabolous Insects. The American Naturalist *117*, 692-709. https://doi.org/10.1086/283753.

Bordbar, A., Feist, A.M., Usaite-Black, R., Woodcock, J., Palsson, B.O., and Famili, I. (2011). A multi-tissue type genome-scale metabolic network for analysis of whole-body systems physiology. BMC Syst Biol *5*, 180. https://doi.org/10.1186/1752-0509-5-180.

Brummel, T., Ching, A., Seroude, L., Simon, A.F., and Benzer, S. (2004). Drosophila lifespan enhancement by exogenous bacteria. Proc. Natl. Acad. Sci. U.S.A. *101*, 12974-12979. https://doi.org/10.1073/pnas.0405207101.

Chen, X., Alonso, A.P., Allen, D.K., Reed, J.L., and Shachar-Hill, Y. (2011). Synergy between (13)C-metabolic flux analysis and flux balance analysis for understanding metabolic adaptation to anaerobiosis in E. coli. Metabolic engineering *13*, 38-48. https://doi.org/10.1016/j.ymben.2010.11.004.

Chien, S., Reiter, L.T., Bier, E., and Gribskov, M. (2002). Homophila: human disease gene cognates in Drosophila. Nucleic Acids Research *30*, 149-151. https://doi.org/10.1093/nar/30.1.149.

Claesson, M.J., O'Sullivan, O., Wang, Q., Nikkilä, J., Marchesi, J.R., Smidt, H., Vos, W.M. de, Ross, R.P., and O'Toole, P.W. (2009). Comparative analysis of pyrosequencing and a phylogenetic microarray for exploring microbial community structures in the human distal intestine. PloS one *4*, e6669. https://doi.org/10.1371/journal.pone.0006669.

Coquin, L., Feala, J.D., McCulloch, A.D., and Paternostro, G. (2008). Metabolomic and flux-balance analysis of age-related decline of hypoxia tolerance in Drosophila muscle tissue. Molecular Systems Biology *4*, 233. https://doi.org/10.1038/msb.2008.71.

Cordes, H., Thiel, C., Baier, V., Blank, L.M., and Kuepfer, L. (2018). Integration of genome-scale metabolic networks into whole-body PBPK models shows phenotype-specific cases of drug-induced metabolic perturbation. NPJ systems biology and applications *4*, 10. https://doi.org/10.1038/s41540-018-0048-1.

Covert, M.W., Famili, I., and Palsson, B.O. (2003). Identifying constraints that govern cell behavior: a key to converting conceptual to computational models in biology? Biotechnology and bioengineering *84*, 763-772. https://doi.org/10.1002/bit.10849.

Crown, S.B., and Antoniewicz, M.R. (2013). Parallel labeling experiments and metabolic flux analysis: Past, present and future methodologies. Metabolic engineering *16*, 21-32. https://doi.org/10.1016/j.ymben.2012.11.010.

Deshpande, S.A., Carvalho, G.B., Amador, A., Phillips, A.M., Hoxha, S., Lizotte, K.J., and Ja, W.W. (2014). Quantifying Drosophila food intake: comparative analysis of current methodology. Nature methods *11*, 535-540. https://doi.org/10.1038/nmeth.2899.

DiAngelo, J.R., and Birnbaum, M.J. (2009). Regulation of fat cell mass by insulin in Drosophila melanogaster. Molecular and cellular biology *29*, 6341-6352. https://doi.org/10.1128/MCB.00675-09.

Dougherty, E.C. (1959). Introduction to Axenic Culture of Invertebrate Metazoa: a Goal. Annals of the New York Academy of Sciences *77*, 27-54. https://doi.org/10.1111/j.1749-6632.1959.tb36891.x.

Douglas, A.E. (2019). Simple animal models for microbiome research. Nature Reviews Microbiology *17*, 764-775. https://doi.org/10.1038/s41579-019-0242-1.

Edelaar, P. (2013). Comment on "Evolutionary trade-offs, Pareto optimality, and the geometry of phenotype space". Science *339*, 757. https://doi.org/10.1126/science.1228281.

Erkosar, B., Defaye, A., Bozonnet, N., Puthier, D., Royet, J., and Leulier, F. (2014). Drosophila microbiota modulates host metabolic gene expression via IMD/NF-κB signaling. PloS one *9*, e94729. https://doi.org/10.1371/journal.pone.0094729.

Feala, J.D., Coquin, L., McCulloch, A.D., and Paternostro, G. (2007). Flexibility in energy metabolism supports hypoxia tolerance in Drosophila flight muscle: metabolomic and computational systems analysis. Molecular Systems Biology *3*, 99. https://doi.org/10.1038/msb4100139.

Feala, J.D., Coquin, L., Zhou, D., Haddad, G.G., Paternostro, G., and McCulloch, A.D. (2009). Metabolism as means for hypoxia adaptation: metabolic profiling and flux balance analysis. BMC Syst Biol *3*, 91. https://doi.org/10.1186/1752-0509-3-91.

Foguet, C., Jayaraman, A., Marin, S., Selivanov, V.A., Moreno, P., Messeguer, R., Atauri, P. de, and Cascante, M. (2019). p13CMFA: Parsimonious 13C metabolic flux analysis. PLOS Computational Biology *15*, e1007310. https://doi.org/10.1371/journal.pcbi.1007310.

Fux, C.A., Costerton, J.W., Stewart, P.S., and Stoodley, P. (2005). Survival strategies of infectious biofilms. Trends in microbiology *13*, 34-40. https://doi.org/10.1016/j.tim.2004.11.010.

Garcia, D.E., Baidoo, E.E., Benke, P.I., Pingitore, F., Tang, Y.J., Villa, S., and Keasling, J.D. (2008). Separation and mass spectrometry in microbial metabolomics. Current opinion in microbiology *11*, 233-239. https://doi.org/10.1016/j.mib.2008.04.002.

García Sánchez, C.E., and Torres Sáez, R.G. (2014). Comparison and analysis of objective functions in flux balance analysis. Biotechnol Progress *30*, 985-991. https://doi.org/10.1002/btpr.1949.

Goelzer, A., and Fromion, V. (2017). Resource allocation in living organisms. Biochemical Society transactions *45*, 945-952. https://doi.org/10.1042/BST20160436.

Goelzer, A., Fromion, V., and Scorletti, G. (2011). Cell design in bacteria as a convex optimization problem. Automatica *47*, 1210-1218. https://doi.org/10.1016/j.automatica.2011.02.038.

Gomes de Oliveira Dal'Molin, C., and Nielsen, L.K. (2018). Plant genome-scale reconstruction: from single cell to multi-tissue modelling and omics analyses. Current Opinion in Biotechnology *49*, 42-48. https://doi.org/10.1016/j.copbio.2017.07.009.

Grafahrend-Belau, E., Junker, A., Eschenröder, A., Müller, J., Schreiber, F., and Junker, B.H. (2013). Multiscale metabolic modeling: dynamic flux balance analysis on a whole-plant scale. Plant physiology *163*, 637-647. https://doi.org/10.1104/pp.113.224006.

Halfvarson, J., Brislawn, C.J., Lamendella, R., Vázquez-Baeza, Y., Walters, W.A., Bramer, L.M., D'Amato, M., Bonfiglio, F., McDonald, D., and Gonzalez, A., et al. (2017). Dynamics of the human gut microbiome in inflammatory bowel disease. Nature Microbiology *2*, 17004. https://doi.org/10.1038/nmicrobiol.2017.4.

Hariharan, D., Vellanki, K., and Kramer, H. (2015). The Western Diet and Chronic Kidney Disease. Current hypertension reports *17*, 16. https://doi.org/10.1007/s11906-014-0529-6.

Heinken, A., and Thiele, I. (2015). Systematic prediction of health-relevant human-microbial co-metabolism through a computational framework. Gut Microbes *6*, 120-130. https://doi.org/10.1080/19490976.2015.1023494.

Heinrich, P., Kohler, C., Ellmann, L., Kuerner, P., Spang, R., Oefner, P.J., and Dettmer, K. (2018). Correcting for natural isotope abundance and tracer impurity in MS-, MS/MS- and high-resolution-multiple-tracer-data from stable isotope labeling experiments with IsoCorrectoR. Sci Rep *8*, 17910. https://doi.org/10.1038/s41598-018-36293-4.

Hjersted, J.L., and Henson, M.A. (2006). Optimization of Fed-Batch Saccharomyces cerevisiae Fermentation Using Dynamic Flux Balance Models. Biotechnol Progress *22*, 1239-1248. https://doi.org/10.1002/bp060059v.

Jayme, D.W., and Smith, S.R. (2000). Media formulation options and manufacturing process controls to safeguard against introduction of animal origin contaminants in animal cell culture. Cytotechnology *33*, 27-36. https://doi.org/10.1023/A:1008133717035.

Kauffman, K.J., Prakash, P., and Edwards, J.S. (2003). Advances in flux balance analysis. Current Opinion in Biotechnology *14*, 491-496. https://doi.org/10.1016/j.copbio.2003.08.001.

Knorr, A.L., Jain, R., and Srivastava, R. (2007). Bayesian-based selection of metabolic objective functions. Bioinformatics (Oxford, England) *23*, 351-357. https://doi.org/10.1093/bioinformatics/btl619.

Krajmalnik-Brown (2012). Effects of gut microbes on nutrient absorption and energy regulation. Nutr. Clin. Pract. Off. Publ. Am. Soc. Parenter Enter Nutr. *27*, 201.

Krause, S.A., Overend, G., Dow, J.A.T., and Leader, D.P. (2022). FlyAtlas 2 in 2022: enhancements to the Drosophila melanogaster expression atlas. Nucleic Acids Research *50*, D1010-D1015. https://doi.org/10.1093/nar/gkab971.

Lacroix, V., Cottret, L., Thébault, P., and Sagot, M.-F. (2008). An introduction to metabolic networks and their structural analysis. IEEE/ACM transactions on computational biology and bioinformatics *5*, 594-617. https://doi.org/10.1109/TCBB.2008.79.

Lambers, H., Posthumus, F., Stulen, I., Lanting, L., Dijk, S.J., and Hofstra, R. (1981). Energy metabolism of Plantago major ssp. major as dependent on the supply of mineral nutrients. Physiol Plant *51*, 245-252. https://doi.org/10.1111/j.1399-3054.1981.tb04472.x.

Lee, J.M., Gianchandani, E.P., and Papin, J.A. (2006). Flux balance analysis in the era of metabolomics. Briefings in bioinformatics *7*, 140-150. https://doi.org/10.1093/bib/bbl007.

Lehninger, A.L., Nelson, D.L., and Cox, M.M. (2013). Principles of biochemistry (New York: W.H. Freeman).

Leisegang, K. (2019). Malnutrition and Obesity. In Oxidants, Antioxidants and Impact of the Oxidative Status in Male Reproduction (Elsevier), pp. 117–134.

Lewis, N.E., Schramm, G., Bordbar, A., Schellenberger, J., Andersen, M.P., Cheng, J.K., Patel, N., Yee, A., Lewis, R.A., and Eils, R., et al. (2010). Large-scale in silico modeling of metabolic interactions between cell types in the human brain. Nature biotechnology *28*, 1279-1285. https://doi.org/10.1038/nbt.1711.

Li, H., Hurlburt, A.J., and Tennessen, J.M. (2018). A Drosophila model of combined D-2- and L-2-hydroxyglutaric aciduria reveals a mechanism linking mitochondrial citrate export with oncometabolite accumulation. Disease models & mechanisms *11*. https://doi.org/10.1242/dmm.035337.

Li, S., Yu, X., and Feng, Q. (2019). Fat Body Biology in the Last Decade. Annu. Rev. Entomol. *64*, 315-333. https://doi.org/10.1146/annurev-ento-011118-112007.

Li, X., Yilmaz, L.S., and Walhout, A.J.M. (2022). Compartmentalization of metabolism between cell types in multicellular organisms: a computational perspective. Current opinion in systems biology *29*. https://doi.org/10.1016/j.coisb.2021.100407.

Lin, R., Liu, W., Piao, M., and Zhu, H. (2017). A review of the relationship between the gut microbiota and amino acid metabolism. Amino Acids *49*, 2083-2090. https://doi.org/10.1007/s00726-017-2493-3.

Liu, Y., Wang, Y., Ni, Y., Cheung, C.K.Y., Lam, K.S.L., Wang, Y., Xia, Z., Ye, D., Guo, J., and Tse, M.A., et al. (2020). Gut Microbiome Fermentation Determines the Efficacy of Exercise for Diabetes Prevention. Cell metabolism *31*, 77-91.e5. https://doi.org/10.1016/j.cmet.2019.11.001.

Ludington, W.B., and Ja, W.W. (2020). Drosophila as a model for the gut microbiome. PLOS Pathogens *16*, e1008398. https://doi.org/10.1371/journal.ppat.1008398.

Lumeng, C.N., and Saltiel, A.R. (2011). Inflammatory links between obesity and metabolic disease. The Journal of clinical investigation *121*, 2111-2117. https://doi.org/10.1172/JCI57132.

Luque, E.M., Tissera, A., Gaggino, M.P., Molina, R.I., Mangeaud, A., Vincenti, L.M., Beltramone, F., Larcher, J.S., Estofán, D., and Fiol de Cuneo, M., et al. (2017). Body mass index and human sperm quality: neither one extreme nor the other. Reproduction, fertility, and development *29*, 731-739. https://doi.org/10.1071/RD15351.

Magazzù, G., Zampieri, G., and Angione, C. (2021). Multimodal regularized linear models with flux balance analysis for mechanistic integration of omics data. Bioinformatics (Oxford, England) *37*, 3546-3552. https://doi.org/10.1093/bioinformatics/btab324.

Magnúsdóttir, S., and Thiele, I. (2018). Modeling metabolism of the human gut microbiome. Current Opinion in Biotechnology *51*, 90-96. https://doi.org/10.1016/j.copbio.2017.12.005.

Martin, A.M., Sun, E.W., Rogers, G.B., and Keating, D.J. (2019). The Influence of the Gut Microbiome on Host Metabolism Through the Regulation of Gut Hormone Release. Frontiers in Physiology *10*, 428. https://doi.org/10.3389/fphys.2019.00428.

Martins Conde, P., Pfau, T., Pires Pacheco, M., and Sauter, T. (2021). A dynamic multi-tissue model to study human metabolism. NPJ systems biology and applications *7*, 5. https://doi.org/10.1038/s41540-020-00159-1.

Merkey, A.B., Wong, C.K., Hoshizaki, D.K., and Gibbs, A.G. (2011). Energetics of metamorphosis in Drosophila melanogaster. Journal of Insect Physiology *57*, 1437-1445. https://doi.org/10.1016/j.jinsphys.2011.07.013.

Millington, J.W., Biswas, P., Chao, C., Xia, Y.H., Wat, L.W., Brownrigg, G.P., Sun, Z., Basner-Collins, P.J., Klein Geltink, R.I., and Rideout, E.J. (2022). A low-sugar diet enhances Drosophila body size in males and females via sex-specific mechanisms. Development (Cambridge, England) *149*. https://doi.org/10.1242/dev.200491.

Mirth, C., Truman, J.W., and Riddiford, L.M. (2005). The role of the prothoracic gland in determining critical weight for metamorphosis in Drosophila melanogaster. Current biology : CB *15*, 1796-1807. https://doi.org/10.1016/j.cub.2005.09.017.

Mirth, C.K., and Shingleton, A.W. (2012). Integrating body and organ size in Drosophila: recent advances and outstanding problems. Frontiers in endocrinology *3*, 49. https://doi.org/10.3389/fendo.2012.00049.

Musselman, L.P., Fink, J.L., Narzinski, K., Ramachandran, P.V., Hathiramani, S.S., Cagan, R.L., and Baranski, T.J. (2011). A high-sugar diet produces obesity and insulin resistance in wild-type Drosophila. Disease models & mechanisms *4*, 842-849. https://doi.org/10.1242/dmm.007948.

Musselman, L.P., and Kühnlein, R.P. (2018). Drosophila as a model to study obesity and metabolic disease. The Journal of experimental biology *221*. https://doi.org/10.1242/jeb.163881.

Nunney, L. (1996). The Response to Selection for Fast Larval Development in Drosophila melanogaster and its Effect on Adult Weight: An Example of a Fitness Trade-Off. Evolution; international journal of organic evolution *50*, 1193-1204. https://doi.org/10.1111/j.1558-5646.1996.tb02360.x.

Orth, J.D., Fleming, R.M.T., and Palsson, B.Ø. (2010a). Reconstruction and Use of Microbial Metabolic Networks: the Core Escherichia coli Metabolic Model as an Educational Guide. EcoSal Plus *4*. https://doi.org/10.1128/ecosalplus.10.2.1.

Orth, J.D., Thiele, I., and Palsson, B.Ø. (2010b). What is flux balance analysis? Nature biotechnology *28*, 245-248. https://doi.org/10.1038/nbt.1614.

Ow, D.S.-W., Lee, D.-Y., Yap, M.G.-S., and Oh, S.K.-W. (2009). Identification of cellular objective for elucidating the physiological state of plasmid-bearing Escherichia coli using genome-scale in silico analysis. Biotechnol Progress *25*, 61-67. https://doi.org/10.1002/btpr.51.

Phan-Thanh, L., and Gormon, T. (1997). A chemically defined minimal medium for the optimal culture of Listeria. International journal of food microbiology *35*, 91-95. https://doi.org/10.1016/S0168-1605(96)01205-6.

Piper, M.D.W., Blanc, E., Leitão-Gonçalves, R., Yang, M., He, X., Linford, N.J., Hoddinott, M.P., Hopfen, C., Soultoukis, G.A., and Niemeyer, C., et al. (2014). A holidic medium for Drosophila melanogaster. Nature methods *11*, 100-105. https://doi.org/10.1038/nmeth.2731.

Piper, M.D.W., Soultoukis, G.A., Blanc, E., Mesaros, A., Herbert, S.L., Juricic, P., He, X., Atanassov, I., Salmonowicz, H., and Yang, M., et al. (2017). Matching Dietary Amino Acid Balance to the In Silico-Translated Exome Optimizes Growth and Reproduction without Cost to Lifespan. Cell metabolism *25*, 610-621. https://doi.org/10.1016/j.cmet.2017.02.005.

Plauth, M., Raible, A., Gregor, M., and Hartmann, F. (1993). Inter-organ communication between intestine and liver in vivo and in vitro. Seminars in cell biology *4*, 231-237. https://doi.org/10.1006/scel.1993.1027.

Pramanik, J., and Keasling, J.D. (1997). Stoichiometric model of Escherichia coli metabolism: Incorporation of growth-rate dependent biomass composition and mechanistic energy requirements. Biotechnol. Bioeng. *56*, 398-421. https://doi.org/10.1002/(SICI)1097-0290(19971120)56:4<398::AID-BIT6>3.0.CO;2-J.

Reiter, L.T., Potocki, L., Chien, S., Gribskov, M., and Bier, E. (2001). A systematic analysis of human disease-associated gene sequences in Drosophila melanogaster. Genome Research *11*, 1114-1125. https://doi.org/10.1101/gr.169101.

Ridley, E.V., Wong, A.C.-N., Westmiller, S., and Douglas, A.E. (2012). Impact of the resident microbiota on the nutritional phenotype of Drosophila melanogaster. PloS one *7*, e36765. https://doi.org/10.1371/journal.pone.0036765.

Robertson, F.W. (1963). The ecological genetics of growth in Drosophila 6. The genetic correlation between the duration of the larval period and body size in relation to larval diet. Genet. Res. *4*, 74-92. https://doi.org/10.1017/S001667230000344X.

Roszak, D.B., and Colwell, R.R. (1987). Survival strategies of bacteria in the natural environment. Microbiol Rev *51*, 365-379. https://doi.org/10.1128/mr.51.3.365-379.1987.

Russo, S.E., Ledder, G., Muller, E.B., and Nisbet, R.M. (2022). Dynamic Energy Budget models: fertile ground for understanding resource allocation in plants in a changing world. Conservation physiology *10*, coac061. https://doi.org/10.1093/conphys/coac061.

Savinell, J.M., and Palsson, B.O. (1992). Network analysis of intermediary metabolism using linear optimization. I. Development of mathematical formalism. Journal of Theoretical Biology *154*, 421-454. https://doi.org/10.1016/S0022-5193(05)80161-4.

Schleucher, J., Vanderveer, P.J., and Sharkey, T.D. (1998). Export of carbon from chloroplasts at night. Plant physiology *118*, 1439-1445. https://doi.org/10.1104/pp.118.4.1439.

Schönborn, J.W., Jehrke, L., Mettler-Altmann, T., and Beller, M. (2019). FlySilico: Flux balance modeling of Drosophila larval growth and resource allocation. Sci Rep *9*, 17156. https://doi.org/10.1038/s41598-019-53532-4.

Schönborn, J.W., Stewart, F.A., Enriquez, K.M., Akhtar, I., Droste, A., Waschina, S., and Beller, M. (2021). Modeling Drosophila gut microbe interactions reveals metabolic interconnectivity. iScience *24*, 103216. https://doi.org/10.1016/j.isci.2021.103216.

Schuetz, R., Kuepfer, L., and Sauer, U. (2007). Systematic evaluation of objective functions for predicting intracellular fluxes in Escherichia coli. Molecular Systems Biology *3*, 119. https://doi.org/10.1038/msb4100162.

Schuetz, R., Zamboni, N., Zampieri, M., Heinemann, M., and Sauer, U. (2012). Multidimensional optimality of microbial metabolism. Science *336*, 601-604. https://doi.org/10.1126/science.1216882.

Sender, R., Fuchs, S., and Milo, R. (2016). Revised Estimates for the Number of Human and Bacteria Cells in the Body. PLOS Biology *14*, e1002533. https://doi.org/10.1371/journal.pbio.1002533.

Sharma, R., Biedenharn, K.R., Fedor, J.M., and Agarwal, A. (2013). Lifestyle factors and reproductive health: taking control of your fertility. Reproductive biology and endocrinology : RB&E *11*, 66. https://doi.org/10.1186/1477-7827-11-66.

Shaw, R., and Cheung, C.Y.M. (2018). A Dynamic Multi-Tissue Flux Balance Model Captures Carbon and Nitrogen Metabolism and Optimal Resource Partitioning During Arabidopsis Growth. Frontiers in plant science *9*, 884. https://doi.org/10.3389/fpls.2018.00884.

Shin, S.C., Kim, S.-H., You, H., Kim, B., Kim, A.C., Lee, K.-A., Yoon, J.-H., Ryu, J.-H., and Lee, W.-J. (2011). Drosophila microbiome modulates host developmental and metabolic homeostasis via insulin signaling. Science *334*, 670-674. https://doi.org/10.1126/science.1212782.

Shingleton, A.W., Frankino, W.A., Flatt, T., Nijhout, H.F., and Emlen, D.J. (2007). Size and shape: the developmental regulation of static allometry in insects. BioEssays : news and reviews in molecular, cellular and developmental biology *29*, 536-548. https://doi.org/10.1002/bies.20584.

Shoval, O., Sheftel, H., Shinar, G., Hart, Y., Ramote, O., Mayo, A., Dekel, E., Kavanagh, K., and Alon, U. (2012). Evolutionary trade-offs, Pareto optimality, and the geometry of phenotype space. Science *336*, 1157-1160. https://doi.org/10.1126/science.1217405.

Shoval, O., Sheftel, H., Shinar, G., Hart, Y., Ramote, O., Mayo, A., Dekel, E., Kavanagh, K., and Alon, U. (2013). Response to comment on "Evolutionary trade-offs, Pareto optimality, and the geometry of phenotype space". Science *339*, 757. https://doi.org/10.1126/science.1228921.

Shupletsov, M.S., Golubeva, L.I., Rubina, S.S., Podvyaznikov, D.A., Iwatani, S., and Mashko, S.V. (2014). OpenFLUX2: (13)C-MFA modeling software package adjusted for the comprehensive analysis of single and parallel labeling experiments. Microbial cell factories *13*, 152. https://doi.org/10.1186/s12934-014-0152-x.

Sláma, K. (1964). Hormonal control of respiratory metabolism during growth, reproduction, and diapause in female adults of Pyrrhocoris apterus L. (Hemiptera). Journal of Insect Physiology *10*, 283-303. https://doi.org/10.1016/0022-1910(64)90013-7.

Sommer, M.O.A. (2015). Advancing gut microbiome research using cultivation. Current opinion in microbiology *27*, 127-132. https://doi.org/10.1016/j.mib.2015.08.004.

Sparkman, O.D., Penton, Z., and Kitson, F.G. (2011). Gas chromatography and mass spectrometry. A practical guide (Burlington, MA: Academic Press).

Stephanopoulos, G., Aristidou, A.A., and Nielsen, J. (1998). Metabolic Engineering. Principles and Methodologies (Elsevier Science).

Storelli, G., Defaye, A., Erkosar, B., Hols, P., Royet, J., and Leulier, F. (2011). Lactobacillus plantarum promotes Drosophila systemic growth by modulating hormonal signals through TOR-dependent nutrient sensing. Cell metabolism *14*, 403-414. https://doi.org/10.1016/j.cmet.2011.07.012.

Szekely, P., Korem, Y., Moran, U., Mayo, A., and Alon, U. (2015). The Mass-Longevity Triangle: Pareto Optimality and the Geometry of Life-History Trait Space. PLOS Computational Biology *11*, e1004524. https://doi.org/10.1371/journal.pcbi.1004524.

Thiele, I., and Palsson, B.Ø. (2010). A protocol for generating a high-quality genome-scale metabolic reconstruction. Nat Protoc *5*, 93-121. https://doi.org/10.1038/nprot.2009.203.

Thiele, I., Sahoo, S., Heinken, A., Hertel, J., Heirendt, L., Aurich, M.K., and Fleming, R.M. (2020). Personalized whole-body models integrate metabolism, physiology, and the gut microbiome. Molecular Systems Biology *16*, e8982. https://doi.org/10.15252/msb.20198982.

Tilg, H., and Kaser, A. (2011). Gut microbiome, obesity, and metabolic dysfunction. The Journal of clinical investigation *121*, 2126-2132. https://doi.org/10.1172/JCI58109.

Troncoso, B., Godoy-Herrera, R., and Mora, W. (1987). The development of larval movement patterns in Drosophila. Heredity *58*, 321-329. https://doi.org/10.1038/hdy.1987.58.

Turnbaugh, P.J., and Gordon, J.I. (2009). The core gut microbiome, energy balance and obesity. The Journal of Physiology *587*, 4153-4158. https://doi.org/10.1113/jphysiol.2009.174136.

van Ankeren, S.C., and Wheeler, K.T. (1985). Relationship between DNA repair and cell recovery: importance of competing biochemical and metabolic processes. Radiat Environ Biophys *24*, 271-280. https://doi.org/10.1007/BF01210934.

van de Kerkhof, E.G., Graaf, I.A.M. de, and Groothuis, G.M.M. (2007). In vitro methods to study intestinal drug metabolism. Current drug metabolism *8*, 658-675. https://doi.org/10.2174/138920007782109742.

Varma, A., and Palsson, B.O. (1994). Metabolic Flux Balancing: Basic Concepts, Scientific and Practical Use. Nature biotechnology *12*, 994-998. https://doi.org/10.1038/nbt1094-994.

Waldbauer, G.P., and Friedman, S. (1991). Self-Selection of Optimal Diets by Insects. Annu. Rev. Entomol. *36*, 43-63. https://doi.org/10.1146/annurev.en.36.010191.000355.

Wolfe, R.R., and Chinkes, D.L. (2005). Isotope tracers in metabolic research. Principles and practice of kineticanalysis (Hoboken . Wiley-Liss: John Wiley & Sons).

Yoon, S.H., Han, M.-J., Jeong, H., Lee, C.H., Xia, X.-X., Lee, D.-H., Shim, J.H., Lee, S.Y., Oh, T.K., and Kim, J.F. (2012). Comparative multi-omics systems analysis of Escherichia coli strains B and K-12. Genome Biology *13*, R37. https://doi.org/10.1186/gb-2012-13-5-r37.

Zamboni, N. (2011). 13C metabolic flux analysis in complex systems. Current Opinion in Biotechnology *22*, 103-108. https://doi.org/10.1016/j.copbio.2010.08.009.

6. List of Figures

7. List of Tables

8. List of Abbreviations

Abbreviation	Definition
°C	degree Celsius
µg	microgram
µL	microlitre
µM	micromolar
µmol	micromol
^{13}CMFA	^{13}C metabolic flux analysis
ACE medium	*Acetobacter*-selective medium
AEL	after egg-laying
AMP	Adenosine 5'-monophosphate
ATP	adenosine triphosphate
CMP	Cytidine 5'-monophosphate
dAMP	2'-Deoxyadenosine 5'-monophosphate
dCMP	2'-Deoxycytidine 5'-monophosphate
dFBA	dynamic flux balance analysis
dGMP	2'-Deoxyguanosine 5'-phosphate
DNA	deoxyribonucleic acid
dTMP	2'-Deoxythymidine 5'-phosphate
dw/DW	dry weight
EAA	essential amino acids
EC	enzyme commission numbers
EDTA	ethylenediaminetetraacetic acid
EGTA	egtazic acid
FBA	flux balance analysis
g	gram
g/h	gram per hour
GAM	growth associated maintenance
GC-MS	gas chromatography–mass spectrometry
GMP	Guanosine 5'-phosphate

h	hour
HD	*holidic diet*
HPLC	high performance liquid chromatography
HSD	high sugar diet
ISTD	internal standard
LSD	low sugar diet
MFA	metabolic flux analysis
mg	milligram
mL	millilitre
mm	millimeters
mM	millimolar
mm²	square millimeters
mm³	cubic millimetres
mmol	millimol
MRS medium	*Lactobacillus-promoting* medium
MS	mass spectrometry
MS/MS	tandem mass spectrometry
NADH	nicotinamide adenine dinucleotide and hydrogen
NADPH	nicotinamide adenine dinucleotide phosphate and hydrogen
ng	nanogram
NGAM	non-growth associated maintenance
nmol	nanomol
OD600	optical density at λ=600 nm
PBS	phosphate buffered saline
PCR	polymerase chain reaction
pg	picogram
RBA	Resource Balance Analysis
RNA	ribonuleic acid
S2R+	S2 receptor plus
TAG	triglyceride
TCA-Cycle	tricarboxylic acid cycle
UMP	Uridine 5'-monophosphate
WMM	weighted mean of metabolite
WMMC	weighted mean metabolite coefficient
Yaa	Yeast-like amino acid

9. Eidesstattliche Erklärung

Ich, Jürgen Wilhelm Schönborn, versichere an Eides Statt, dass die Dissertation von mir selbständig und ohne unzulässige fremde Hilfe unter Beachtung der „Grundsätze zur Sicherung guter wissenschaftlicher Praxis an der Heinrich-Heine-Universität Düsseldorf“ erstellt worden ist.

Diese Dissertation wurde in noch keiner anderen Fakultät zur Prüfung vorgelegt.

_____ _____

Ort, Datum Unterschrift